PTT-26

Some Properties of Mechanically Alloyed Oxide Dispersion Strengthened Metals

By

Adebayo Yekeen Badmos
Churchill College, Cambridge

Department of Materials Science and Metallurgy
Pembroke Street
Cambridge CB2 3QZ

A dissertation submitted for the degree of
Doctor of Philosophy
at the University of Cambridge
October 1997

PREFACE

This dissertation is submitted for the degree of Doctor of Philosophy at the University of Cambridge. The investigation described herein was carried out under the supervision of Dr. H. K. D. H. Bhadeshia in the Department of Materials Science and Metallurgy, University of Cambridge, between October 1994 and September 1997. Except where acknowledgement and reference to previous work is made, this work is, to the best of my knowledge, original and carried out without collaboration. Neither this , nor any similar dissertation has been or is being submitted for any degree, diploma or other qualification at any other University.

The contents of Chapters Four and Five have been accepted for publication and Chapter Six submitted for publication with the details as below.

(i) A. Y. Badmos and H. K. D. H. Bhadeshia (1997), "The Evolution of Solutions: A Thermodynamic Analysis of Mechanical Alloying' *Metallurgical Transactions A,* **28** 1–6.

(ii) A. Y. Badmos, H. K. D. H. Bhadeshia, and D.J.C. Mackay (1997), "Neural Network Models for the Tensile Properties of Mechanically Alloyed ODS Iron–Alloys" - Accepted for publication in *Materials Science and Technology.*

(iii) A. Y. Badmos and H. K. D. H. Bhadeshia (1997), "Yield Strength of Mechanically Alloyed ODS Iron Alloys : Physical Interpretation" - Submitted for publication in *Materials Science and Technology.*

Adebayo Yekeen Badmos

ACKNOWLEDGEMENTS

To Almighty God is due every praise and glory for the successful completion of this work. With gratitude I acknowledged the enormous financial commitments of my sponsors, Cambridge Commonwealth Trust for the Blue Circle Scholarship and the Committee of Vice–Chancellors and Principals of Universities, UK, for the Overseas Research Studentship (ORS).

I am particularly grateful to my supervisor, Dr. H. K. D. H. Bhadeshia without whose inspirational supervision, the timely completion of this work would not have been possible. His enthusiasm, patience, encouragement and seemingly inexhaustible pool of ideas have been found tremendously helpful in every aspect of this research. I wish to thank Professor Alan Windle for the provision of laboratory facilities in the Department of Materials Science and Metallurgy at the University of Cambridge. The help from the technical staff in the Department has been much appreciated, especially from Brian Whitmore, Brian Barber, Carol Best, Graham Morgan, Dave Nicol, Robinson Taylor and Kelvin Robert. I am also grateful to the entire members of my research group (Phase Transformation) for providing the friendly and stimulating working environment.

I would like to express my indebtedness to INCO Alloy, Hereford, UK, for the supply of the materials used in the experimental investigation of this work. Also, the intellectual contributions of the officers from the Research and Development Departments of INCO Alloy and National Power Plc. during the discussions at our series of meetings are acknowledged with thanks. I thank Dr. A.R. Jones, Liverpool University, UK., for providing some data for neural network analysis.

I warmly acknowledged the special position of my wife during the course of this work. Her moral support and encouragement were the sources of my emotional strength at those difficult times of the usual research frustration and low morale. Finally, I would like to say a big "THANK YOU" to my parents for their support and encouragement. This thesis is dedicated to them for all they went through for my education.

ABSTRACT

Oxide dispersion strengthened (ODS) superalloys are generally made using the mechanical alloying technique. In this, the powdered components are attrited together to form a solid solution with finely dispersed oxide particles. The material produced by compacting the powder using extrusion and rolling has exceptionally high creep resistance after a recrystallization heat–treatment. A great deal is understood about the microstructure but not the mechanical properties. The main purpose of this work was to model some of the mechanical properties of iron–base ODS alloys.

A brief introduction to the aim is followed by an extensive literature review dealing with all aspects of the process and the physical metallurgy of the resulting alloys. The experimental techniques used in the course of the investigations are described in Chapter Three.

The evolution of a solution during the attrition of mixtures of powders has been studied by developing a novel thermodynamic analysis which incorporates large particles rather than just atoms. Normal thermodynamic theory for solutions begins with the mixing of components atoms. However, in mechanical alloying, solutions are prepared by mixing together lumps of the components, each of which might contain millions of identical atoms. It has never been clear as to when the component powders become more like a solution than a mechanical mixture. It is predicted that solution formation by the mechanical alloying of solid components cannot occur unless there is a gain in coherency as the particles become small. The existence of a barrier to the evolution of solution due to interfacial energy is also identified.

The relationship between the tensile properties and a number of variables known to affect mechanical properties is studied using an artifitial neural network applied to the published data. Models have thus been produced dealing with the yield strength, ultimate tensile strength and elongation (Chapter Five). The analysis revealed patterns which are metallurgically significant and which permit

the quantitative estimation of mechanical properties as a function of important processing and service variables together with an indication of confidence limits.

The neural network models can express the output as a function of a very large number of interesting variables. An alternative approach involves modelling based on physical principles. The components of the yield strength of MA956, a mechanically alloyed ODS ferritic steel have been investigated quantitatively in Chapter Six. The ambient temperature yield strength of the alloy in the as–processed condition originates from its ultra–fine grain size, the intrinsic strength of ferritic iron, dispersoid strenthening via the yttria compounds and finally, the dislocation density. The contributions of these components decrease in the order stated. The contribution from dispersion strengthening has been estimated using dislocation theory and has been demonstrated to be consistent with that measured experimentally. It is found that much of the difference in strength between the recrystallised and unrecrystallised forms can be explained in terms of the grain structure.

Appendices I and II report the experimental investigations relating to the characteristic anisotropic mechanical behaviour of the alloys. Some tensile tests conducted to verify some of the results of the neural network analysis are reported in Appendix III.

CONTENTS

NOMENCLATURE AND ABBREVIATIONS

MA	Mechanical Alloying
ODS	Oxide Dispersion Strengthened
ΔG_f	Free energy of formation
γ'	Intermetallic phase in nickel–base alloys
F_r	Retarding force per unit area
f	Volume fraction of particles
r	Particle radius
γ_{gb}	Grain boundary energy per unit area
T	Temperature
T_m	Melting temperature
τ_{OR}	Orowan shear stress
f.c.c.	Face centered cubic
b.c.c.	Body centered cubic
σ_y	Yield strength
d	Grain size
σ_i	Lattice friction stress
k_o	Grain boundary locking parameter
τ_p	Resolved shear stress for dislocation by–pass
G	Shear modulus
b	Burgers vector
λ	Interparticle spacing
K',K'',K'''	Constants
H	Total hardness

H_m	Hardness due to matrix
K_p	Material constant for dispersed phase
GAR	Grain aspect ratio
σ_{eff}	Effective strength
σ_m	Inherent strength of ODS matrix
f_a	Volume average of dispersed particles
K	An interaction parameter for creep
δ_b	Gap between grain boundaries
σ_{Fe}	Strength of pure iron
σ_s	Solid solution strengthening
σ_p	Particle strengthening
σ_g	Grain boundary strengthening
σ_d	Dislocation strengthening
D_o	Pre-exponential component of self-diffusion coefficent
ρ	Dislocation density
$\dot{\epsilon}$	Shear strain rate
a_v	Area associated with a vacancy
k	Boltzmann constant
y	Output of neural network
x_j	Input of neural network
w_j	Weight of neural network
θ_i	Bias of neural network
h_i	Hyperbolic transfer function of neural network
x_N	Normalized value of input x_j
x_{min}	Minimum value of input x_j
x_{max}	Maximum value of input x_j

μ_A^o	Molar free energy of a pure component A
m_A	Atoms per powder particle of A
N_a	Avogadro number
ΔS_M	Entropy of mixing
ΔG_M	Free energy of mixing
ΔH_M	Enthalpy of mixing
ΔH_I	Change in energy due to interfaces
ϵ_{AA}	Binding energy between atoms of A

CHAPTER ONE

Introduction

1.1 Mechanically Alloyed ODS Superalloys

The need for materials with good high temperature capabilities has led to the development of the mechanical alloying (MA) technique for the production of oxide dispersion strengthened (ODS) superalloys. This includes both iron–base and nickel–base superalloys with fine and stable inert-oxide dispersions which improve the resistance to creep deformation. It is significant that with the MA process, the matrix composition and the nature of the dispersoids can be manipulated independently. The matrix composition can be tailored to optimize corrosion resistance and the dispersoids for strength. The nominal compositions of the commercially available mechanically alloyed oxide dispersion strengthened alloys are given in Table 1.1 and discussed in detail in Chapter Two.

Mechanical alloying involves the creation of an alloy by the intense mechanical deformation of mixtures of elemental or master–alloy powders. The powders are then consolidated by various powder metallurgical processes such as hot–isostatic pressing and extrusion. After mechanical alloying and consolidation, the alloys have a very fine grained microstructure and a very high hardness. A recrytallization heat–treatment is used to soften the alloy and to form a coarse columnar grain structure suitable for applications where creep resistance is important (Figure 1.1). The outstanding high temperature properties (about 1000 °C) of the alloys are therefore due to the uniform distribution of fine oxide particles, the coarse columnar grain structure, and the stable and adherent surface layer of protective oxide. Figure 1.2 illustrates a common method of manufacture for engineering applications.

Table 1.1 : Chemical compositions (wt.%) of some typical commercial MA–ODS alloys.

Steels	C	Cr	Al	Mo	Ti	N	Ti_2O_3	Y_2O_3	Fe
MA957	0.01	14.0	–	0.3	1.0	0.012	–	0.27	Balance
DT2203Y05		13.0	–	1.5	2.2		–	0.5	Balance
ODM 331		13.0	3.0	1.5	0.6		–	0.5	Balance
ODM 751		16.5	4.5	1.5	0.6		–	0.5	Balance
ODM 061		20.0	6.0	1.5	0.6		–	0.5	Balance
MA956	0.01	20.0	4.5	–	0.5	0.045	–	0.50	Balance
PM2000	< 0.04	20.0	5.5		0.5		–	0.5	Balance
PM2010	< 0.04	20.0	5.5		0.5		–	1.0	Balance
DT(DT2906)		13.0	–	1.5	2.9		1.8	–	Balance
DY(DT2203Y03)		13.0	–	1.5	2.2		0.9	0.5	Balance

Ni–Base	C	Cr	Al	Ti	W	Fe	N	Total O	Y_2O_3	Ni
MA754	0.05	20.0	0.3	0.5	–	–	–	0.37	0.6	Balance
MA6000	0.06	15.0	4.5	2.3	3.9	1.5	0.2	0.57	1.1	Balance
MA760	0.06	19.5	6.0	–	3.4	1.2	0.3	0.6	1.0	Balance
MA758	0.05	30.0	0.3	–	0.5	–	–	0.37	0.6	Balance

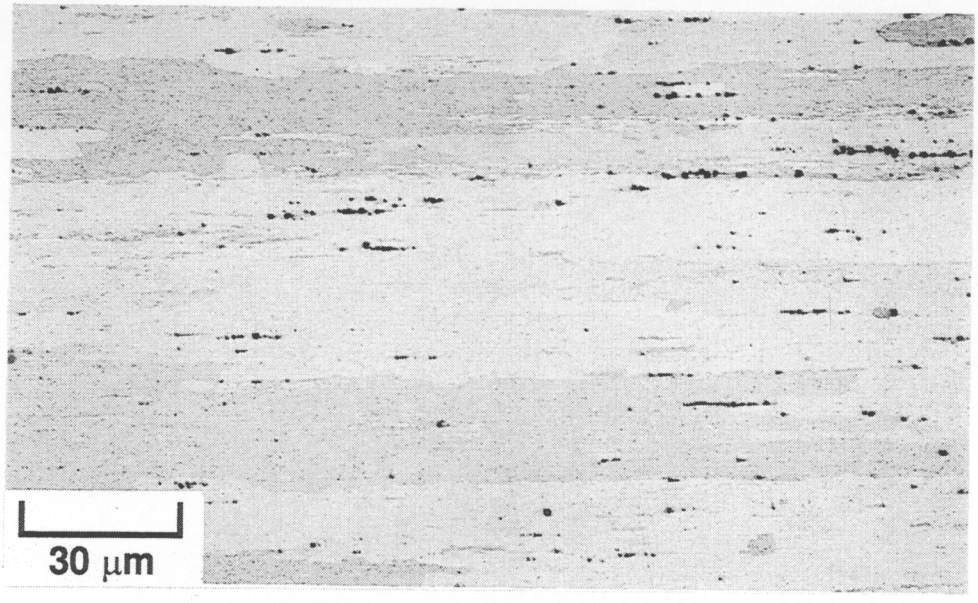

Figure 1.1: Typical microstructure of the mechanically alloyed ODS metal, MA956, after a recrystallization heat–treatment. The extrusion is horizontal in this micrograph.

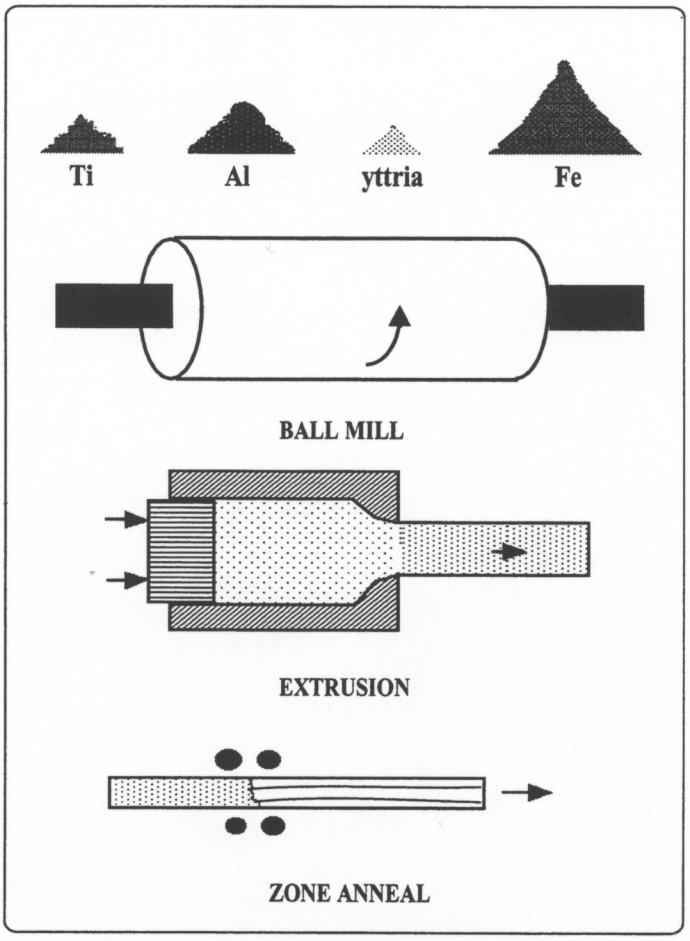

Figure 1.2 : Schematic illustration of the manufacturing process for mechanically alloyed metals.

1.2 Aims and objectives

Although, mechanically alloyed oxide dispersion stenghtened alloys are already available in commercial quantities, the technique is nevertheless special and a large number of important phenomena are not yet understood. Previous work has focussed on the control of microstructure but there has been no work on the way in which a solution evolves during the mechanical alloying process, nor on the modelling of mechanical properties. The evolution of the solid solution during the MA process is not understood even from a thermodynamic view point. Experimental measurements of the mechanical properties of the alloys are not yet exhaustive and the published data have not been properly coordinated to provide a definite pattern with regard to the numerous variables known to be important in understanding the service behaviour of the alloys. The columnar grain structure produced by directional recrystallisation is ideal for elevated temperature applications where creep resistance along the longitudinal direction is important. It is, however, less resistant to transverse stresses, which is a major disadvantage for tubular forms of the kind typical in heat exchangers. It is necessary therefore to understand the anisotropy inherent in the commercially available mechanically alloyed metals. The main objective of this work was to attempt to create quantitative models for some properties of these alloys.

CHAPTER TWO

Literature Review

2.1 Oxide Dispersion Strengthened (ODS) Alloys

When fine second phase particles are distributed in a crystalline matrix, a microstructure is formed which can be much stronger than the matrix phase alone. Such alloys are termed dispersion-strengthened materials [Ansell, 1966]. Oxides make the best dispersoids because of their high hardness, stability at high temperatures, inertness or insolubility in the matrix metals, and availability in fine particulate form. Oxides of reactive elements such as aluminium, silicon, beryllium, magnesium thorium, zirconium, and yttrium are preferable, because they are more stable at high temperatures than oxides of the more noble metals such as copper and nickel, which are suitable as matrix metals. There are many ways of adding oxide particles to metals.

The simple mechanical mixing technique involves the use of a high speed blender [Gregory and Goetzel, 1958; Zwilsky and Grant, 1962] or a ball mill [Tracey and Worn, 1962] to coat the surface of metallic powders with oxide. The interparticle spacing in the consolidated alloy produced from these powders is limited by the starting powder particle size. Powder sizes of less than 5 nm are required to get sufficiently fine interparticle spacings even with large mechanical reductions during consolidation and subsequent working operations. Powders this fine containing γ' (Ni_3[Al, Ti]) formers such as Al and Ti are very reactive because of their high specific surface area and complete or nearly complete oxidation of Al and Ti can result [Benjamin, 1970].

Ignition coating involves mixing alloy powders with a liquid solution of a salt of a reactive metal.

This mixture is dried and pulverized and the powders are heated in an inert or reducing environment to convert the salt into a refractory oxide [Murphy and Grant, 1962]. This technique also produces oxide coated powders which therefore have the same disadvantages as powders produced by the simple mechanical mixing technique. There is a greater degree of contamination because of the oxidizing potential of the reaction products from the salt decomposition step [Benjamin 1970].

Internal oxidation involves exposing metal powders or thin metal strip containing a dilute solid solution of a reactive element to an oxidizing environment at elevated temperatures. The reactive element is then converted into a dispersoid by diffusing oxygen [Chaston, 1945; Bonis and Grant, 1962; Spengler, 1964; Adachi and Grant, 1960]. It has been found experimentally that the particle size of the dispersoid increases with increasing depth of penetration of the internal oxidation front into the metal [Adachi and Grant, 1960]. Very fine, contamination-prone powders or expensive ultra-thin strips are required to obtain sufficiently fine dispersoid particle sizes. When the alloy also contains γ' forming elements, the oxygen potential has to be controlled to only oxidize the desired species.

In the selective reduction process an intimate mixture of metal oxides is produced and the oxide of the matrix alloy is selectively reduced leaving the dispersoid unaffected [Alexander *et al.*, 1961]. If Al and Ti are to be present in the matrix alloy, the reduction step is not possible with gases because of the stability of Al_2O_3 and TiO_2. These oxides can be reduced by the use of molten alkali and alkaline earth metals. However, this causes excessive growth of the dispersoid particles, and it is necessary to remove the reaction product oxides and carrier agent, usually a salt [Benjamin, 1970].

Mechanically alloyed ODS alloys are produced by deformation, a method which produces metal powder with controlled, extremely fine microstructures. The technique circumvents the shortcomings described earlier and permits the effective combination of oxide dispersion strengthening and γ' precipitation hardening in nickel-base superalloys. From the initial laboratory success in 1968 [Benjamin, 1970], the process has been developed into a well-controlled production operation. A range of nickel,

iron, aluminium and other alloys have been designed specifically for the process and techniques have been developed to form and fabricate the alloys into useful components [Benjamin and Volin, 1974; Weber,1980; Curwick, 1981; Gilman and Benjamin, 1983; Hack, 1984; McColvin and Smith, 1985; Arzt, 1988; Benjamin, 1988; Benn and Mirchandani, 1988; Whittenberger, 1989; Fischer and Weber 1990; Rühle and Korb 1991; Schaffer and McCormick, 1992].

2.2 Commercial MA–ODS Superalloys

There are two major commercial variants of MA superalloys (Table 1.1) the nickel-base alloys, intended for aerospace applications [Fleetwood, 1986; Sundaresan and Froes, 1987] and the more successful iron-base alloys for lower temperature applications. The density of the ferritic alloys is about 10 % lower than that of the nickel-base alloys, providing a significant strength/weight advantage, together with a lower thermal expansion coefficient which is beneficial when thermal fatigue is an important design criterion [Fischer *et al.*, 1977].

2.2.1 Iron–Base MA–ODS Alloys

There is growing technological interest in ferritic ODS alloys for possible use as heat exchanger process tubing, furnace and structural components. The alloys developed so far (Table 1.1) are designed to be oxidation and corrosion resistant, but with a greater creep strength when compared with equivalent cast alloys, due to the dispersion of fine yttria particles. MA956 has the greater oxidation resistance due to the high chromium concentration and its large aluminium content. Normal ferritic steels tend to undergo a marked loss in creep strength at temperatures in excess of 600 °C; the ODS alloys discussed here can in principle be used at much higher temperatures.

The excellent high temperature corrosion resistance of MA956 results principally from the formation of a stable, tightly adherent α–Al_2O_3 oxide coating. This oxide forms during the final heat treatment of mill products [Benn, 1983]. The high stability of dispersoids within the alloy matrix allows the

retention of usable strength at temperatures up to about $0.9T_m$ [McColvin, 1985].

Because of its formability, MA956 has been produced in the widest range of product forms of any mechanically alloyed ODS alloy. The alloy was originally developed for use in sheet form gas-turbine combustors, but with its combination of high strength up to 1300 °C, corrosion resistance and formability, the alloy has found a number of other applications. The gas-turbine applications under development include fabricated nozzles, compressor nozzle parts of vehicle turbines, rings for aero-engine combustors, and combustor baffle for industrial turbines. Use in power stations include oil and coal burners and swirlers, and fabricated tube assemblies for fluidized bed combustion. Burner flame stabilisers made from MA956 sheet and rivets are used in severely corrosive environments in which metal temperatures up to 1230 °C are experienced [Macdonald, 1981]. MA956 used in fliudized bed combustion has been evaluated successfully for local gasification in which its resistance to sulphidation and carburization is outstanding [Lloyd and Cooke, 1981]. The oxidation resistance of alumina forming MA956 is generally regarded as superior to that of materials which develop chromia scales [McColvin and Smith, 1987].

The ferritic iron alloys have been considered for fast-breader nuclear reactor structural materials because they do not embrittle at high temperatures and have lower swelling rate during neutron bombardment [Huet and Leroy, 1974]. Conventional ferritic steels are unsuitable because the operating temperatures of these reactors are around 650 °C. Carbide strengthening is not acceptable because carbon can be leached out or picked-up in a sodium environment. MA957 and a similar steel DT2203Y05 are therefore designed for nuclear reactor applications, for use in a liquid sodium environment at temperatures of the order of 700 °C. Both have a high void swelling resistances and a low carbon concentration in order to avoid the formation of titanium carbides [Asano *et al.*, 1988, Little *et al.*, 1991]. The titanium is meant to combine with chromium, molybdenum and iron to form a stable body centred cubic FeCrTiMo intermetallic χ–phase during ageing at around 800 °C, which can further boost the creep strength [Okafor and Carlson, 1978; Snykers and Huck, 1974].

The 'ODM' alloys are ferritic oxide dispersion microforged materials produced using the mechanical alloying technique. The compositions of ODM751 and ODM331 are very similar to MA956 alloy except that they contain 1.5 wt.% Mo with less chromium and more titanium. The rupture strength of ODM751 is larger than that of MA956 [Kazimierzak *et al.*, 1990]. The additional 1.5 wt.% Mo, either via the χ–phase or through solid solution strengthening, presumably adds to the creep strength of ODM751. However, the results are confusing because PM2000, which does not contain molybdenum, virtually matches the rupture strength of ODM751 [Bhadeshia, 1997]. The ODM alloys can be used for a wide range of high temperature applications including heat exchangers for advanced energy conversion systems, as well for chemical processes, gas turbines combustion chambers, diesel engine components, thermocouple shielding, resistors and other miscellaneous chemical applications.

PM2000 and PM2010 are ferritic MA–ODS superalloys. The former is claimed to show reduced pore formation during service and improved mechanical properties and weldability [Ruhl and Korb, 1991]. It shows a lower weight gain than MA956 during isothermal and cycling oxidation [Daeubler and Frischammer, 1990; Ruhle and Korb, 1991]. Results from tensile and stress-rupture tests as well as from oxidation and corrosion investigations are superior to those of other commercial ODS alloys [Daeubler and Froschammer, 1990]. PM 2000 can be used in gas-turbines (aircraft, marine, automotive etc.) combustion chambers, flame tubes, exhaust units, furnace construction, chemical processing equipments, glass and ceramic industries.

2.2.2 Nickel–Base MA–ODS Alloys

Incoloy MA754 and MA758 are nickel–base mechanical alloys without γ' strengthening. MA754 was the first mechanically alloyed ODS superalloy to be produced on a large scale. The material is basically a Ni–20 wt.% Cr alloy strengthened by about 1 vol. % Y_2O_3 (Table 1.1). It is comparable to TD–NiCr (an earlier ODS material strengthened with thoria, ThO_2) but has a non–radioactive dispersoid. The yttria dispersoid imparts exceptional high-temperature strength and creep resistance to the alloy. MA754 is used currently in military aircraft engines and offers an effective alternative to single crystal

castings and directionally solidified components [Fleetwood, 1986]. MA758 is a higher chromium version of MA754 (Table 2.1), developed for oxidation resistance. Its mechanical properties are similar to those of MA754 when identical product forms and grain structures are compared. MA758 has found applications in the metal processing industry and in the glass–processing industry.

The nickel–base alloys MA6000 and MA760 are both γ' strengthened. The dispersion strengthening with yttria allows the strength to be maintained to much higher temperatures. For example, at 1093 °C, the 1000 hour rupture strength of MA6000 is twice that of conventional nickel–base superalloys [Fleetwood, 1986]. For reasons which are not clear, the (low and high cycle) fatigue resistance of MA6000 is much better than that of conventional alloys, as is its thermal fatigue resistance [Gessinger, 1984].

A lot of the oxidation resistance of MA6000 relies on the formation of chromia at the surface. However, chromia is not very resistant to sulphidation. Resistance to sulphide attack is important in industrial gas turbine manufacture, where the ODS alloys have applications as vanes. MA760 has a higher sulphidation and oxidation resistance, due to its higher chromium and aluminium concentrations, the latter inducing the formation of surface alumina [Bhadeshia, 1997].

2.3 The Mechanical Alloying Process

The starting powders for mechanical alloying contain at least one ductile metal to act as a host or binder to hold the other ingredients together. They consist typically of a mixture of commercially available metal powders (or master alloy powders), fine refractory oxides and reactive elements. Since the use of elemental mixes in the starting powder often leads to the formation of inclusions of incompletely processed raw materials, pre-alloyed master alloy powders are preferred [Elliott *et al.*, 1991]. The pre-alloyed master alloy also reduces oxidation of reactive additives and the newly alloyed powder. Fine refractory oxides such as yttria are sometimes added to provide dispersion strengthening to $0.9T_m$ [Arzt, 1988]. Reactive elements (Ti, Al) provide oxidation resistance in the final product. In nickel-base

alloys, Ti and Al also provide intermediate temperature strength by precipitation of the γ', $Ni_3(Al, Ti)$ [Gilman and Benjamin, 1983]. The powders are produced in high-energy attrition mills or special large-ball mills, consolidated by various combinations of hot–isostatic pressing and extrusion and finally heat–treated, either isothermally or in a temperature gradient to induce recrystallisation (Figure 1.1).

2.3.1 High-Energy Milling

Mechanical alloying makes possible the combination of dispersion, solid-solution and precipitation strengthening by mixing all the constituents in powder form ever more intimately until the formation of a true alloy powder leaving only the oxides dispersed in the solid solution [Gilman and Benjamin, 1983]. Mixing is achieved by dry high-energy ball milling, under conditions which cause fragmentation and welding together, a process prevented in conventional ball milling by the use of liquids and surfactants.

During mechanical alloying, the particles become trapped between the colliding balls producing intense plastic deformation and fracture. The ductile metal powders are flattened and where they overlap, the atomically clean surfaces just created weld together, building up layers of composite powders and the dispersoid. At the same time work hardened elemental or composite powders fracture. A qualitative description of these repeated fragmentation and coalescence processes by Gilman and Benjamin (1983) is shown in Figure 2.1. The legends in Fig. 2.1 indicate the events that might occur depending on the impact angle. High strain–rate fracture is favoured for normal impact. Other modes such as forging fracture and shear fracture occur at glancing angles. Direct seizure is a coalescence event favoured by normal impacts. At other impact angles, indirect seizure (i.e, seizure preceded by sliding deformation) would be a preferred coalescence mechanism.

These competing processes of cold welding and fracture occur repeatedly throughout the milling, gradually kneading the composites so that their structure is continually refined and homogenised. The processes from the initial stage to the completion are schematically illustrated in Figure 2.2. After the initial stage of milling the composite shows coarse layers of identifiable starting materials, with the

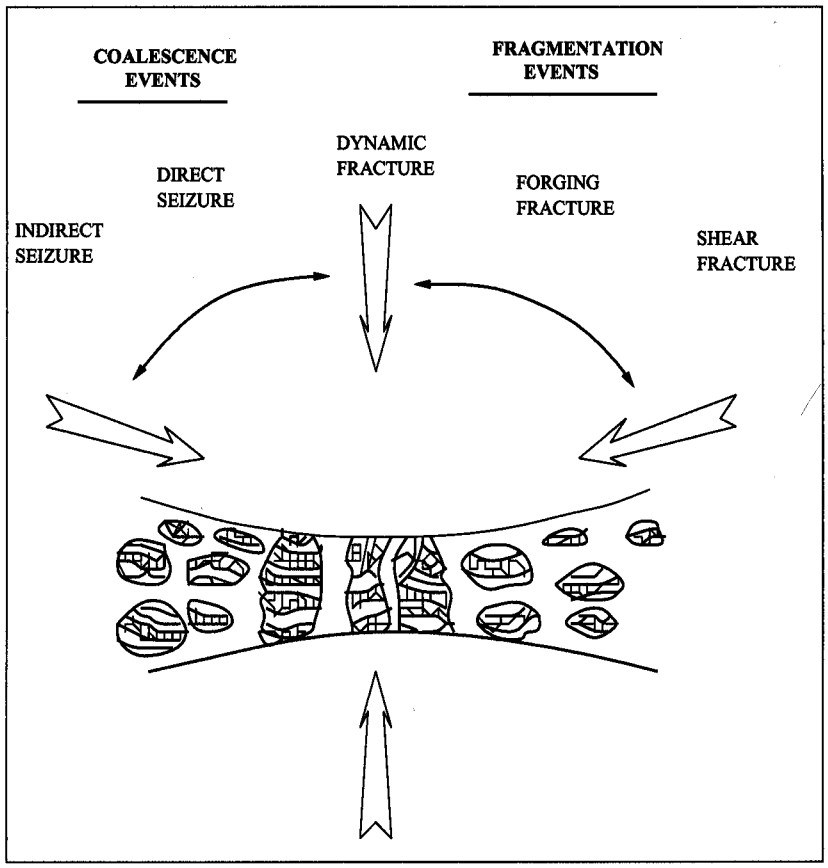

Figure 2.1 : Schematic illustration of the repeated fragmentation and coalescence processes in mechanical alloying [Gilman and Benjamin, 1983].

dispersoid closely spaced along the welds (Fig. 2.2a). After more refinement through fracture and welding, the composite develops a structure of convoluted lamellae of decreasing thickness between welded surfaces along which dispersoids are closely spaced (Fig. 2.2b). At this stage the average spacing of yttria dispersoids at the layer interfaces is similar to the average layer thickness resulting in an ideal random distribution of the oxide with an interparticle spacing of less than 0.5 μm [Hack, 1984]. The combination of severe cold-work and possible heating from the kinetic energy of balls aids diffusion and as diffusion distances decrease continually by the finer mixing of constituents, solute elements dissolve, areas of solid solution grow in composite powders and metastable phases may precipitate.

In the final stage of milling the lamellae become more convoluted and thin (Fig. 2.2c). The compositions of individual particles converge to the overall composition of the starting powder blend. Precipitation of

equilibrium phases may occur, work hardening and softening reaches a balance and the microhardness of the individual powder particles attains a saturation value of around 650 kg mm^{-2} for Fe–Cr alloys [Gilman and Benjamin, 1983]. Finally the lamellae are no longer resolvable optically and the distance between dispersoid particles along the weld interfaces, approximately equal to the spacing between the welds, (Fig. 2.2d). The composition of individual powder particles is then equivalent to that of the starting blend and mechanical alloying is said to be complete [Fleetwood, 1986].

The structures that develop during high energy ball milling of powders are dependent on the process variables and the nature of the powder components. These include the type and energy of the mill, the milling media, the milling temperature and atmosphere, the weight ratio of the powder to steel balls, the mechanical behaviour of the component powder mixtures and the chemistry and phase equilibra of the components [Koch, 1989].

The processing time for mechanical alloying depends upon the size and type of the mill used, the powder volume and the elastic constants of the powder [Courtney and Maurice, 1989]. It is not the number of ball/powder collisions but the energy absorbed per particle during a collision which controls the milling time [Aiken *et al.*, 1991]. Mechanical alloying processing times of 40 h or less are usually adequate for obtaining powder homogeneity [Benjamin, 1970].

To prevent uncontrolled oxidation of the metal powders, mechanical alloying is performed using inert process gas. Argon is the most popular gas [Kramer 1977] but some argon may become trapped during processing to precipitate later as very fine bubbles near the fine dispersoids [Jaeger and Jones, 1991, 1992b].

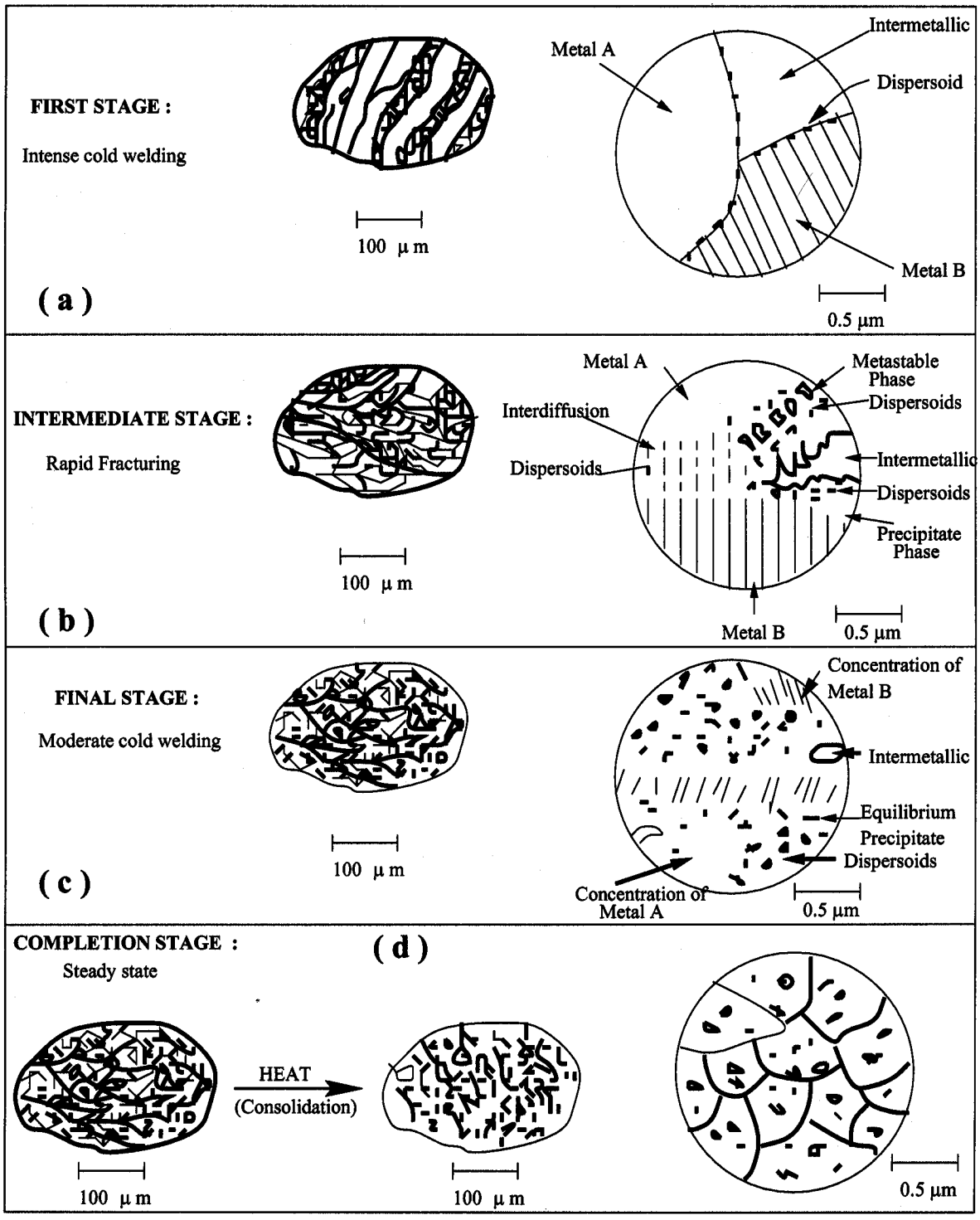

Figure 2.2 : Schematic illustration of the processes at different stages of mechanical alloying [Sundaresan and Froes, 1987].

2.3.2 Thermomechanical Processing

The presence of an oxide coating can inhibit metal powder from densifying on simple sintering [Gilman and Benjamin 1983] and the high hardness of mechanically alloyed powder prevents cold pressing. Therefore, the powder discharged from the mill has to be consolidated using high temperature and high pressure processes such as hot isostatic pressing (HIP), or heating in mild steel sealed cans followed by hot extrusion. The latter method is generally preferred as it is cheaper and able to produce anisotropic structures with good creep properties [Fleetwood, 1986].

The mild steel extrusion cans are filled from the 'alloy blend'. Cans of up to 280 mm diameter and 660 mm length are used, containing up to 170 kg of powder. Several hours of soaking in a furnace at the extrusion temperature is required to ensure that the centre of the powder mass is heated thoroughly. During this time inter–diffusion occurs which causes the highly strained composite powder particles to become chemically homogeneous with all the physical properties of a truly alloyed powder [Nutting *et al.*, 1981]. Extrusion is carried out in commercial 5000–6000 tonne presses at temperatures, reduction ratios and, speeds which are interdependent and which must be determined in conjunction with the subsequent hot-working parameters [Hack 1984]. After extrusion, the cans used for the consolidation are removed either by machining or by pickling, depending on the alloy and the product form.

The MA-ODS alloys in the as-extruded condition are usually too hard to use. They are therefore heat–treated, either isothermally or in a temperature gradient to induce recrystallisation. Recrystallization in MA–ODS alloys usually does not occur until temperatures close to melting are reached [Benjamin and Gilman, 1983; Gessinger, 1984; Hack, 1984]

2.4 Grain Morphology in MA–ODS Alloys

The major peculiar feature of the ODS mechanical alloys is that they tend to recrystallise into a highly anisotropic columnar grain structure. There are two reasons why such grain structures should

arise. Zone annealing, like directional solidification can encourage growth along the associated moving temperature gradient. Secondly, any dispersoids may tend to align along the extrusion direction, so that the Zener pinning force is smallest for growth parallel to the working direction, for both MA957 and MA956 [Chou and Bhadeshia, 1993].

For reasons which have never been explained, nickel–base alloys do not have a pronounced nonuniform distribution of dispersoids [Baloch and Bhadeshia, 1991]. Thus, MA6000, when isothermally annealed, often recrystallises into an equiaxed grain structure (there are batch–to–batch variations). The same alloy will recrystallise directionally when zone annealed. The sense of the columnar grains can be altered by changing the zone annealed direction; cross annealing (*i.e.* zone annealing in a direction normal to the extrusion direction) causes the growth of stubby columnar grains normal to the extrusion direction, confirming a more or less uniform dispersoid distribution. In addition, zone annealing at high speeds leads to a transition from a columnar to equiaxed recrystallised grains [Chou and Bhadeshia, 1993].

The nickel–base alloy MA760 has a response which is similar to that of MA6000, although the signs are that there is a stronger alignment of particles along the extrusion direction. Thus, isothermal annealing does not lead to equiaxed grains, but cross annealing can change the direction of the columnar recrystallised grains.

The mechanically alloyed steels contain a very pronounced alignment of particles along the extrusion direction [Baloch, 1989]. Isothermal heat–treatment of as–worked samples always leads to the development of coarse columnar grains. MA957, which has a rather low yttria content, has relatively stubby columnar grains following isothermal heat treatment. No amount of cross annealing or any other heat treatment has succeeded in causing a change in the direction of columnar grain growth, which is always parallel to the working direction. The importance of a nonuniform dispersion of particles in inducing the development of columnar grains has been emphasized in recent experiments where the introduction

of HfC or TiB_2 led to the formation of anisotropic grains during secondary recrystallisation of the NiAl intermetallic matrix [Jaeger and Jones, 1991].

The roughness of grain boundaries in recrystallised mechanically alloyed nickel–base superalloys and steels has been characterised in detail [Whittenberger, 1981; Jaeger and Jones, 1991; Murakami *et al.*, 1992]. The serrated boundaries arise because of transient pinning by dispersoids. Coarser and smoother boundaries occur when the stored energy is large, simply because it is then easier for the boundary to overcome the pinning force [Murakami *et al.*, 1992].

2.5 Preannealing Effects on the Recrystallization Behaviour of MA-ODS Alloys

Preannealing is a term used to describe a sample which has been heat treated at a temperature which is too low for recrystallisation, but high enough to induce significant changes in the stored energy, and in the subsequent microstructure following an elevated temperature recrystallisation heat treatment.

The effects of preannealing, at temperatures above that at which austenite can form, on MA957 can be summarised as follows [Chou and Bhadeshia, 1994]. A weak preannealing treatment (at about 1150 °C) has little or no effect on subsequent recrystallisation. As the preannealing time is increased, there is a transition from a coarse columnar grain structure to one which is equiaxed (20–40 μm) depending on the exact heat treatment). This is because the reduction in stored energy reduces grain boundary mobility, so that nucleation has an opportunity to develop in several regions of the sample, giving an equiaxed grain structure.

Continued preannealing causes the development of a bimodal equiaxed grain structure. This is because there is an inhomogeneous distribution of pinning particles in the alloy. The now substantial reduction in stored energy due to preannealing, retards recrystallisation more in some regions compared with others which are less strongly pinned. For MA957 the preannealing time at 1150 °C is in excess of 160 hours for this condition to be reached [Bhadeshia, 1997].

Further preannealing leads to such a large reduction in the stored energy that subsequent recrystallisation is suppressed.

It is much more difficult to control the grain structure of MA956 using preannealing heat treatments. Grain refinement certainly occurs, as in MA957, but the fine grains tend not to be equiaxed. This may be because MA956 contains a larger concentration of yttria. The anisotropic pinning due to the inhomogeneous distribution of the oxide particles is more difficult to overcome if the fraction of particles is large. It would be very interesting to test this with MA956 containing a smaller quantity of yttria dispersoids.

2.6 Initial Microstructures

Immediately after the mechanical alloying process, the powders are canned and extruded/hot–rolled to produce the appropriate bulk forms. During heating for either extrusion or rolling, the canned mechanically alloyed powders may recrystallise to a sub–micron grain size which is representative of the grain structure found immediately after consolidation. These incredibly fine grain sizes are a consequence of the strains imparted on the powders during the mechanical alloying process, true strains of the order of 9 (equivalent to stretching a unit length by a factor of 8000). The subsequent consolidation by comparison involves minor degrees of deformation, but much higher bulk temperatures (around 1000 °C). It is known that during the course of consolidation, the material may dynamically recrystallise several times. It should be emphsized that the sub–micron grains referred to above are true grains with large relative misorientations, not simply dislocation cell structures generated by deformation [Bhadeshia, 1997].

Nevertheless, the iron–base alloys immediately after consolidation have a cold–deformed microstructure in which the ultra–fine grains are elongated along the working direction and contain other classic features of cold work, *i.e.* the high dislocation density and a generally convoluted microstructure. The dislocation density has been measured for DT2203Y05 to be about 10^{15} m^{-2} [Little *et al.*, 1991]; although this is

large, it is not particularly high when compared with dislocation densities found in conventional steel martensitic microstructures . Subsequent heat–treatment leads to primary recrystallisation into a very coarse grained microstructure .

The nickel–base superalloys also have an ultra–fine grained microstructure, but one which is the product of primary recrystallisation . The sub–micrometer grains are therefore equiaxed, contain undistorted annealing twins and a clean microstructure. Subsequent heat treatment therefore leads to secondary recrystallisation driven by the grain boundary energy of the fine grained primary recrystallised state. It is not clear why the nickel base alloys are in a primary recrystallised state following extrusion/hot–rolling, whereas the iron–base alloys, which are fabricated under identical conditions, have a cold deformed microstructure.

Irrespective of whether the alloys have a primary or secondary recrystallised microstructure, the ultra–fine grains obtained after recrystallisation make the alloys very hard (Table 2.1) and for most applications unusable without heat treatment which leads to an enormous coarsening of the microstructure with a reduction in the amount of grain surface per unit volume by 2–3 orders of magnitude. The details of recrystallisation are discussed in the next section.

Table 2.1: Typical Vicker's Hardness data before and after recrystallisation into a coarse grained microstructure [Bhadeshia, 1997].

Alloy	HV, Before Recrystallisation	HV, After Recrystallisation
MA957	400–410	230–240
MA956	350–390	225–245
MA956 Sheet	410	250
MA6000	645	500–520
MA760	720–790	500–515
MA758	405	214

The excess energy stored in the mechanically alloyed and consolidated materials described in Table 2.1 is primarily in the form of grain surfaces and to a lesser extent due to dislocations and other high–entropy defects.

Extrusion/rolling leads to an alignment of dispersoid particles along the working direction, the degree of alignment being pronounced in the case of the iron–base alloys. This alignment reflects inhomogeneities in the fabrication process arising at the single particle level and below. Thus, the iron–base alloys almost always tend to recrystallise into a columnar grained microstructure, with the principal growth direction being parallel to the extrusion direction, irrespective of whether the sample is zone annealed, cross annealed or isothermally treated (cross annealing is zone annealing along a direction normal to the extrusion direction). For reasons which are not clear, the anisotropy in particle dispersion is much less for the nickel base superalloys, in which the direction of columnar grain growth can often be controlled by the sense of the temperature gradient during zone annealing. Indeed, equiaxed coarse grained secondary recrystallised microstructures can be readily generated either by isothermal annealing or by zone annealing at high speeds [Baloch and Bhadeshia, 1991].

2.7 The Dispersoids and Precipitates

Fine yttria particles ($\simeq$ 10 nm) are incorporated into the metallic matrix as a consequence of the ball milling operations. Most of these survive as yttrium oxide in spite of consolidation by extrusion and rolling at about 1050 °C. However, heat–treatment causes these particles to react with dissolved aluminium (or titanium) and oxygen to produce a variety of compounds [Krautwasser *et al.*, 1994; Murakami, 1993; Schaffer *et al.*, 1989; Cama and Hughes, 1993]. The possible combinations of yttria and alumina include those listed in Table 2.2.

The alumina particles tend to be some 500 nm in size, the titanium carbonitrides about 100–200 nm in size [Regle, 1994], and both have a much smaller number density than the original yttria particles. Hence, the reaction does not lead to a significant coarsening of the size distribution or inter–particle

Table 2.2: Yttrium–Aluminium–Oxygen compounds reported to occur in mechanically alloyed ODS iron and nickel base alloys.

$3Y_2O_3.5Al_2O_3$	YAG	yttrium aluminium garnet
$Y_2O_3.Al_2O_3$	YAH	yttrium aluminium hexagonal
$2Y_2O_3.Al_2O_3$	YAM	yttrium aluminium monoclinic
$Y_2O_3.Al_2O_3$	YAP	yttrium aluminium perovskite
$Y_2O_3.Al_2O_3$	YAP'	yttrium aluminium pseudo–perovskite
$3Y_2O_3.5Al_2O_3$	YAT	yttrium aluminite tetragonal

spacing. Even extremely severe heat–treatment (72 hours at 1400 °C) has little effect on the yttrium containing particles [Murakami, 1993]. Typical changes in the size of the finer particles are illustrated in Figure 2.3, which represents data for samples annealed for 110 h at the temperatures indicated, for samples of PM2010 [Krautwasser *et al.*, 1994]. Note that these data do not represent coarsening driven by interface energy minimisation, but complicated effects originating in the reactions between the yttria, aluminium and oxygen. Thus, the volume fraction is not constant during heat treatment. The volume fraction of the smaller reactive particles increases, whereas any large alumina particles tend to dissolve as the aluminium reacts with the yttria [Krautwasser *et al.*, 1994].

In the extruded condition, 80 % of the particles in both MA956 and MA957 are less than 15 nm in size, with those in MA956 being much smaller [Regle, 1994]. Nevertheless, the mean particle diameters are quite similar at 11.7 and 11.4 nm for MA957 and MA956 respectively [Regle, 1994], presumably because the fraction of particles is larger in the latter. Some typical particle sizes for the fine particles are presented in Table 2.3.

Table 2.3: Some particle characteristics, with the alloys in the unrecrsytallised "as–received" condition.

Alloy	Mean Particle Size / nm	Reference
MA957	12	Regle (1994)
MA956	12	Regle (1994)
PM2010	15	Krautwasser *et al.* (1994)

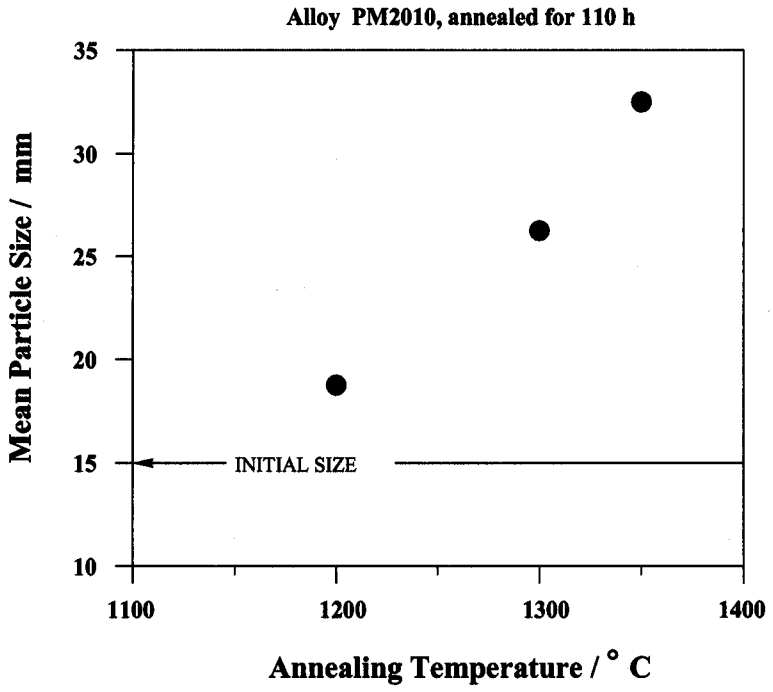

Figure 2.3 : Changes in particle size due to annealing, of alloy PM2010, for 110 h at each of the temperatures indicated. Data from Krautwasser *et al.*, (1994)

Almost all the mechanical alloys contain alumina particles introduced accidentally or as a consequence of internal oxidation during mechanical alloying (alumina is deliberately added to ODM751 at the mechanical alloying stage). These particles are also stable, but are too coarse and few to cause significant Zener pinning. Titanium containing mechanical alloys such as MA957 and MA6000 also contain titanium–rich particles whose exact character is not known; they may be oxides or carbo–nitrides.

The coarsest precipitates, which are not very stable, are the $M_{23}C_6$ particles which are visible optically, and dissolve (at around 1000 °C) during heating to the recrystallisation temperature only to reprecipitate during slow cooling to ambient temperature. These carbides are found in the nickel–base superalloys and not in the iron–base alloys which contain very low carbon concentrations.

To summarise, the yttrium based dispersoids are extremely stable in spite of some reaction with aluminium and oxygen to form garnets. The other particles are likely to be of little consequence to both

the recrystallisation process and the creep resistance of the alloys.

The mechanism by which the fine yttrium containing particles enhance the creep resistance has been studied both for the mechanically alloyed nickel–base superalloys and the steels [Nardone and Tien, 1983; Herrick *et al.*, 1988; Schroder and Arzt, 1985; Preston *et al.*, 1991]. The creep resistance arises from the fact that dislocations have to climb over the hard obstacles. For steels, the consequent improvement in creep resistance allows alloys such as DT2203Y05 to be used at a service temperature of 975 K compared with that for conventional ferritic stainless steels whose maximum service temperature is about 925 K.

For the steels, there is some evidence that the oxide particles and the intermetallic compounds which precipitate in some alloys, inhibit the migration of boundaries [Evans *et al.*, 1992].

2.8 Defects in Mechanically Alloyed Superalloys

Alloys produced by mechanical alloying always exhibit processing defects which include macro- and micro-porosity and inclusion particles. In addition, a peculiar defect called 'intrusion' has also been observed in MA alloys. Fine grains which result from incomplete recrystallization and particle denuded bands due to inadequate milling are also reported in MA ferritic ODS alloys. These defects are discussed below.

2.8.1 Macroporosity

All materials made by conventional powder metallurgy (PM) routes can contain coarse residual porosity usually situated at grain boundaries. Such pores are large and easily seen. Since MA products are subjected to a high level of mechanical working such macropores are unlikely to be retained but form subsequently due to the precipitation of dissolved gases.

2.8.2 Microporosity

During mechanical alloying, the fracture process exposes clean, fresh and rough surfaces which can adsorb gases. These gases, can become trapped between powder particles during welding and then be retained in solid solution. Jaeger and Jones (1991, 1992b) have reported micropores (between 0.1–0.2 mm) containing argon gas around second phase particles in ODM331 bar and tubes. According to Jaeger and Jones (1992b), the association of argon with particles can be due to the release of argon from high-angle grain boundaries that become pinned at particles while migrating during secondary recrystallization.

2.8.3 Intrusion Defects

These are defects observed only in MA-ODS alloys [Cama, 1994]. They are equiaxed and filled with material of matrix composition similar to that in the micro-wrought pre-consolidated powders [Zeizinger and Arzt, 1988; Weisbrodt *et al.*, 1990; Jaeger and Jones, 1991]. The defects are surrounded by discontinuous layers of "debris" in the form of Al-, Y- and Ti-rich particles and their bonding with the surrounding matrix is weak [Korb, 1988]. Intrusion defects pin grain boundaries and hence hinder recrystallization [Jaeger and Jones, 1992b]. They also hamper transverse grain growth [Cairns *et al.*, 1975, Jongenburger and Singer, 1988]. Intrusion defects can be minimized by using clean raw materials and master alloys, avoiding contamination during powder handling, controlling milling parameters and by monitoring the mechanical alloying process very carefully to eliminate any under processed particles [Schneider and Dannhauser, 1991].

2.8.4 Bands of Fine Grains

In many MA superalloys, recrystallization may not reach completion, leaving elongated regions of fine-grained materials [Cairns *et al.*, 1975]. These regions can reduce creep performance [Zeizinger and Arzt, 1988; Jaeger and Jones, 1992b]. The defects have been observed in MA ferritic alloys and ODM751 [Jaeger and Jones, 1992b] and in nickel-base MA6000 [Arzt, 1988; Weisbrodt *et al.*,

1990]. Randomly distributed fine grains (length about 1 mm), depleted of dispersoids have also been recently reported in an experimental iron-base ODS alloy DYAL (with nominal composition : 13Cr–3Al–1.5Mo–0.6Ti–0.5Y_2O_3) similar to ODM751 [Kehagias *et al.*, 1993].

2.8.5 Particle Denuded Bands

Particle-denuded bands are a consequence of inadequate milling due to "dead zones" in the mills used for mechanical alloying. Jaeger and Jones (1992b) have reported dispersoid-free zones in ferritic MA–ODS alloys, ODM331 and ODS751. Kehagias *et al.*, (1993) also reported similar particle denuded bands (of width approx. 2 mm) in an experimental ferritic ODS alloy DYAL. These regions are weak and can act as centres for strain localisation during deformation [Jaeger and Jones, 1992b].

2.9 Strengthening in ODS Alloys

Strengthening in ODS alloys is achieved by dispersoid particles acting as barriers to dislocation motion during deformation and as a result increasing the load required to tear away a dislocation or bulge it through an array of particles. Here the strengthening can be described by the various mechanisms by which dislocations interact with or by-pass the obstacles. For optimum dispersion strengthening, distributing a given volume fraction of dispersoids more finely is more effective than increasing the volume fraction [Benn and Mirchandani, 1988; Rosler and Arzt,1990]. The ability of dispersoid phases to impede dislocation motion at elevated temperatures has also been related empirically to their free energies of formation, $-\Delta G_f$ [Benn and Mirchandani, 1988]. Refractory oxides such as zirconia, alumina and yttria (stability in increasing that order) have $-\Delta G_f$ values several fold higher than γ' or metal carbides and thus offer more stable configurations [Lawn *et al.*, 1976; Lupis, 1983; and Elliott, 1991].

In addition to acting as barriers to dislocation motions, particles also exert a retarding force on migrating grain boundaries. The retarding force per unit area, F_r, is according to Zener, (1948), given by:

$$F_r \simeq \frac{3f\gamma_{gb}}{2r} \tag{2.1}$$

where f is the volume fraction of particles of uniform radius r and γ_{gb} is the grain boundary energy per unit area [Martin and Doherty, 1980]. Hence, for a given volume fraction of particles, the smaller particles offer a greater hindrance to the migrating grain boundary compared to that offered by the larger particles.

2.9.1 Dislocation–Particle Interactions

There are several ways in which fine particles can act as barriers to dislocations. They can act as strong impenetrable particles through which the dislocations can move only by sharp changes in curvature of the dislocation line. On the other hand, they can act as coherent particles through which dislocations can pass, but only at stress levels much above those required to move dislocations through the matrix phase. There are four essential ways by which dislocations overcome particles that are present on their slip planes:

(i) Orowan bowing;

(ii) cross-slip;

(iii) climb over particles;

(iv) particle shearing.

Dislocation bowing and cross–slip occur for $T < 0.5T_m$, where T is the absolute temperature of deformation and T_m is the melting point. According to Orowan (1946), when a dislocation encounters two particles on its glide plane, it expands in the region between them until the segments on either side of the particle meet and form a dislocation loop around the particle. Dislocations may not always be confined to their slip planes during the bowing out process since cross-slip can occur. When by-pass is complete, residual loops remain associated with the particle [Wilcox and Clauer, 1972a]. According

to Ashby (1969), the initial flow stress of dispersion strengthened crystals is most probably controlled by Orowan by-passing rather than cross slip. The situation may be more favourable for cross slip to occur if Orowan loops are left first or if misfits strains around the particles exist which might be developed during cooling from high temperature owing to differences in thermal contraction [Singer and Gessinger, 1984]. Cross slip becomes more difficult as the stacking-fault energy is decreased. This is because of the additional force which is required to constrict a more widely split dislocation before cross slip can occur [Singer and Gessinger, 1984]. Chrumium additions decrease the stacking-fault energy in Ni-Cr alloys [Beeston and France, 1968]. Thus cross slip is expected to be unlikely in alloys with high chromium concentrations.

High temperatures enable dislocations to overcome the oxide particles by thermally activated climb, while at low temperatures where diffusion is slow, dislocation by-pass is assumed to occur by Orowan looping. If the spacing of the particles is small, then the applied stresses cannot bend the dislocation to a radius comparable to the particle spacing and the dislocations shear the particle. Also if a dislocation bows around a particle, especially a soft one, it is possible that the particle will be sheared as an alternative [Wilcox and Clauer, 1972b].

In dispersion strengthened alloys the overall material strength has contributions from both the matrix grain structure and the second phase dispersion.

2.9.2 Matrix Strengthening

In polycrystalline materials grain refinement represents a very useful and economical method of improving both the strength and fracture resistance. At low temperatures, the yield strength, σ_y, of a material is related to its grain size, d, by an empirical expression originally proposed by Hall (1951) and greatly extended by Petch (1953). The expression, which is known as Hall-Petch equation, has the form given as :

$$\sigma_y = \sigma_i + k_o d^{1/2} \tag{2.2}$$

where σ_i is the "lattice friction stress" which is temperature dependent and represents the overall resistance of the crystal lattice to dislocation movement, and k_o is the "locking parameter", a constant which is independent of temperature, composition and strain rate and reflects the difficulty in spreading slip across the grain boundaries. k_o measures the relative hardening contribution of the grain boundaries.

2.9.3 Dispersoid Strengthening

The strengthening from dispersoids comes from the need to move the dislocations past the particles. The resolved shear stress (τ_p) required for dislocation by-pass according to the Orowan (1946) model is

$$\tau_p = \frac{K'Gb}{\Lambda} \tag{2.3}$$

where G is the shear modulus of the matrix, b is the magnitude Burgers vector of the dislocation, Λ is the interparticle spacing and K' is a numerical constant. Ashby (1966) modified the Orowan model to take account of the interaction between neighbouring dislocations which had bowed, the line energy of the dislocations and the interparticle spacing. His model resulted in a reduction of the applied stress required for by-passing to occur.

$$\tau_p = \frac{K''Gb}{\Lambda} \ln\left(\frac{\bar{x}}{2b}\right) \simeq k'''\Delta\sigma_y \tag{2.4}$$

where $\bar{x}$ is the average diameter of the circle of intersection between the particle and the slip plane, $\Delta\sigma_y$ is the increase in the tensile stress for dispersion–strengthened alloys with uniform spherical particles and K''' is a constant.

Assuming that hardness H is proportional to the yield strength, it follows that

$$H = H_m + k_p d^{-1/2} \tag{2.5}$$

where H_m is the hardness of the matrix and k_p is another constant [Ashby and Jones, 1980]. For a fixed volume fraction of dispersed particles, the hardness should increase with decreasing particle diameter and for a fixed particle size, the hardness should increase with increasing volume fraction

of dispersoids. Therefore strengthening is increased if the volume fraction of dispersoids is high, the particles are fine, the particle distribution uniform and for high temperature applications, the particles inert [Tien and Purushothaman, 1976].

2.10 Effects of Grain Shape and Particle Distribution on the Creep Properties of MA–ODS Alloys

The grain structure developed in MA–ODS alloys depends strongly on the thermomechanical processing history. Either grain structures which have micron or submicron scale grain size, or very coarse secondary recrystallized grain structures with high GAR can be produced. A high aspect ratio grain structure can be produced over quite short distances in a sufficiently steep stationary temperature gradient. Alternatively, extremely high aspect ratio structures can be developed a length of 1 m or more by the application of a moving hot zone annealing technique [Cairns, *et al.*, 1975; Benn *et al.*, 1981].

The development of high GAR structure in ODS materials can also be influenced by the range of inert particles present in the alloy; these particles may be strengthening or non-strengthening depending on their size. Incorporation of a dispersion strengthening phase can improve the elevated temperature performance of alloys. However, the improvement in strength can depend strongly on the size, distribution and type of particle present.

2.10.1 Effect of Grain Aspect Ratio (GAR)

The good high-temperature properties of ODS superalloys correlate directly with their coarse elongated grain structures [Wilcox and Clauer, 1972; Benjamin and Bomford, 1974]. The grain aspect ratio (GAR) of a material is the average length to breadth ratio of the grains. Wilcox and Clauer (1972) found that the creep and yield strength at 1093 °C in nickel based thoria dispersion strengthened alloys increased linearly with increasing GAR. Similarly, as illustrated in Figure 2.4, Benjamin and Bomford, (1974) reported that elevated temperature mechanical properties of an experimental MA753 are proportional

to the grain aspect ratio up to about 6:1. In practice, a minimum grain aspect ratio of 8:1 is normally considered acceptable [Hack, 1984].

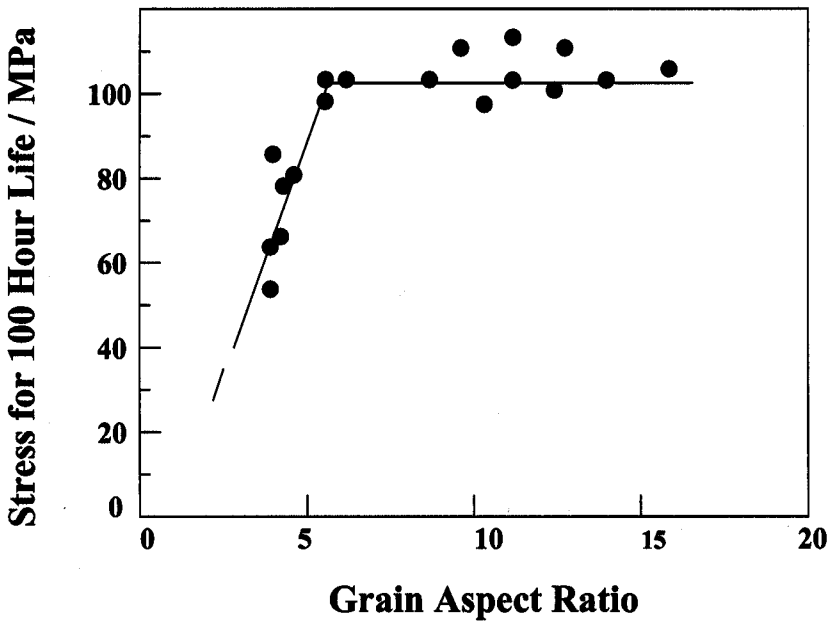

Figure 2.4 : Relationship between 100 hrs life at 1038 $^{\circ}C$ and grain-aspect ratio in experimental INCOLOY alloy MA753 [Benjamin and Bomford, 1974].

A high GAR can in principle improve the creep properties in the following ways:

(i) inhibition of creep damage accumulation;

(ii) retardation of diffusional creep;

(iii) retardation of grain boundary sliding.

Wilcox and Clauer (1972) suggested that the increased creep and yield strength with increasing GAR in thoria dispersion strengthened nickel based alloys was due to retardation of grain boundary sliding.

Reducing grain boundary sliding through the control of GAR has been postulated as the reason for the improved creep strength observed by Arzt (1984) in tests on MA 6000. Arzt tested materials with different GAR ranging from 4 to 60 at 950 °C and showed that the time to rupture showed a pronounced

dependence on the GAR. Below a value of 15, fracture was mainly intergranular, whereas at higher values of GAR rupture times became less sensitive to GAR, and failure was mainly transgranular. It was suggested that at values of low GAR grains readily slide past each other and intergranular fracture by cavity growth can occur unimpeded. As the GAR increases, sliding is impeded and cavity growth is retarded. Arzt (1984) suggested that a threshold stress exists below which sliding does not take place. A threshold stress of 6 MPa was given for the MA6000 tested.

Other work on MA6000 by Zeizinger and Arzt (1988) revealed that the transition between intergranular and transgranular failure was at a GAR of about 18, showing good agreement with that found by Arzt (1984). However, experiments to determine the cavity growth accommodation mechanism revealed that, contrary to the above, grain boundary sliding did not control creep damage accumulation. In fact, a mechanism based on dislocation creep was suggested to be rate-controlling. The authors proceeded to develop a model for time to fracture as a function of GAR in which the decisive parameter for creep accommodation necessary for cavity growth was the GAR. In the derivation of the model they assumed no grain boundary sliding, and that damage accumulation was by dislocation creep. From this it seems that the main parameter determining accommodation of damage should be one based upon inhibition of dislocation movement rather than one based on GAR. Nevertheless, the model agrees well with experimental observations by Zeizinger and Arzt (1988) and by Wilcox and Clauer (1972).

As the GAR of a material increases, the shear stresses on longitudinal grain boundaries are reduced and accommodation by grain boundary sliding becomes more difficult. However, high GAR is not the only factor to play a significant role in preventing sliding. Grain boundary particles can inhibit the movement of grain boundary dislocations and may be poor sources and sinks for vacancies. As grain boundary sliding takes place by movement of grain boundary dislocations then grain boundary particles will restrict dislocation movement and inhibit sliding.

The capacity of grain boundaries to slide may also be influenced by the level of texture developed

within the alloy. Sellars and Petkovic-Luton (1980), found that the degree of crystallographic texture increased with GAR. So these may not be independent parameters. Lund and Nix (1976) identified that an increased degree of texture leads to a prevalence of grain boundaries of low misorientation. These low misorientations or low angle boundaries could be less favourable sources and sinks for vacancies than more general high angle boundaries. Low angle boundaries are also less likely to undergo grain boundary sliding. Zeizinger and Arzt (1988) have further suggested that it is not the grain aspect ratio which determines the accommodation of damage but rather the interlocking between individual grains. This increases with the GAR. It is difficult however, to see how the serrated nature of the grain boundary is directly related to the GAR which is governed by a combination of the level of prior deformation, loading and the size and distribution of second phase particles. For example, work by Sellars and Petkovic-Luton (1980) showed that, with increasing GAR, the grain boundaries tend to lie preferentially along stringers of high oxide content. It is most likely that the particles will play the dominating role in determining the level of grain boundary serration and not the GAR.

2.10.2 Effect of Second Phase Particles

The presence of a uniform dispersion of fine inert particles provides an effective barrier to dislocation movement in ODS materials. Thorium oxide (ThO_2) was selected as the dispersoid phase for early alloys but yttria gives a better distribution during mechanical alloying and unlike thoria is not radioactive.

It might be assumed that an increase in the yttria content should lead to a corresponding increase in the creep resistance. This must be the case as the concentration is increased from zero, but recent work [Krautwasser *et al.*, 1994] indicates that there may be an optimum concentration of yttria. In a series of experiments carried out on alloys PM2000 and PM2010, which differ only in the yttria content (0.5, 1.0 wt.% respectively), it was found that the higher quantity in PM2010 does not lead to a significantly larger number density of fine dispersoids (< 100 nm). It was predicted therefore that PM2010 should not have a higher creep strength than PM2000 [Krautwasser *et al.*, 1994]. This result remains to be verified.

The volume fraction and size of particles chosen can vary from alloy to alloy and from one product to another. Typical concentrations (wt.%) and particle sizes of Y_2O_3 in a number of ODS alloys are given below in Table 2.4.

Table 2.4 : Size and wt.% of dispersoid in MA–ODS alloys.

Alloy	Product form	Y_2O_3 (wt.%)	Y_2O_3 (size, nm)	Reference
MA956	Sheet	1.2	250	Whittenberger (1978)
MA956	Bar	0.58	30	Haghi (1990)
MA754	Bar	1.3	5-100	Howson (1980)
MA6000	Bar	2.5	100	Zeizinger (1988)

In addition to the strengthening phase, MA–ODS alloys usually contain distributions of other, coarser dispersoids, which have either been carried through to the final product as part of the processing route or have been precipitated during processing. Examples of these coarser dispersoids are given below in Table 2.5. The size and volume fraction of fine dispersoid can affect the evolution of microstructure and the elevated temperature strength of ODS alloys. Benjamin and Bomford (1974) examined the effect of dispersoid volume fraction in a Y_2O_3 strengthened, nickel-base superalloy. The volume fraction of dispersoid added ranged from 0 to 0.045 while the size ranged from 15–58 nm. The combination of high volume fraction and small particle size produced an alloy with a low GAR and poor stress rupture properties at both 1038 °C and 760 °C. Apart from this, the stress rupture strengths at 760 °C were insensitive to variations in particle size and volume fraction. However, the dispersoid greatly affected the GAR [Benjamin and Bomford, 1974]. This in turn, influenced the rupture properties. For GAR less than 6 the 1038 °C ruptured strength was controlled by GAR while at higher GAR it was found to be controlled by a dispersoid parameter ratio f/f_a, where f is the volume fraction and f_a is the volume

Table 2.5 : Typical coarse oxides found in MA–ODS alloys.

Alloy	Product form	Dispersoid type	wt.%	Size (nm)	Reference
MA956	Sheet	$Spinel + Cr_2O_3$ $Cr_2O_3 + Y_2O_3$	2.0	450	Whittenberger *et al.*, (1978)
PM2000	Bar	Al_2O_3 $Al_2O_3 + Y_2O_3$	0.80	360	Jaeger (1994)
MA754	Bar	$Ti(CN)Al_2O_3$ $Y_2O_3Al_2O_3$	-	100-900	Howson *et al.*, (1980)
ODM751	Tube	$Ti(CN)Al_2O_3$ $Y_2O_3Al_2O_3$	0.6	300	Jaeger (1994)

average of the oxide particle size.

2.11 Threshold Creep Stress in MA–ODS Alloys

The elevated temperature deformation behaviour of ODS alloys is characterized by a threshold stress below which the creep rate is negligible. Whittenberger (1977) observed threshold stresses of around 53 MPa for thoria dispersion strengthened nickel and thoria dispersion strengthened NiCrAl tested at 1100 °C. He also observed that for MA754, the threshold stress was dependent on the GAR with the threshold value of 72 MPa for materials with a GAR of 3.5 tested parallel to the extrusion direction and 17 MPa when tested in the long transverse direction where the GAR was < 1. Petkovic-Luton *et al.* (1983) also found a threshold stress of around 70 MPa in single crystal MA956 tested between 1050 and 1150 °C while Haghi and Anand (1990), ascribed a threshold stress of 31 MPa to MA956 tested at 900 °C.

The existence of a threshold stress has been attributed to a number of mechanisms including :

(i) repulsive dislocation-particle interactions;

(ii) dislocation-particle interactions involving localized climb;

(iii) attractive dislocation-particle interactions.

The repulsive dislocation-particle interaction mechanism involves dislocations either looping the particles, as in the Orowan mechanism described previously, or by dislocation climb. In each case the threshold stress is the stress required for dislocation by-pass.

Evidence for Orowan dislocation interactions has been observed by Haghi and Anand (1990), who found dislocation loops around yttrium oxide dispersoids in MA956 tested at 1000 °C. However, they also found that the measured threshold stress was only about half the calculated Orowan stress. They concluded that the threshold stress is due to a combination of repulsive and attractive dislocation particle interactions. Further work by Petkovic-Luton *et al.* (1983) on the same material found no evidence of dislocation loops or debris expected from an Orowan mechanism.

It would appear, therefore, that the Orowan stress cannot be identified with the values of threshold stress found in ODS alloy system. This has led to the development of models based on processes by which dislocations can cirumvent particles, especially by climb. One such process proposed by Brown and Ham (1971) assumed that dislocation climb is local, *i.e.,* is confined to the portion of the dislocation close to the particle/matrix interface. This segment undergoes climb while the remaining dislocation line stays in the glide plane. Climb by-pass of dispersoid particles leads to an overall increase in dislocation line length. The increase in line length necessary to surmount the particle needs an increase in energy and this is provided by the applied stress. A threshold stress must be exceeded before the energy requirements are achieved and localized climb occurs. Arzt and Wilkinson (1986), however, suggested that the sharp dislocation curvature necessary for localized climb cannot be sustained at the point of dislocation–particle contact as it would rapidly relax by diffusion, leading to more general climb. A threshold stress would still exist from the general climb of dislocations but this has been estimated by Shewfelt and Brown (1977) and Arzt and Ashby (1982) as less than 10 % of the Orowan stress.

2.12 Elevated–Temperature Failure in ODS Alloys

The failure mode in ODS materials operating at elevated temperatures depends on a number of parameters such as the operating temperature, strain rate and microstructure. Whereas a fine grained ODS alloy may show superplasticity, the same alloy tested under identical conditions but in coarse grained secondary recrystallized condition is likely to fail by cavity formation. For example, Wiegert and Henricks (1980) tested secondary recrystallized MA 956 and a developmental iron-base alloy HDA8077, and found that a critical strain rate of 5×10^{-3} min^{-1} existed above which the materials had high ductility and failure was by microvoid coalescence. However, below the critical strain rate the material failed intergranularly, through cavity linkage, with low ductility.

There is a large body of evidence to indicate that under typical creep and stress rupture conditions, failure of ODS alloys, in the secondary recrystallized condition, is governed largely by the ease with which creep cavities nucleate, grow and eventually coalesce. For example, Howson *et al.* (1980) showed that MA754 failed by intergranular cavitation at grain boundaries transverse to the applied stress when creep tested in the temperature range 760–1093 °C. Zeizinger and Arzt, (1988) showed that when creep testing MA6000 at 850 and 950 °C the developing fracture modes changed from mainly transgranular to intergranular when the grain aspect ratio was greater than 18 with both failure mechanisms strongly influenced by cavity formation. Failure by cavity formation has also been observed in iron-base ODS materials by Wiegert and Henricks (1980) who tested MA956 bar at 1093 °C at a strain rate of between 10–9 and 10–5 min^{-1} and by Whittenberger (1978) and (1979) who creep tested MA956 sheet and bar at 1100 °C.

2.12.1 Creep Cavity Nucleation

Nucleation of a cavity always occurs where deformation is inhomogeneous [Goods and Brown, 1979]. In non-particle hardened systems this takes place at the grain boundary triple points, grain boundary irregularities or blocked slip bands. Homogeneous cavity nucleation by vacancy accumulation is

considered improbable at high temperatures as the vacancy supersaturation necessary to form the void would probably not be achieved during deformation [Balluffi and Seigle, 1955]. Nix (1982) has indicated that even if diffusion processes were not a factor in limiting supersaturation, normal stresses in excess of yield strength of YS/100 GPa, would be necessary to provide sufficient supersaturation to nucleate a void. These stresses can not be achieved by the applied stresses alone.

In ODS materials cavity nucleation is associated with dispersoids. Goods and Brown (1979) have suggested that nucleation can take by mechanical decohesion between the particles and the matrix. This mechanism is favoured by most researchers such as Harris, (1965), Rukwied (1973) and Fleck *et al.* (1975). It involves the particle behaving as a discontinuity in the boundary plane and acting as a stress concentrator in the event of grain boundary sliding. Cavitation results either from rupture of the particle or the particle/matrix interface.

Creep cavity nucleation may also occur through intense thermomechanical processing. For example, Pilling and Ridley (1988) suggested that the association of cavities with particles in the superplastic materials can be related to pre-existing defects such as regions of particle/interface decohesion. These are believed to have developed during the intense thermomechanical processing applied to a material in order to produce the fine grain sub–grain superplastic microstructure.

2.12.2 Cavity Growth

A cavity whether pre-existing or nucleated by vacancy condensation at a particle/matrix interface or by plastic flow of the matrix, can grow by a number of mechanisms. If grain boundary sliding is the mechanism for cavity nucleation, it seems reasonable that continued sliding should lead to continued cavity growth. The evidence, however, does not wholly support this, since cavities often appear to be reasonably uniform in size across a grain boundary facet whereas the sliding displacements are usually non-uniform [Evans and Wilshire, 1985].

Although it is unlikely that vacancy diffusion alone can nucleate cavities at high temperatures, diffusion

produces cavity growth. Figure 2.5 shows schematically the mechanisms which can cause cavity growth at high temperatures. These are: diffusion-controlled (a and b); and dislocation creep-controlled (c) [Arzt, 1984]. Growth by diffusion is stress directed with the tensile stress component governing the diffusion process. Where boundary diffusion alone controls growth (Fig. 2.6a) matter diffuses out of the growing void and deposits onto the grain boundary. The void is assumed to maintain its spherical shape during growth because surface diffusion is generally fast compared to grain boundary diffusion. This assumption may not be wholly justified under conditions where void growth is controlled by surface diffusion (Fig. 2.6b). When surface diffusion is slow, the void ceases to grow as a sphere. Matter from the cavity tip diffuses into the boundary at a rate which is faster than can be replaced by diffusion from other parts of the cavity surface. The void then becomes flatter and more crack-like.

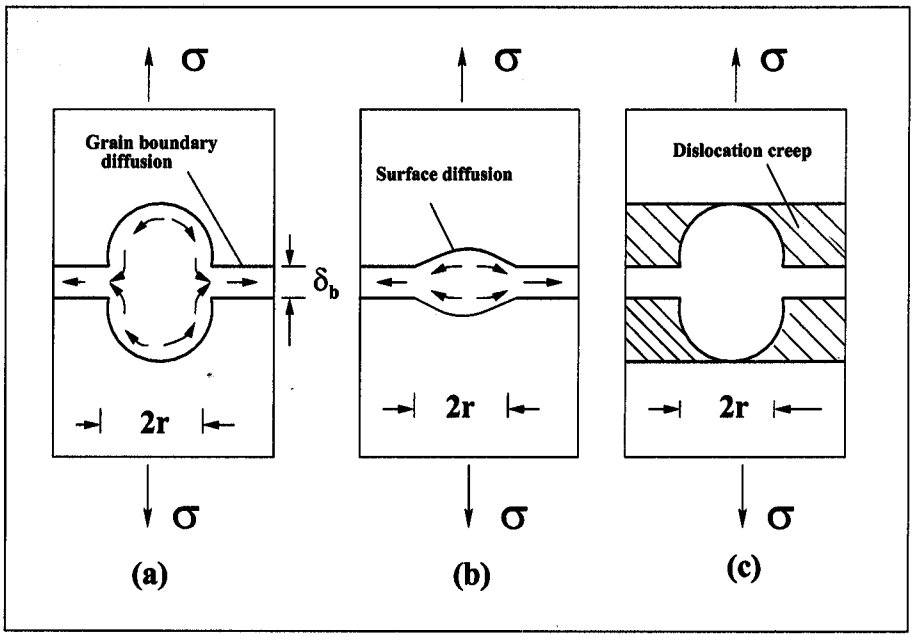

Figure 2.5 : Schematic of cavity growth mechanisms [Arzt, 1984]. (δ_b is the gap between boundaries, $2r$ is void size)

2.12.3 Constrained Cavity Growth

The cavity growth models described earlier generally assume that the total load on each grain boundary is constant, implying that each grain is free to slide and that no constraints exist. Dyson (1976), however, proposed that in a polycrystalline material cavity growth is constrained by the ability of neighbouring grains to accommodate shape changes and maintain contiguity by dislocation creep or grain boundary sliding. This mechanism of constrained cavity growth assumes that cavitation is a continuous process, with grain boundaries having different cavity nucleation rates. Hence a cavitated grain boundary can be surrounded by uncavitated grain boundaries. Such inhomogeneous distributions of grain boundary cavities have been observed by Tipler *et al.* (1970) from an examination of creep fracture surfaces. The mechanism of constrained cavity growth can be explained through Figure 2.6, where cavitation at the boundary between grains A and B has caused the grains to move apart. Cavity free grains C and D however do not move apart and a compressive stress can build up at EF.

This build up of compressive stress can be relieved by material diffusion or by plastic flow of the grain interiors. Then cavities will grow by a rate determined by the specific stress relaxation mechanism. At low stresses the relief mechanism is by diffusional creep while at higher stresses grain interior dislocation creep dominates. The relief of compressive stresses is easiest with dislocation creep and cavity growth is more rapid. However, if the grain interior is resistant to dislocation creep, as is the case for ODS materials, then diffusional relief mechanism will dominate. Similarly if the grain boundaries are not free to slide, as may be for MA–ODS materials with highly serrated grain boundary topography, then cavity growth will be limited.

2.12.4 Accommodation of Creep Damage

A grain boundary cavity grows by the displacement to material within the microstructure. This displacement of material needs to be accommodated to maintain compatibility and can be achieved by the mechanisms described in the previous section, namely; grain boundary sliding; stress directed diffusion;

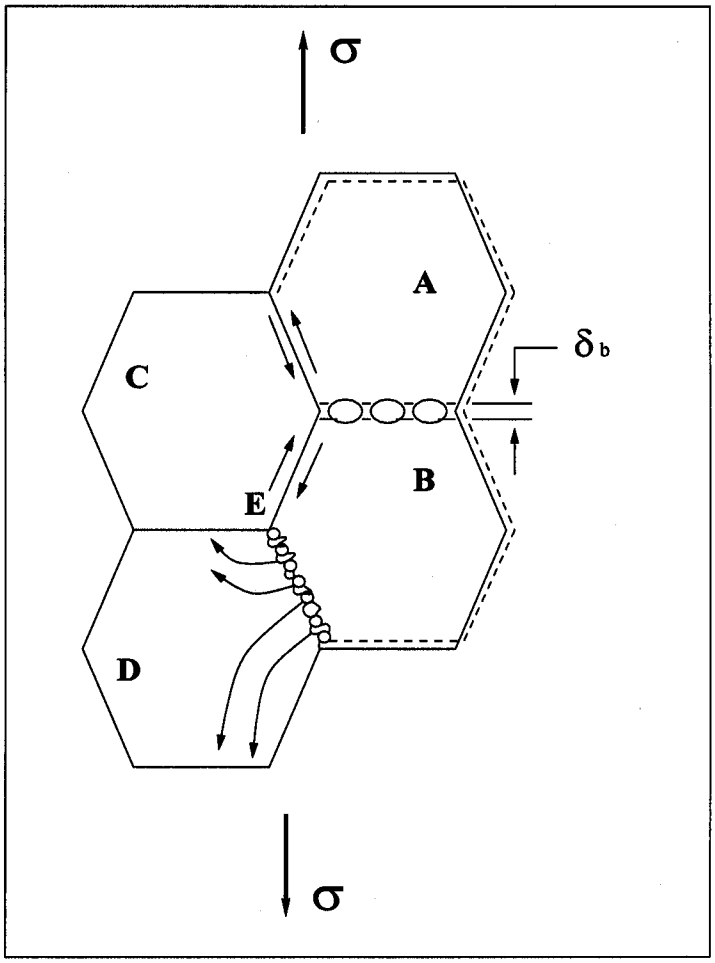

Figure 2.6 : Schematic diagram of constrained cavity growth mechanism (Dyson, 1976).

or dislocation creep of the surrounding matrix. More reasonably, the accommodation mechanisms are likely to be a combination of the above, as indicated by Raj and Ghosh, (1981) and Timmins and Arzt (1988). These accommodation mechanisms may also control the rate of cavity growth so, by limiting one or more of these mechanisms cavity growth will be limited and the creep strength will be increased.

In ODS materials dislocation creep is strongly suppressed by the effectiveness of the dispersoid in resisting dislocation motion. This will therefore limit the growth of cavities in a situation where the dislocation creep of the material surrounding the cavity is rate controlling. In addition, for some MA–ODS alloys, for example, MA6000, examined by Arzt (1988), where thermomechanical processes have produced a highly elongated grain structure containing serrated grain boundaries, grain boundary

sliding is limited by the keying in of the serrations and, therefore, cavity growth controlled by sliding is also limited. Grain boundary sliding is further inhibited as the resolved shear stresses necessary for sliding will be greatly reduced when the grain boundary is aligned parallel to the stress direction, as is the case for alloys with high GAR. Cavity growth by stress directed diffusion of vacancies may also be inhibited when the grain size is large because the diffusion distances between vacancy sinks and sources are large. This reduction in diffusional creep can become even more evident when the coupled with the inability of grain boundaries to slide [Nix, 1981]. Inhibition of growth of cavities by serrated grain boundaries is only applicable where the applied stress and other factors favour sliding. For alloys where the long axis of the developed high GAR grain structure is aligned parallel to the applied stress, where the resolved shear stresses are low this is not a problem. However, some engineering applications require loading where the short axis of the elongated grain structure is aligned with the stress axis, for example, internally pressurised tube. Here cavities will form on longitudinal grain boundaries and the transverse boundaries will need to be serrated in order to resist sliding and limit cavity growth. In this case the problem may be exacerbated as the transverse boundaries are often observed to be nearly aligned to the maximum principal shear stress.

2.13 Anisotropic Mechanical Behaviour in MA–ODS Alloys

Oxide dispersion strengthened alloys produced by mechanical alloying have been found to show anisotropic mechanical behaviour with the strength along the transverse direction lower than that along the extrusion or rolling direction.

Whittenberger, (1981) investigated the elevated temperature tensile properties of MA956 bars and their results are as shown in Figure 2.7. The longitudinal direction was shown to be stronger with greater ductility than the transverse direction.

Alamo *et al.* (1992) evaluated the tensile strength of 25 % cold-worked bars of MA957 and a summary of their data on the proof stress (PS) and ultimate tensile strength (UTS) measured in the longitudinal

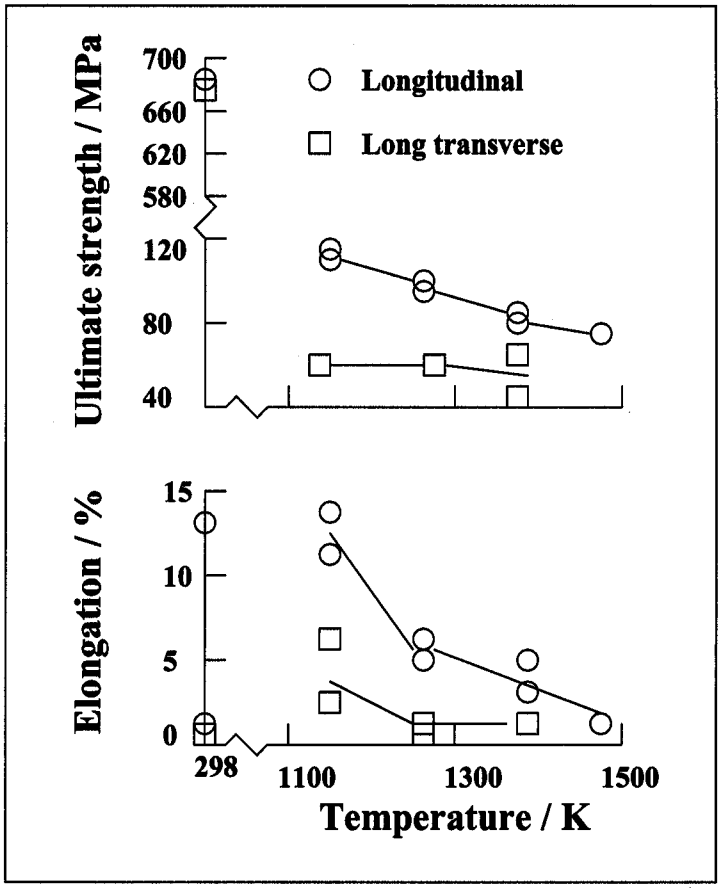

Figure 2.7 : Tensile Properties as a function of temperature for MA956 tested in the longitudinal and long transverse bar direction [Whittenberger, 1981].

and radial directions is shown in Table 2.6. The strength measured along the radial direction was shown to be about 200 to 300 MPa lower than values obtained in the longitudinal direction. Similar observations have been made previously for cold-worked tubes of MA956 and MA957, [Alamo *et al.*, 1990].

The anisotropic behaviour is most probably the consequence of the thermomechanical treatment rather than the mechanical alloying itself. A thin sheet of thoria dispersed nickel-base alloy, TD–NiCr (Ni–20Cr–2ThO_2) produced by internal oxidation of thorium and a standard commercial sheet manufacturing process had been reported to exhibit a similar anisotropic behaviour [Whittenberger, 1976]. For any heat (production batch) of the alloy the tensile properties, stress-rupture strength, and creep strength

Table 2.6 : Tensile strength of 25 % Cold-worked bars of MA957, determined along the radial and the longitudinal directions.

	Radial Direction		Longitudinal Direction	
Test Temperature /°C	0.2 % PS /MPa	UTS /MPa	0.2 % PS /MPa	UTS /MPa
20	893	1035	1360	1388
20	908	1032	1184	1216
450	654	718	1000	1016
450	706	785	965	973

were reported higher for specimens taken parallel to the rolling direction than those of specimens taken normal to the rolling direction. Figure 2.8 shows the stresses necessary to produce 0.1 % creep in 100 h as a function of temperature, direction and sheet thickness. It can be seen that the creep strength of TD–NiCr sheet is greater parallel to the rolling direction than normal to the rolling direction.

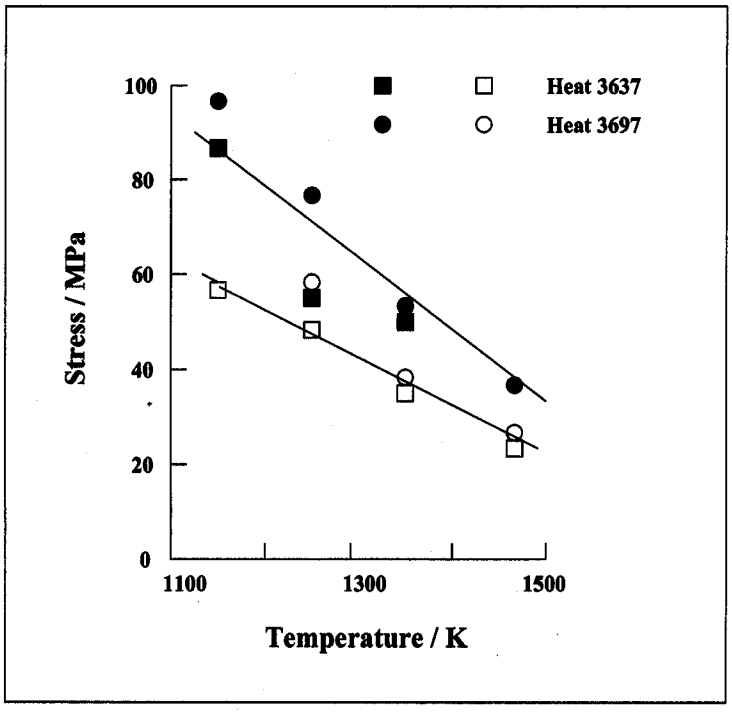

Figure 2.8 : Stress to produce 0.1% creep in 100 h in thin (0.025 cm) TD–NiCr sheet as a function of temperature and direction [Whittenberger, 1976].

However, the compressive strength of mechanically alloyed ODS alloys has been shown to be isotropic. Whittenberger, (1984), conducted a study of the compressive-flow-strength/strain-rate behaviour of MA6000 and observed that the compressive strength was independent of orientation. According to Whittenberger (1984), the inherent strength of ODS alloys is similar in all test directions and the low strength in tension can be traced to the inability of grain boundaries to support large tensile stresses. It follows therefore, that the elongated grain structure with boundaries aligned parallel to the extrusion, direction must have been responsible for the weaker transverse strength.

2.14 Summary

The mechanical alloying technique for the production of oxide dispersion strengthened alloys is a technically viable and potentially promising method for the growing industrial demands for superalloys with better high-temperature capabilities. Mechanically alloyed metals have been developed with a unique coarse columnar grain structure that gives an outstandingly high creep resistance, fine dispersion of inert oxide particles that ensures higher stability at high temperatures, and introduction of reactive elements (Al and Cr) with the attendant higher corrosion resistance and intermediate temperature strength. The alloys have been used in varieties of high temperature industrial applications. However, quite a lot of work is still required in order to understand many of the unusual characteristics of the technique.

CHAPTER THREE

Experimental Techniques

3.1 Materials

The experimental investigations were carried out mainly on MA956, a mechanically alloyed, oxide dispersion strengthened ferritic stainless steel (Table 1.1). The alloy was provided by INCO Alloys, Hereford, U.K. MA956 is produced by charging three primary powders, elemental iron, a pre–alloyed chromium-rich master alloy and yttria, into a water cooled vertical attritor and milled. The resultant powder is consolidated by extrusion at 1000 °C and finally rolled also at 1000 °C. A high–temperature annealing treatment usually at 1300 °C for 30 min is applied to develop the coarse columnar grain structure required to resist creep deformation.

The alloy was supplied as round or rectangular bars and in both the as-extruded and recrystallized conditions. The microstructures in both conditions are shown in Figure 3.1. The as–extruded microstructure consists of elongated grains of less than one micron diameters and grain aspect ratio up to 30 whilst the recrystallized microstructure has coarse grains (10–50 μm) elongated along the extrusion direction with aspect ratio of about 10 [Alamo *et al.*, 1992].

3.2 Stress–Rupture Tests

Samples of MA956 were subjected to various forms of heat–treatments in order to manipulate the grain structure and their stress–rupture properties were tested using facilities at INCO Alloys. Threaded-end specimens with gauge section parallel to the extrusion direction (longitudinal) and perpendicular to the extrusion direction (transverse) were produced. Most of the longitudinal specimens were "standard test pieces", with a gauge diameter and length of 4.51 mm and 23 mm respectively. All of the transverse

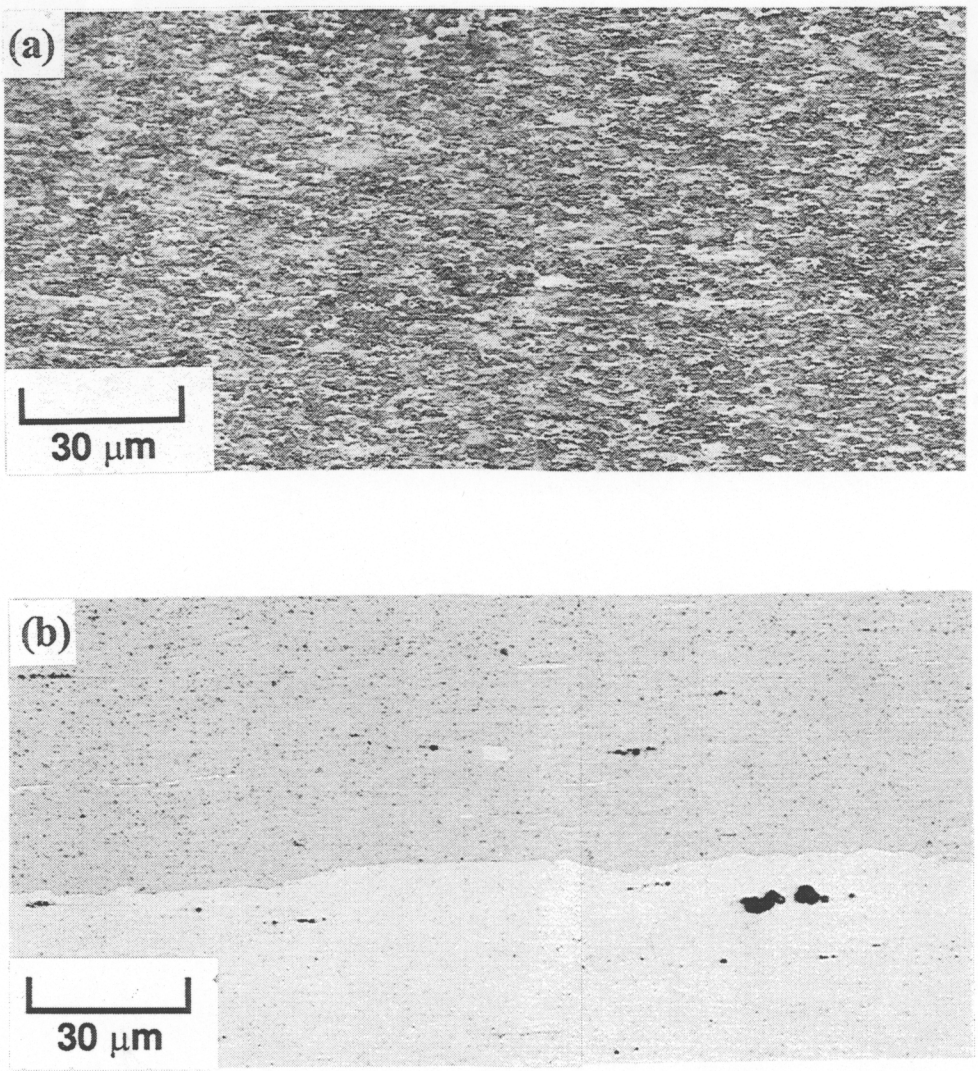

Figure 3.1: Microstructures of MA–ODS ferritic stainless steel, MA956. (a) before recrystallization heat–treatment; (b) after recrystallization heat–treatment (30 min/1300 °C).

specimens and some of the longitudinal specimens were "miniature", with gauge diameter and length of 3 mm and 15 mm respectively, due to the limited size of the bar stock. The stress-rupture tests were conducted in air at 1095 °C in a constant-load tensile creep testing machine under stresses in the range 28 to 79 MPa. The creep ductility was measured using a high temperature extensometry system.

3.3 Hardness Tests

The hardness measurements were made on polished samples using a Vickers pyramid hardness testing machine with an indentation load of 10 kg and a $\frac{2}{3}''$ objective. A minimum of five readings were obtained from each sample and the mean value calculated.

3.4 Tensile Tests

Some room temperature and high temperature tensile tests were conducted on the recrystallized and unrecrystallized MA956. The room temperature tensile samples were machined from a rectangular bar of MA956 in the as-extruded condition, both along the working direction and normal to the working direction. The samples used in the investigation of the temperature dependence of the tensile properties of the alloy in the as-extruded condition were machined from a different batch of the material, in the form of a round bar of 10 mm diameter. Only logitudinal samples could be obtained in that case. The specimens for high temperature testing were slightly bigger than those for ambient tests because different accessories are required when the testing machine is fitted with a heating furnace (Figure 3.2).

The room temperature tests were carried out on a "Schenck Trebel", universal screw–driven test machine with a maximum loading capacity of 50 kN. The high temperature tests were on a "MAND" universal testing machine which is similar to the Schenck Trebel machine but with a design which makes it suitable for use with a furnace assembly.

3.5 Optical Microscopy

Samples were prepared for optical metallography by hot mounting in conductive bakelite powder, followed by grinding on SiC paper to 1200 grit and polishing with 1 μm cloth coated with diamond paste. They were etched using a reagent which is made up of 2 g CuCl2, 40 ml HCl and, 40 to 80 ml ethanol. Optical micrographs were taken with an Axiotech microscope with a Yashica camera attached.

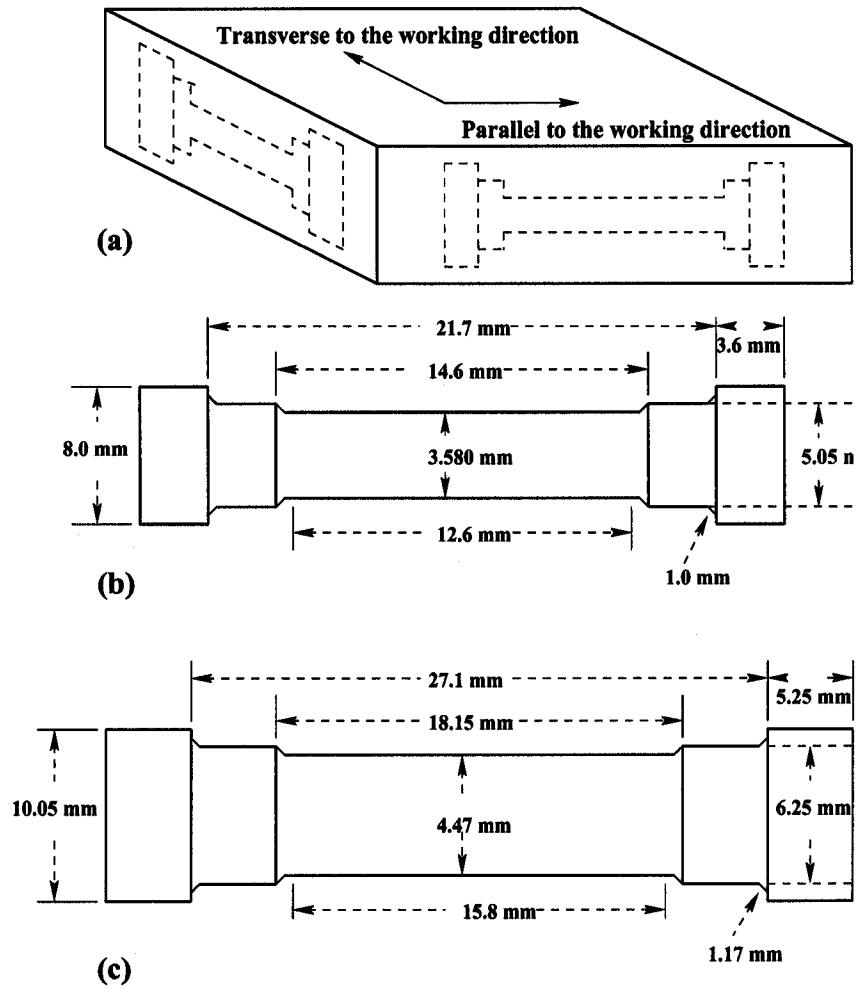

Figure 3.2 : Specimens used for the tensile tests, (a) rectangular bar showing sample orientations, (b) room temperature test specimen, and (c) high temperature test specimen.

3.6 Scanning Electron Microscopy (SEM)

A Jeol–820 scanning electron microscope was used to examine some metallographic specimens and fracture surfaces. Fractured Samples were mounted onto stubs using an Araldite adhesive mixed with graphite powder to prevent charging during imaging. An FP4 film was used on the attached camera.

3.7 Energy Dispersive X–ray (EDX) Microanalysis

Chemical microanalysis was carried out using an EDX system on a Camscan S4 scanning electron microscope. ZAF4, is a suite of computer programs which permits the calibration and routine quanti-

tative electron microprobe analysis. The X–ray emissions were interpreted using these programs. The microscope was operated at 20 kV with the stage tilted at 45°. The specimen is inserted in the EDX holder with the Co standard on the rim. The system is calibrated by the reference spectrum collected from the analysis of the Co standard and the quality of the subsequent analysis depends on the accuracy of the calibration.

3.8 Transmission Electron Microscopy

Carbon extraction replicas were prepared to oxide particles in a Phillips 400T transmission electron microscope operated at 120 kV.

Single–stage carbon extraction replicas were prepared using the method described by Smith and Nutting (1956) from optical microscopy samples using a light etch (2 g CuCl2, 40 ml HCl and, 40 to 80 ml ethanol). A carbon coating of 200-300 Å(colour blue–brown) was deposited in a vacuum of 10^{-5} torr on to the etched specimens. The carbon film was scored using a sharp blade to enable the removal of several small sections covering the whole area of the sample. The film was then removed by electrolytic etching in a solution containing 5 % hydrochloric acid in methanol at +1.5 V. The film was washed in industrial methylated spirits and floated off in distilled water and then collected on 200 square mesh copper grids for examination in the TEM.

CHAPTER FOUR

Thermodynamic Analysis of Mechanical Alloying

4.1 Introduction

It has always been a question as to when a mixture of powders becomes a solution during the mechanical alloying process. Normal thermodynamic theory for solutions begins with the mixing of component atoms. Many solutions are, however, prepared by mixing together lumps of the components, each of which might contain millions of identical atoms. We examine here the way in which a solution evolves from these large clusters of components, from a purely thermodynamic point of view. There are some interesting results including the prediction that solution formation by the mechanical alloying of solid components cannot occur unless there is a gain in coherency as the particles become small. The nature of the barrier to mechanical alloying is discovered. There is also the possibility of a metastable state prior to the achievement of full solution, when the component atoms prefer like–neighbours.

4.2 Thermodynamic Analysis

Consider the pure components A and B with molar free energies μ_A^o and μ_B^o respectively. If the components are initially in the form of powders then the average free energy of mixture of such powders is given by

$$G\{\text{mixture}\} = (1-x)\mu_A^o + x\mu_B^o \tag{4.1}$$

where x is the mole fraction of B. It is assumed that the powder particles are so large that the A and B atoms do not "feel" each other's presence via interatomic forces between unlike atoms. It is also assumed that the number of ways in which the mixture of powder particles can be arranged is not

sufficiently different from unity to give a significant contribution to a configurational entropy of mixing. Thus, a blend of powders which obeys equation 4.1 is called a *mechanical mixture.* It has a free energy that is simply a weighted mean of the components, as illustrated by the point u in Figure 4.1 for a mean composition x.

A solution, on the other hand, describes a mixture of atoms or molecules, *i.e.* the smallest particle in the present context since mixing cannot be achieved on an even finer scale. There will in general be an enthalpy change associated with the change in near neighbour bonds. Because the total number of ways in which the "particles" can arrange is now very large, there will always be a significant contribution from the entropy of mixing. The free energy of the solution is therefore different from that of the mechanical mixture, as illustrated by the point v on Figure 4.1. The difference in the free energy between these two states of the components is the free energy of mixing, the essential term in all thermodynamic models for solutions.

In practice, many solutions do not form instantaneously from a mixture of large particles to an intimate mixture of atoms. Instead, the system must go through a series of transition states involving ever decreasing particle sizes and increasing number densities as the particles are subdivided. One example is the process of mechanical alloying [Benjamin, 1970] in which a mixture of large particles is attrited until the subdivision of particles ultimately leads to the formation of a solution. The violent mixing of two initially immiscible liquids is another example.

4.2.1 Configurational Entropy

We consider a binary system consisting of pure components A and B. In contrast to the conventional approach for solution theory, the equation for the free energy of mixing must contain particle sizes which can be much greater than an atom.

The change in configurational entropy as a consequence of mixing can be obtained using the Boltzmann equation $S = k \ln\{w\}$ where w is the number of configurations and k has its usual meaning.

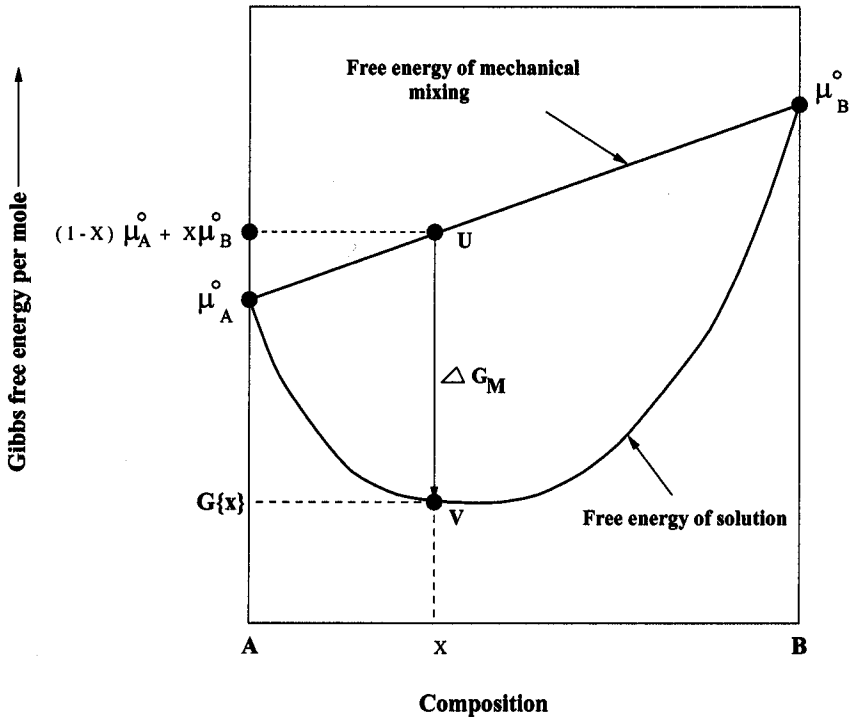

Figure 4.1 : Plot of the molar Gibbs free energy versus composition (mole fraction), both for mechanical mixtures and for solutions. $G\{x\}$ is the free energy of the solution of composition x whereas $(1-x)\mu_A^\circ + x\mu_B^\circ$ is the free energy of the corresponding mechanical mixture of large particles of A and B.

Suppose that there are m_A atoms per powder particle of A, and m_B atoms per particle of B; the powders are then mixed in a proportion which gives an average concentration of B which is the mole fraction x.

There is only one configuration when the heaps of pure powders are separate. When the powders are randomly mixed, the number of possible configurations for a mole of atoms becomes:

$$\frac{(N_a([1-x]/m_B + x/m_A))!}{(N_a[1-x]/m_A)!\ (N_a x/m_B)!} \tag{4.2}$$

where N_a is Avogadro's number. The numerator in equation 4.2 is the total number of particles and the denominator the product of the factorials of the A and B particles respectively. Using Stirling's approximation we obtain the molar entropy of mixing as

$$\begin{aligned}\frac{\Delta S_M}{kN_a} = &\frac{(1-x)m_B + xm_A}{m_A m_B}\ln\left\{N_a\frac{(1-x)m_B + xm_A}{m_A m_B}\right\} \\ &- \frac{1-x}{m_A}\ln\left\{\frac{N_a(1-x)}{m_A}\right\} \\ &- \frac{x}{m_B}\ln\left\{\frac{N_a x}{m_B}\right\}\end{aligned} \tag{4.3}$$

subject to the condition that the number of particles remains integral and non–zero. As a check, it is easy to show that this equation reduces to the familiar

$$\Delta S_M = -kN_a[(1-x)\ln\{1-x\} + x\ln\{x\}]$$

when $m_A = m_B = 1$.

Naturally, the largest reduction in free energy occurs when the particle sizes are atomic. This is illustrated in Figure 4.2 which shows the molar free energy of mixing for a case where the average composition is equiatomic assuming that only configurational entropy contributes to the free energy of mixing. An equiatomic composition maximises configurational entropy. When it is considered that phase changes often occur at appreciable rates when the accompanying reduction in free energy is just $10\,\mathrm{J\,mol^{-1}}$, Figure 4.2 shows that the entropy of mixing cannot be ignored when the particle size is less than a few hundreds of atoms. In commercial practice, powder metallurgically produced particles are typically 100 μ m in size, in which case the entropy of mixing can be neglected entirely, though solution formation must be considered to be advanced when the processing reduces particle dimensions to some 10^2 atoms. These comments must be qualified by the fact that we have neglected any enthalpy changes, which are treated in the next section.

4.2.2 Enthalpy

A major component of the excess enthalpy of mixing comes from the fact that there will in most cases be a change in the energy when new kinds of bonds are created during the formation of a solution.

In the regular solution model, the enthalpy of mixing is obtained by counting the different kinds of near neighbour bonds when the atoms are mixed at random. This information, together with the binding energies, gives the required change in enthalpy on mixing. The binding energy may be defined by considering the change in energy as the distance between a pair of atoms is decreased from infinity to an equilibrium separation. The change in energy during this process is the binding energy, which for a pair of A atoms is written $-2\epsilon_{AA}$. It follows that when $\epsilon_{AA} + \epsilon_{BB} < 2\epsilon_{AB}$, the solution will have a larger

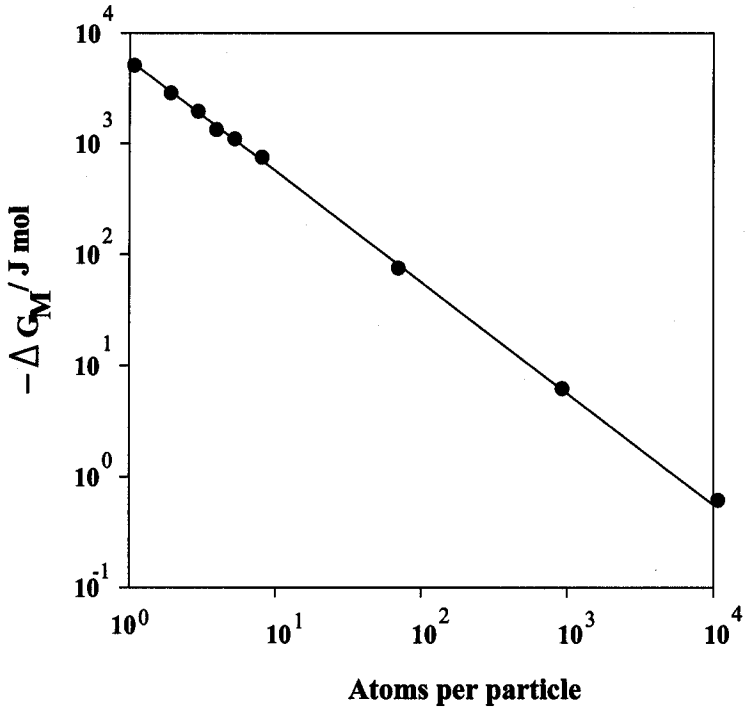

Figure 4.2 : The molar Gibbs free energy of mixing, $\Delta G_M = -T\Delta S_M$, for a binary alloy, as a function of the particle size when all the particles are of uniform size in a mixture whose average composition is equiatomic. $T = 1000\,K$.

than random probability of bonds between unlike atoms. The converse is true when $\epsilon_{AA} + \epsilon_{BB} > 2\epsilon_{AB}$ since atoms then prefer to be neighbours to their own kind.

With the approximation that atoms in a solution are randomly dispersed, the number of A–A bonds in a mole of solution is $zN_a(1-x)^2$, B–B bonds $zN_a x^2$ and A–B bonds $2zN_a(1-x)x$ where z is the co–ordination number. It follows that the molar enthalpy of mixing is given by:

$$\Delta H_M \simeq N_a z(1-x)x\omega \tag{4.4}$$

where

$$\omega = \epsilon_{AA} + \epsilon_{BB} - 2\epsilon_{AB} \tag{4.5}$$

The product $zN_a\omega$ is often called the regular solution parameter which we shall label Ω in subsequent discussion.

This treatment of the enthalpy of mixing has to be adapted for particles which are not monoatomic. For example, only those atoms at the interface between the A and B particles will feel the influence of the

unlike atoms. Assuming cubic particles, each of volume V_i and surface area $S = 6(V_i)^{2/3}$, we have

$$V_i = m_i\Phi_i \qquad \text{and} \qquad V_T = \sum_i \frac{N_a x_i}{m_i} V_i$$

where the subscript i represents the component, Φ_i is the volume per atom, x_i is the mole fraction, V_T is the total volume and N_a is Avogadro's number.

The total *surface area* of n_i isolated particles is $S_T = \sum_i n_i S$ but the total *grain boundary area* when the particles are compacted is half this value. It follows that the grain boundary area per unit volume, S_V is given by

$$S_V = \left(\frac{1}{2}\sum_i n_i 6(m_i\Phi_i)^{\frac{2}{3}}\right) \Big/ \left(\sum_i \frac{N_a x_i}{m_i} V_i\right) \tag{4.6}$$

If it is assumed that the boundary has a thickness 2δ (two monolayers) then the volume fraction of material within the boundary is $S_V \times 2\delta$. The enthalpy of mixing can only be generated within this region where the unlike atoms meet. It follows that

$$\Delta H_M = \Omega \; 2\delta S_V \; x(1-x) \tag{4.7}$$

4.2.3 Interfacial Energy

The role of the interface as discussed in the previous section is simply to identify the number of different atoms that are physically close enough to interact. However, there is a further term which must be taken into account, which does not occur in conventional solution theory. This comes from the inevitable disorder present at the interface, giving a structural component of the interfacial energy as σ per unit area. The chemical component of interfacial energy is already included in the enthalpy of mixing term. The net cost due to the structural component is

$$\Delta H_I = V_m S_V \sigma \tag{4.8}$$

where V_m is the molar volume.

ΔH_I is the *change* in enthalpy content due to interfaces. It is assumed that $S_V \simeq 0$ for very large particles. The process is envisaged as one in which the very large particles are reduced to smaller ones on the route towards the formation of a solution. This is a reasonable description of the mechanical alloying process. It is also assumed in this analysis that σ is identical for interfaces between $A - A$ particles, $B - B$ particles and $A - B$ particles.

4.3 Results & Discussions

The modelling of atomic solutions is well–established but Figure 4.3 nevertheless presents the results for particles which are one–atom in size. This is to illustrate the magnitude of the free energy changes involved for comparison against later results, and to highlight the fact that the energy of mixing is zero for the pure components. There are three cases illustrated corresponding to solutions in which like–atoms tend to cluster ($\Omega > 0$), those in which they tend to order ($\Omega < 0$) and lastly, the ideal solution ($\Omega = 0$). The calculations are for 1000 K, the temperature dependence appearing only via the $(-T\Delta S_M)$ term. Finally, interfacial energy does not feature in these plots because the solution is atomic and therefore fully coherent.

Difficulties arise when considering the evolution of a solution from a mixture of large particles to mixtures with ever decreasing sizes. This scenario precisely describes mechanical alloying, where the component powders are repeatedly fractured and deformed until an atomic solid solution is formed. The refinement of particle size leads to an increase in the amount of interface per unit volume (S_V). If the interface energy is constant then the cost indicated by equation 4.8 must eventually overwhelm any advantage from the entropy or enthalpy of mixing. The inescapable conclusion is that mechanical alloying cannot occur unless there is a gain in coherency, *i.e.* a reduction in the interfacial energy as atomic dimensions are approached. This is not surprising in hindsight, since the process envisaged is the opposite of the normal precipitation and growth event in which a small particle begins coherently and loses coherency as it grows.

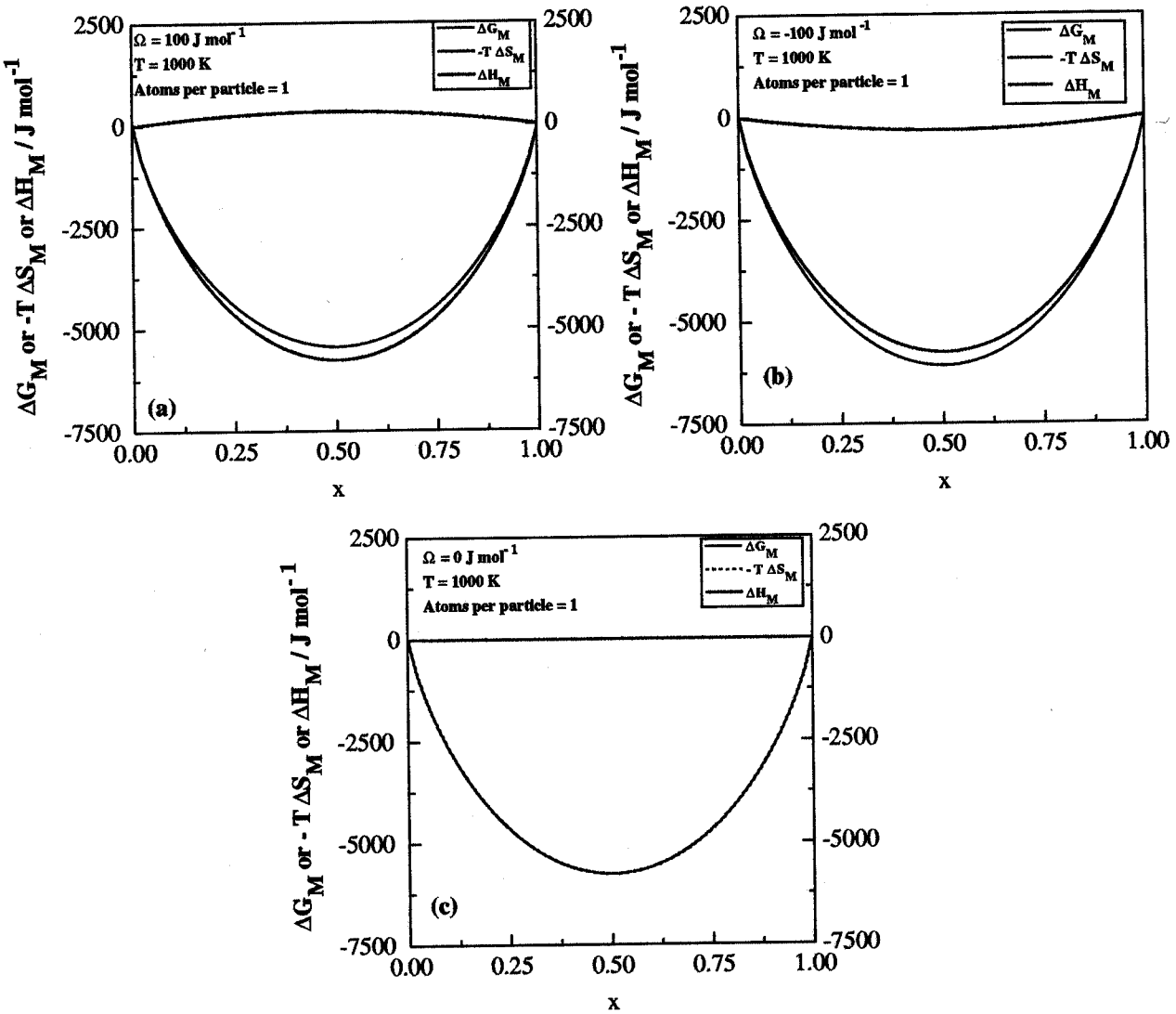

Figure 4.3 : Plots of the free energy, entropy and enthalpy of mixing in a binary system at 1000 K. (a) $\Omega = 100\,\mathrm{J\,mol^{-1}}$, (b) $\Omega = -100\ \mathrm{J\,mol^{-1}}$ and (c) $\Omega = 0\,\mathrm{J\,mol^{-1}}$.

Since the change in the interfacial energy with particle size is not known, we have assumed that σ remains constant until a size of 10^7 atoms is reached. Beyond that the energy decreases linearly to zero when the particle size is one atom:

$$\begin{aligned} \sigma &= 0.5\ \mathrm{J\,m^{-2}} && m > 10^7 \text{atoms per particle} \\ \sigma &= 0.5\left(1 - \frac{10^7 - m}{10^7}\right)\ \mathrm{J\,m^{-2}} && m \leq 10^7 \text{atoms per particle} \end{aligned} \tag{4.9}$$

The results as a function of particle size are illustrated in Figure 4.4. A typical powder particle at the

beginning of the mechanical alloying process might be some 10^{17} atoms in size but the calculations begin at 10^9 in order to see significant effects. The free energy change as the particle size is reduced to 10^9 atoms is at first mainly a contribution from the increase in the structural component of interfacial energy. The net free energy change remains positive until contributions from the enthalpy and entropy of mixing begin to become significant and when the interfacial energy term begins to decrease below 10^7 atoms due to a gain in coherency.

The energy changes are all very much smaller than associated with the direct formation of an atomic solution (cf. Fig. 4.3). This is because the contribution from configurational entropy is small until the particle size reaches about 100 atoms, and that from enthalpy is small because only those atoms at unlike–particle interfaces can interact. The details also depend on the nature of the solution, the sign and size of Ω. For the case where like atoms tend to cluster ($\Omega > 0$), a pair of minima develop, in the A and B rich regions, in the ΔG_M function as the particle size is reduced. Solution formation is not favoured when the concentrations of the two components are about equal. The opposite is true when $\Omega \geq 0$ and mixing is favoured at all compositions once the particle size becomes small enough for coherency to set in.

Figure 4.5 shows how there is a barrier to the formation of a solid solution during the mechanical alloying process. The barrier occurs for all the examples illustrated because of the incorporation of interfacial energy in the analysis. This dominates in the early stages as the particle size is reduced, until a size is achieved below which coherency begins to set in. It is important to note that when $\Omega > 0$, there is an energy barrier even in the absence of interfacial energy since the alloying forces unlike atoms to mix leading to an increase in enthalpy. Naturally, this latter effect is minimised at low or high concentrations which are A–rich or B–rich respectively. Figure 4.5a reveals the possibility that there is an energy well in the curve of energy versus particle size, suggesting a possible metastable state making the alloying process particularly difficult. However, the general result is that there is a certain particle size below which mechanical alloying proceeds rapidly with a reduction in free energy.

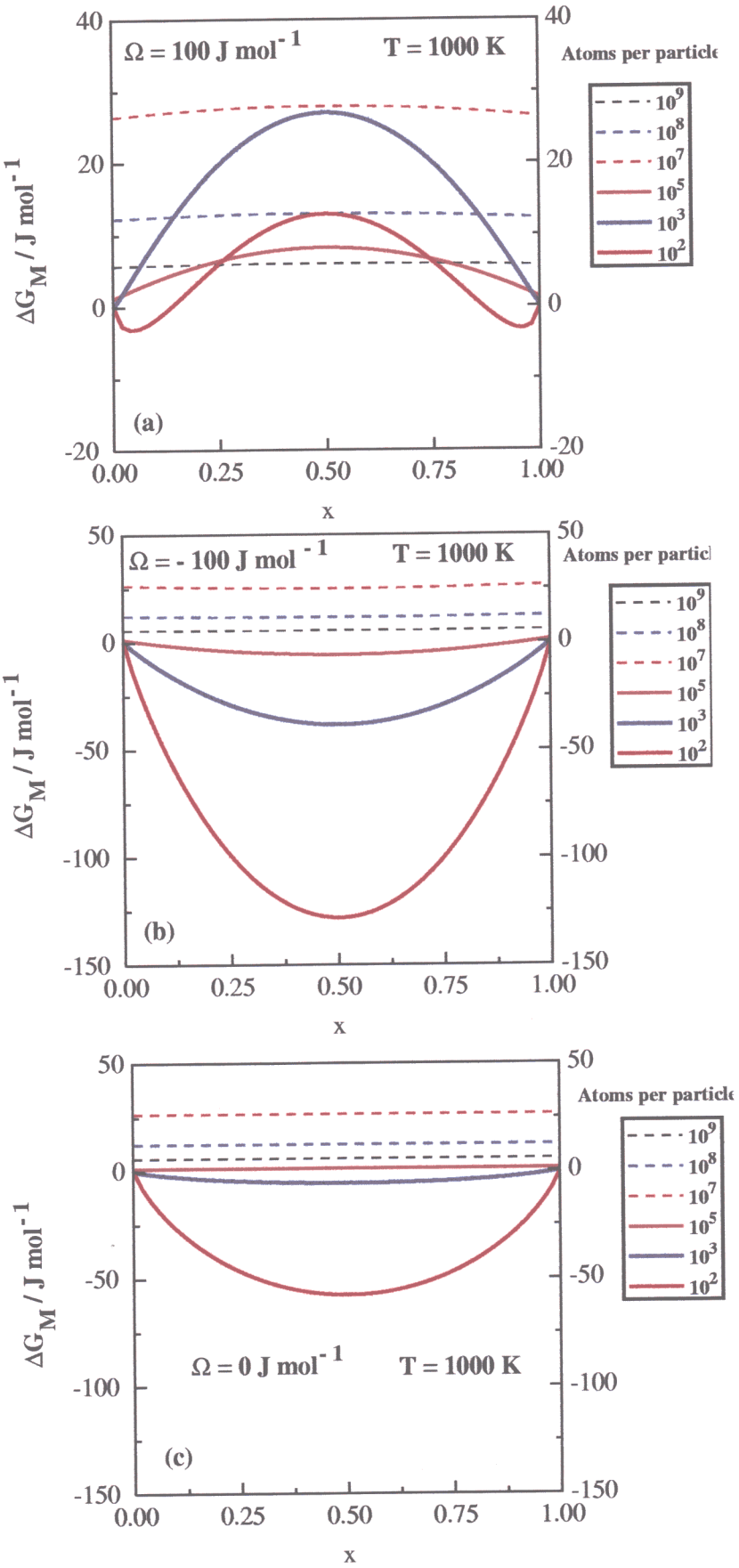

Figure 4.4 : Plots of the free energy, entropy and enthalpy of mixing in a binary system at 1000 K, as a function of the number of atoms in the particles. (a) $\Omega = 100\,\mathrm{J\,mol^{-1}}$, (b) $\Omega = -100\,\mathrm{J\,mol^{-1}}$ and (c) $\Omega = 0\,\mathrm{J\,mol^{-1}}$.

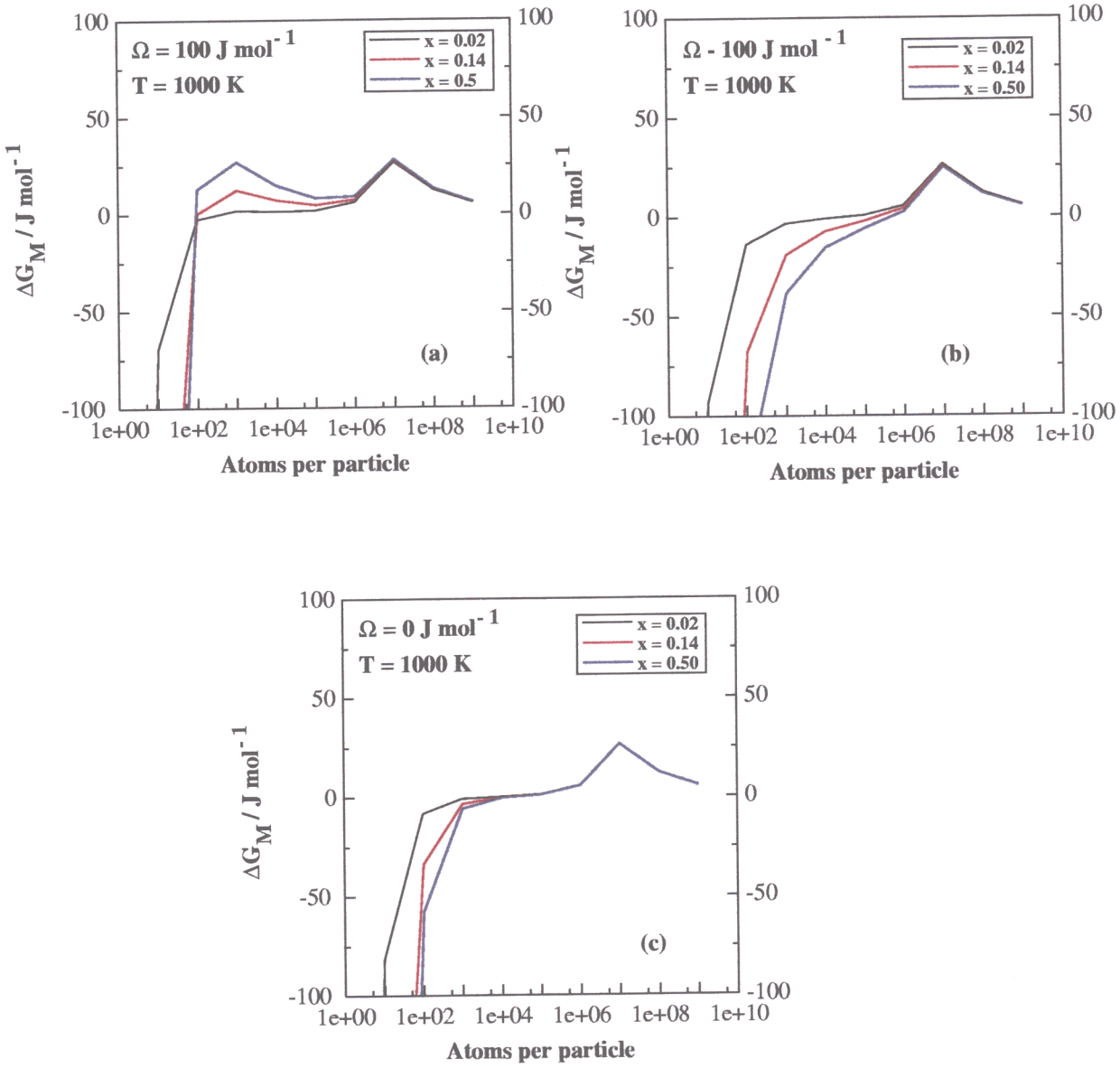

Figure 4.5 : Free energy versus the number of atoms per particle as a function of the concentration, at $T = 1000K$. (a) $\Omega = 100\,\mathrm{J\,mol^{-1}}$, (b) $\Omega = -100\,\mathrm{J\,mol^{-1}}$ and (c) $\Omega = 0\,\mathrm{J\,mol^{-1}}$. The jagged appearance is because the calculated points have been connected with straight segments. The true variation is expected to be smooth.

Finally, the entropy term $-T\Delta S$ ensures that the effect of increasing the temperature is, for all finite x, to make the alloying process easier (Figure 4.6).

4.4 Conclusions

A model has been developed to deal with a situation in which a solution is created by continuously refining a mixture of powder particles of the pure components. This process of solution formation is a good representation of the mechanical alloying process.

It is predicted that mechanical alloying is not possible unless initially incoherent interfaces approach coherency and eventually disappear as true solution is approached. The inclusion of interfacial energy also predicts the existence of a barrier to the evolution of the solution. For cases where like atoms tend to cluster, it is possible in principle to obtain a metastable state before solution formation is completed.

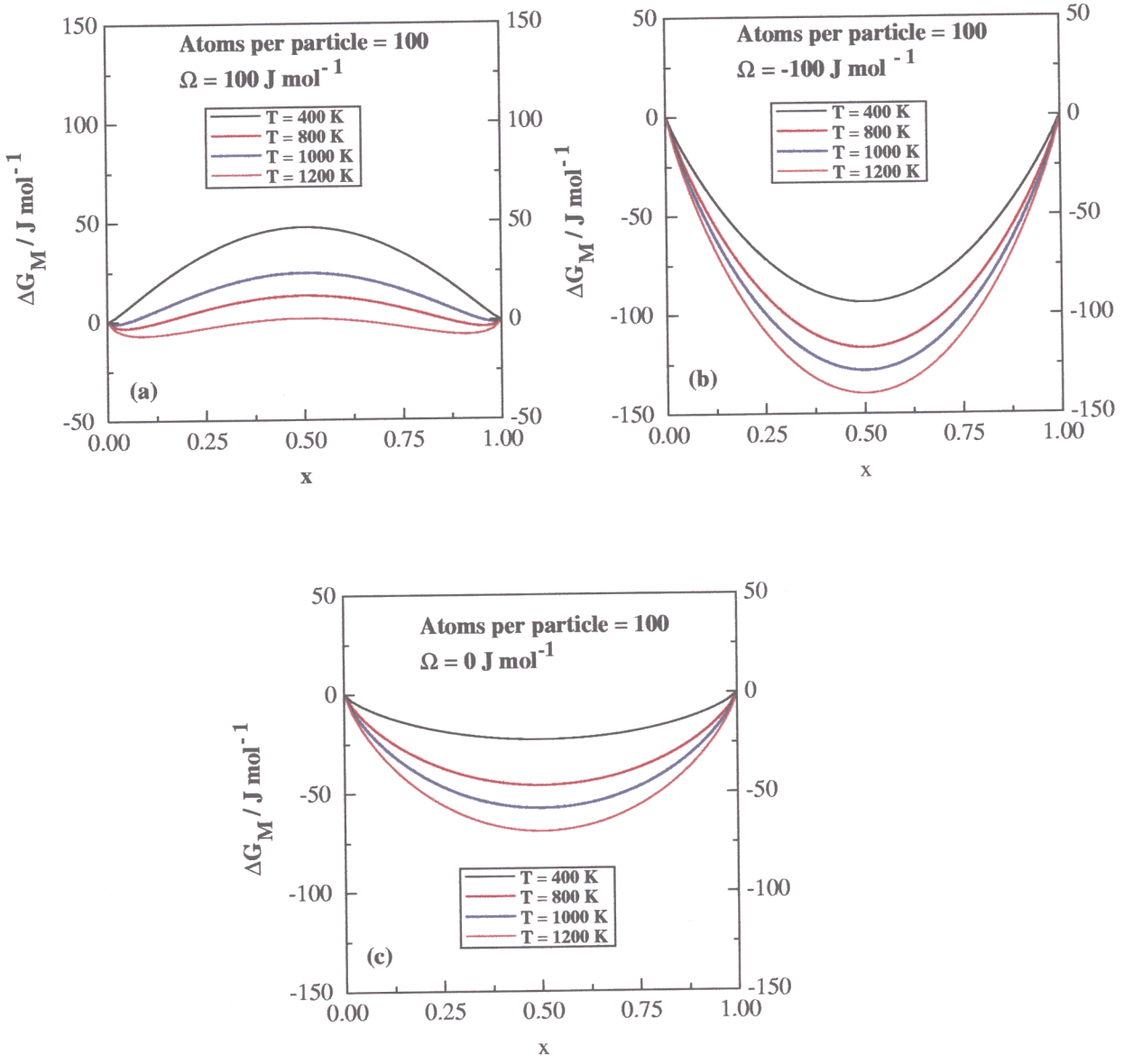

Figure 4.6 : Effect of temperature on the free energy of mixing for a particle size containing 100 atoms per particle (a) $\Omega = 100\,\mathrm{J\,mol^{-1}}$, (b) $\Omega = -100\,\mathrm{J\,mol^{-1}}$ and (c) $\Omega = 0\,\mathrm{J\,mol^{-1}}$.

CHAPTER FIVE

Neural Network Models for the Tensile Properties Of Mechanically Alloyed ODS Iron–Alloys

5.1 Introduction

Very limited information is available in the published literature on the mechanical properties of mechanically alloyed materials. The experimental data which are available do not seem to have been adequately interpreted in terms of the numerous variables known to affect the mechanical properties. The technique of mechanical alloying is unconventional and this is coupled with the complex microstructures. The objective of this work was to investigate whether an artificial neural network [Rumelhart *et al.*, 1986] can be trained to predict the yield strength, ultimate tensile strength and elongation of the mecanically alloyed ferritic stainless steels as a non-linear function of the important processing and service variables.

This chapter is presented first with an introduction to the neural network technique, followed by a description of how the optimum model was obtained in each case. The final section deals with the use of the models to ensure as far as is possible that the percieved relationships are metallurgically significant.

5.2 The Neural Network

Most people are familiar with regression analysis, where data are best-fitted to a specified relationship which is usually linear. The result is an equation in which each of the inputs x_j is multiplied by a weight w_j. The sum of all such products and a constant θ then gives an estimate of the output $y = \sum_j w_j x_j + \theta$.

It is well understood that there are dangers in using such relationships beyond the range of fitted data.

A neural network is a more general method of regression analysis. As before, the input data x_j are multiplied by weights, but the sum of all these products forms the argument of a hyperbolic tangent. The output y is therefore a non-linear function of x_j, the function usually chosen being the hyperbolic tangent because of its flexibility. The exact shape of the hyperbolic tangent can be varied by altering the weights (Figure 5.1a). Further degrees of non-linearity can be introduced by combining several of these hyperbolic tangents (Figure 5.1b), so that the neural network method is able to capture almost arbitrarily non-linear relationships. It is well known that the effect of chromium on the microstructure of steels is quite different at large concentrations than in dilute alloys. Ordinary regression analysis cannot cope with such changes in the form of relationships.

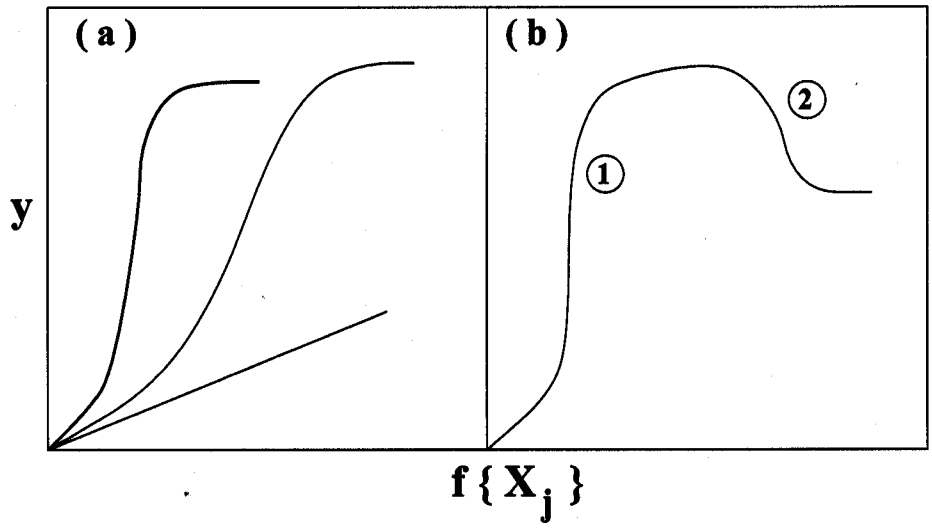

Figure 5.1 : (a) Three different hyperbolic tangent functions - the 'strength' of each depends on the weight (b) A combination of two hyperbolic tangents to produce a more complex model.

A neural network is 'trained' on a set of examples of input and output data. The outcome of the training is a set of coefficients (*weights*) and a specification of the functions which in combination with the weights relate the input to the output. The training process involves a search for the optimum non-linear

relationship between the input and the output data and is computer intensive. Once the network is trained, estimation of the outputs for any given inputs is very rapid.

One of the difficulties with blind data modelling is that of 'overfitting', in which spurious details and noise in the training data are overfitted by the model (Figure 5.2). This gives rise to solutions that generalise poorly. Mackay (1992, 1994, 1995, 1997) has developed a Bayesian framework for neural networks in which the appropriate model complexity is inferred from the data. The Bayesian theory is a subject in its own right and beyond the scope of the present work.

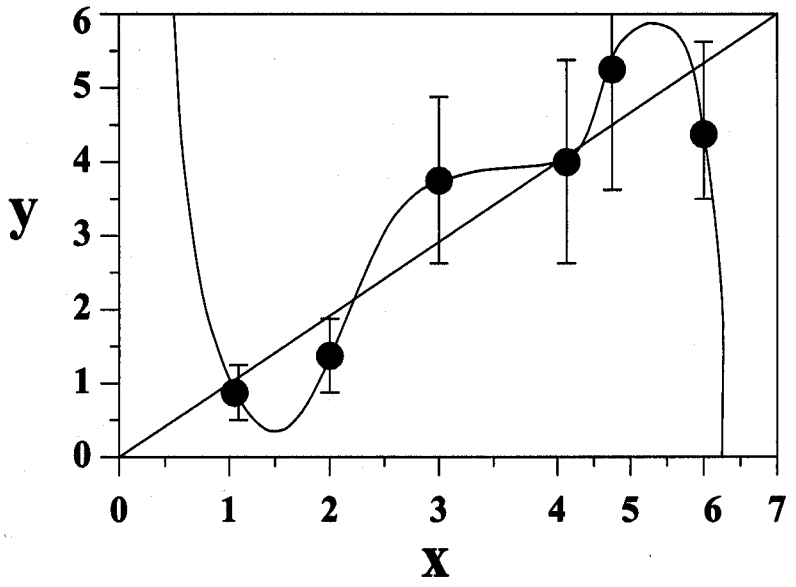

Figure 5.2 : A complicated model may fit the data, but in this case, a linear relationship may be all that is justified by the noise in the data.

However, the Bayesian framework for neural networks has two important advantages. First, the significance of the input variables with respect to explaining the variation in the output is automatically quantified. Consequently the significance perceived by the model of each input variable can be compared against metallurgical theory. Second, the network's predictions are accompanied by error bars which depend on the specific position in input space. These quantify the model's certainty about its predictions. The error bars are therefore not fixed as in conventional regression analysis.

The neural network method has recently been applied to many materials problems and examples include: the impact toughness of C–Mn steel arc welds by Bhadeshia *et al.* (1995); an analysis of the strength of Ni-base superalloys by Jones *et al.* (1995); austenite formation in steels by Garvard *et al.* (1996); yield and ultimate tensile strength of steel welds by Cool *et al.* (1997); fatigue crack growth rate in nickel base superalloys by Fujii *et al.* (1996); mechanical properties in the HAZ of power plant steels by Cool *et al.* (1997); prediction of martensite-start temperature by Vermeulen *et al.* (1996); prediction of the continuous cooling transformation diagram of some selected steels by Vermeulen *et al.* (1997), and prediction of the measured temperature after the last finishing stand in hot rolling, by Vermeulen *et al.* (1997).

5.3 The Analysis

Both the input and output variables were first normalized with the range $+0.5$ to -0.5. The normalisation is obtained through a procedure which is expressed quantitatively as :

$$x_N = \frac{x - x_{min}}{x_{max} - x_{min}} - 0.5 \tag{5.1}$$

where x_N is the normalized value of x, which has the minimum and maximum values given by x_{min} and x_{max} respectively. The nomalisation is not necessary for the analysis but it enables an easier subsequent comparison of the significance of each of the variables.

Figure 5.3 shows a typical network. Each network consisted of input nodes (one for each variable x), a number of hidden nodes, and an output node. Linear functions of the inputs x_j are operated on by a hyperbolic tangent transfer function:

$$h_i = \tanh\left(\sum_j w_{ij}^{(1)} x_j + \theta_i^{(1)}\right) \tag{5.2}$$

so that each input contributes to every hidden unit. The bias is designated θ_i and is analogous to the

constant that appears in linear regression analysis. The strength of the transfer function is in each case determined by the weight w_{ij}. The transfer to the output y is linear:

$$y = \sum_i w_{ij}^{(2)} h_i + \theta^{(2)} \tag{5.3}$$

The specification of the network structure, together with the set of weights, is a complete description of the formula relating the input to the output. The weights are determined by training the network.

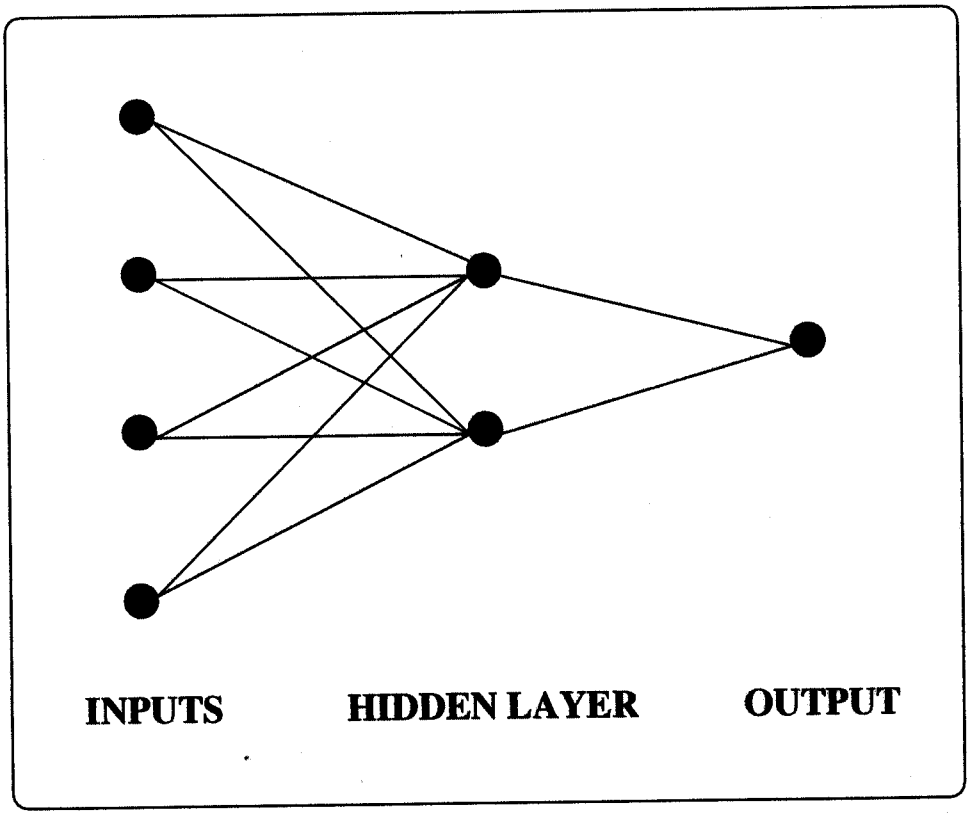

Figure 5.3 : Typical network used in the analysis.

5.4 Training and Optimisation

The 'training' is the time consuming stage in the production of a functioning neural network. A neural network as defined in equations (3.2) and (3.3) is trained using a data set $D = \{x^m, t^m\}$ by adjusting **w** so as to minimize an error function, e.g.,

$$E_D(w) = \frac{1}{2}\sum_m (y(x^m; w) - t^m)^2 \tag{5.4}$$

This objective function is a sum of terms, one for each input-target pair $\{x, t\}$, measuring how close the output is to the target **t** (Mackay, 1995).

The minimization is based on the repeated evaluation of the gradient of E_D using 'backpropagation'[Rumelhart *et al.*, 1986]. The backpropagation algorithm computes for each input-output pair m the gradient of $\frac{1}{2}\left(y(x^m; w) - t^m\right)^2$ by following the 'forward pass' of equations (3.2–3.3) by a 'backward pass', in which information about the errors $\left(y(x^m; w) - t^m\right)$ propagates back through the network by the chain rule. Often, regularization is included, modifying the objective function to

$$M(w) = \beta E_D + \alpha E_W \tag{5.5}$$

where, for example, $E_W = \frac{1}{2}\sum w_i^2$. This additional term favours small values of **w** and thus encourages the model to find simpler solutions with less tendency to 'overfit' noise in the data. The control parameters, α and β define the assumed Gaussian noise level $\sigma_\nu^2 = \frac{1}{\beta}$ and the assumed weight variances $\sigma_w^2 = \frac{1}{\alpha}$. σ_ν is the noise level inferred by the model. The parameter α has the effect of encouraging the weights to decay. Therefore, a high value of σ_w implies that the input parameter concerned explains a relatively large amount of the variation in the output. Thus, σ_w is regarded as a good expression of the significance of each input though not of the sensitivity of the output to that input. The values of the hyperparameters are inferred from the data using the Bayesian method by [Mackay, 1992].

The complexity of the model is controlled by the number of hidden units and the values of the regularization constants (σ_w), one associated with each of the inputs, one for biases and one for all weights connected to the output. The noise level, σ_ν, decreases monotonically as the number of hidden units increases. However, the complexity of the model also increases with the number of hidden units. A high degree of complexity may not be justified if the model attempts to fit the noise in the experimental data. Mackay (1992, 1993, 1994, 1997) has made a detailed study of this problem and defined a quantity (the 'evidence') which comments on the probability of a model. In circumstances where two models give similar results for the known dataset, the more probable model would be predicted to be that which is simpler; this simple model would have a higher value of evidence. The evidence framework is used to control the regularisation constants and the noise level . The number of hidden units is set by examining performance on test data. A combination of Bayesian and pragmatic statistical techniques are therefore used to control the complexity of the model. A further procedure used to avoid the overfitting problem was to randomly divide the experimental data into two equal sets, the *training* and *test* datasets. The models are developed using just the training data. The unseen test data are then used to assess how the model generalizes. A good model would produce similar levels of errors in both the test and training data whereas an overfitted model might accurately predict the training data but badly estimate the unseen test data. Once the correct complexity of the model has been chosen using this procedure, it can be retrained using all the data with a small but significant reduction in the error.

The test error (sum squared error, E_D) is a reflection of the ability of the model to predict the target values in the test data. It is popular to use the test error as the default performance measure whereby the model with the lowest test error is reckoned to be the best [Mackay, 1994]. In many applications there will be an opportunity not to simply make a scalar prediction, but rather to make a prediction with error bars, or maybe an even more complicated predictive performance. It is then reasonable to compare models in terms of their predictive performance as measured by the log predictive probability of the test data. Under the log predictive error, as contrasted with the test error, the penalty for making a wild

prediction is much less if the wild prediction is accompanied by appropriately large error bars [Mackay, 1997]. Assuming that for each example m the model gives a prediction with error, $(y^{(m)}, \sigma^{(m)2})$, the log predictive error (LPE) is [Mackay, 1997]:

$$LPE = \sum_m \left[\frac{1}{2} \left(t^{(m)} - y^{(m)} \right)^2 / \sigma_y^{(m)^2} + \log(\sqrt{2\pi}\sigma_y^{(m)}) \right] \tag{5.6}$$

5.5 Committee Model

It is common practice in the application of neural networks to train many different candidate networks from the same data by varying either the number of hidden units or starting value of σ_w, and then to select the best on the basis of the test error or log predictive error, and to keep only this network and discard the rest. There are two disadvantages with such an approach. First, all of the effort involved in training the remaining networks is wasted. Second, the generalization performance on the validation set has a random component due to the noise on the data, and so the network which had best performance on the validation set might not be the one with the best performance on new test data.

These drawbacks can be reduced by combining the networks together to form a *committee* [Perrone and Cooper, 1993; Perrone, 1994; Mackay, 1994]. The importance of such an approach is that it can lead to significant improvements in the predictions on new data, while involving little additional computational effort. In fact the performance of a commitee can be better than the performance of the best single network used in isolation, although there is an optimum size to the committee.

Suppose we have a set of L trained network models y_i where $i = 1, ..., L$. The commitee output is taking to be the average of the outputs of the L networks which comprise the committee. Thus, the commitee prediction, $\overline{y}$ is written as:

$$\overline{y} = \frac{1}{L}\sum_{i}^{L} y_i \tag{5.7}$$

The optimum size of the committee is determined from the validation error of the committee's predictions using the test dataset. The test error of the predictions made by a committee is calculated by replacing the y in equation (3.5) with $\overline{y}$.

5.6 The Database

The database used for the analysis was compiled from published literature. There are 232 data points in the database. The dataset is restricted because at the moment, published information on the mechanical properties of mechanically alloyed materials is very limited. Moreover, discrepances in the experimental conditions and inadequate reporting in some cases necessitated the exclusion of some published data.

Table 5.1 shows the chemical compositions of some commercial MA-ODS steels which are represented in the data used for the analysis [Whittenberger, 1981; Singer and Gessinger, 1994; Zakine *et al.*, 1993; Dubiel *et al.*, 1994; Hendrix and Vandermeulen, 1982; Alamo *et al.*, 1990, 1992; Regle, 1994 etc.].

Table 5.1 : Chemical composition (wt.%) of some commercial MA-ODS steels.

Steel	Cr	Al	Mo	Ti	Y_2O_3	Fe
MA956	20.0	4.5	-	0.5	0.5	Balance
MA957	14.0	-	0.3	1.0	0.27	Balance
DY (DT2203Y05)	13.0	-	1.5	2.2	0.5	Balance
DT (DT2906)	13.0	-	1.5	2.9	-	Balance

5.7 The yield strength model

The technique was applied to the variables listed in Table 5.2 for the analysis of the yield strength. There were 232 data, 12 input variables and one output which is the yield strength. The major alloying elements (Cr, Al, Ti, Mo) are expected to influence the yield strength primarily via solid solution strengthening. In some alloys molybdenum, titanium and chromium also precipitate as an intermetallic compound, χ-phase (FeCrTiMo) after a low-temperature ageing treatment [Hendrix and Vandermeulen, 1982]. Yttrium oxide is present as a very fine dispersion and must enhance strength at all temperatures by impeding the glide of dislocations. The recrystallisation heat-treatment has a very severe effect on the microstructure since it changes an ultrafine primary recrystallised grain structure to one which is coarse and columnar. Cold work is naturally expected to increase the yield strength; the dataset included a variety of methods of cold deformation including rolling and swaging. The yield strength of body-centred cubic metals is particularly sensitive to temperatrure because of the large Peierls barriers to dislocation motion. A further temperature dependence comes from the possibility of the climb of dislocations over dispersoids. There may, in unrecystallised alloys be an additional effect due to the onset of dynamic recrystallisation.

The plot of σ_{ν}, as a function of the complexity of the models is shown in Figure 5.4 . Note that a number of values are presented for each hidden unit because the training process was started off using different randomly chosen seeds which determine the starting values of the weights. The test error and log predictable error versus hidden units are shown in Fig. 3.5.

The numerical data for the top ten models ranked by their test error are shown in Table 5.3. Table 4 shows the test errors of the ten committees formed, starting with the best model and progressively increasing the number of models in the committee. The plots of the test errors of the top ten models and those of the committees are shown in Figure 5.6 plotted to the same scale to show the usual reduction in test error when an appropriate committee is formed. The committee consisting of five top ranking

Table 5.2 : The variables used in the analysis of the yield strength.

Variable	Range	Mean	Standard Deviation
Chromium, wt%	13-20	17.30	3.20
Aluminium, wt%	0-4.5	2.62	2.23
Titanium, wt%	0.5-3.50	1.03	0.86
Molybdenum, wt%	0-1.5	0.35	0.56
Yttria, wt%	0-0.5	0.41	0.15
Recrystallisation temperature, °C	20-1330	697	595
Recrystallization time, s	0-120	28.44	33.38
Ageing temperature, °C	20-800	163.3	303
Ageing time, s	0-2888	327	739
Cold Work, %	0-70	10.43	19.64
Test temperature, °C	0-1200	562.1	340.4
Strain rate, s^{-1}	0.00000003-0.03	0.000989	0.0025
Yield strength, MPa	63-1600	497	388

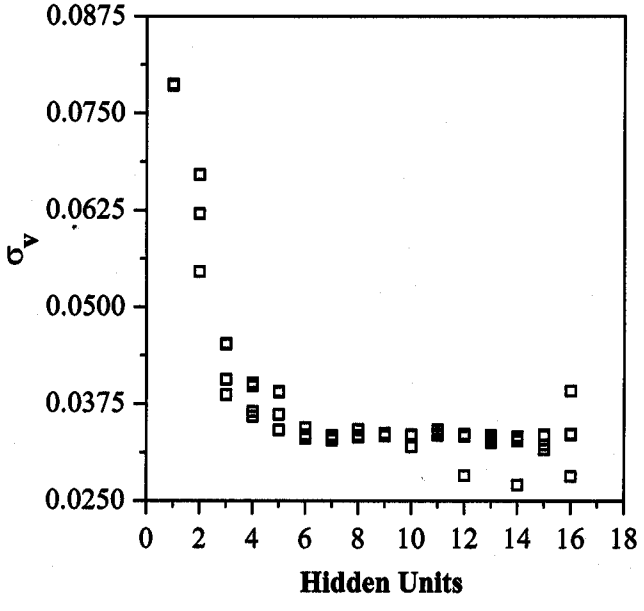

Figure 5.4 : Variation in σ_v as a function of hidden units.

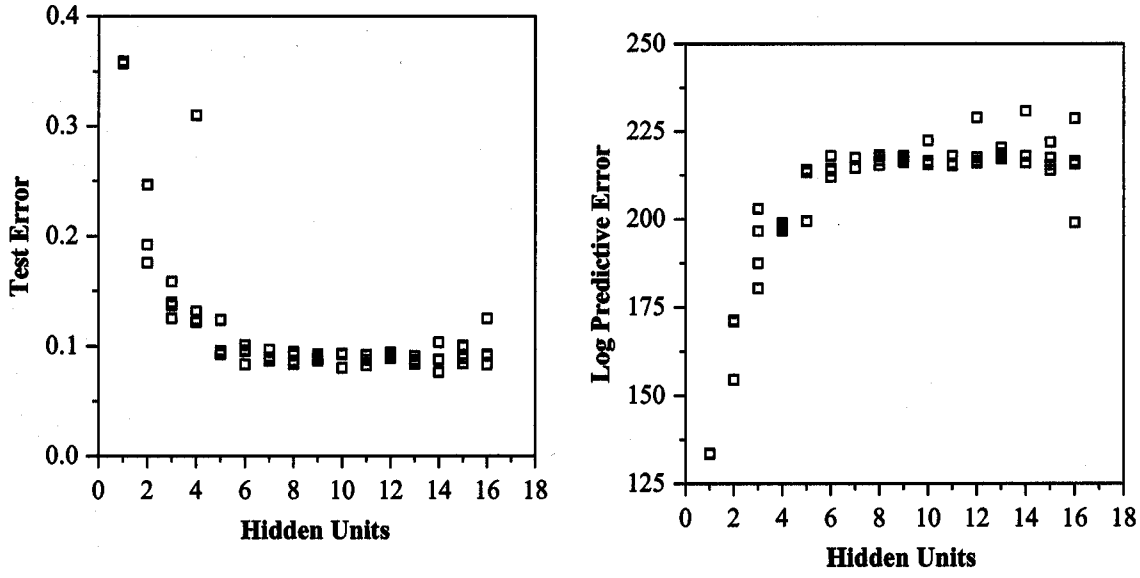

Figure 5.5 : Variation in test error and log predictive error as functions of the number of hidden units. Note that a larger log predictive error stands for a better model.

models has the least test error and was used for the study of the yield strength presented later.

The plots of the predicted values versus experimental values of the training and test dataset for the single best model and the commitee are shown in Figures 3.7 and 3.8 respectively. Figure 3.9 shows the plot for the committee after retraining using the whole dataset.

The perceived significance of each of the input variables by the various models contained in the committee is shown by σ_w in Figure 5.10. The parameter σ_w, is rather like a partial correlation coefficient in that it represents the amount of variation in the output that can be attributed to any particular input parameter and does not necessarily represent the sensitivity of the output to the each of the inputs. As expected, the yield strength correlates strongly with temperature.

Table 5.3 : Ranking by test error of the ten best models of the yield strength

Ranking	Hidden units	Seed	Test error	Log predictive error
1	14	100	0.0764770	230.75
2	10	100	0.080370	222.37
3	11	100	0.082443	217.96
4	16	30	0.083116	228.67
5	6	30	0.083576	218.03
6	8	100	0.083781	217.81
7	13	10	0.083790	220.32
8	15	30	0.084411	221.84
9	13	100	0.085464	218.76
10	6	10	0.086566	218.26

Table 5.4 : Test errors of the committees. Notice that the test error of the best committee is less than that of the single best model.

Number of models in committee	Test error
1	0.07648
2	0.07309
3	0.07128
4	0.07137
5	0.07104
6	0.07170
7	0.07221
8	0.07257
9	0.07322
10	0.07403

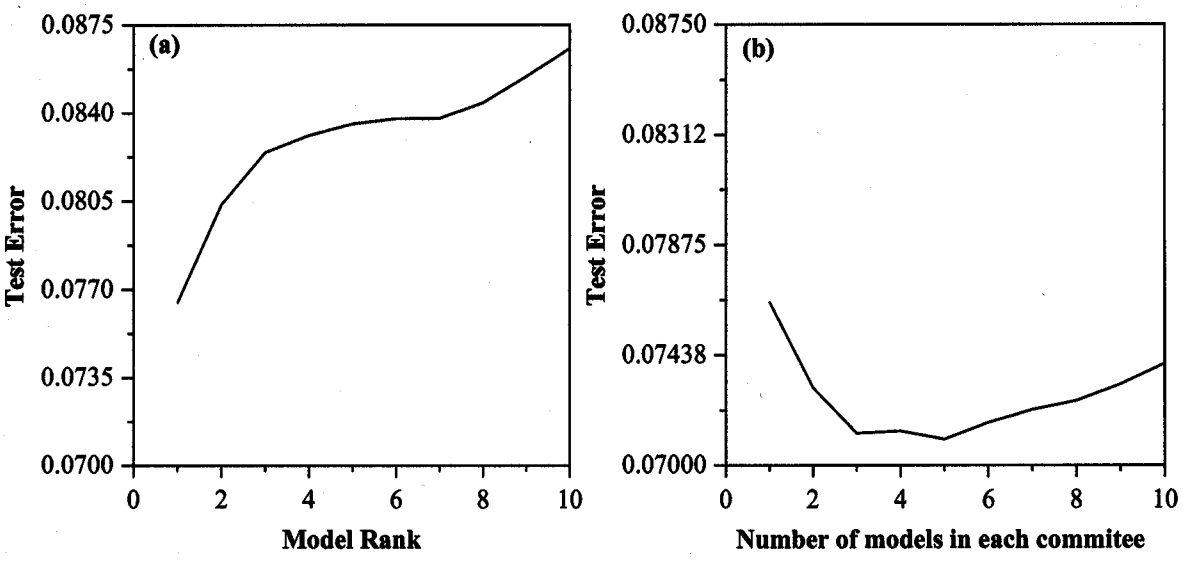

Figure 5.6 : (a) Test errors of the top ten of yield strength models; and (b) corresponding test errors for the commitee models.

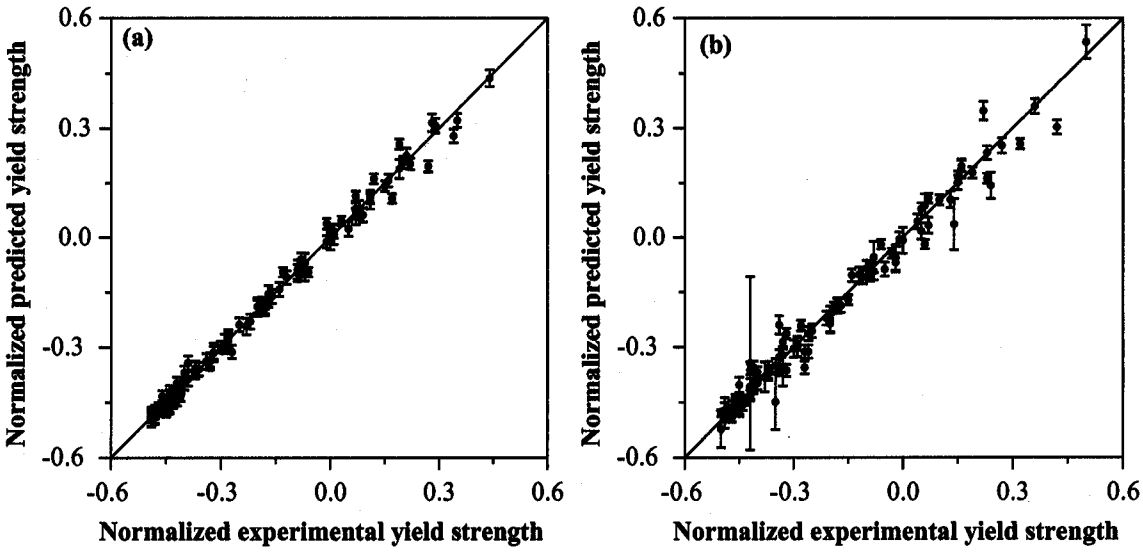

Figure 5.7 : Predicted versus experimental results using single best model. (a) training dataset, (b) test dataset.

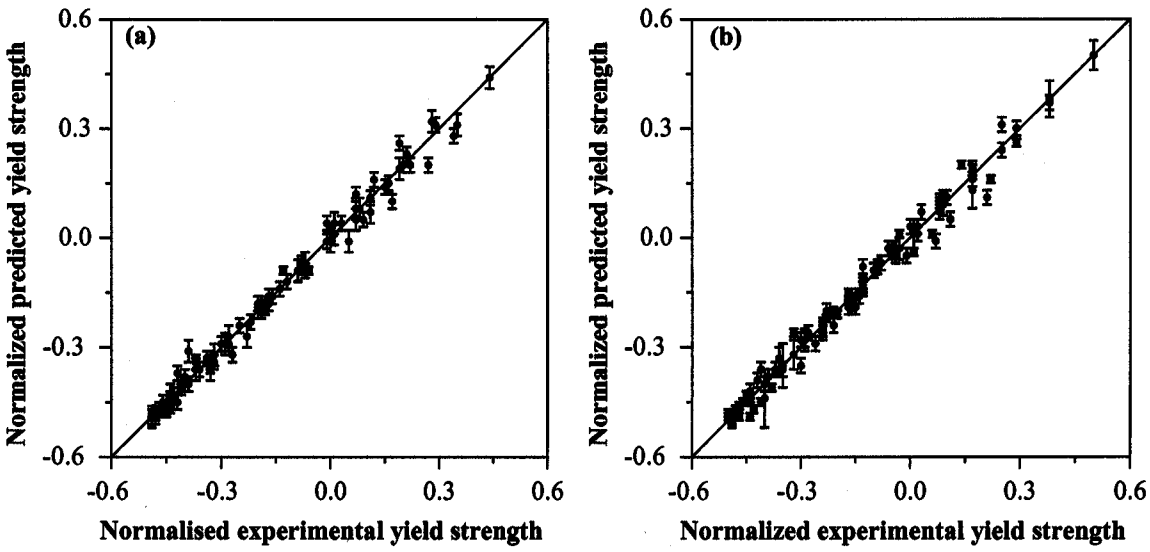

Figure 5.8 : Predicted versus experimental results using the optimum committee. (a) training dataset, (b) test dataset.

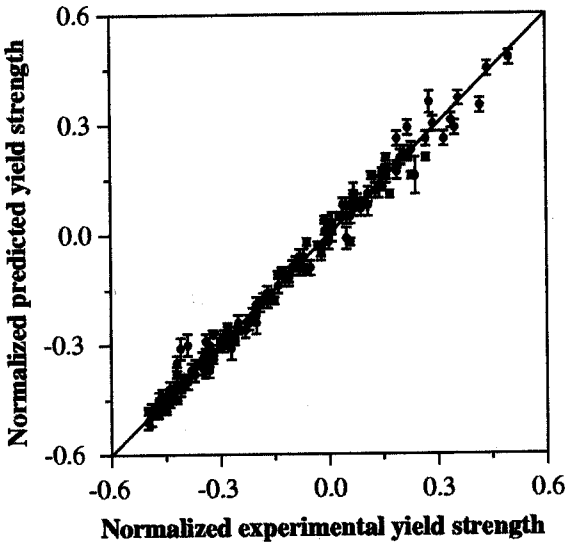

Figure 5.9 : Predicted versus experimental results for the whole dataset after retraining, using the optimum committee.

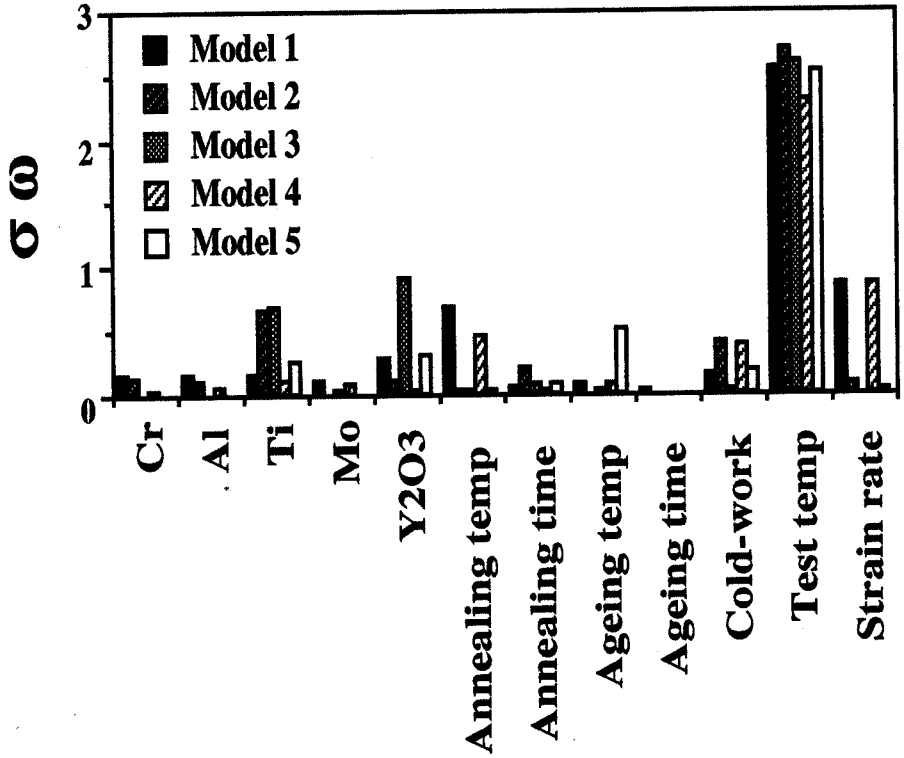

Figure 5.10 : The model-percieved significance of the input parameters for the committee model trained on all data. The σ_w value for all the members of the committee are presented for each of the variables.

5.8 The ultimate tensile strength model

The neural network technique was applied to the ultimate strength data shown in Table 5.5. The variables are identical to those used for the yield strength analysis. It would ideally be interesting to include the strain hardening coefficient since this determines the plastic instability which defines the ultimate strength. However, such data were not found at all in the published literature. There were 12 input variables and one output variable, the ultimate tensile strength. A total of 232 data were used. The data were divided equally and randomly into a 'test' dataset and a 'training' dataset. The 'training' dataset was used to train the model and the ability of the model to generalise was examined by checking its performance on the unseen 'test' data.

Table 5.5 : The variables used in the analysis of the ultimate tensile strength.

Variable	Range	Mean	Standard Deviation
Chromium, wt%	13-20	17.19	3.22
Aluminium, wt%	0-4.5	2.54	2.24
Titanium, wt%	0.5-3.50	1.1	0.87
Molybdenum, wt%	0-1.5	0.37	0.58
Yttria, wt%	0-0.5	0.41	0.15
Recrystallization temperature, °C	20-1330	684	594
Recrystallization time, s	0-120	27.56	33.24
Ageing temperature, °C	20-800	174.7	311.7
Ageing time, s	0-2888	361	781
Cold work, %	0-70	10.47	19.71
Test temperature, °C	0-1200	561.1	347.6
Strain rate, s^{-1}	0.00000003-0.03	0.0011	0.0025
UTS, MPa	70.7-1680	575.3	407.3

Figure 5.11 shows the plot of σ_ν versus hidden units. As expected, the inferred noise level decreases monotonically as the number of hidden units increases.

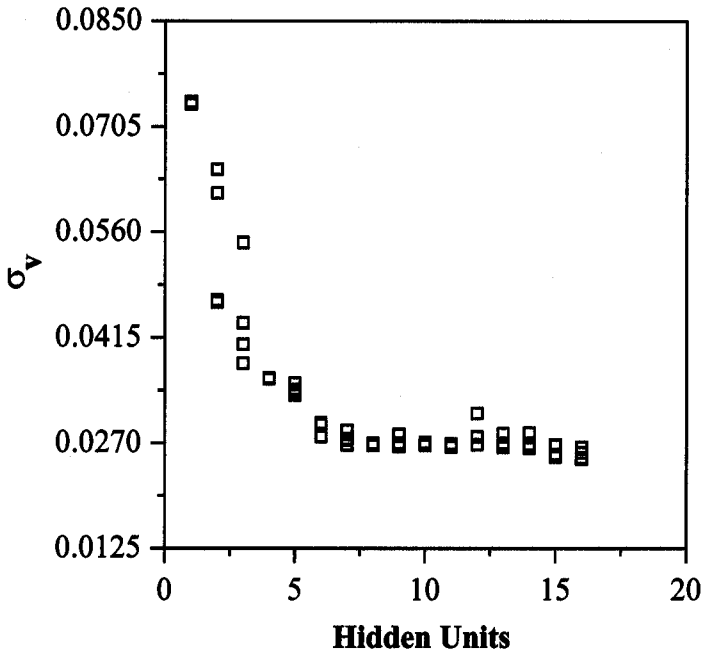

Figure 5.11 : Variation in σ_ν as a function of hidden units. Several values are presented for each set of hidden units because the training for each network was started with a variety of random seeds.

Figure 5.12 show the variation of test error and log predictive error as functions of the number of hidden units. The calculated test error goes through a minimum at 16 hidden units and the log predictive error also goes through a maximum at the same number of hidden units. This would have been the optimum model if a single model were to be used for the analysis.

A committee model was used. Based on the values of the test error and log predictive error, four models were selected as best. The models were ranked using their test error values as shown in Table 5.6.

The optimum number of models in the committee was determined from the calculated validation errors of the different possible committees. Figure 5.13 shows the variation of the test error of the best models

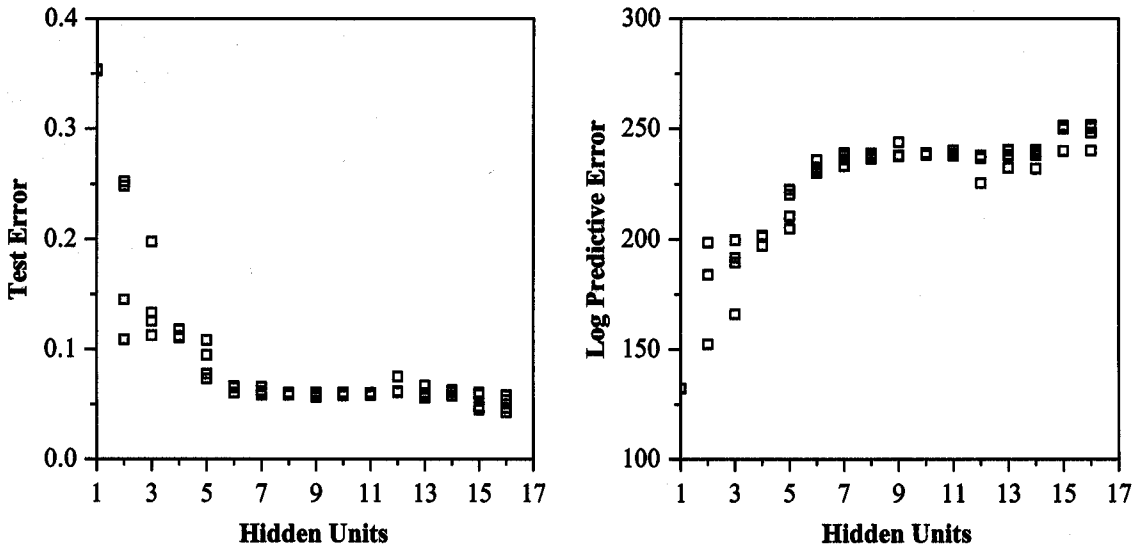

Figure 5.12 : Variation in test error and in log predictive error as functions of the number of hidden units.

Table 5.6 : Ranking by test error for the four best models of ultimate strength .

Ranking	Hidden units	Seed	Test energy	Log predictive error
1	16	30	0.042786	250.73
2	15	30	0.045090	250.15
3	16	100	0.046607	250.49
4	15	100	0.047735	251.45

as a function of their position on the ranking table and the test error of the commitees as a function of the number of models. It is evident that forming a commitee reduces the test error, and hence improves predictions.

As shown in Fig. 11 the commitee that is made up of the top three models shows the least test error and was used for the analysis. The agreement between the predicted and experimental values for the training and test datasets are shown in Figures 3.14 and 3.15 for the single best model and the committee respectively.

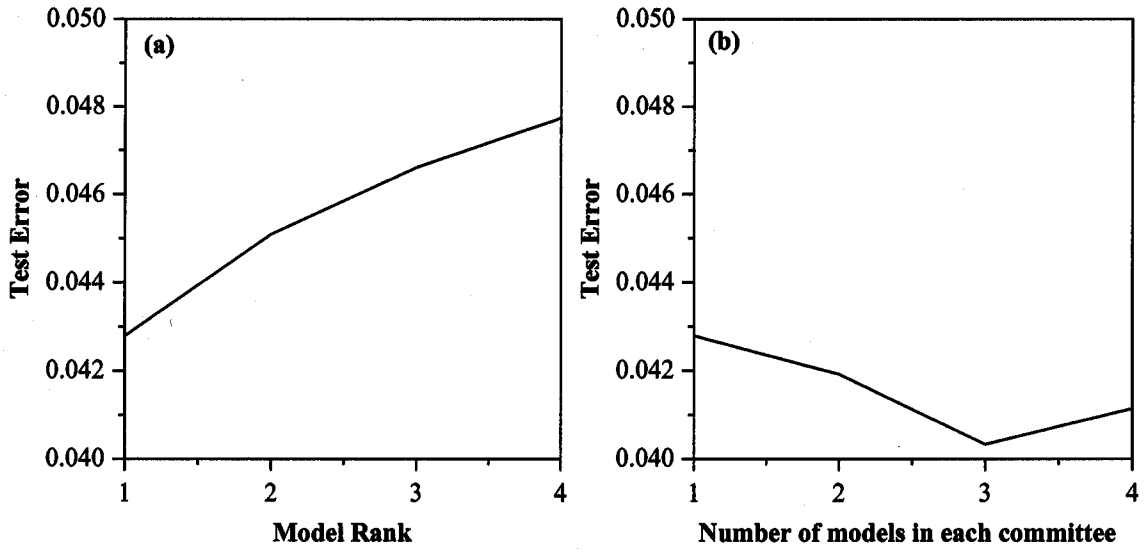

Figure 5.13 : (a) Test error of the four best ultimate tensile strength models and, (b) corresponding test errors for commitees of models.

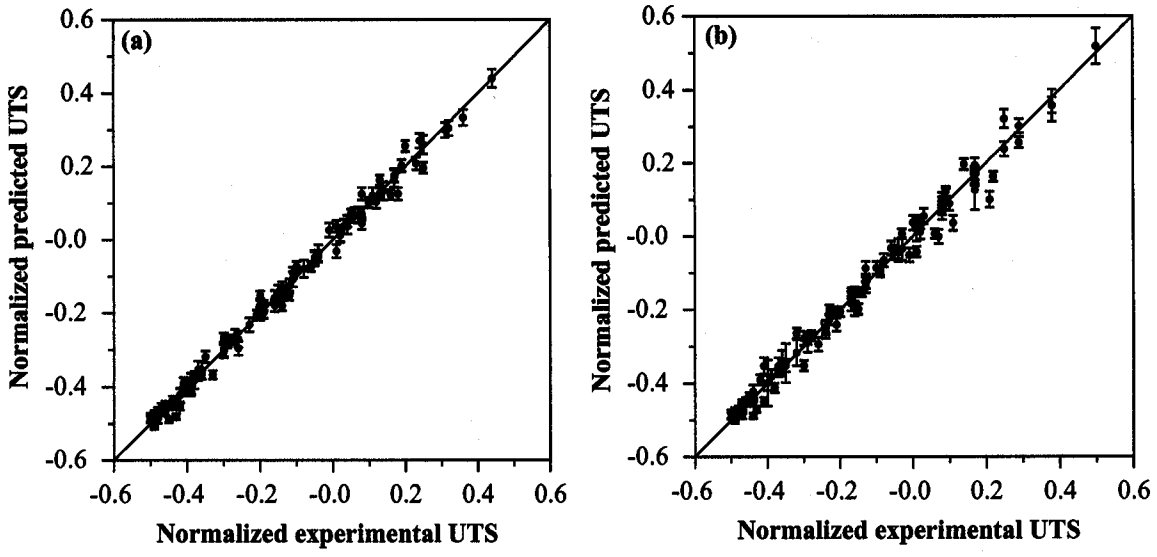

Figure 5.14 : Predicted versus experimental results using the single best model. (a) training dataset (b) test dataset.

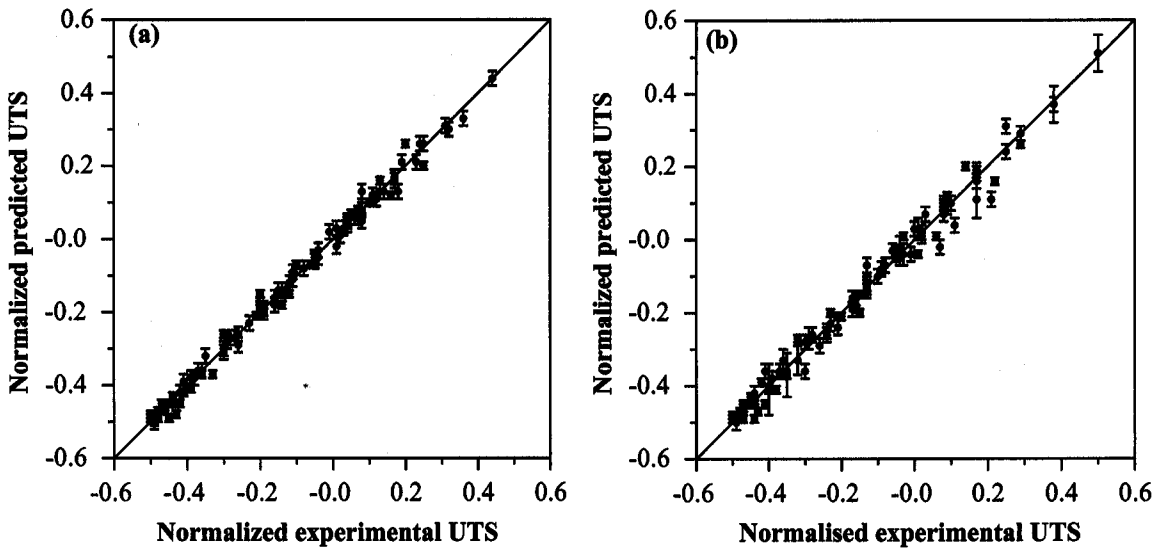

Figure 5.15 : Predicted versus experimental results using the optimum committee. (a) training dataset (b) test dataset.

The committee models were then retrained on the whole dataset beginning with the weights determined from the previous training exercise. Figure 5.16 shows the plot of the predicted values versus experimental values of the whole dataset after the retraining. The retraining is shown to have significantly improved the model with the reduction in error bars and the apparent absence of outliers.

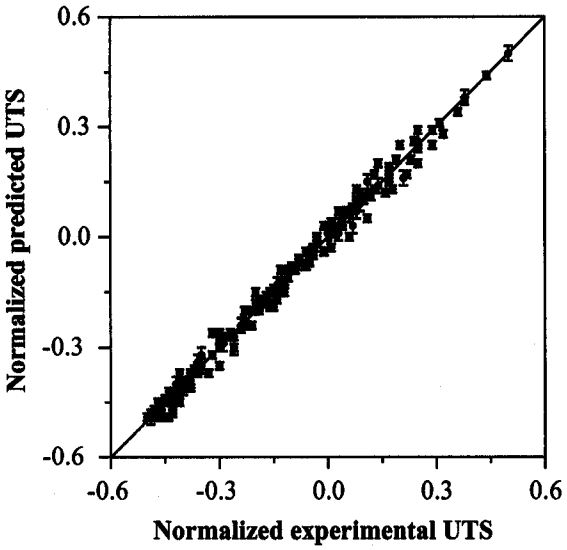

Figure 5.16: Predicted versus experimental results for the whole dataset after the retraining using the committee.

The perceived significance of each of the input variables by the various models contained in the committee is shown by σ_w in Figure 5.17 . The test temperature is shown to have the largest σ_w for all the three models in the committee. This shows the models have recognised a correct pattern because temperature is mostly varied than any other input in the database. Moreover, temperature is known to affect strength very significantly.

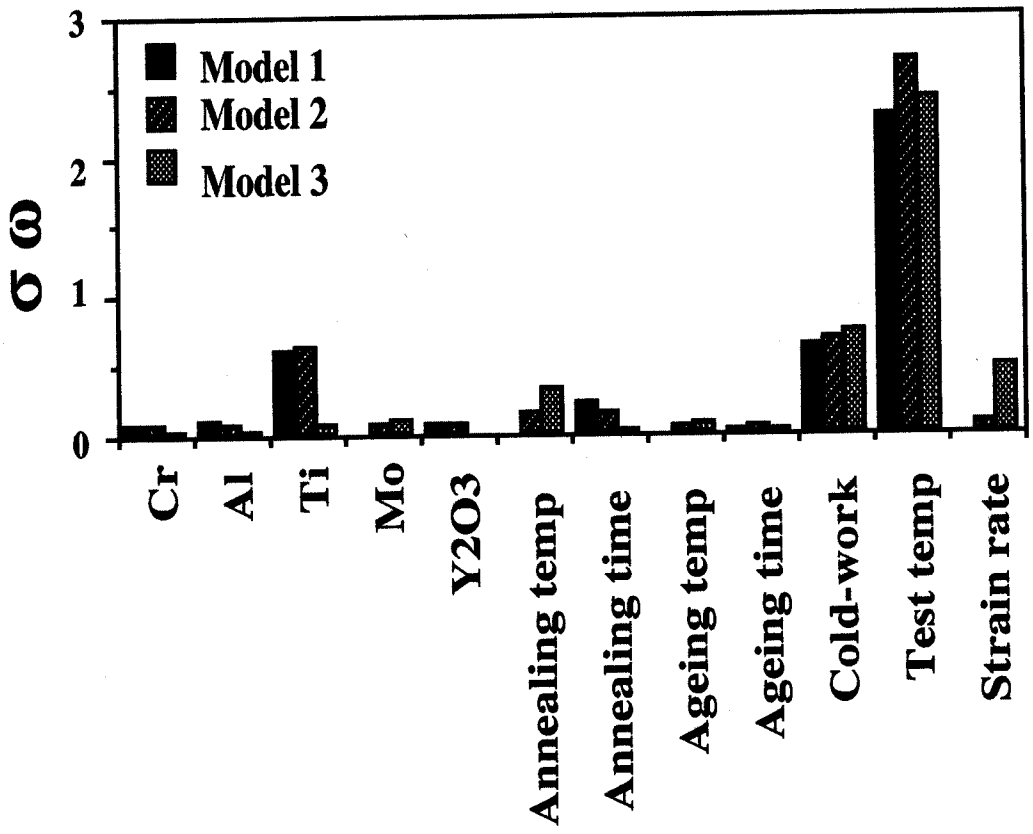

Figure 5.17: The model-percieved significance of the input parameters for the committee model trained on all data. The σ_w value for all the members of the committee are presented for each of the variables.

5.9 Elongation model

The ultimate tensile strength and yield strength were included as input variables in addition to the 12 input variables used in the strength analysis (Table 5.7). The inclusion of the strength parameters became necessary after the initial attempts to train the network without the parameters failed to produce good result. The reason for this behaviour is obvious, ductility of a material is a function of strength. The database consists of 232 examples and the noise level in the data is as plotted in Figure 5.18. Test error and log predictive error as functions of hidden units are shown in Figure 3.19.

Table 5.8 gives the numerical data of the ten best models ranked according to their log predictive errors. Though the ranking of the models was by their log predictable error the optimum committee was determined using the validation error. The test errors of the ten committees are shown in Table 3.9

Table 5.7 : The variables used in the analysis of elongation.

Variable	Range	Mean	Standard Deviation
Chromium, wt%	13-20	17.45	3.19
Aluminium, wt%	0-4.5	2.74	2.20
Titanium, wt%	0.5-3.50	1.02	0.86
Molybdenum, wt%	0-1.5	0.35	0.58
Yttria, wt%	0-0.5	0.42	0.15
Recrystallization temperature, °C	20-1330	729	585
Recrystallization time, s	0-120	28.92	33.72
Ageing temperature, °C	20-800	171	309
Ageing time, s	0-2888	354.8	778
Cold work, %	0-70	11.4	22.59
Test temperature, °C	0-1250	561.4	340.2
Strain rate, s^{-1}	0.00000003-0.03	0.0013	0.0027
UTS, MPa	70.7-1680	545	390
Yield strength, MPa	63-1600	468	367
Elongation, MPa	0.8-49.29	12.13	8.18

and Figure 5.20 shows the test error versus ranking of the best models and test errors of the committees.

As shown in Fig. 3.20(b) the commitee consisting of the top six models shows the least energy error and was therefore chosen as the optimum model. Figures 3.21 and 3.22 give the plots of the predicted values versus experimental values for the single best model and the committee respectively. The plot for the committee after retraining the committee models with the whole dataset is given in Figure 3.23.

Figure 5.24 shows the plot of σ_ν, the model percieved significance of the variables for the six models contained in the committee. Test temperature is shown to have a large effect on elongation. This is expected and it is exciting to note the consistency with the patterns shown in the yield and ultimate strength models. The percieved influence of yield strength on elongation is slightly higher than for ultimate tensile strength on elongation. This is expected metallurgically since it is the difference between the yield strength and UTS that relates to the uniform component of elongation.

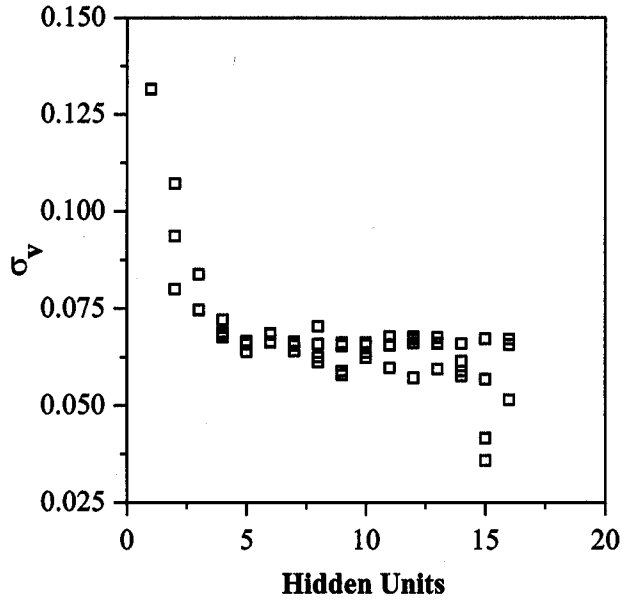

Figure 5.18: Variation in σ_ν as a function of hidden units.

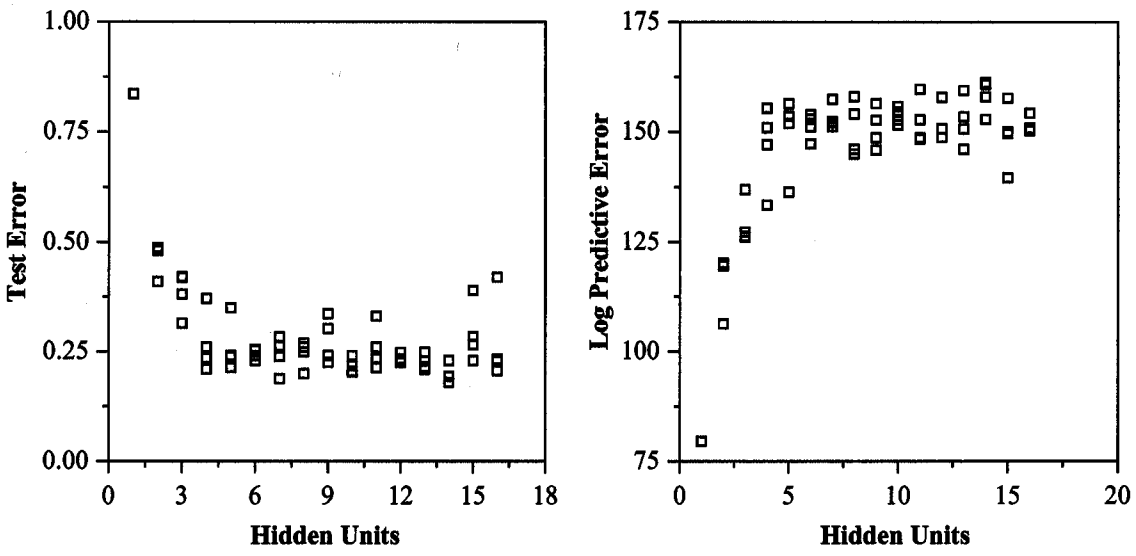

Figure 5.19: Variation in test error and log predicive error as functions of hidden units.

Table 5.8 : Ranking by log predictive error for the ten best models of the elongation

Ranking	Hidden units	Seed	Test error	Log predictive error
1	14	50	0.17988	161.23
2	14	30	0.19329	160.86
3	11	30	0.21316	159.76
4	13	50	0.20960	159.47
5	8	100	0.19966	158.05
6	7	50	0.18807	157.47
7	5	100	0.21390	156.42
8	4	30	0.21008	155.44
9	10	100	0.20382	155.81
10	10	10	0.20522	154.51

Table 5.9 : Test errors of the committees.

Models in committee	Test error
1	0.17987
2	0.17642
3	0.17930
4	0.17921
5	0.18035
6	0.17368
7	0.17504
8	0.17702
9	0.17639
10	0.17726

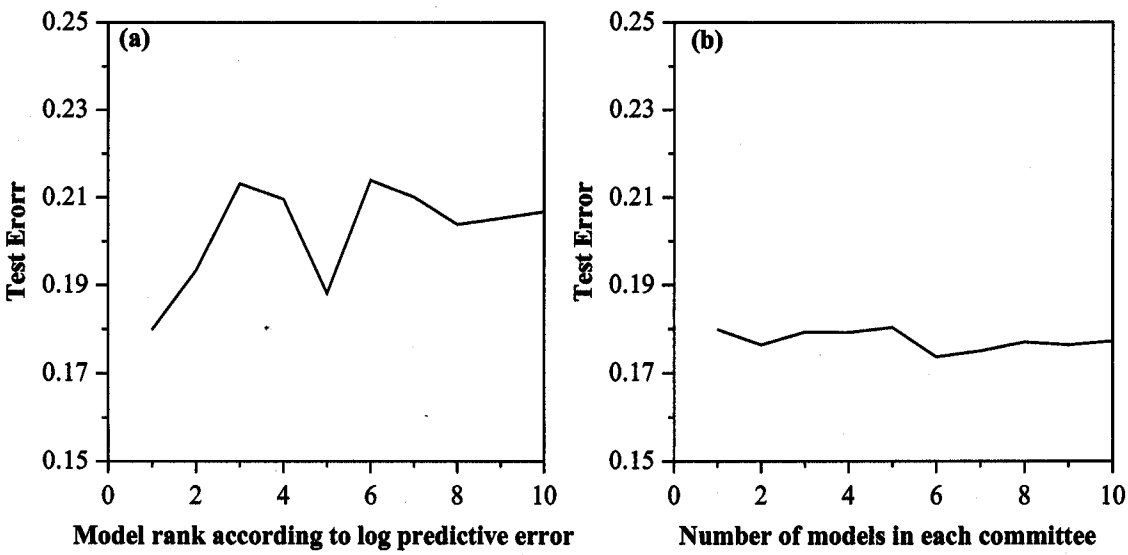

Figure 5.20: (a) Test errors of the top ten of the elongation models and, (b) corresponding test errors for commitees of models.

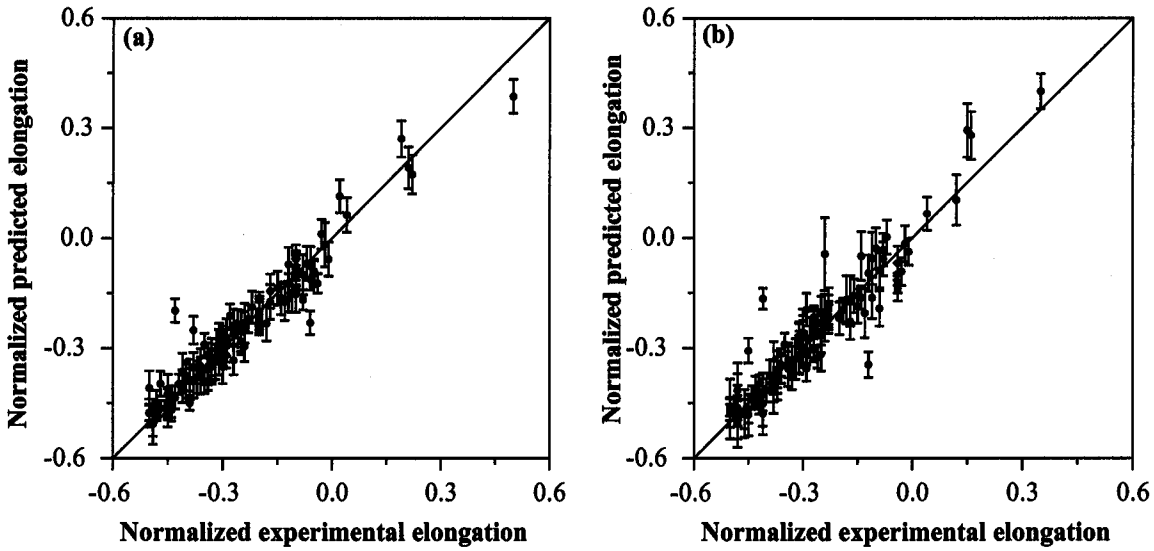

Figure 5.21: Predicted versus experimental results using the single best model. (a) training dataset (b) test dataset.

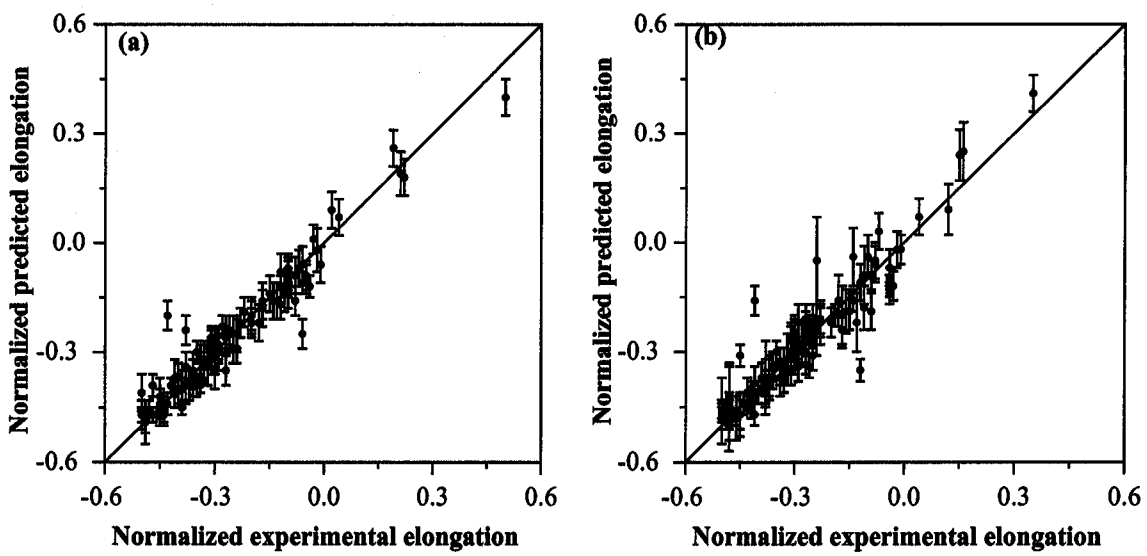

Figure 5.22 : Predicted versus experimental results using the optimum committee. (a) training dataset (b) test dataset.

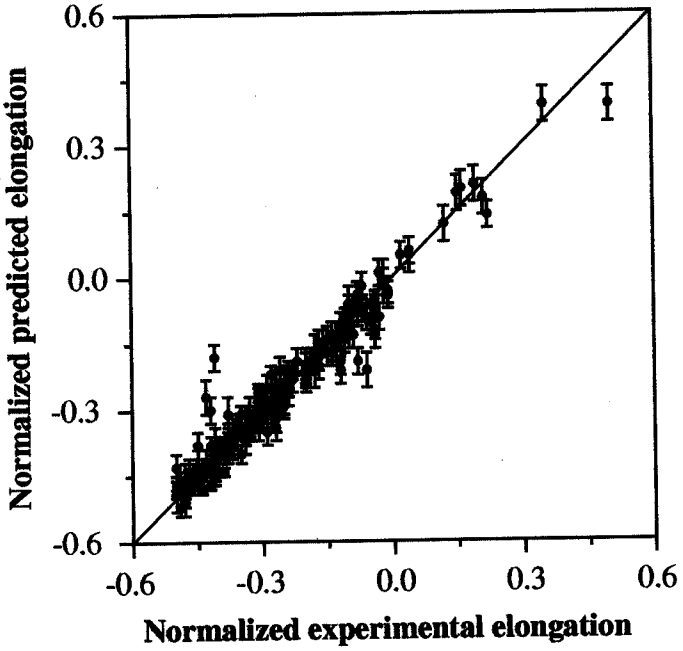

Figure 5.23 : Predicted versus experimental results for the whole dataset after the retraining using the committee.

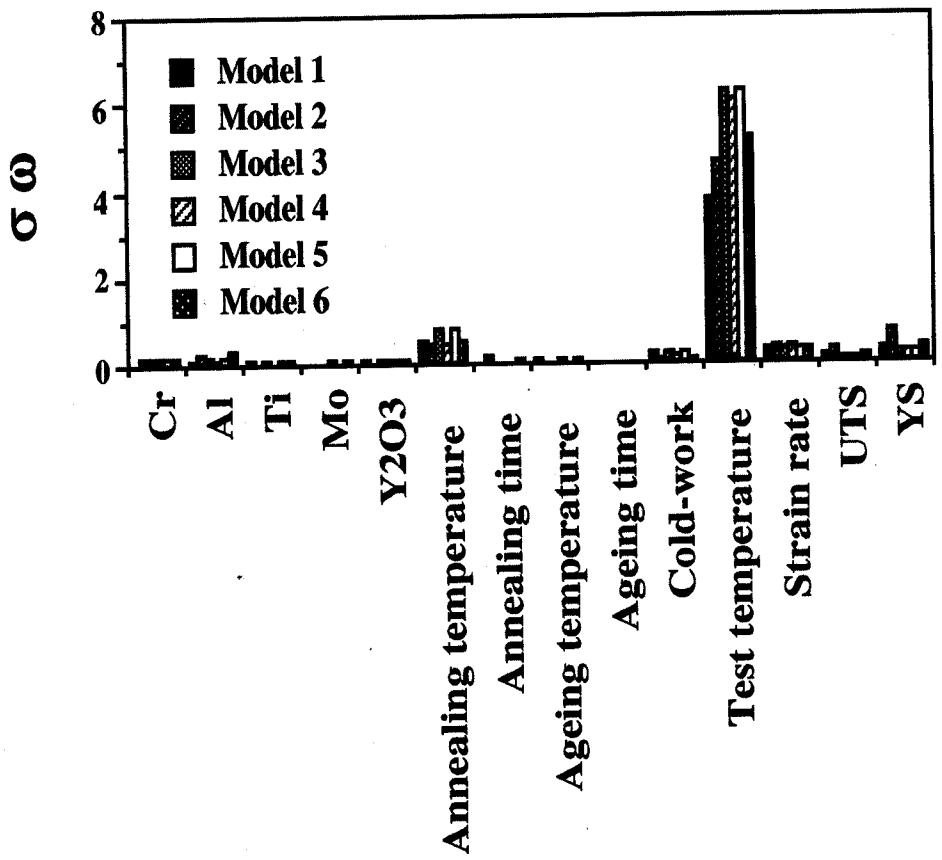

Figure 5.24 : The model-percieved significance of the input parameters for the committee model trained on all data. The σ_w value for all the members of the committee are presented for each of the variables.

5.10 Application of the models

Attempts were made to use the commitee models to predict the influence of the variables on the ultimate tensile strength, yield strength and percent elongation of the iron-base MA-ODS alloys and to see if the perceived relationships are reasonable from the point of view of the established metallurgical facts. All the results are presented along with the ± 1 standard deviation predicted error bars.

5.10.1 Effect of temperature

Figure 5.25 shows the predicted effect of test temperature on the ultimate strength, yield strength and elongation of MA956 for both recrystallized and unrecrystallised conditions.

The predicted patterns are quite reasonable. There is no significant fall in strength until around 500°C. Similarly, there isn't any noticeable change in elongation until precisely the same region of fall in strength when the elongation increases. This is consistent with the established facts that increasing temperature leads to decrease in strength and an increase in elongation. However, the sharp drop in strength and corresponding sharp rise in elongation is peculiar though well known [Alamo *et al.*, 1990, 1992; Regle, 1994]. An explanation that the sharp changes occur at a temperature where the dislocation density effectively drops would have been appropriate if the pattern had not been the same for both the recrystallized and unrecrystallized conditions. It may be the case that dislocations climb over the fine yttria particles becomes prominent in the regime where the sharp drop is observed. The alloy is seen to show higher percent elongation in the unrecrystallised condition than the recrystallised. This seems unusual as the alloys in the unrecrystallised condition are harder and would be expected to be less ductile. However, this result is consistent with the extensive experimental work by Alamo (1992) which indicates that it is the coarse columnar grain structure which leads to poor ductility in the recrystallised alloys.

The strengths and percent elongation of the various commercial MA-ODS ferritic steels are compared in Figure 5.26.

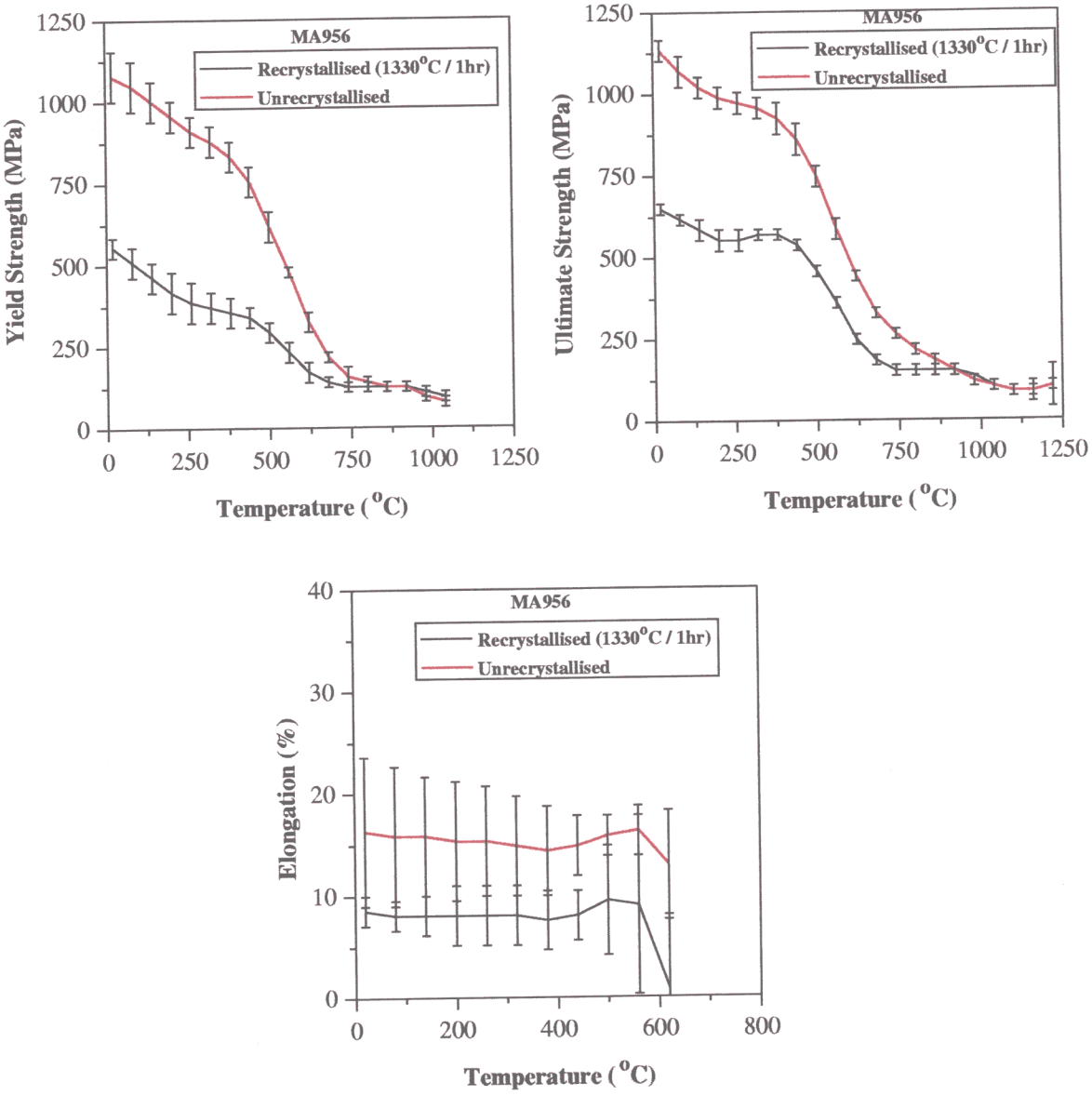

Figure 5.25: Effect of temperature on the yield strength, ultimate strength and percent elongation of MA956.

The heat-treatment conditions of the alloys are as for commercial applications. DT and DY are given ageing treatment to precipitate χ-phase for higher strength. This effect is correctly predicted with higher ultimate strength for DT and DY than MA956 which contains no χ-phase. DY contains yittria particles whereas DT doesn't and this explains the higher strength of DY than DT alloy. As shown the yield strength of MA956 is higher than DT despite the fact that DT contains χ-phase. This is because of the yittria particles in MA956 and clearly demonstrates that the effect of dispersoids strengthening

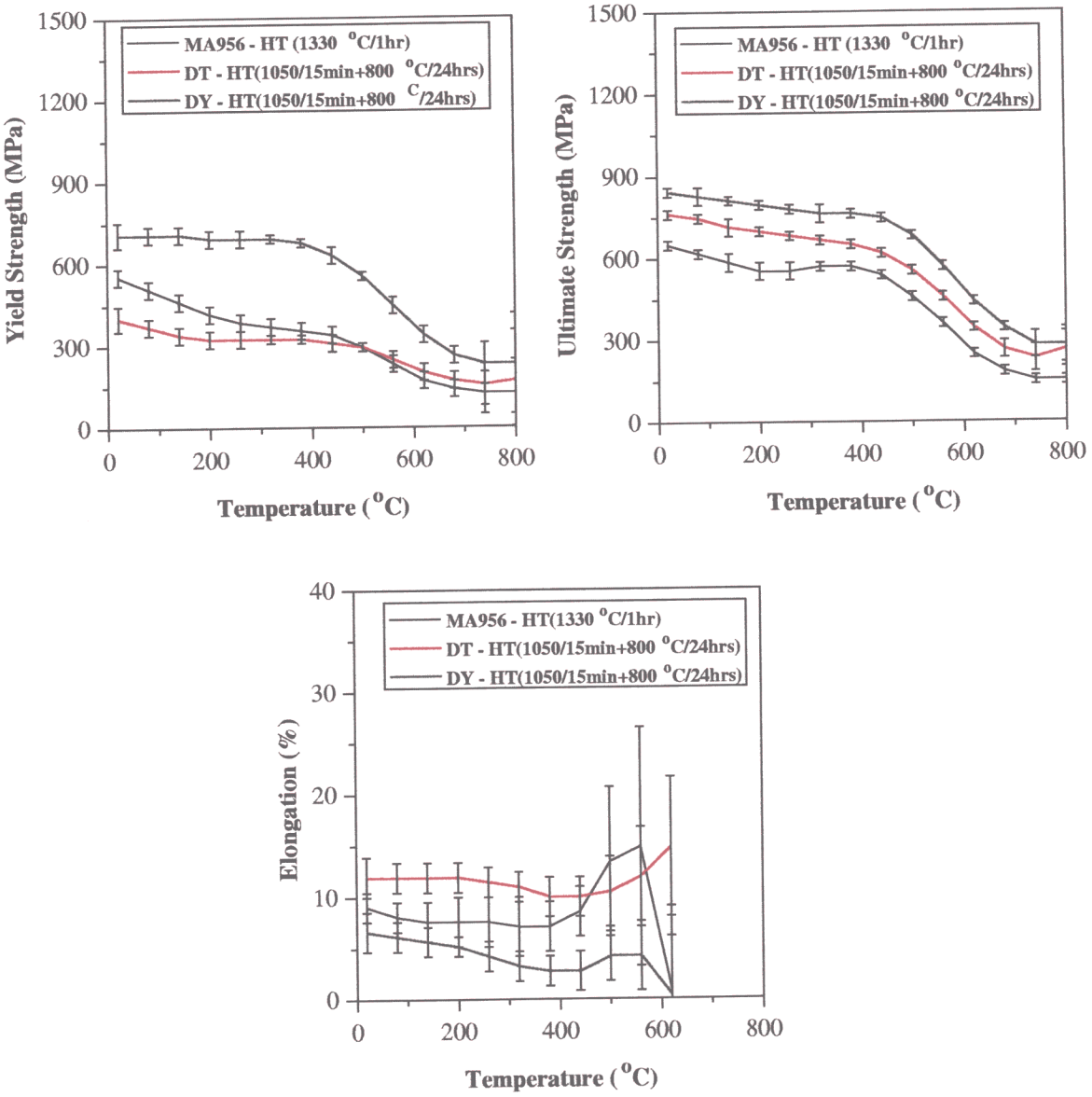

Figure 5.26: Comparison of the predicted properties of some MA-ODS ferritic steels.

is primarily on the yield strength rather than on the ultimate strength. The plots of percent elongation further show the effects of dispersoids with DT showing a better ductility because yittria particles are not present. It can then be summarized that yittria particles increases yield strength and reduces ductility and that the lower ductility in DY in which both χ-phase and yittria particles are present is as a result of the yittria particles.

5.10.2 Effect of Titanium, Molybenum and Yttria content

Figure 5.27 shows the effects of titanium, yittria , and molybdenum on the ultimate strength, yield strength and elongation of MA956. The ultimate strength and yield strength increase with weight percent content of titanium, elongation, however, appears insensitive. The increase in strength with increasing titanium is supposed to be via χ-phase but this is not formed in MA956, in which the titaninum solid solution strengthens, thus affecting both the ultimate and yield strength almost equally. The effect of yittria content is slightly more pronunced on the yield than the ultimate tensile strength, though the error bars are large. The bar charts of the model percieved significance of variables for the ultimate strength and yield strength in Figures 3.10 and 3.17 respectively, agreeably show a higher yittria effect for the yield strength than the ultimate strength. The results of an experimental work by Kawasaki *et al.*(1996) on the effect of dispersoids on tensile deformation of Fe-20Cr ODS alloys has helped to establish the reliability of the predicted patterns. Addition of ytrria particles was reported [Kawasaki, *et al.*, 1996] to increase the 0.2% yield stress all over the experimental temperature range (300–1073 K) and that at higher temperatures than 673 K, the increament of work hardening due to the dispersoids is small. The ultimate tensile strength is a function of work hardening and this probably explains why the predicted effect of dispersoids on the ultimate tensile strength is generally smaller than for the yield strength. These predicted behaviours with respect to titanium and yittria concentrations are significant as they seem to corroborate the explanation given earlier for the predicted tensile properties of the different MA-ODS steels. Titanium through χ-phase is responsible for the higher ultimate strength of DT and DY than MA956. The higher yield strength of MA956 than DT and the higher ductility of DT than MA956 and DY is because of the yittria particles in MA956 and DT. Strength and elongation are shown to be insensitive to molybdenum content in MA956. Apart from being a solid solution strengthener, molybdenum is a constituent in χ-phase and as such increasing its concentration is expected to contribute positively to strength. However, the titanium level upon which formation of χ-phase depends is very low in MA956 compared to the levels in the alloys where χ-phase is formed so

increasing molybdenum concentration may not have any effect. The model seems to have recognised correct patterns.

5.10.3 Effect of Chromium and Aluminium

The predicted effects of chromium and aluminium on the tensile properties of MA956 are shown in Figure 5.28 . Changes in concentration have negligible effects on the strength and elongation of MA956. However, the error bars are so large that it is not possible to reach a satisfactory conclusion. Large error bars occur either due to noisy data or due to sparce data. It is suspected that both of these factors are responsible for the lack of a significant relationship for chromium or aluminium.

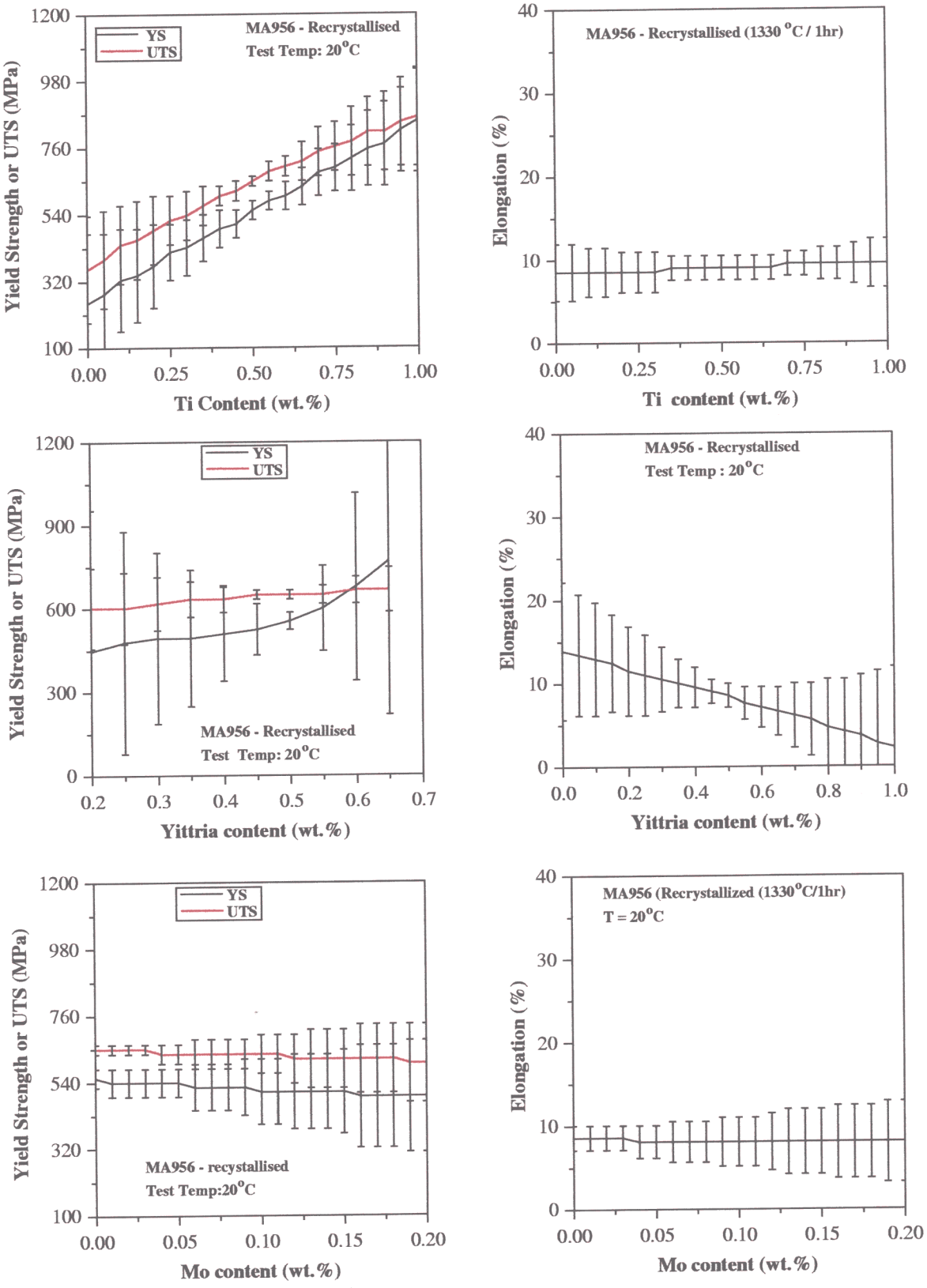

Figure 5.27 : Predicted effect of titanium, yttria and molybdenum on the yield strength, ultimate strength and percent elongation of MA956.

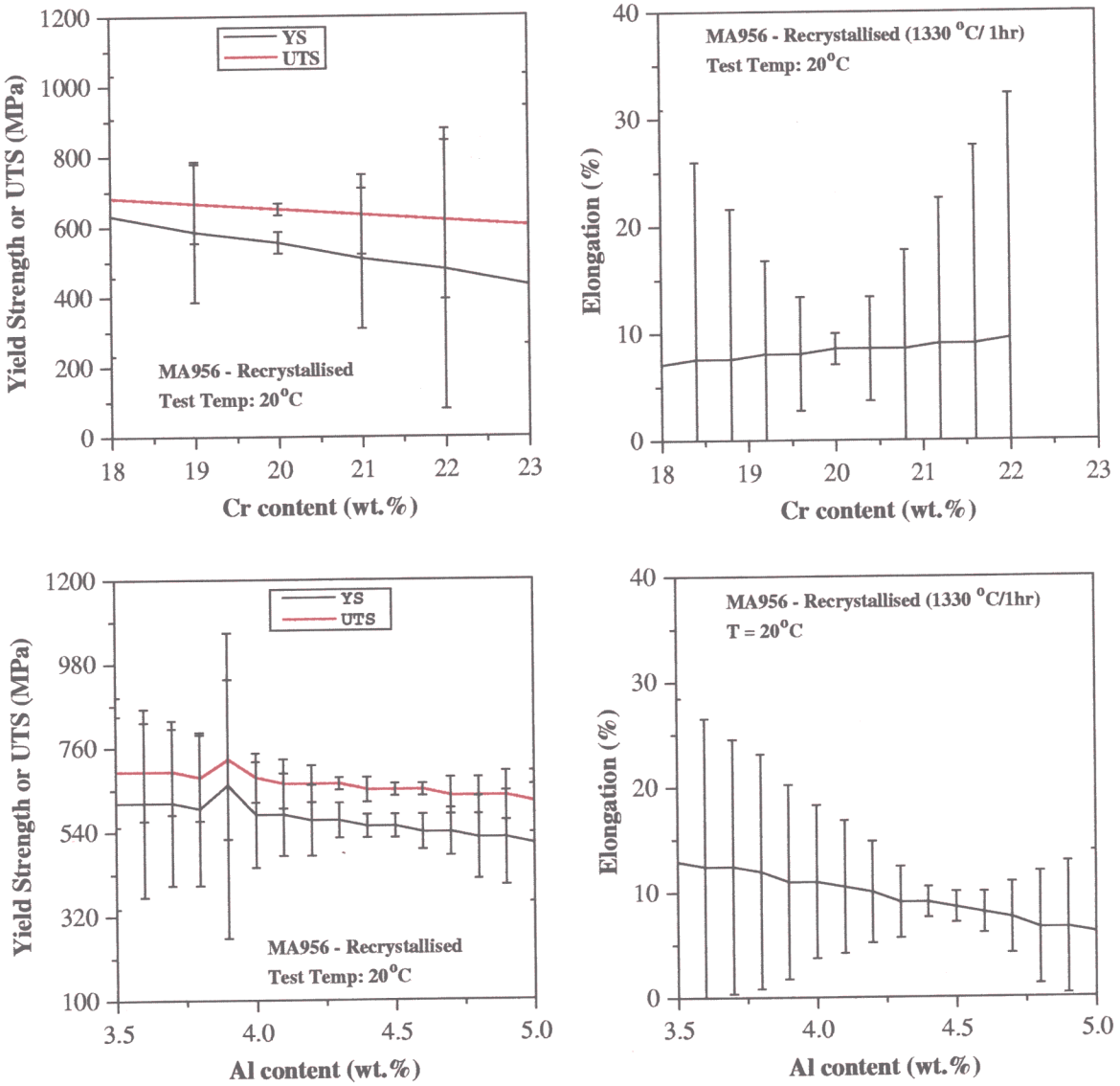

Figure 5.28 : Predicted effect of chromium and aluminium on the yield strength, ultimate strength and percent elongation of MA956.

5.10.4 Effects of recrystallisation temperature and time

The effects of the recrystallisation temperature and recrystallisation time on the ultimate strength, yield strength and elongation are shown in Figure 5.29 . As expected the ultimate strength and yield strength decrease with increasing recrystallisation temperature and time whilst the elongation increases.

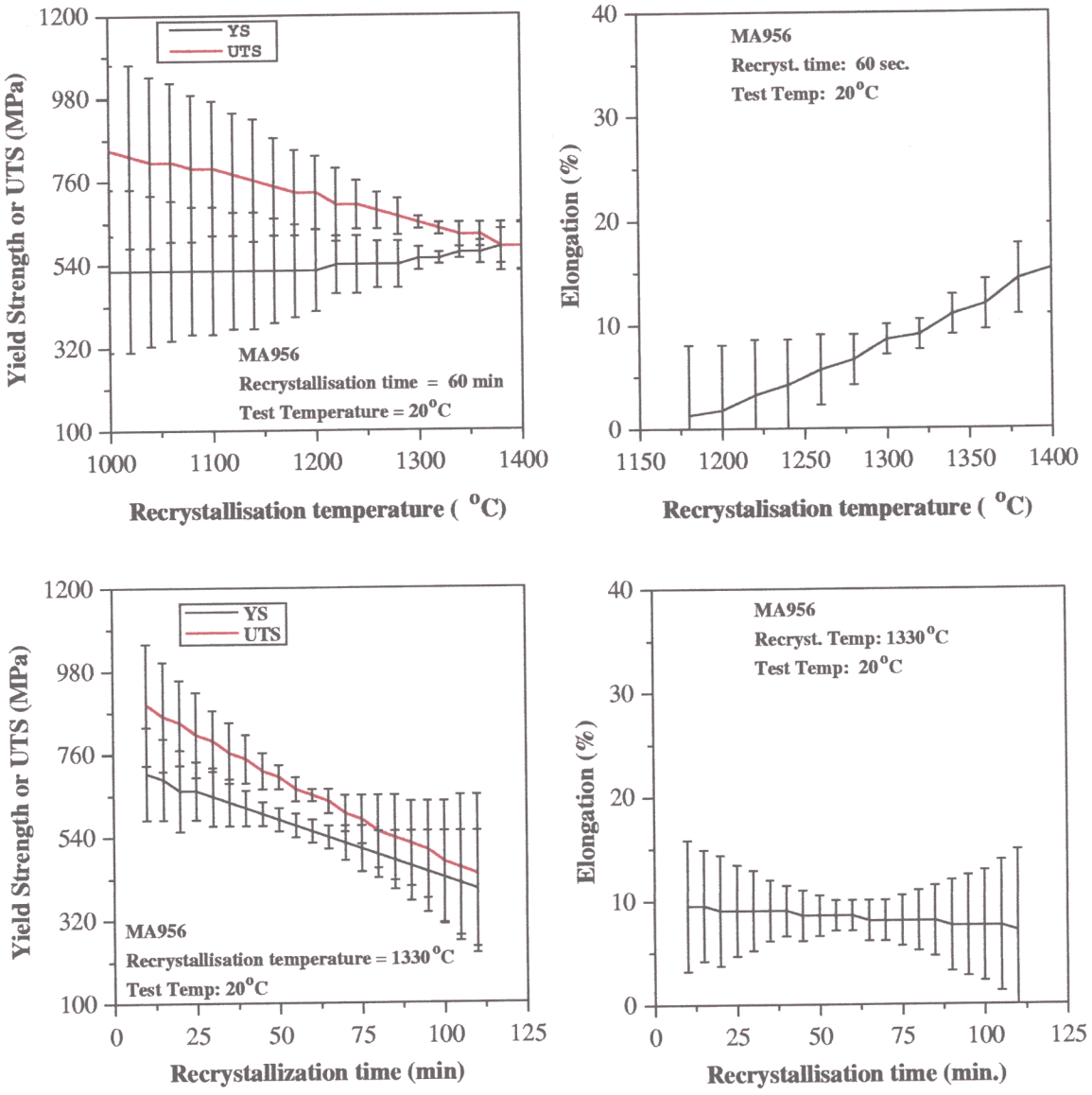

Figure 5.29 : Effects of recrystallisation temperature and recrystallisation time on the tensile properties of MA956.

5.10.5 Effects of cold-work and strain rate

Figure 5.30 shows the the predicted effects of cold-work and strain rate on the ultimate strength, yield strength and elongation of MA956. As expected, increasing cold-work increases the ultimate strength and the yield strength and saturation level is predicted above which further cold-work does not lead to increase in strength. Though the error bars are large for the elongation, the predicted pattern is what is expected, decreasing ductility with increasing cold-work. The large error bar is due to the reason that there is very limited examples where cold-work is varied in the database. The strength and elongation

are shown to be insensitive to low strain rate but at high strain rate, strengths increase and elongation decreases accordingly with increasing strain rate. These results are in excellent agreement with the report of an experimental work by [Whittenberger, 1979].

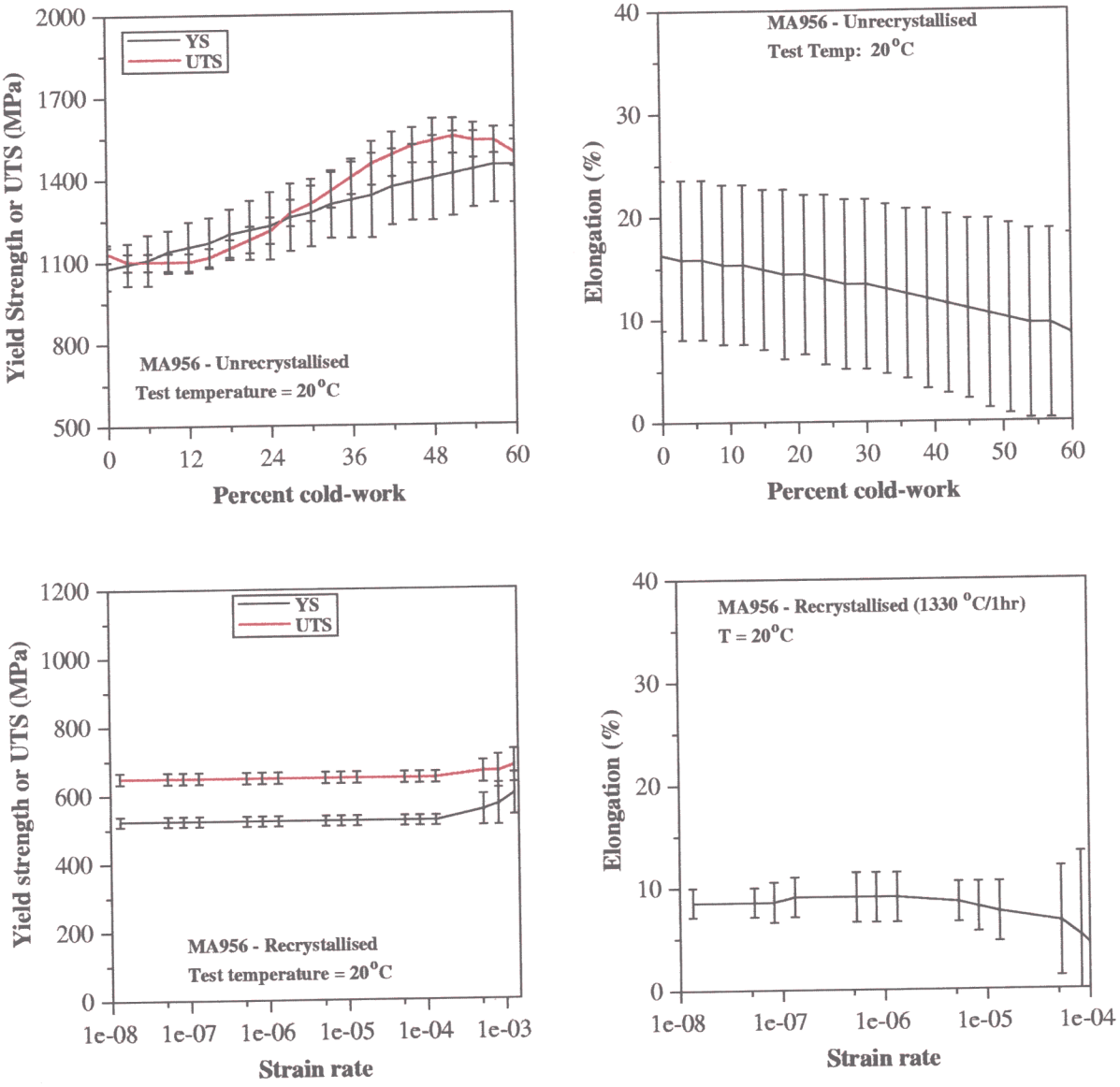

Figure 5.30 : Effects of cold-work and strain rate on the tensile properties of MA956.

5.11 Summary

Tensile properties data for mechanically alloyed, oxide dispersion strengthened ferritic stainless steels have been analysed using a neural network technique within a Bayesian framework. The analysis, though empirical, can after appropriate training and with the use of committee of models, produce results which are metallurgically reasonable.

Our experience of the neural network method suggests that it has considerable potential for useful applications in materials science. It is particularly useful in circumstances where there is extreme complexity, such that physical models are not available to construct within a reasonable time scale.

Neural networks are frequently used for regression problems in which continuous variables are modelled. They can also be applied to classification problems where the variables to be predicted adopt discrete values [Ichikawa, *et al.*, 1996].

The technique is extremely powerful; it can in principle produce a model for a random set of points. There are many models available, for example, on the world-wide web or from commercial sources. Care must however, be taken to select those which have a good strategy for avoiding the problem of overfitting the data. Methods in which the error bar depends on the position in the input space are particularly safe.

Finally, the neural network, like all regression methods, is a purely mathematical tool which cannot necessarily distinguish between cause and effect. The selection of proper inputs and outputs is important in deducing physically sound relationships.

CHAPTER SIX

Physical Interpretation of the Yield Strength of Mechanically Alloyed ODS Iron Alloys

6.1 Introduction

In Chapter four, an empirical neural network analysis of the mechanical properties of mechanically alloyed iron–base ODS alloys was presented as a function of a large number of variables. The neural network analysis produced models which are non–linear and incorporate interactions between variables. Such models are extremely useful in alloy design and data interpretation, but any model which includes a large number of interacting variables becomes difficult to interpret using the principles of physical metallurgy. This is because the latter are simple in the context of sophisticated industrial alloys, but in some circumstances can nevertheless give great insight and understanding on a level which is easier to picture.

The neural network analysis dealt with the yield and ultimate tensile strength and the elongation. Of these, the yield strength should be the best behaved mechanical property given that the other two rely on complex phenomena related to large degrees of homogeneous and inhomogeneous deformation. The purpose of the work reported in this Chapter was, therefore, to attempt a better *physical* understanding of the yield strength of the mechanically alloyed ODS materials.

MA 956, which is the focus of the present work, is a ferritic MA–ODS steel with the nominal composition Fe–20Cr–4.5Al–0.5Ti–0.5Y_2O_3 wt.%. It is strengthened against creep by a highly stable fine dispersion

of yttrium oxide [Benjamin, 1970; Benjamin and Cairns, 1971]. By conventional standards, this dispersion changes little even as the melting temperature is approached. In the as-extruded condition, the alloy has a microstructure with less than one micrometre grain size and a grain aspect ratio of about 30, while in the recrystallized condition the grain size is about 10–50 μ m and the aspect ratio is about 10 [Alamo *etal.*, 1992]. The yttria particles added to the starting powders react with aluminium and oxygen from the solid solution to form very fine dispersions of mixed (Y, Al) oxides [Cama and Hughes, 1994]. The average dispersoid diameter in the as–extruded condition is about 11 nm [Regle, 1994].

The essential problem which is addressed in this Chapter is the results of neural network analysis, summarised in Figure 6.1 which shows the variation in the yield strength of recrystallised and unrecrystallised MA956 as a function of the temperature. The curves represent a best–fit empirical interpretation of a large quantity of experimental data with the caveat that overfitting has been avoided as explained in Chapter 4. The error bars correspond to $\pm 1\sigma$ and give an indication of the uncertainty in the experimental data as well as the uncertainty in interpretating those data. The major aim of the work presented here is to explain the curves in Figure 6.1 on the basis of strengthening theories.

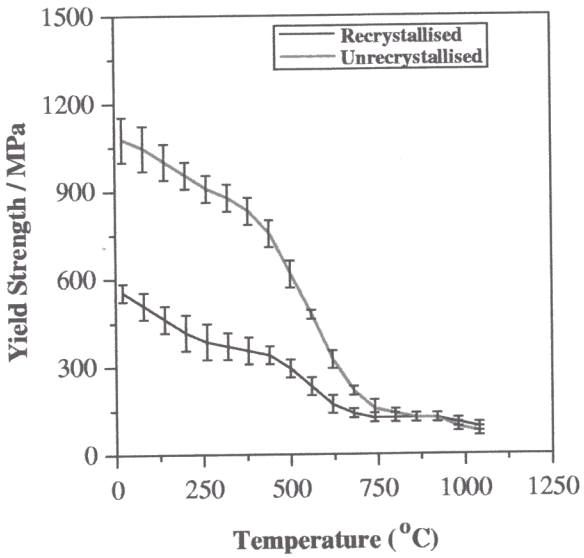

Figure 6.1 : Neural network predictions for the yield strength of the recrystallized and unrecrystallized MA956 [Chapter 4].

6.2 Strength of Recrystallized MA956

It is usual to express the yield strength as a linear combination of contributions from a number of mechanisms using the approximation that these mechanisms are essentially non–interacting:

$$\sigma_y = \sigma_{Fe} + \sigma_s + \sigma_p + \sigma_g + \sigma_d \tag{6.1}$$

where

σ_{Fe}	is the strength of the pure, annealed matrix,
σ_s	is solid solution strengthening,
σ_p	is the particle strengthening,
σ_g	is the grain boundary strengthening,
σ_d	is the dislocation strengthening.

The yield strength σ_{Fe} of pure, annealed iron at room temperature was calculated as in [Young and Bhadeshia, 1994] with the temperature dependence according to the experimental results by Leslie (1972) who studied interstitial–free Ti-gettered iron. Leslie also reported the temperature dependence of solid solution strenghtening by a number of solutes in iron. Although the concentrations he studied did not achieve the levels of interest in the present work, his data for 6 at.% solute were used to obtain the temperature dependence of solution strengthening for each solute. The absolute values of the room temperature solid solution strengthening were obtained from an empirical expression for fully recrystallised ferritic stainless steels (17–25 wt.% Cr) by Lewis and Pickering (1983):

$$\sigma_y = 36 + 8.5(\text{wt.\% Cr}) + 58(\text{wt.\% Mo}) - 107(\text{wt.\% Ti}) + 15.9d^{-\frac{1}{2}} \quad \text{MPa} \tag{6.2}$$

so that $\sigma_s = 8.5(\text{wt.\% Cr}) + 58(\text{wt.\% Mo}) - 107(\text{wt.\% Ti})$ MPa

The negative coefficient for Ti shows some effect of interstitial solutes [Lewis and Pickering, 1983]. Ti removes interstitial solutes as TiC or TiN.

Shewfelt and Brown (1977) modelled dispersion strengthening as a function of temperature assuming that the dislocations remain on their slip planes except when they are able to overcome the obstacles by

climb. Whether or not climb occurs depends on the strain rate and temperature. By comparing theory against experimental data (1974) they obtained

$$\sigma_p = \frac{Gb}{\lambda}\left[(0.51 \pm 0.01) + (0.12 \pm 0.02)\log\left\{\frac{\dot{\epsilon} k T R^2}{4\pi\rho b^2 a_v G\lambda D_o}\right\} + (0.052 \pm 0.009)\left(\frac{Q}{kT}\right)\right] \quad \text{MPa} \tag{6.3}$$

where G is the shear modulus, b is the Burgers vector, D_o is the pre–exponential component of the self–diffusion coefficient of ferritic iron, Q is the activation energy for this self–diffusion coefficient, k is the Boltzmann constant, ρ is the dislocation density, $\dot{\epsilon}$ is the shear strain rate, R is the particle radius, λ is the square lattice spacing of the particles and a_v is the area associated with a vacancy. Table 6.1 shows the values of these parameters for MA 956 and the references where the information is from literature. The value for the particle spacing, λ, has been calculated using an expression by Kelly and Nicholson (1963):

$$\lambda = \sqrt{\frac{2\pi}{3}}\left(\frac{R^2}{f}\right)^{\frac{1}{2}} \tag{6.4}$$

where R is the particle radius, and f is the volume fraction of particles. The area associated with a vacancy was calculated using $a_v = \pi(b/2)^2$.

Table 6.1 : Parameters for the particle strengthening calculation. a is the lattice parameter of ferrite, taken as 2.87 Å

Parameter	Value	Reference
Shear modulus, G^*	80 GPa	Ubhi *et al.*, 1981
Burgers vector, b	$a\sqrt{\frac{3}{4}} = 2.485$ Å	-
Particle radius, R	5.695 nm	Regle, 1994
Dislocation density, ρ	10^{15} m^{-2}	Little *et al.*, 1991
D_o of α–Fe	5×10^{-5} m^2 s^{-1}	Honeycombe and Bhadeshia, 1995
Activation energy, Q	240000 J mol^{-1}	Honeycombe and Bhadeshia, 1995

The calculated components of strength are given in Table 6.2 and are illustrated as functions of temperature in Figure 6.2a for recrystallised MA956. It is seen that the major contribution is from the

to float off. The remaining particles coagulate and segregate making them ineffective as strengthening dispersoids†. At the same time, the other strengthening terms are unaffected by this procedure when the comparison is with a recrystallised MA956 sample.

Arc melting might seem a drastic method to eliminate dispersoid strengthening. It is nevertheless necessary because the yttria is added because of its stability in iron. Attempts to coarsen the dispersion would not only be ineffective but also unconvincing in the present context.

Figure 6.3 shows the optical microstructures and TEM of the replicas of the samples before melting and after melting. The optical micrographs show that the grain sizes of the two samples are comparable whereas the replica images show that the experiment has been successful in removing fine dispersoids from the melted sample. This is reflected in the measured hardness values which were found to be in the range 248–253 HV (mean 251 HV) and 188–196 HV (mean 192 HV) for the unmelted and melted samples.

† This is why yttria is not incorporated into the alloy by melting, but by mechanical alloying.

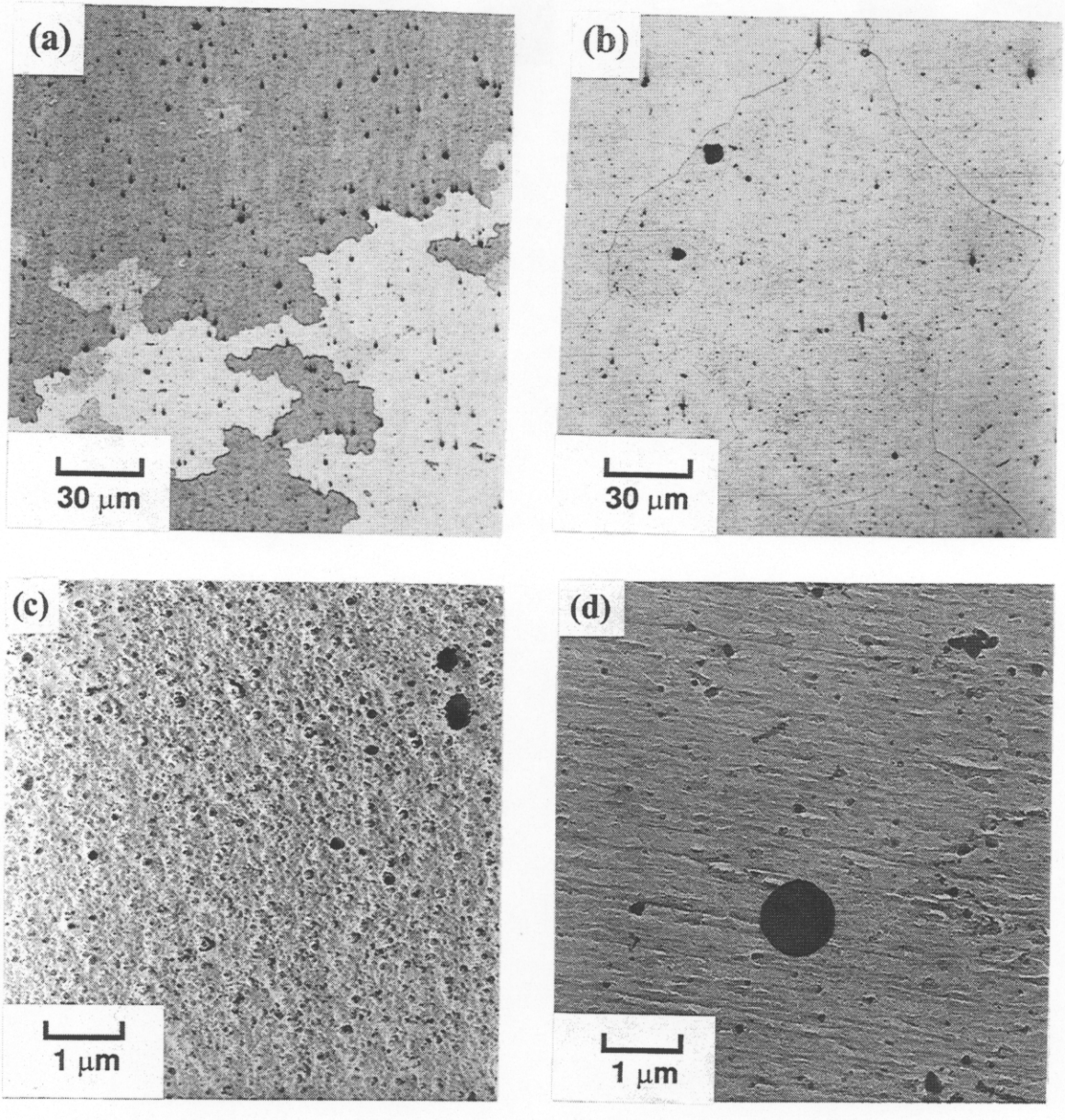

Figure 6.3: Optical micrographs of the samples of MA956 (a) before and (b) after melting. Corresponding TEM replica images of the samples of MA956 (c) before and (d) after melting.

Nominal stress/nominal strain curves are presented in Figure 6.4 which show that there is a reduction of 250 MPa in the yield strength for the melted sample. This is in remarkable agreement with the calculated room temperature particle strengthening of 248 MPa, giving confidence in the model†

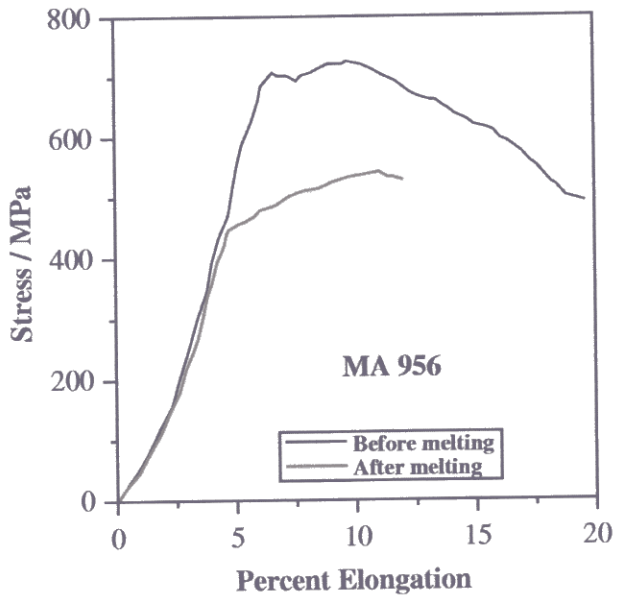

Figure 6.4 : Tensile properties of MA956 before melting and after melting.

6.4 Unrecrystallized MA956

There is a remarkable difference in the grain size of recrystallised MA956 (about 10 mm) and the unrecrystallized alloy which has grains less than one micron diameter. Grain size must therefore represent the major component of the reduction in strength following a recrystallisation heat treatment. If this is the case then the strength of the unrecrystallized MA956 is simply that of the recrystallized sample and the grain boundary strengthening.

This assumption can be verified by comparing calculated grain size strengthening values with the measured difference between the strength of the recrystallized and unrecrystallised MA956 as manifested in

† The incidental observation that a larger elongation is observed in the unmelted sample is because the melted sample fractured eventually by a cleavage mechanism. The reason for this has not been investigated in detail.

the neural network analysis [Chapter 4]. The Hall-Petch [Hall, 1951; Petch, 1953] relation is expressed as:

$$\sigma_g = k_o d^{-\frac{1}{2}} \tag{6.5}$$

where k_o is a constant which is a measure of the grain boundary resistance and d, is the grain size. According to equation 3, the value of k_o for ferritic stainless steels is $15.9\text{MPa}\,\text{mm}^{-\frac{1}{2}}$ [Lewis and Pickering, 1983].

Although the grain size strengthening can be calculated using the Hall–Petch relation, there is no adequate theory for its temperature dependence. We have therefore estimated the temperature dependence using the neural network model and the assumption that the difference between the recrystallised and unrecrystallised samples is essentially due to the respective grain structures. The ratio of the difference relative to that at room temperature was used to scale the results according to equation 6.5.

Figure 6.5 shows the calculated yield strength of the unrecrystallized MA956 as a function of the grain size in the range 0.5–1.0 μm. As before, the results are compared against the neural network interpretation of the experimental data. The yield strength can be explained rather well with the grain size set at about 0.9 μm.

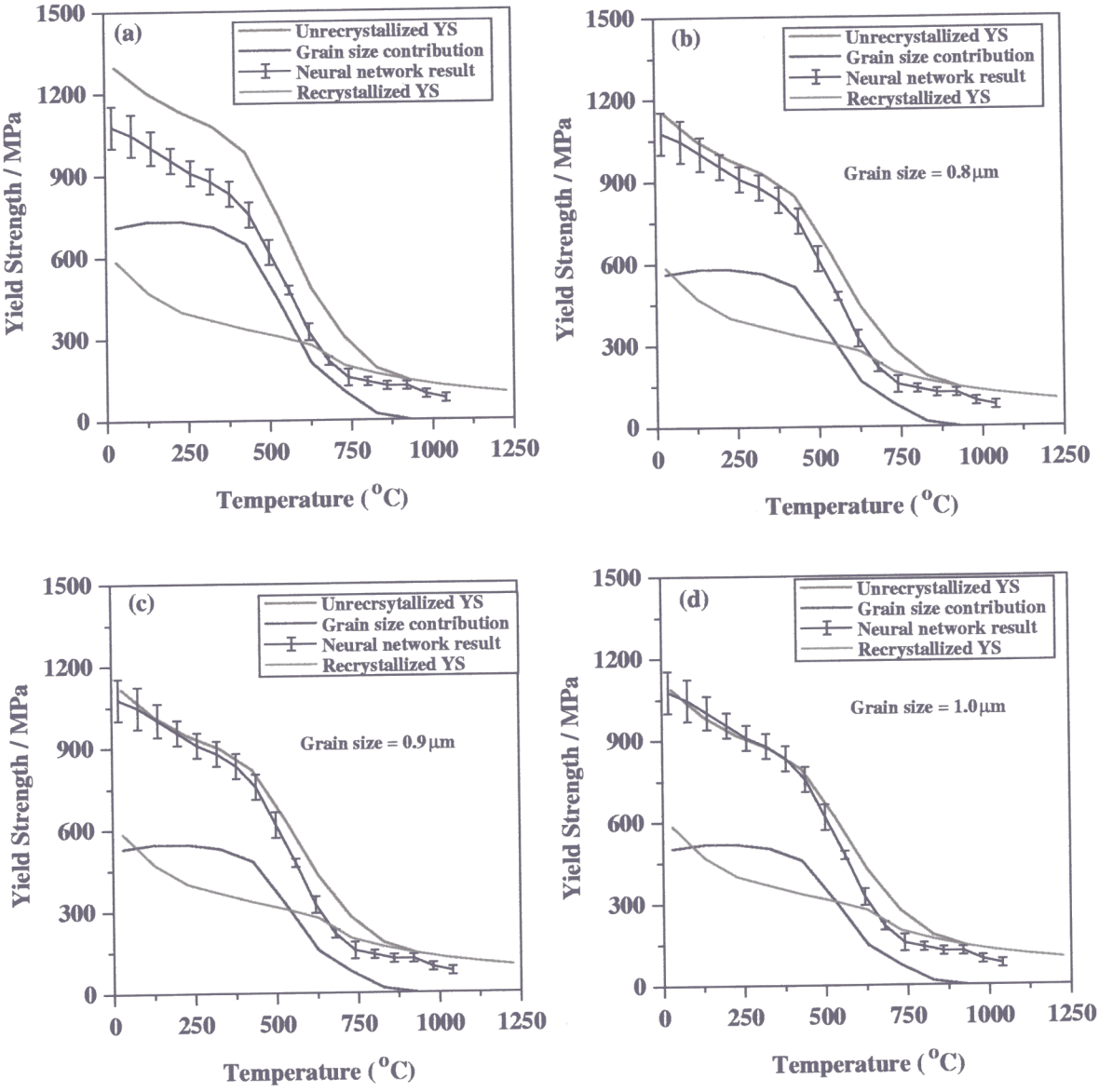

Figure 6.5 : Calculated yield strength of unrecrystallized MA956 using different grain sizes and compared with the neural network results. The plots are for grain sizes (a) 0.5 μm, (b) 0.8 μm, (c) 0.9 μm and (d) 1.0 μm.

There is a slight increase in grain size strengthening with temperature over the range 30–300 °C. This increase may not be significant given the uncertainty in the experimental data as apparent in the error bars, but it could be a consequence of strain ageing associated with the small concentration of interstitial carbon in MA956. A similar effect is found in the temperature dependence of the strength in ordinary ferritic steels [Tapsell, 1931].

The more significant decrease in the contribution from grain size strenghening occurs at higher temperatures. For austenitic steels, the reduction in grain size strengthening with increasing temperature has been associated with a weakening of dislocation locking effects at grain boundaries [Rao *etal.*, 1975]. This might apply to MA956, but a more likely explanation is that there is dynamic recrystallisation accompanying deformation at high temperatures. This has been observed experimentally by Chou and Bhadeshia [Chou and Bhadeshia, 1995] during the hot deformation of MA956 and MA957 (another ODS mechanically alloyed ferritic stainless steel). The dynamic recrystallisation could be observed even when the deformation temperatures was far less than the ordinary recrystallization temperature of the alloys. This would also explain why the grain size contribution remains constant until about 500 °C, because grain boundaries are not expected to be able to migrate until the iron and substitutional atoms acquire sufficient mobility.

To assess this, the grain sizes necessary to explain the reduction in the strengthening contribution σ_g were calculated from the difference between the recrystallised and unrecrystallised alloy strengths as a function of temperature (Figure 6.6). The grain sizes estimated for all cases are seen to be quite reasonable in the sense that a fully recrystallised microstructure will have grains some 10–50 μm in size [Alamo *etal.*, 1992].

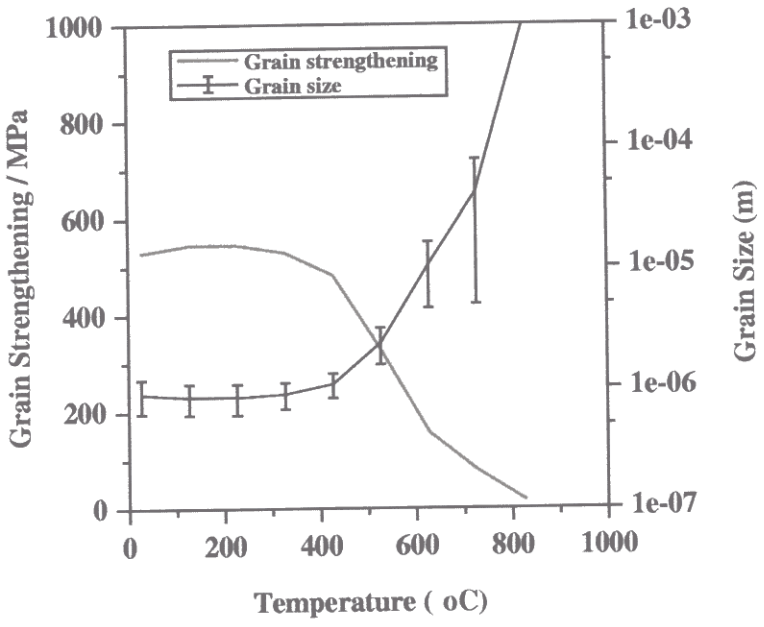

Figure 6.6 : Grain strengthening and estimated grain size of samples of MA956 which are unrecrystallized prior to testing as a function of temperature.

6.5 Summary

The ambient temperature yield strength of mechanically alloyed MA956 in the as–processed condition originates from its ultra–fine grain size, the intrinsic strength of ferritic iron, dispersoid strenthening via the yttria compounds and finally, the dislocation density. The contributions of these components decrease in the order stated. The dispersoids contribute only about 250 MPa, but it is emphasized that their prime purpose is to provide creep resistance, a property not discussed here.

Recrystallisation has the effect of virtually eliminating grain size strengthening but leaving the other contributions essentially unchanged.

The temperature dependence of the strength has also been estimated. The relatively sharp decline in the strength in the recrystallised condition beyond about 500 °C replicates the decrease in the strength of iron. It is believed that a further large temperature dependence in the case of the unrecrystallised sample comes from dynamic recrystallisation during testing which reduces the grain size contribution to strength.

Finally, it is interesting that we have used our earlier neural network analysis of a vast quantity of published data to validate the physical models. Mechanically alloyed materials are notorious in their variability so this is a good method of providing an assessed experimental datum. Furthermore, the network provides estimates of uncertainty in the experimental data which are useful in the validation excercise.

CHAPTER SEVEN

Conclusions and Further Work

7.1 Conclusions

A variety of studies have been conducted into the mechanical alloying process and the tensile properties of the mechanically alloyed oxide dispersion strengthened superalloys, with some fascinating results.

A model has been developed to deal with a situation in which a solution is created by continuously refining a mixture of powder particles of the pure components as in mechanical alloying. It is predicted that solution formation by the mechanical alloying of solid components cannot occur unless there is a gain in coherency as the particles become small. The inclusion of interfacial energy also predicts the existence of a barrier to the evolution of the solution. For cases where like atoms tend to cluster, it is possible in principle to obtain a metastable state before solution formation is completed.

A neural network technique trained within a Bayesian framework has been applied to the analysis of the yield strength, ultimate tensile strength and percent elongation of mechanically alloyed oxide dispersion strengthened ferritic steels as functions of variables which are known to influence mechanical properties. The analysis has produced patterns which are metallurgically reasonable, and which permit the quantitative estimation of mechanical properties together with an indication of confidence limits.

The components of the yield strength of a mechanically alloyed oxide–dispersion strengthened iron–base superalloy, MA956, have been investigated quantitatively. It is found that much of the difference in strength between the recrystallised and unrecrystallised forms can be explained in terms of the grain structure. The contribution from dispersion strengthening has been estimated using dislocation theory and has been demonstrated to be consistent with that measured experimentally. The temperature

dependence of the yield strength has also been studied; some of the effects observed in the range 500–600 °C can be attributed to the change in the intrinsic strength of pure, annealed iron.

7.2 Further Work

The thermodynamic treatment of the evolution of solutions in mechanical alloying is at present qualitative. The model could be applied to specific alloy systems where the interatomic interactions are used.

The neural network models produced are based on the data available in the literature which at moment are not very exhaustive, as more data become available the analysis will be repeated periodically to ensure that the models are firmly based and reliable. In the present state, the models have been shown to reproduce experimental results reasonably well, attempts will be made to use the models in the design of new alloys.

Only the tensile properties of the iron–base MA–ODS alloys have been analysed. Neural network analysis of the creep properties of the iron–base alloys will be conducted and similar analysis will be made for the tensile and creep properties of the nickel–base alloys.

The physical interpretation of the yield strength of MA956 shows that the temperature dependence of the yield strength of MA–ODS alloys in the as-extruded condition is to a large extent, dominated by dynamic recrystallization and grain growth. It is necessary to investigate the kinetics of the recrystallization and grain growth in order to understand the stress versus temperature relationship as it affects the phenomena.

Finally, we are no further in understanding the anisotropic mechanical behaviour in MA–ODS alloys which must be related to the deformation processing and consequent dispersoid alignment combined with crystallographic texture issues.

APPENDIX ONE

Effect of Grain Structure on the Creep Properties of MA956

A1.1 Introduction

Chou and Bhadeshia, (1993), determined that most of the stored energy of an alloy like unrecrystallized MA956 is in the form of grain boundaries and that the stored energy is so large that moving grain boundaries can easily overcome any drag from the particle dispersion. Furthermore, the alignment of oxide particles along the extrusion direction would lead to the development of a columnar recrystallized grain structure. They proposed and verified that a reduction in the stored energy via some process before recrystallization would lead to a more isotropic grain structure. This is because the grain velocity along the extrusion direction would be reduced. The objective of the work reported here was to see whether a more isotropic recrystallized structure improves the stress-rupture properties of MA956, especially the relatively poor transverse properties.

Various heat treatments procedures were employed in order to systematically vary the grain size and shape. In addition to the conventional recrystallization heat-treatment for the alloy, two other experimental heat-treatments were investigated. The latter involved the control of stored energy before recrystallization by "preannealing" the alloy at a temperature high enough to permit recovery but not recrystallization. The heat-treatments are described in Table A1.1. The heat-treatments were performed in air prior to the machining of test specimens for the stress-rupture tests.

Table A1.1 : Heat-reatments investigated for grain structure control.

Class	Type	Detail
A	Conventional	Recrystallization at 1315 $°C$ for 50 min
B	Experimental	Preannealing at 1050 $°C$ for 455 h + Recrystallization at 1315 $°C$ for 20 min
C	Experimental	Preannealing at 1100 $°C$for 150 h + Recrystallization at 1300 $°C$ for 15 min

A1.2 **Results and Discussions**

A1.2.1 *Structure*

The microstructures of the samples due to the different heat-treatments are shown in Figure A1.1 for sections taken parallel and transverse to the extrusion direction. The conventional heat-treatment A has led to a complete recrystallization with a coarse and uniform columnar grain structure. The experimental heat-treatment B produced refined elongated grains which are distributed non-uniformly within the structure, whilst the experimental heat-treatment C has produced a structure which is composed of elongated grains which are finer than the A–structure but coarser than B and are uniformly distributed within the structures. The longer preannealing time in B relative to C produced a higher reduction in stored energy and consequently, the driving force for recrystallization is lower in B than C. However, the persistent anisotropic grain shape suggests that stored energy is probably not the only controlling factor. The reduction in the stored energy can reach a level where the microstructure becomes sensitive to any inhomogeneous distribution of particles and the grain size begins to be limited by Zener pinning, as the pinning force becomes comparable to the driving force for grain boundaries migration [Chou and Bhadeshia, 1993]. This may explain the non–uniform structure in B.

A1.2.2 *Hardness Values*

The results of the hardness measurements are shown in Table A1.2. The samples are identified by heat–treatment (A, B or C), orientation with respect to the extrusion direction (L for longitudinal, T for transverse) and the sample serial number. As expected, there is no significant variation between the samples as a function of heat–treatment or plane of section. After all, the observed variation in grain structure is not very large and hardness tests, because of their 3–dimensional nature, are unlikely to be sensitive to the plane of section.

Table A1.2 : Vickers Hardness values of MA956 for different heat-treatment conditions.

Heat-Treatment	Specimen	Hardness (VHN)
A	AL1	261
	AL2	258
15 min / 1315 °C	AT1	265
B	BL1	258
455 h / 1050 °C	BL2	257
+ 20 min / 1315 °C	BT1	246
C	CL1	269
160 h / 1100 °C	CL2	241
+ 15 min / 1300 °C	CT1	264

A1.2.3 *Stress-Rupture Properties*

The stress–rupture properties of MA956 are summarized in Table A1.3. The number of hours at stress before failure are indicated below the respective stresses of 38, 48, 59, 69 and 79 MPa. Samples with a minimum of 24 hours life at 48 MPa are reckoned commercially as having passed. Where a sample was not tested at a particular load, it is indicated by NT. There are four results for each of the heat–treatments samples stressed in the longitudinal direction, and two in the transverse dirction.

The stress–rupture properties measured along the transverse direction are poor compared with the

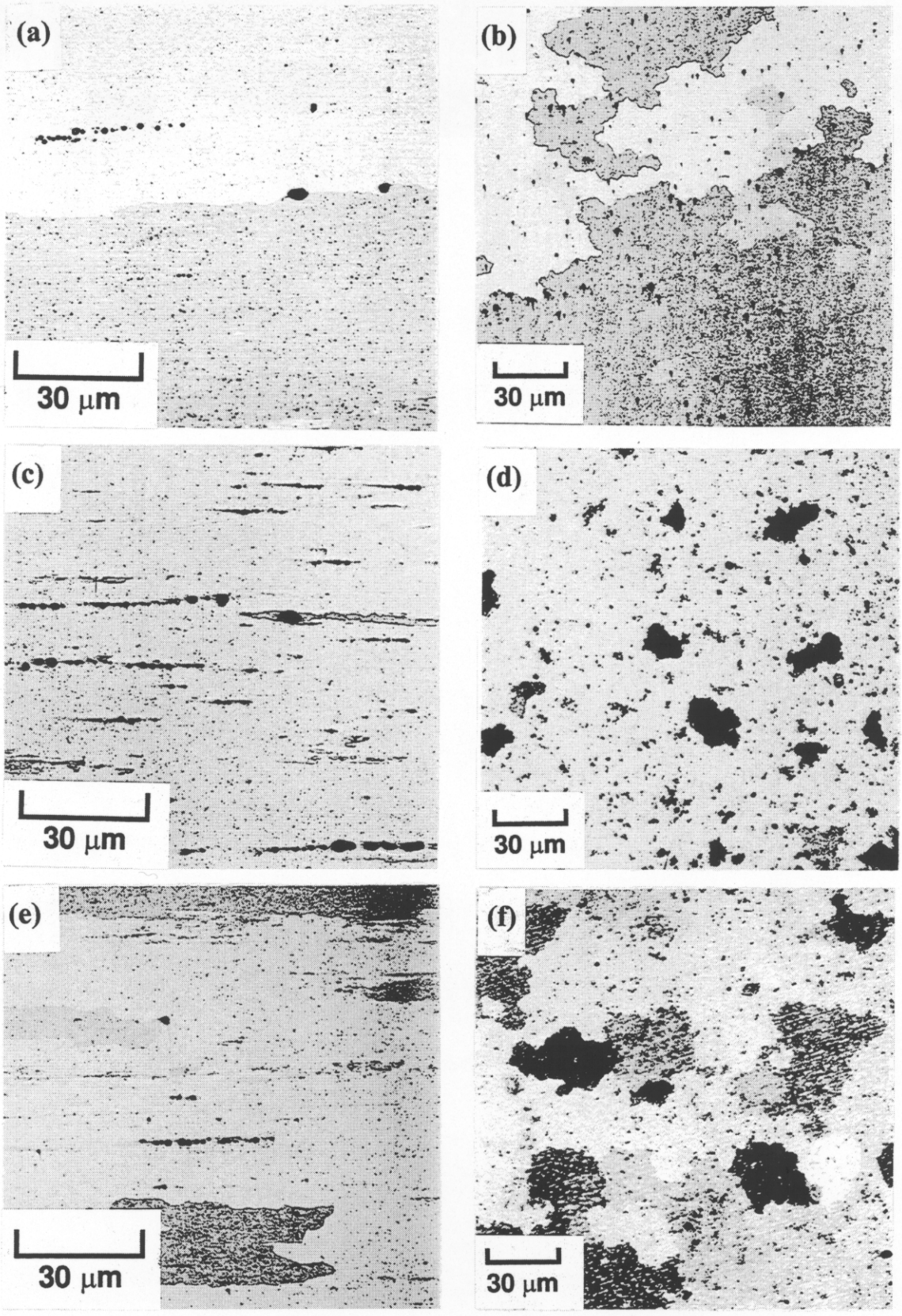

Fig. A1.1: Microstructures of sections parallel and transverse to the extrusion direction after heat-treatment. (a), (c) and (e) longitudinal sections after heat-treatments A, B, and C respectively (b), (d) and (f) transverse sections after heat-treatment A, B, and C respectively.

longitudinal samples for all the test conditions. The properties are generally better for the conventionally heat-treated samples. Heat-treatment C produced the worst effect on the stress-rupture strength of the alloy but with improved the transverse creep ductility. The refinement of the grains in the structure by the experimental heat-treatments B and C reduces the grain aspect ratio of the grains and have produces poorer stress-rupture properties. However, the refinement has not led to an equiaxed grained structure hence there is no significant improvement in the transverse stress–rupture strength.

Table A1.3 : Stress-rupture properties of MA956 alloy and the different heat-treatment conditions.

Heat-Treatment	Specimen	Hours at various Stresses					Elongation	Remark
		38 MPa	48 MPa	59 MPa	69 MPa	79 MPa	(%)	Pass or Fail
A	AL1	24	24	24	8	0	10.4	Pass
	AL2	24	24	24	24	3	11.7	Pass
15 min / 1315 °C	AL3	24	24	24	100	-	9.0	Pass
	AL4	24	24	24	24	83	7.4	Pass
	AT1	0	0	0	0	0	2.1	Fail
	AT2	0	0	0	0	0	1.9	Fail
B	BL1	24	24	24	6	0	14.9	Pass
	BL2	24	24	24	5	0	7.6	Pass
455 h / 1050 °C	BL3	24	24	24	4	0	11.5	Pass
+	BL4	24	24	24	0	0	16.1	Pass
20 min / 1315 °C	BT1	0	0	0	0	0	3.3	Fail
	BT2	0	0	0	0	0	3.0	Fail
C	CL1	24	3	0	0	0	5.8	Fail
	CL2	17	0	0	0	0	4.3	Fail
160 h / 1100 °C	CL3	24	24	24	1	0	9.1	Pass
+	CL4	24	24	24	24	0	10.2	Pass
15 min / 1300 °C	CT1	0	0	0	0	0	3.7	Fail
	CT2	0	0	0	0	0	14.9	Fail

Pronounced delamination was observed in one of the experimental transverse samples, CT2 (Figure A1.2). The delamination occurred over about 10 mm along the length of the specimen and the cracks

Fig. A1.2 : Optical micrograph of the section through delaminated region on sample CT2.

contained particles which were analysed using energy dispersive X–ray (EDX) microanalysis method (Figure A1.3). Some of the contents of the cracks are simply large regions of the alloy which have become detached during the delamination process. However, a large number of the particles which imaged brightly in the scanning electron microscope were aluminium rich, perhaps alumina. Alumina is an insulating phase and would therefore tend to charge up during scanning electron microscopy and hence appear bright (Figure A1.3).

A1.3 *Summary*

The original notion that the transverse rupture properties might improve with the refinement of grain structure, or with a decrease in the anisotropy of grain structure (Chou and Bhadeshia, 1993) appears incorrect. After all, heat-treatments *B* and *C* gave generally the worst stress-rupture properties in all the test orientations.

The results can in fact be understood if the grain boundaries which are normal to the stress axis become particularly susceptible to oxidation. There is an established phenomenon known as "stress-assisted grain boundary embrittlement by oxygen" (Smith *et al.*, 1980 and 1984; Bricknell and Woodford,

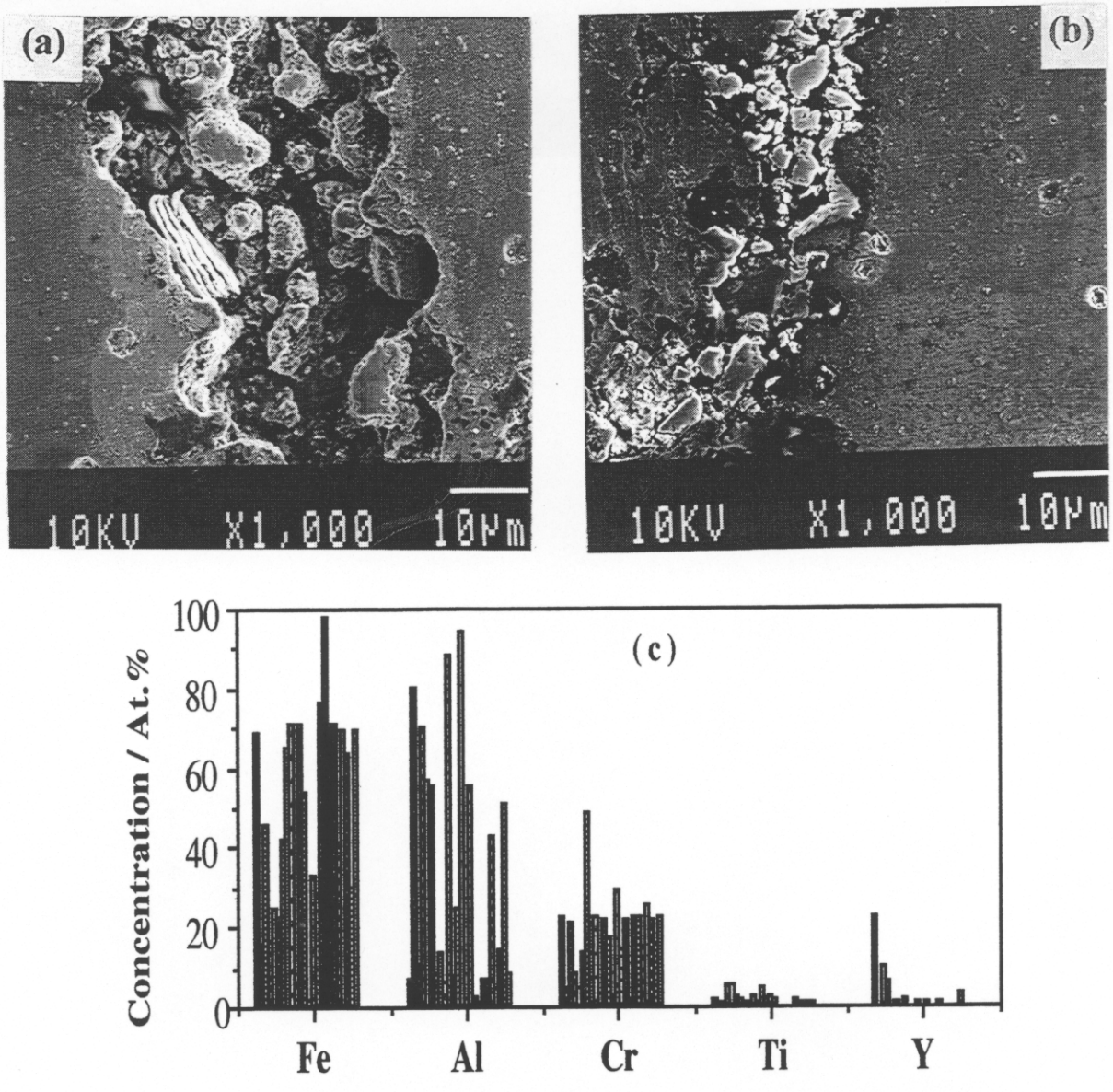

Fig. A1.3 : Scanning electron micrograph of the delaminated sample CT2 and the energy dispersive X-ray analysis of the particles. (a) particles which are chunks of matrix metal, (b) typical particles with high aluminium concentration and (c), EDX analysis of a number of particles chosen at random.

1981). The ODS alloy studied here should be particularly susceptible to oxygen effects because of the high concentration of aluminium which has a strong affinity for oxygen. When a sample is tested parallel to the columnar grains, the amount of grain surface normal to the stress axis should be minimal. Consequently, failure during a stress-rupture test should involve considerable ductile deformation. There should exist a high probability for the formation of alumina films at the grain boundaries for tests in which the stress is applied perpendicular to the columnar grains. This would lead to premature failure

with little plastic deformation. This theory is illustrated schematically in Figure A1.3. The hypothesis is consistent with the observation of substantial alumina particles at the cracks in the failed transverse samples, although this may have occurred after failure.

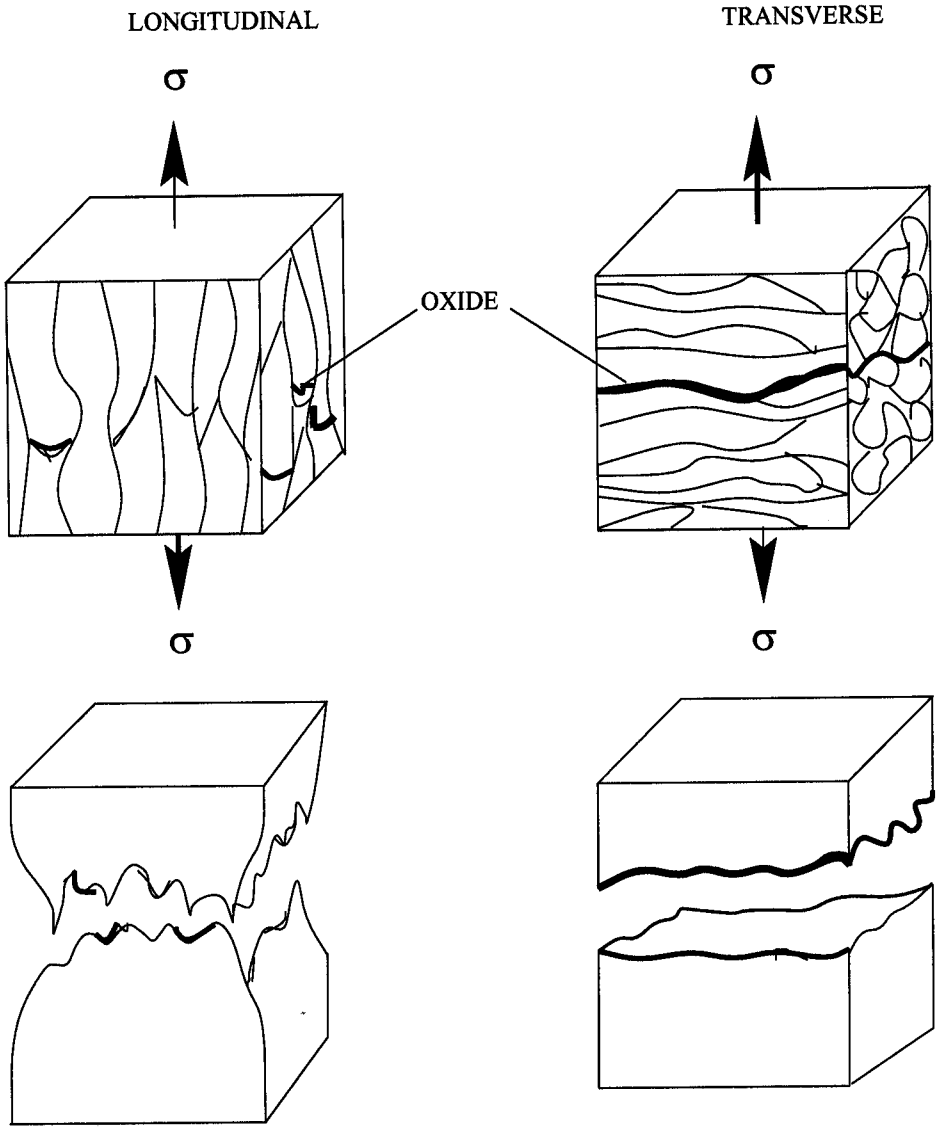

Fig. A1.3 : Schematic illustration of the effect of stress versus grain-boundaries relation on the "stress-assisted grain boundary embrittlement by oxygen".

APPENDIX TWO

Grain Boundary Oxidation in MA-ODS Alloys

A2.1 Introduction

The observation of aluminium–rich particles in the cracks in a delaminated stress–rupture specimen (Appendix 1) prompted a further investigation on possible grain boundary oxidation in mechanically alloyed ODS metals. A nickel–base ODS alloy (MA758, Table 1.1) was used to investigate this phenomenom. MA758 is a nickel–base mechanical alloy without γ' strengthening. It is the higher-chrominum version of MA754 (Table 1.1), the first mechanically alloyed ODS superalloy to be produced on a large scale. MA758 was developed for applications in which the higher chromium content is needed for greater oxidation resistance. Its mechanical properties are comparable to those of MA754. The alloy is used in metal processing industry and in the glass-processing industry. Variants of the alloy exist with difference only in their aluminium concentrations. MA758 with 0.36 wt.% Al has been found to fail in service by cracking. The work reported here deals with two variants of MA758 having different aluminium contents.

A2.2 Experimental Procedures

Two forms of MA758 alloy; one containing 0.36 wt.% Al and the other 0.22 wt.% Al were provided by INCO Alloy. The sample with 0.36 wt.% Al was a failed nozzle while the 0.22 wt.% Al sample was in the form of a round bar in a recrystallised condition. The nozzel is produced by forging the recrystallized alloy. The recrystallization heat–treatment is by zone annealing whereby a hot zone is passed along the bar and recrystallization takes place under the influence of a temperature gradient.

intrinsic strength of iron. Although this intrinsic resistance to dislocation motion becomes smaller at high temperatures, it never vanishes but reaches a limiting value known as the athermal resistance [Seeger, 1954]. The athermal resistance arises from the long–range stress fields of obstacles. Fluctuations caused by thermal vibrations are important over distances of the order of a few atoms and hence cannot assist the dislocations to overcome any fields which extend over large distances. This is why the strength of the iron does not tend to zero with increasing temperature (Figure 6.2a).

The next largest contributions to the overall strength come from the dispersoids and solid solution strengthening. These contributions naturally depend on the particle characterisitics and solute concentrations respectively so it is not possible to make general comments about their magnitudes.

Table 6.2 : Calculated yield strength of recrystallized MA956

Temperature / °C	Y.S. of pure iron / MPa	Solutes contribution / MPa	Dispersoids contribution / MPa	Total Y.S. / MPa
27	216	116	248	580
127	158	113	193	465
227	144	92	160	396
327	144	80	139	362
427	144	63	123	330
527	144	48	112	304
627	129	39	103	271
727	72	32	95	199
827	52	26	89	168
927	38	21	85	144
1027	28	17	80	125
1127	20	14	77	111
1227	15	11	74	100

Figure 6.2b shows the comparison of the calculated yield strength with the experimental data as represented by the neural network estimates (Chapter four). The agreement is impressive indicating

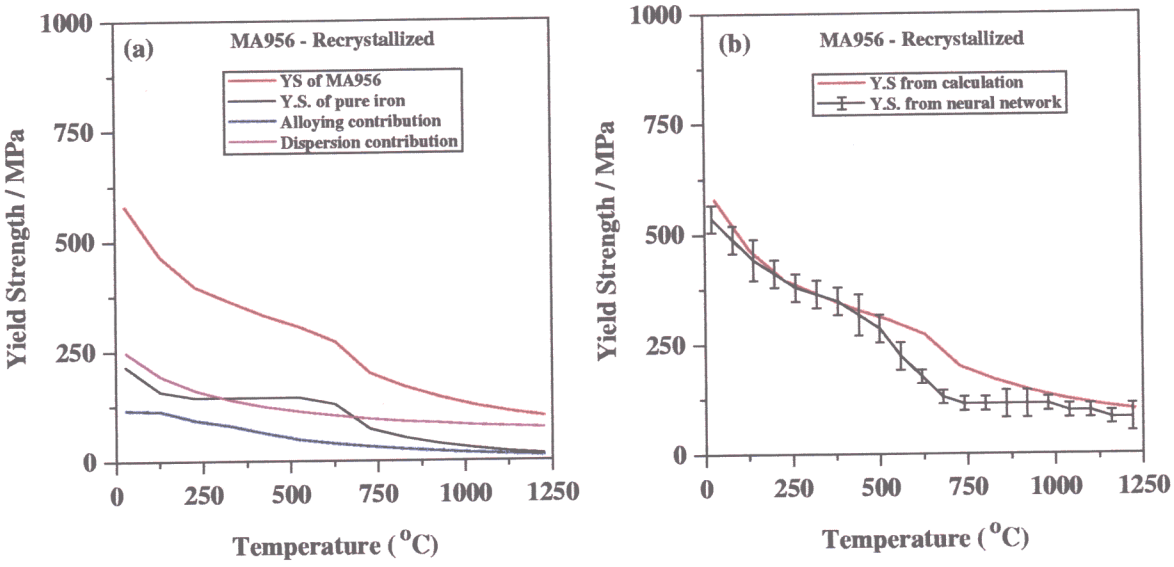

Figure 6.2 : (a) Calculated yield strength of MA956 and contributions from the various components as functions of temperature. (b) Calculated yield strength compared with the result of a neural network analysis.

that the factorisation of strength is reasonable. Furthermore, the accelerating decrease in strength observed in the temperature range 550–650 °C is, by comparison with Figure 6.2a, seen to be a consequence of the similar variation in the strength of the pure iron. Such behaviour is expected because iron atoms become significantly mobile in this temperature range when considered for the slow strain rates typical of tensile tests. There are many other phenomena which reflect the mobility in this temperature range; for example, secondary hardening in alloyed steels.

6.3 Measured Dispersoid Strengthening

There might be considerable uncertainties in the estimation of dispersion strengthening. For example, the particles may not be uniformly distributed and are unlikely to have a uniform size [Krautwasser *et al.*, 1994; Dubiel *et al.*, 1994]. To gain more confidence in the analysis, the dispersoids were effectively removed from a recrystallised sample and the strength measured. This was done by arc melting the alloy in an argon atmosphere, which causes many of the oxides (which have a relatively low density)

The temperature range between the start of recrystallization T_{sR} and melting T_M is 100 °C–150 °C (Jongenburger *et al.*, 1987).

For the purpose of this investigation the samples were again heat-treated in air at 1150 °C for 1 hour and their microstructures were studied metallographically using optical and scanning electron microscopies.

A2.3 Results and Summary

Figure A2.1 shows the microstuctures of the two variants of MA758 after heat–treatment. The grain boundaries of the 0.36 wt.% Al sample are decorated with a phase which appears bright in the scanning electron microscope (Figure A2.1c). The phase is likely to be oxide which tends to charge up under the influence of electron beam and hence as a result appear bright.

The higher aluminium variant is therefore found to be more susceptible to grain boundary oxidation, although direct evidence for oxide formation has not yet been obtained.

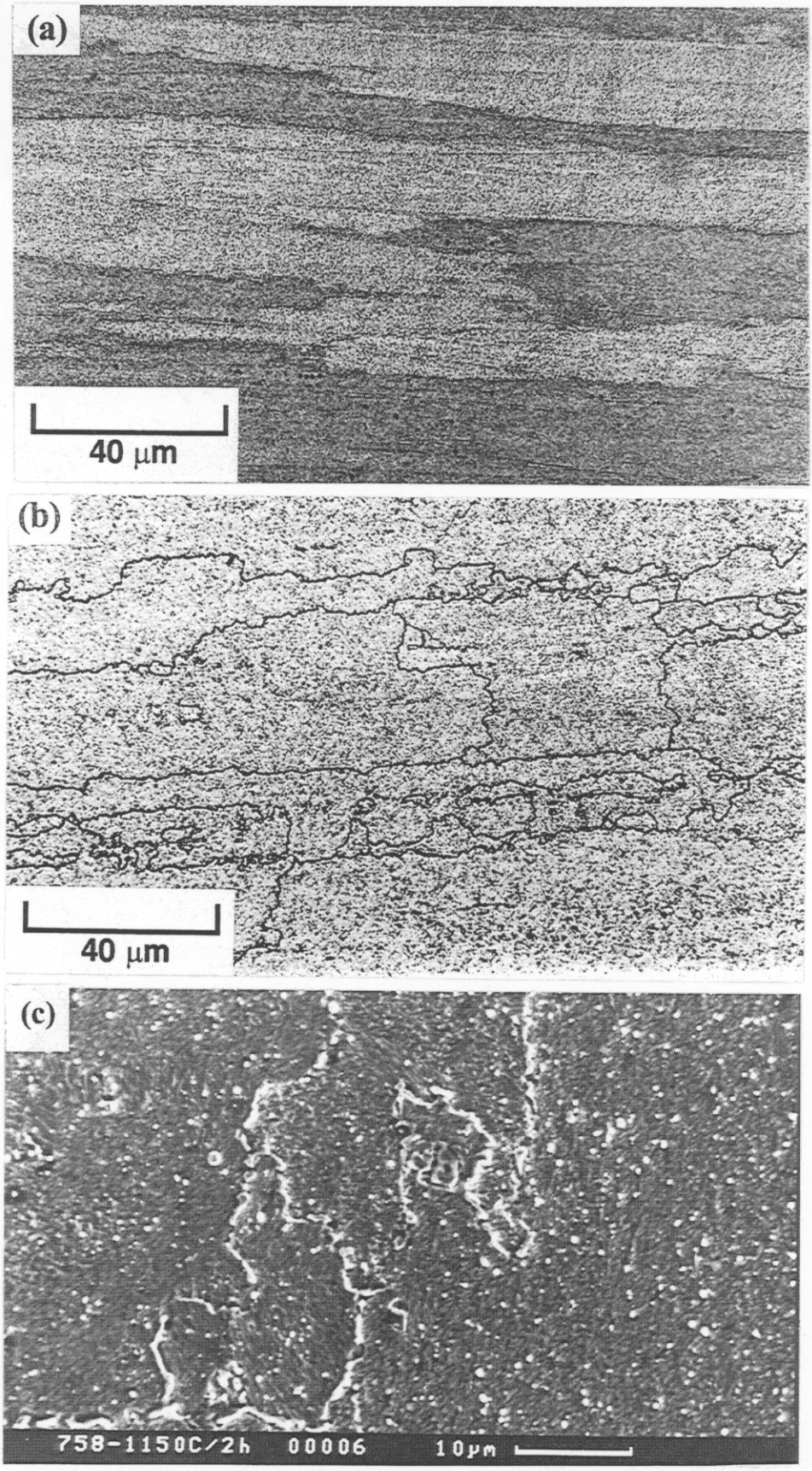

Fig. A2.1 : Optical micrographs of the samples of MA758 after heat–treatment. (a) 0.22 wt.% Al, (b) 0.36 wt.% Al, and (c) Scanning electron micrograph of the sample with 0.36 wt.% Al.

APPENDIX THREE

Some Tensile Tests on MA956

A3.1 **Introduction**

Anisotropic mechanical behaviour MA–ODS steels has been sutied mostly using high temperature tests (Whittenberger, 1981, 1984, Alamo *et al.*, 1992) but the corresponding behaviour at room temperature is not well established. The work reported here was an attempt to investigate the room temperature tensile properties of MA956. The neural network analysis (Chapter five) showed that the unrecrystallized alloy is not only stronger but also more ductile than when it is in the recrystallized condition, when the stress is applied parallel to the working direction. This is unusual given the high hardness in the unrecrystallized condition.

Standard tensile specimens were machined from a rectangular bar of MA956 in the as-extruded condition both along the direction parallel and normal to the extrusion direction. After the machining, a number of longitudinal and transverse samples were recrystallized by annealing at 1300 °C for 30 min before the test.

A3.2 **Results and Discussion**

The plots of stress versus percent elongation for the room temperature tests along the longitudinal and transverse directions are shown in Figure A3.1 for both the recrystallized and the unrecrystallized conditions. The strength in the recrystallized sample is higher along the longitudinal direction than along the transverse direction but the ductility is identical in both directions. For the unrecrystallized sample the strength is isotropic but the longitudinal ductility far exceeds that along the transverse

direction. Naturally, the unrecrystallized sample is always stronger than the recrystallized sample (Figure A3.1c,d), although its ductility is more anisotropic.

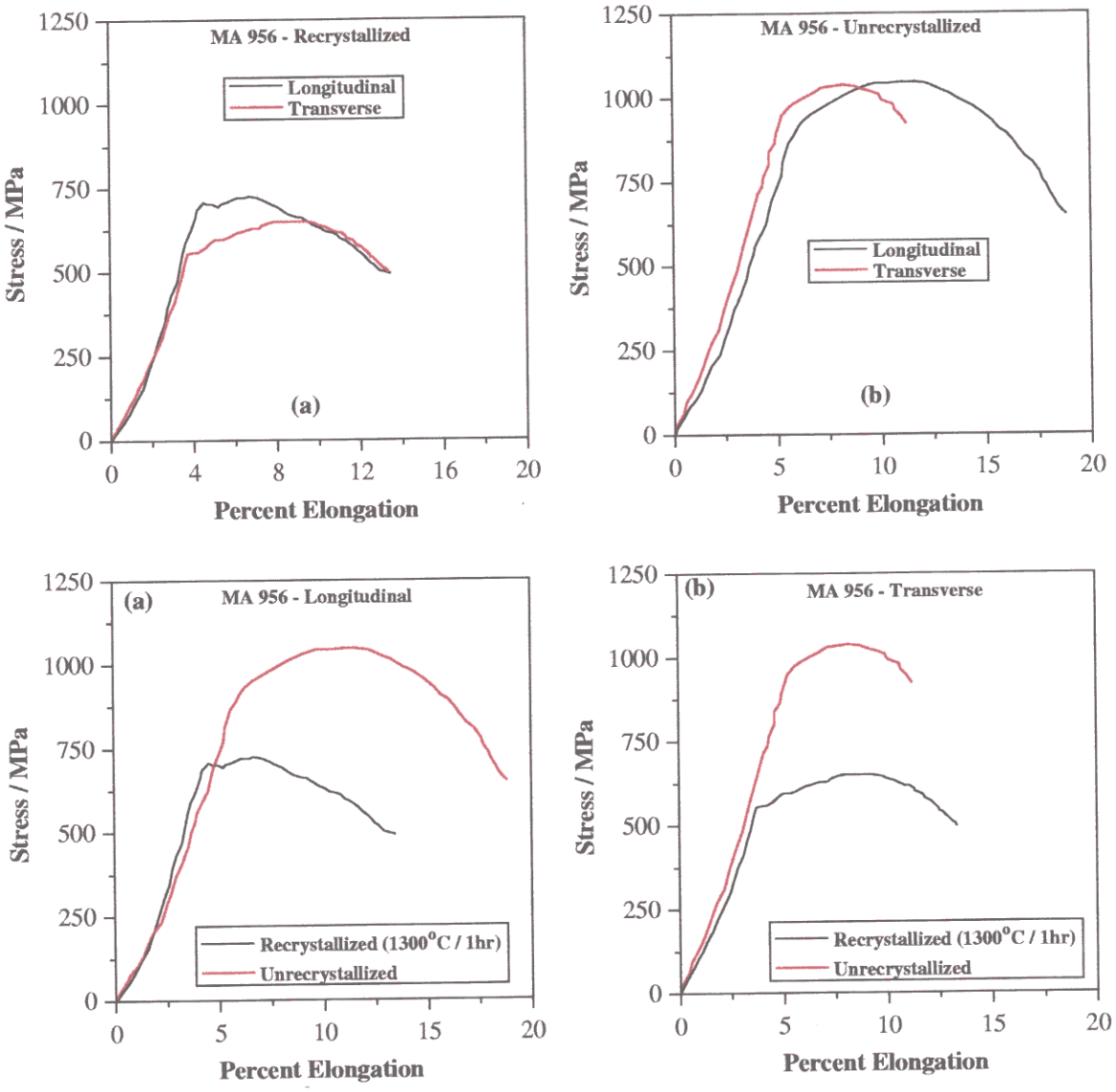

Fig. A3.1 : Stress versus percent elongation for the room temperature tensile testings along the longitudinal and transverse directions. (a) recrystallized, (b) unrecrystallized, (c) longitudinal recrystallized and unrecrystallized compared and (d) transverse recrystallized and unrecrystallized compared.

The elongation results are difficult to interpret given the complex nature of the failures illustrated in Figure A3.2. Deformation is clearly anisotropic and there are signs of delamination along the rolling

plane for both the recrystallized and unrecrystallized samples. There are longitudinal features even on the transverse samples. The ductility of the transverse recrystallized sample is low because the fracture facets are able to propagate over large distances due to the coarse grain structure.

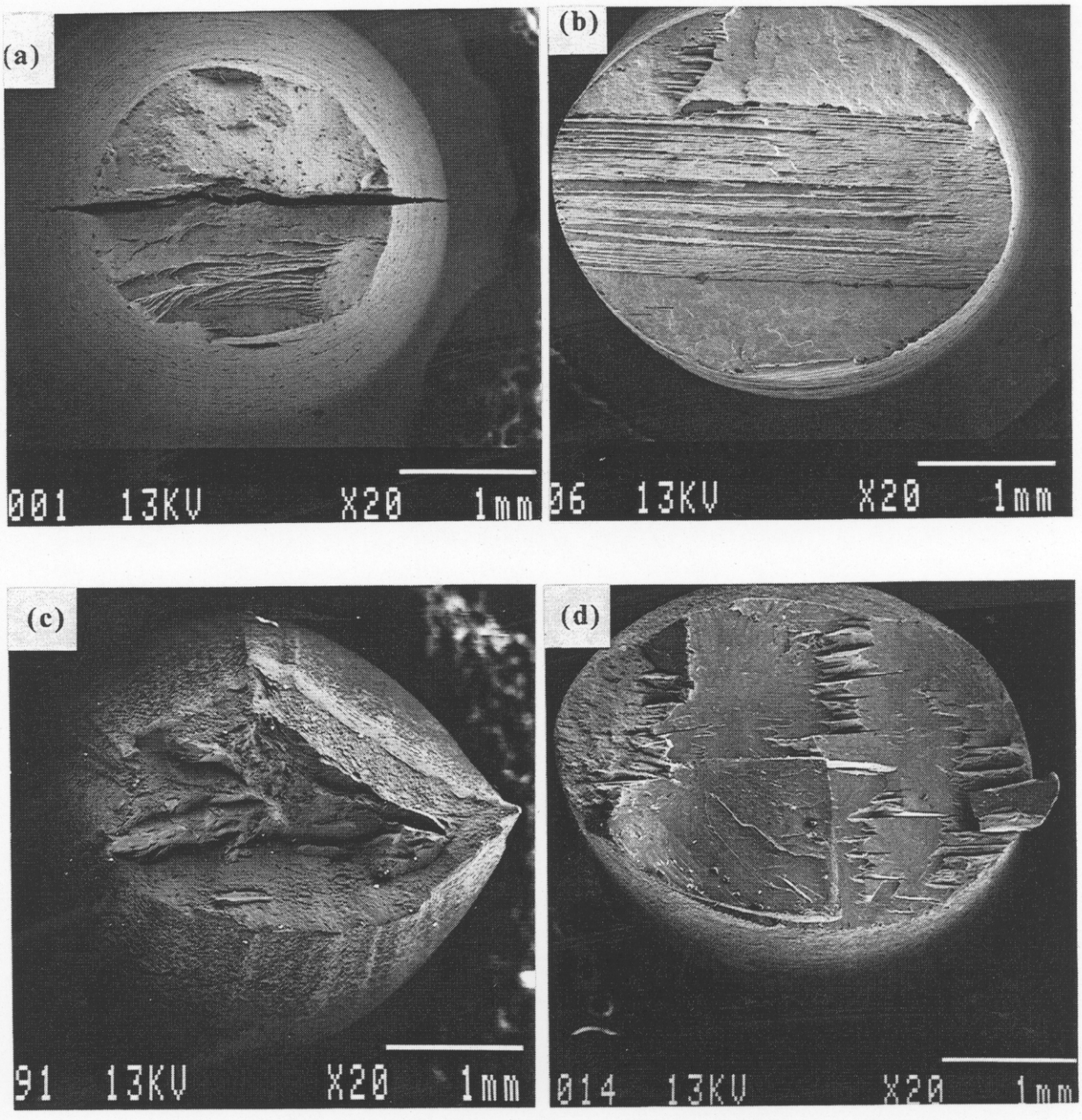

Fig. A3.2 : Scanning electron micrographs showing the fracture surfaces after the room temperature tensile tests. (a) and (b), unrecrystallized longitudinal and transverse samples respectively; (c) and (d), recrystallized longitudinal and transverse samples respectively.

Figure A3.3 shows the measured stress versus percent elongation data for different temperatures for the unrecrystallized MA956. The strength falls sharply between 450 °C and 600 °C, and the ductility increases with the test temperature. The sudden decrease is, as indicated by the physical model (Chapter six), due to dynamic recrystallization (Figure A3.4). These results are consistent with Regle (1994) and and with the neural network analysis (Chapter five). The slight drop in strength between room temperature and 200 °C is interesting. Though, this is not apparent in the earlier work by Regle (1994), it is consistent with the neural network analysis and the results of the physical model as compared in Figure A3.5

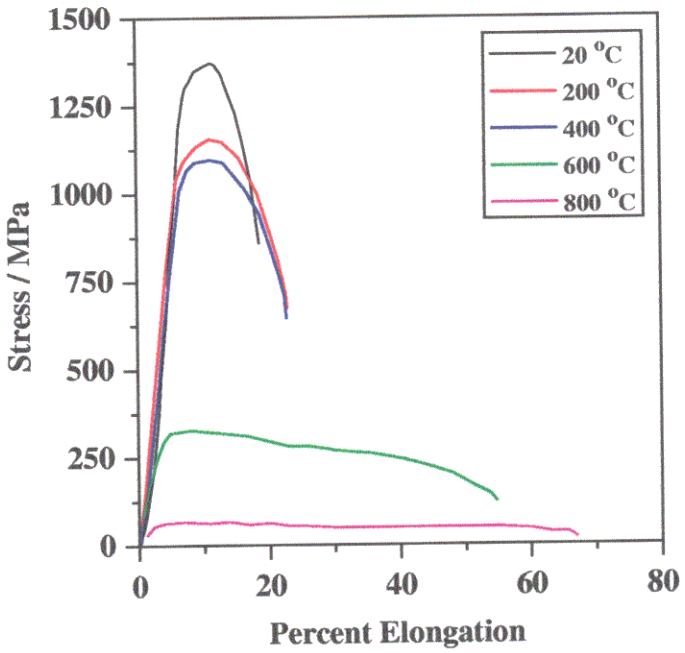

Fig. A3.3 : Temperature dependence of the tensile properties of unrecrystallized MA956.

A3.3 Summary

The room temperature tensile properties of recrystallized MA956 reveal a greater strength along the longitudinal direction than the transverse direction but isotropic ductility. By contrast, the strength is isotropic but the ductility is poor along the transverse direction for the unrecrystallized samples.

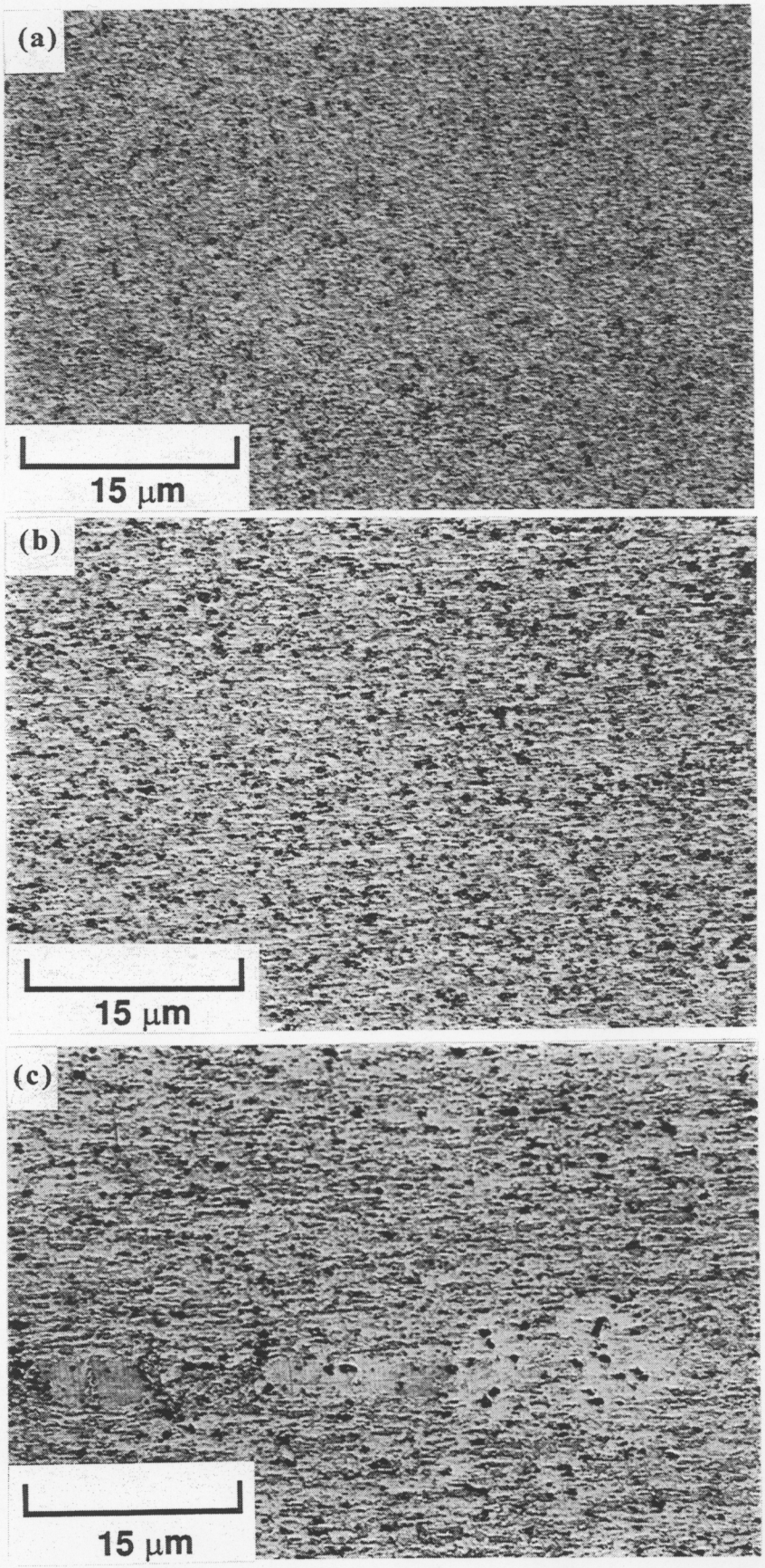

Fig. A3.4 : Microstructures at the fracture regions of the samples of unrecrystallized MA956 tested at different temperatures. (a) 20 $°C$ (b) 600 $°C$ and, (c) 800 $°C$.

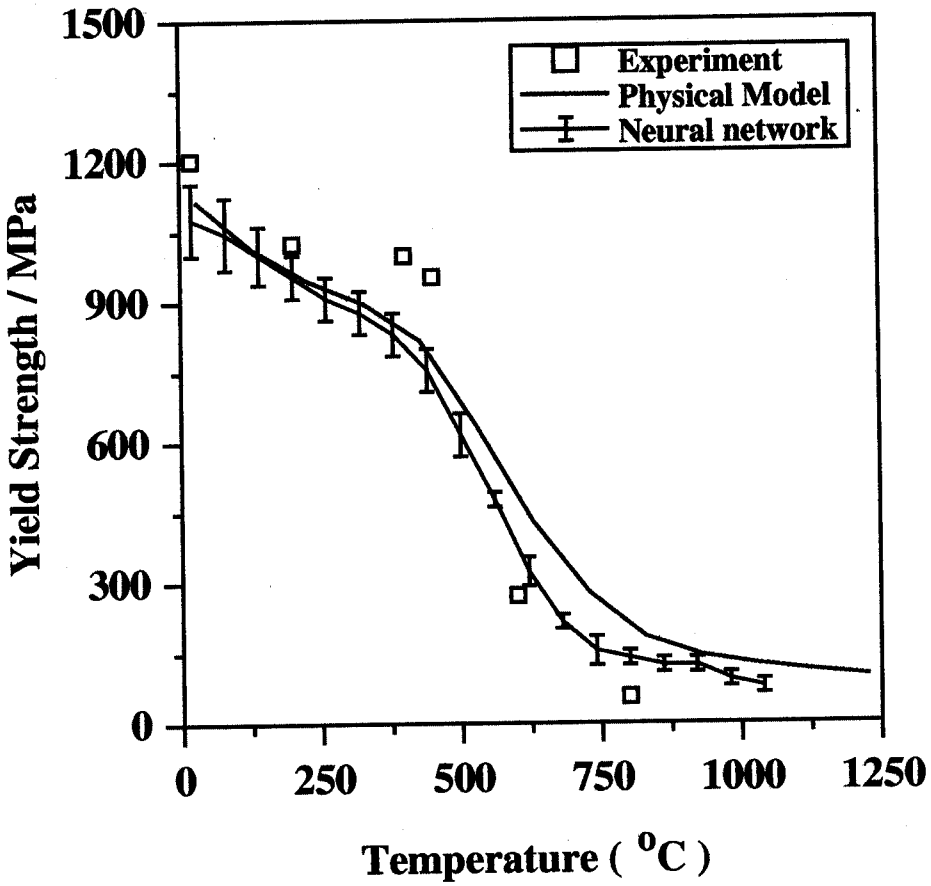

Fig. A3.5 : Yield strength of MA956 at different temperatures compared with the neural network and physical model results.

APPENDIX FOUR

Data for the Neural Network Analysis

PM2000 → 5.5 AL

Cr	Al	Ti	Mo	Y_2O_3	Annealing		Ageing		CW	T	SR	UTS	YS	EL	Ref.
					Temp.	Time	Temp.	Time	/%		/s	/MPa	/MPa	/%	
20	4.50	0.50	0.00	0.50	1300	60	20.0	0.0	0	20	8.33E-5	645.00	553	10.00	INCO Alloy
20	4.50	0.50	0.00	0.50	1300	60	20.0	0.0	0	400	8.33E-5	543.00	423	11.00	INCO Alloy
20	4.50	0.50	0.00	0.50	1300	60	20.0	0.0	0	600	8.33E-5	275.00	201	21.00	INCO Alloy
20	4.50	0.50	0.00	0.50	1300	60	20.0	0.0	0	800	8.33E-5	139.00	122	12.00	INCO Alloy
20	4.50	0.50	0.00	0.50	1300	60	20.0	0.0	0	900	8.33E-5	115.00	108	8.00	INCO Alloy
20	4.50	0.50	0.00	0.50	1300	60	20.0	0.0	0	1000	8.33E-5	100.00	97	4.50	INCO Alloy
20	4.50	0.50	0.00	0.50	1300	60	20.0	0.0	0	1100	8.33E-5	91.00	85	3.50	INCO Alloy
20	4.50	0.50	0.00	0.50	1300	60	20.0	0.0	0	1200	8.33E-5	79.00	76	2.00	INCO Alloy
13	0.00	2.90	1.50	0.00	1050	15.0	800	1444	0	20	8.10E-4	752.48	386	12.92	Zakine *et al.*, 1993
13	0.00	2.90	1.50	0.00	1050	15.0	800	1444	0	100	8.10E-4	722.77	366	12.08	Zakine *et al.*, 1993
13	0.00	2.90	1.50	0.00	1050	15.0	800	1444	0	200	8.10E-4	696.34	336	10.83	Zakine *et al.*, 1993
13	0.00	2.90	1.50	0.00	1050	15.0	800	1444	0	300	8.10E-4	663.37	321	10.01	Zakine *et al.*, 1993
13	0.00	2.90	1.50	0.00	1050	15.0	800	1444	0	400	8.10E-4	633.66	310	9.17	Zakine *et al.*, 1993
13	0.00	2.90	1.50	0.00	1050	15.0	800	1444	0	450	8.10E-4	598.32	287	9.17	Zakine *et al.*, 1993
13	0.00	2.90	1.50	0.00	1050	15.0	800	1444	0	500	8.10E-4	554.46	277	10.83	Zakine *et al.*, 1993
13	0.00	2.90	1.50	0.00	1050	15.0	800	1444	0	550	8.10E-4	485.05	257	12.92	Zakine *et al.*, 1993
13	0.00	2.90	1.50	0.00	1050	15.0	800	1444	0	600	8.10E-4	386.14	227	19.17	Zakine *et al.*, 1993
13	0.00	2.90	1.50	0.00	1050	15.0	800	1444	0	650	8.10E-4	305.93	198	27.08	Zakine *et al.*, 1993
13	0.00	2.90	1.50	0.00	1050	15.0	800	1444	0	700	8.10E-4	257.43	168	35.02	Zakine *et al.*, 1993
13	0.00	2.90	1.5	0.5	1050	15.0	800	1444	0	20	8.10E-4	831.68	702	7.08	Zakine *et al.*, 1993
13	0.00	2.90	1.5	0.5	1050	15.0	800	1444	0	100	8.10E-4	811.88	693	5.42	Zakine *et al.*, 1993
13	0.00	2.90	1.5	0.5	1050	15.0	800	1444	0	200	8.10E-4	797.80	712	5.01	Zakine *et al.*, 1993
13	0.00	2.90	1.5	0.5	1050	15.0	800	1444	0	300	8.10E-4	792.08	702	3.33	Zakine *et al.*, 1993
13	0.00	2.90	1.5	0.5	1050	15.0	800	1444	0	400	8.10E-4	752.48	653	2.51	Zakine *et al.*, 1993
13	0.00	2.90	1.5	0.5	1050	15.0	800	1444	0	450	8.10E-4	693.07	613	3.33	Zakine *et al.*, 1993
13	0.00	2.90	1.5	0.5	1050	15.0	800	1444	0	500	8.10E-4	663.37	565	4.17	Zakine *et al.*, 1993
13	0.00	2.90	1.5	0.5	1050	15.0	800	1444	0	550	8.10E-4	613.86	445	5.01	Zakine *et al.*, 1993
13	0.00	2.90	1.5	0.5	1050	15.0	800	1444	0	600	8.10E-4	544.55	386	8.35	Zakine *et al.*, 1993
13	0.00	2.90	1.5	0.5	1050	15.0	800	1444	0	650	8.10E-4	396.04	316	10.02	Zakine *et al.*, 1993
13	0.00	2.90	1.5	0.5	1050	15.0	800	1444	0	700	8.10E-4	297.03	247	11.25	Zakine *et al.*, 1993

CW–cold work; T–test temperature; SR–strain rate; UTS–ultimate tensile strength; YS–yield strength; EL–elongation. Compositions are in wt.%; temperature in °C; time in second.

Cr	Al	Ti	Mo	Y_2O_3	Annealing		Ageing		CW	T	SR	UTS	YS	EL	Ref.
					Temp.	Time	Temp.	Time	/%		/s	/MPa	/MPa	/%	
20	4.50	0.50	0.00	0.50	1300	60	20.00	0.00	0.00	350	8.33E-08	319.74	230	10.62	Whittenberger, 1981
20	4.50	0.50	0.00	0.50	1300	60	20.00	0.00	0.00	400	8.33E-08	302.25	198	8.5	Whittenberger, 1981
20	4.50	0.50	0.00	0.50	1300	60	20.00	0.00	0.00	500	8.33E-08	280.4	186	6.75	Whittenberger, 1981
20	4.50	0.50	0.00	0.50	1300	60	20.00	0.00	0.00	600	8.33E-08	258.54	183	5	Whittenberger, 1981
20	4.50	0.50	0.00	0.50	1300	60	20.00	0.00	0.00	700	8.33E-08	236.69	169	4.25	Whittenberger, 1981
20	4.50	0.50	0.00	0.50	1300	60	20.00	0.00	0.00	800	8.33E-08	219.21	153	3.25	Whittenberger, 1981
20	4.50	0.50	0.00	0.50	1300	60	20.00	0.00	0.00	900	8.33E-08	206.09	149	2.38	Whittenberger, 1981
20	4.50	0.50	0.00	0.50	1300	60	20.00	0.00	0.00	1000	8.33E-08	188.62	147	1.75	Whittenberger, 1981
20	4.50	0.50	0.00	0.50	1300	60	20.00	0.00	0.00	1050	8.33E-08	179.87	138	1.75	Whittenberger, 1981
20	4.50	0.50	0.00	0.50	1300	60	20.00	0.00	0.00	1100	8.33E-08	166.75	140	1.75	Whittenberger, 1981
20	4.50	0.50	0.00	0.50	1300	60	20.00	0.00	0.00	1152	8.33E-08	158.01	139	1.5	Whittenberger, 1981
20	4.50	0.50	0.00	0.50	1300	60	20.0	0.0	0	1093	3.33E-2	84.10	81	24.00	Whittenberger, 1979
20	4.50	0.50	0.00	0.50	1300	60	20.0	0.0	0	1093	8.33E-3	80.10	78	19.00	Whittenberger, 1979
20	4.50	0.50	0.00	0.50	1300	60	20.0	0.0	0	1093	8.33E-4	80.40	79	6.10	Whittenberger, 1979
20	4.50	0.50	0.00	0.50	1300	60	20.0	0.0	0	1093	3.33E-4	81.00	79	4.50	Whittenberger, 1979
20	4.50	0.50	0.00	0.50	1300	60	20.0	0.0	0	1093	8.33E-5	77.20	75	1.90	Whittenberger, 1979
20	4.50	0.50	0.00	0.50	1300	60	20.0	0.0	0	1093	8.33E-6	77.10	75	1.00	Whittenberger, 1979
20	4.50	0.50	0.00	0.50	1300	60	20.0	0.0	0	1093	3.33E-6	76.90	76	1.00	Whittenberger, 1979
20	4.50	0.50	0.00	0.50	1300	60	20.0	0.0	0	1093	8.33E-7	77.80	76	1.00	Whittenberger, 1979
20	4.50	0.50	0.00	0.50	1300	60	20.0	0.0	0	1093	8.33E-8	73.30	73	1.00	Whittenberger, 1979
20	4.50	0.50	0.00	0.50	1300	60	20.0	0.0	0	1093	3.33E-8	70.70	69	1.00	Whittenberger, 1979
20	4.50	0.50	0.00	0.50	1300	60	20.0	0.0	0	1092	5.8E-3	94.30	91	4.8	Whittenberger, 1978
20	4.50	0.50	0.00	0.50	1300	60	20.0	0.0	0	1092	1.5E-3	92.50	85	4.1	Whittenberger, 1978
20	4.50	0.50	0.00	0.50	1300	60	20.0	0.0	0	1092	1.5E-4	87.30	80	2.1	Whittenberger, 1978
20	4.50	0.50	0.00	0.50	1300	60	20.0	0.0	0	1092	1.5E-5	76.10	71	1.4	Whittenberger, 1978
14	0.00	1.00	0.30	0.27	20.00	0.00	20.00	0.00	0	20	7.10E-04	1011.21	994	18.54	Alamo *et al.*, 1992
14	0.00	1.00	0.30	0.27	20.00	0.00	20.00	0.00	0	150	7.10E-04	924.11	934	17.71	Alamo *et al.*, 1992
14	0.00	1.00	0.30	0.27	20.00	0.00	20.00	0.00	0	300	7.10E-04	867.14	826	16.88	Alamo *et al.*, 1992
14	0.00	1.00	0.30	0.27	20.00	0.00	20.00	0.00	0	500	7.10E-04	668.13	657	20.02	Alamo *et al.*, 1992
14	0.00	1.00	0.30	0.27	20.00	0.00	20.00	0.00	0	600	7.10E-04	498.16	487	26.88	Alamo *et al.*, 1992
14	0.00	1.00	0.30	0.27	20.00	0.00	20.00	0.00	0	750	7.10E-04	213.3	191	32.45	Alamo *et al.*, 1992
14	0.00	1.00	0.30	0.27	1000.00	120.00	20.00	0.00	0	20	7.10E-04	1145.23	1124	15.21	Alamo *et al.*, 1992
14	0.00	1.00	0.30	0.27	1000.00	120.00	20.00	0.00	0	150	7.10E-04	1041.12	1029	13.96	Alamo *et al.*, 1992
14	0.00	1.00	0.30	0.27	1000.00	120.00	20.00	0.00	0	300	7.10E-04	972.21	946	13.54	Alamo *et al.*, 1992
14	0.00	1.00	0.30	0.27	1000.00	120.00	20.00	0.00	0	500	7.10E-04	813.2	795	16.88	Alamo *et al.*, 1992
14	0.00	1.00	0.30	0.27	1000.00	120.00	20.00	0.00	0	600	7.10E-04	564.35	546	20.34	Alamo *et al.*, 1992
14	0.00	1.00	0.30	0.27	1000.00	120.00	20.00	0.00	0	700	7.10E-04	356.24	324	18.45	Alamo *et al.*, 1992

Cr	Al	Ti	Mo	Y_2O_3	Annealing		Ageing		CW	T	SR	UTS	YS	EL	Ref.
					Temp.	Time	Temp.	Time	/%		/s	/MPa	/MPa	/%	
20	4.5	0.5	0	0.5	1330	60	20.00	0.00	0.00	0	8.10E-4	645.12	563	12.92	Singer and Gessinger, 1984
20	4.5	0.5	0	0.5	1330	60	20.00	0.00	0.00	150	8.10E-4	610.21	522	11.96	Singer and Gessinger, 1984
20	4.5	0.5	0	0.5	1330	60	20.00	0.00	0.00	300	8.10E-4	568.23	482	10.01	Singer and Gessinger, 1984
20	4.5	0.5	0	0.5	1330	60	20.00	0.00	0.00	400	8.10E-4	498.67	434	10	Singer and Gessinger, 1984
20	4.5	0.5	0	0.5	1330	60	20.00	0.00	0.00	500	8.10E-4	387.54	337	19.17	Singer and Gessinger, 1984
20	4.5	0.5	0	0.5	1330	60	20.00	0.00	0.00	600	8.10E-4	296.45	209	23.19	Singer and Gessinger, 1984
20	4.5	0.5	0	0.5	1330	60	20.00	0.00	0.00	800	8.10E-4	189.89	128	21.9	Singer and Gessinger, 1984
20	4.5	0.5	0	0.5	1330	60	20.00	0.00	0.00	900	8.10E-4	173.43	120	12.23	Singer and Gessinger, 1984
20	4.5	0.5	0	0.5	1330	60	20.00	0.00	0.00	1000	8.10E-4	115.56	104	8.45	Singer and Gessinger, 1984
20	4.5	0.5	0	0.5	1330	60	20.00	0.00	0.00	1100	8.10E-4	113.53	104	4.5	Singer and Gessinger, 1984
20	4.5	0.5	0	0.5	1330	60	20.00	0.00	0.00	1200	8.10E-4	99.34	88	3.5	Singer and Gessinger, 1984
20	4.5	0.5	0	0.5	1330	60	20.00	0.00	0.00	1250	8.10E-4	89.78	76	2.9	Singer and Gessinger, 1984
20	4.5	0.5	0	0.5	1330	60	20.00	0.00	0.00	20	8.33E-5	647	550	10	INCO Alloy
20	4.5	0.5	0	0.5	1330	60	20.00	0.00	0.00	20	8.33E-5	556	549	10.5	INCO Alloy
20	4.5	0.5	0	0.5	1330	60	20.00	0.00	0.00	20	8.33E-5	624	551	8	INCO Alloy
20	4.5	0.5	0	0.5	1330	60	20.00	0.00	0.00	20	8.33E-5	624	552	8	INCO Alloy
20	4.5	0.5	0	0.5	20	0	20.00	0.00	0.00	20	8.33E-5	1218	1208	1.6	INCO Alloy
20	4.5	0.5	0	0.5	20	0	20.00	0.00	0.00	200	8.33E-5	1007	1001	0.8	INCO Alloy
20	4.5	0.5	0	0.5	1330	60	20.00	0.00	0.00	400	8.33E-5	545	422	11	INCO Alloy
20	4.5	0.5	0	0.5	1330	60	20.00	0.00	0.00	400	8.33E-5	542	425	10.5	INCO Alloy
20	4.5	0.5	0	0.5	1330	60	20.00	0.00	0.00	400	8.33E-5	555	424	10.5	INCO Alloy
20	4.5	0.5	0	0.5	1330	60	20.00	0.00	0.00	400	8.33E-5	552	422	10.5	INCO Alloy
20	4.5	0.5	0	0.5	20	0	20.00	0.00	0.00	400	8.33E-5	987	915	9.6	INCO Alloy
20	4.5	0.5	0	0.5	1330	60	20.00	0.00	0.00	500	8.33E-5	418	334	12	INCO Alloy
20	4.5	0.5	0	0.5	1330	60	20.00	0.00	0.00	600	8.33E-5	272	200	19	INCO Alloy
20	4.5	0.5	0	0.5	1330	60	20.00	0.00	0.00	600	8.33E-5	279	203	23	INCO Alloy
20	4.5	0.5	0	0.5	1330	60	20.00	0.00	0.00	600	8.33E-5	279	204	23	INCO Alloy
20	4.5	0.5	0	0.5	20	0	20.00	0.00	0.00	600	8.33E-5	494	305	19.5	INCO Alloy
20	4.5	0.5	0	0.5	1330	60	20.00	0.00	0.00	650	8.33E-5	218	154	22	INCO Alloy
20	4.5	0.5	0	0.5	1330	60	20.00	0.00	0.00	700	8.33E-5	173	138	23	INCO Alloy
13	0.00	2.2	1.50	0.5	1050	15.0	800	1444	0.00	22	5.0E-3	874	724	10.3	Hendrix and Vandermeulen, 1982
13	0.00	2.2	1.50	0.5	1050	15.0	800	1444	0.00	22	5.0E-3	930	768	10.3	Hendrix and Vandermeulen, 1982
13	0.00	2.2	1.50	0.5	1050	15.0	800	1444	0.00	500	5.0E-3	622	546	15.2	Hendrix and Vandermeulen, 1982
13	0.00	2.2	1.50	0.5	1050	15.0	800	1444	0.00	500	5.0E-3	624	542	15.3	Hendrix and Vandermeulen, 1982
13	0.00	2.2	1.50	0.5	1050	15.0	800	1444	0.00	700	5.0E-3	236	216	20.0	Hendrix and Vandermeulen, 1982
13	0.00	2.2	1.50	0.5	1050	15.0	800	1444	0.00	700	5.0E-3	240	217	20.6	Hendrix and Vandermeulen, 1982

Cr	Al	Ti	Mo	Y_2O_3	Annealing		Ageing		CW	T	SR	UTS	YS	EL	Ref.
					Temp.	Time	Temp.	Time	/%		/s	/MPa	/MPa	/%	
13	0.00	2.2	1.50	0.5	1050	15.0	800	2888	0.00	500	5.0E-3	660	560	12.6	Hendrix and Vandermeulen, 1982
13	0.00	2.2	1.50	0.5	1050	15.0	800	2888	0.00	500	5.0E-3	661	550	12.7	Hendrix and Vandermeulen, 1982
13	0.00	2.2	1.50	0.5	1050	15.0	800	2888	0.00	600	5.0E-3	413	366	24.6	Hendrix and Vandermeulen, 1982
13	0.00	2.2	1.50	0.5	1050	15.0	800	2888	0.00	600	5.0E-3	410	365	21.0	Hendrix and Vandermeulen, 1982
13	0.00	2.2	1.50	0.5	1050	15.0	800	2888	0.00	700	5.0E-3	247	219	21.6	Hendrix and Vandermeulen, 1982
13	0.00	2.2	1.50	0.5	1050	15.0	800	2888	0.00	700	5.0E-3	248	213	23.2	Hendrix and Vandermeulen, 1982
13	0.00	2.2	1.50	0.5	1050	15.0	800	2888	0.00	22	5.0E-3	1000	795	7.7	Hendrix and Vandermeulen, 1982
13	0.00	2.2	1.50	0.5	1050	15.0	800	2888	0.00	22	5.0E-3	991	768	7.7	Hendrix and Vandermeulen, 1982
13	0.00	2.2	1.50	0.5	1050	15.0	800	2888	0.00	200	5.0E-3	909	692	7.0	Hendrix and Vandermeulen, 1982
13	0.00	2.2	1.50	0.5	1050	15.0	800	2888	0.00	200	5.0E-3	909	697	7.0	Hendrix and Vandermeulen, 1982
13	0.00	2.2	1.50	0.5	1050	15.0	800	2888	0.00	400	5.0E-3	804	653	5.7	Hendrix and Vandermeulen, 1982
13	0.00	2.2	1.50	0.5	1050	15.0	800	2888	0.00	400	5.0E-3	808	658	6.0	Hendrix and Vandermeulen, 1982
20	4.50	0.50	0.00	0.50	1330	60	20.00	0.00	0.00	400	1.00E-03	632.04	521	10.23	Dubiel *et al.*, 1994
20	4.50	0.50	0.00	0.50	1330	60	20.00	0.00	0.00	600	1.00E-03	344.75	322	20.4	Dubiel *et al.*, 1994
20	4.50	0.50	0.00	0.50	1330	60	20.00	0.00	0.00	800	1.00E-03	159.12	145	12.42	Dubiel *et al.*, 1994
13	0.00	3.50	1.50	0.00	1050	15.0	800	1444	0.00	0	8.10E-4	1148.21	1054	15.21	Dubiel *et al.*, 1984
13	0.00	3.50	1.50	0.00	1050	15.0	800	1444	0.00	150	8.10E-4	1098.78	956	13.96	Dubiel *et al.*, 1984
13	0.00	3.50	1.50	0.00	1050	15.0	800	1444	0.00	200	8.10E-4	1056.45	945	13.96	Dubiel *et al.*, 1984
13	0.00	3.50	1.50	0.00	1050	15.0	800	1444	0.00	300	8.10E-4	1023.43	917	13.54	Dubiel *et al.*, 1984
13	0.00	3.50	1.50	0.00	1050	15.0	800	1444	0.00	530	8.10E-4	776.48	683	18.56	Dubiel *et al.*, 1984
13	0.00	3.50	1.50	0.00	1050	15.0	800	1444	0.00	610	8.10E-4	626.58	522	21.4	Dubiel *et al.*, 1984
20	4.50	0.50	0.00	0.50	20.00	0.00	20.00	0.00	70.00	450	4.10E-03	623.02	543	21	Alamo *et al.*, 1990
20	4.50	0.50	0.00	0.50	20.00	0.00	20.00	0.00	70.00	500	4.10E-03	505.28	432	26.14	Alamo *et al.*, 1990
20	4.50	0.50	0.00	0.50	20.00	0.00	20.00	0.00	70.00	550	4.10E-03	382.64	234	33	Alamo *et al.*, 1990
20	4.50	0.50	0.00	0.50	20.00	0.00	20.00	0.00	70.00	600	4.10E-03	230.57	197	49.29	Alamo *et al.*, 1990
20	4.50	0.50	0.00	0.50	20.00	0.00	20.00	0.00	70.00	650	4.10E-03	142.26	121	42	Alamo *et al.*, 1990
20	4.50	0.50	0.00	0.50	20.00	0.00	20.00	0.00	70.00	700	4.10E-03	112.83	87	34.29	Alamo *et al.*, 1990
20	4.50	0.50	0.00	0.50	1125	5	20.00	0.00	10.00	20	4.10E-03	932.29	834	1.82	Alamo *et al.*, 1990
20	4.50	0.50	0.00	0.50	1125	5	20.00	0.00	10.00	200	4.10E-03	786.32	657	1.36	Alamo *et al.*, 1990
20	4.50	0.50	0.00	0.50	1125	5	20.00	0.00	10.00	400	4.10E-03	630.94	523	3.18	Alamo *et al.*, 1990
20	4.50	0.50	0.00	0.50	1125	5	20.00	0.00	10.00	500	4.10E-03	484.98	324	5	Alamo *et al.*, 1990
20	4.50	0.50	0.00	0.50	1125	5	20.00	0.00	10.00	600	4.10E-03	343.72	231	20.45	Alamo *et al.*, 1990
20	4.50	0.50	0.00	0.50	1125	5	20.00	0.00	10.00	650	4.10E-03	258.97	200	19.55	Alamo *et al.*, 1990
20	4.50	0.50	0.00	0.50	1125	5	20.00	0.00	10.00	700	4.10E-03	202.47	156	16.36	Alamo *et al.*, 1990
20	4.50	0.50	0.00	0.50	20.00	0.00	20.00	0.00	70.00	20	4.10E-03	1108.68	1064	3.43	Alamo *et al.*, 1990

Cr	Al	Ti	Mo	Y_2O_3	Annealing		Ageing		CW	T	SR	UTS	YS	EL	Ref.
					Temp.	Time	Temp.	Time	/%		/s	/MPa	/MPa	/%	
20	4.50	0.50	0.00	0.50	20.00	0.00	20.00	0.00	70.00	100	4.10E-03	1059.62	946	7.24	Alamo *et al.*, 1990
20	4.50	0.50	0.00	0.50	20.00	0.00	20.00	0.00	70.00	150	4.10E-03	1000.62	903	7.74	Alamo *et al.*, 1990
20	4.50	0.50	0.00	0.50	20.00	0.00	20.00	0.00	70.00	200	4.10E-03	978.68	956	8.4	Alamo *et al.*, 1990
20	4.50	0.50	0.00	0.50	20.00	0.00	20.00	0.00	70.00	250	4.10E-03	966.63	948	8.56	Alamo *et al.*, 1990
20	4.50	0.50	0.00	0.50	20.00	0.00	20.00	0.00	70.00	300	4.10E-03	946.79	850	9.5	Alamo *et al.*, 1990
20	4.50	0.50	0.00	0.50	20.00	0.00	20.00	0.00	70.00	350	4.10E-03	892.83	745	12.86	Alamo *et al.*, 1990
20	4.50	0.50	0.00	0.50	20.00	0.00	20.00	0.00	70.00	400	4.10E-03	750.57	670	18.43	Alamo *et al.*, 1990
20	4.5	0.5	0	0.5	1330	60	20.00	0.00	0.00	20	8.33E-5	647	550	10	INCO Alloy
20	4.5	0.5	0	0.5	1330	60	20.00	0.00	0.00	20	8.33E-5	556	549	10.5	INCO Alloy
20	4.5	0.5	0	0.5	1330	60	20.00	0.00	0.00	20	8.33E-5	624	551	8	INCO Alloy
20	4.5	0.5	0	0.5	1330	60	20.00	0.00	0.00	20	8.33E-5	624	552	8	INCO Alloy
20	4.5	0.5	0	0.5	20	0	20.00	0.00	0.00	20	8.33E-5	1218	1208	1.6	INCO Alloy
20	4.5	0.5	0	0.5	20	0	20.00	0.00	0.00	200	8.33E-5	1007	1001	0.8	INCO Alloy
20	4.5	0.5	0	0.5	1330	60	20.00	0.00	0.00	400	8.33E-5	545	422	11	INCO Alloy
20	4.5	0.5	0	0.5	1330	60	20.00	0.00	0.00	400	8.33E-5	542	425	10.5	INCO Alloy
20	4.5	0.5	0	0.5	1330	60	20.00	0.00	0.00	400	8.33E-5	555	424	10.5	INCO Alloy
20	4.5	0.5	0	0.5	1330	60	20.00	0.00	0.00	400	8.33E-5	552	422	10.5	INCO Alloy
20	4.5	0.5	0	0.5	20	0	20.00	0.00	0.00	400	8.33E-5	987	915	9.6	INCO Alloy
20	4.5	0.5	0	0.5	1330	60	20.00	0.00	0.00	500	8.33E-5	418	334	12	INCO Alloy
20	4.5	0.5	0	0.5	1330	60	20.00	0.00	0.00	600	8.33E-5	272	200	19	INCO Alloy
20	4.5	0.5	0	0.5	1330	60	20.00	0.00	0.00	600	8.33E-5	279	203	23	INCO Alloy
20	4.5	0.5	0	0.5	1330	60	20.00	0.00	0.00	600	8.33E-5	279	204	23	INCO Alloy
20	4.5	0.5	0	0.5	20	0	20.00	0.00	0.00	600	8.33E-5	494	305	19.5	INCO Alloy
20	4.5	0.5	0	0.5	1330	60	20.00	0.00	0.00	650	8.33E-5	218	154	22	INCO Alloy
20	4.5	0.5	0	0.5	1330	60	20.00	0.00	0.00	700	8.33E-5	173	138	23	INCO Alloy
20	4.5	0.5	0	0.5	1330	60	20.00	0.00	0.00	1200	8.33E-5	80	76	3	INCO Alloy
20	4.5	0.5	0	0.5	1330	60	20.00	0.00	0.00	1200	8.33E-5	78	75	1	INCO Alloy
20	4.5	0.5	0	0.5	1330	60	20.00	0.00	0.00	1200	8.33E-5	76	78	1	INCO Alloy
20	4.5	0.5	0	0.5	20	0	20.00	0.00	0.00	700	8.33E-5	298	211	22.5	INCO Alloy
20	4.5	0.5	0	0.5	1330	60	20.00	0.00	0.00	750	8.33E-5	155	122	16	INCO Alloy
20	4.5	0.5	0	0.5	1330	60	20.00	0.00	0.00	800	8.33E-5	140	124	10	INCO Alloy
20	4.5	0.5	0	0.5	1330	60	20.00	0.00	0.00	800	8.33E-5	138	120	13	INCO Alloy
20	4.5	0.5	0	0.5	1330	60	20.00	0.00	0.00	800	8.33E-5	135	121	12	INCO Alloy
20	4.5	0.5	0	0.5	20	0	20.00	0.00	0.00	800	8.33E-5	137	122	11	INCO Alloy
20	4.5	0.5	0	0.5	20	0	20.00	0.00	0.00	800	8.33E-5	233	162	10	INCO Alloy
20	4.5	0.5	0	0.5	20	0	20.00	0.00	0.00	800	8.33E-5	257	166	11	INCO Alloy

Cr	Al	Ti	Mo	Y_2O_3	Annealing		Ageing		CW	T	SR	UTS	YS	EL	Ref.
					Temp.	Time	Temp.	Time	/%		/s	/MPa	/MPa	/%	
20	4.5	0.5	0	0.5	20	0	20.00	0.00	0.00	800	8.33E-5	244	180	11	INCO Alloy
20	4.5	0.5	0	0.5	1330	60	20.00	0.00	0.00	900	8.33E-5	115	107	9	INCO Alloy
20	4.5	0.5	0	0.5	1330	60	20.00	0.00	0.00	900	8.33E-5	116	109	7.5	INCO Alloy
20	4.5	0.5	0	0.5	20	0	20.00	0.00	0.00	900	8.33E-5	170	118	6.5	INCO Alloy
20	4.5	0.5	0	0.5	20	0	20.00	0.00	0.00	900	8.33E-5	157	109	6	INCO Alloy
20	4.5	0.5	0	0.5	20	0	20.00	0.00	0.00	900	8.33E-5	170	118	5.5	INCO Alloy
20	4.5	0.5	0	0.5	20	0	20.00	0.00	0.00	950	8.33E-5	147	95	4	INCO Alloy
20	4.5	0.5	0	0.5	20	0	20.00	0.00	0.00	950	8.33E-5	145	98	3.5	INCO Alloy
20	4.5	0.5	0	0.5	20	0	20.00	0.00	0.00	982	8.33E-5	124	96	3.5	INCO Alloy
20	4.5	0.5	0	0.5	1330	60	20.00	0.00	0.00	1000	8.33E-5	100	97	4.5	INCO Alloy
20	4.5	0.5	0	0.5	1330	60	20.00	0.00	0.00	1000	8.33E-5	101	97	5	INCO Alloy
20	4.5	0.5	0	0.5	1330	60	20.00	0.00	0.00	1000	8.33E-5	101	94	6.5	INCO Alloy
20	4.5	0.5	0	0.5	1330	60	20.00	0.00	0.00	1000	8.33E-5	101	93	5	INCO Alloy
20	4.5	0.5	0	0.5	20	0	20.00	0.00	0.00	1000	8.33E-5	130	93	5.4	INCO Alloy
20	4.5	0.5	0	0.5	20	0	20.00	0.00	0.00	1000	8.33E-5	113	94	1.2	INCO Alloy
20	4.5	0.5	0	0.5	20	0	20.00	0.00	0.00	1000	8.33E-5	110	97	1.8	INCO Alloy
20	4.5	0.5	0	0.5	20	0	20.00	0.00	0.00	1030	8.33E-5	92	72	3	INCO Alloy
20	4.5	0.5	0	0.5	20	0	20.00	0.00	0.00	1093	8.33E-5	81	63	1	INCO Alloy
20	4.5	0.5	0	0.5	1330	60	20.00	0.00	0.00	1100	8.33E-5	91	85	3.5	INCO Alloy
14	0.00	1.00	0.30	0.27	20.00	0.00	20.00	0.00	25	0	7.10E-04	1270.64	1163	10.40	Regle, 1994
14	0.00	1.00	0.30	0.27	20.00	0.00	20.00	0.00	25	100	7.10E-04	1196.27	1127	10.40	Regle, 1994
14	0.00	1.00	0.30	0.27	20.00	0.00	20.00	0.00	25	150	7.10E-04	1173.73	1092	10.40	Regle, 1994
14	0.00	1.00	0.30	0.27	20.00	0.00	20.00	0.00	25	200	7.10E-04	1154.18	1063	10.50	Regle, 1994
14	0.00	1.00	0.30	0.27	20.00	0.00	20.00	0.00	25	250	7.10E-04	1102.27	1023	11.80	Regle, 1994
14	0.00	1.00	0.30	0.27	20.00	0.00	20.00	0.00	25	300	7.10E-04	1101.73	1018	13.40	Regle, 1994
14	0.00	1.00	0.30	0.27	20.00	0.00	20.00	0.00	25	350	7.10E-04	1079.18	987	13.80	Regle, 1994
14	0.00	1.00	0.30	0.27	20.00	0.00	20.00	0.00	25	400	7.10E-04	1012.45	945	14.40	Regle, 1994
14	0.00	1.00	0.30	0.27	20.00	0.00	20.00	0.00	25	450	7.10E-04	948.73	872	15.20	Regle, 1994
14	0.0	1.00	0.30	0.27	20.00	0.00	20.00	0.00	25	500	7.10E-04	834.45	745	18.45	Regle, 1994
14	0.00	1.00	0.30	0.27	20.00	0.00	20.00	0.00	25	550	7.10E-04	721.36	636	20.0	Regle, 1994
14	0.00	1.00	0.30	0.27	20.00	0.00	20.00	0.00	25	650	7.10E-04	501.00	400	24	Regle, 1994
14	0.00	1.00	0.30	0.27	20.00	0.00	20.00	0.00	25	750	7.10E-04	463.27	327	20.40	Regle, 1994
14	0.00	1.00	0.30	0.27	20.00	0.00	20.00	0.00	60	0	7.10E-04	1680.3	1600	6.40	Regle, 1994
14	0.00	1.00	0.30	0.27	20.00	0.00	20.00	0.00	60	100	7.10E-04	1579.09	1509	6	Regle, 1994
14	0.00	1.00	0.30	0.27	20.00	0.00	20.00	0.00	60	200	7.10E-04	1481.82	1381	6.4	Regle, 1994
14	0.00	1.00	0.30	0.27	20.00	0.00	20.00	0.00	60	300	7.10E-04	1372.73	1272	6.80	Regle, 1994

Cr	Al	Ti	Mo	Y_2O_3	Annealing		Ageing		CW	T	SR	UTS	YS	EL	Ref.
					Temp.	Time	Temp.	Time	/%		/s	/MPa	/MPa	/%	
14	0.00	1.00	0.30	0.27	20.00	0.00	20.00	0.00	60	400	7.10E-04	1281.82	1181	6.4	Regle, 1994
14	0.00	1.00	0.30	0.27	20.00	0.00	20.00	0.00	60	450	7.10E-04	1156.73	1072	6.8	Regle, 1994
14	0.00	1.00	0.30	0.27	20.00	0.00	20.00	0.00	60	500	7.10E-04	1009.09	909	10.4	Regle, 1994
14	0.00	1.00	0.30	0.27	20.00	0.00	20.00	0.00	60	550	7.10E-04	908.18	818	13.60	Regle, 1994
14	0.00	1.00	0.30	0.27	20.00	0.00	20.00	0.00	60	600	7.10E-04	717.18	618	16.80	Regle, 1994
14	0.00	1.00	0.30	0.27	20.00	0.00	20.00	0.00	60	650	7.10E-04	556.27	527	14.40	Regle, 1994
14	0.00	1.00	0.30	0.27	20.00	0.00	20.00	0.00	60	700	7.10E-04	496.55	454	12.00	Regle, 1994
14	0.00	1.00	0.30	0.27	20.00	0.00	20.00	0.00	60	720	7.10E-04	450.00	400	11.78	Regle, 1994
14	0.00	1.00	0.30	0.27	20.00	0.00	20.00	0.00	60	750	7.10E-04	401.82	381	10.40	Regle, 1994
20	4.5	0.5	0	0.5	20	0	20.00	0.00	0.0	0	7.10E-04	1055.32	931	9.26	Regle, 1994
20	4.5	0.5	0	0.5	20	0	20.00	0.00	0.00	100	7.10E-04	996.70	896	9.96	Regle, 1994
20	4.5	0.5	0	0.5	20	0	20.00	0.00	0.00	200	7.10E-04	943.96	843	11.96	Regle, 1994
20	4.5	0.5	0	0.5	20	0	20.00	0.00	0.00	300	7.10E-04	908.79	808	12.96	Regle, 1994
20	4.5	0.5	0	0.5	20	0	20.00	0.00	0.00	450	7.10E-04	794.88	720	16.26	Regle, 1994
20	4.5	0.5	0	0.5	20	0	20.00	0.00	0.00	550	7.10E-04	609.89	509	19.30	Regle, 1994
20	4.5	0.5	0	0.5	20	0	20.00	0.00	0.00	650	7.10E-04	306.74	263	23.43	Regle, 1994
20	4.5	0.5	0	0.5	20	0	20.00	0.00	0.00	750	7.10E-04	192.08	123	23.43	Regle, 1994
20	4.5	0.5	0	0.5	20	0	20.00	0.00	0.00	800	7.10E-04	188.08	121	11.43	Regle, 1994
20	4.5	0.5	0	0.5	20	0	20.00	0.00	0.00	850	7.10E-04	178.08	115	10.43	Regle, 1994
20	4.5	0.5	0	0.5	20	0	20.00	0.00	25	10	7.10E-04	1242.86	1142	8.43	Regle, 1994
20	4.5	0.5	0	0.5	20	0	20.00	0.00	25	131	7.10E-04	1154.95	1054	7.74	Regle, 1994
20	4.5	0.5	0	0.5	20	0	20.00	0.00	25	273	7.10E-04	1031.87	931	8.74	Regle, 1994
20	4.5	0.5	0	0.5	20	0	20.00	0.00	25	465	7.10E-04	891.21	791	13.65	Regle, 1994
20	4.5	0.5	0	0.5	20	0	20.00	0.00	25	557	7.10E-04	652.64	562	20	Regle, 1994
20	4.5	0.5	0	0.5	20	0	20.00	0.00	25	658	7.10E-04	396.48	316	24.39	Regle, 1994
20	4.5	0.5	0	0.5	20	0	20.00	0.00	25	749	7.10E-04	198.24	158	22.65	Regle, 1994
20	4.5	0.5	0	0.5	20	0	20.00	0.00	60	20	7.10E-04	1486.92	1476	5.22	Regle, 1994
20	4.5	0.5	0	0.5	20	0	20.00	0.00	60	120	7.10E-04	1453.85	1353	7.83	Regle, 1994
20	4.5	0.5	0	0.5	20	0	20.00	0.00	60	212	7.10E-04	1348.35	1248	9.13	Regle, 1994
20	4.5	0.5	0	0.5	20	0	20.00	0.00	60	293	7.10E-04	1260.44	1160	9.13	Regle, 1994
20	4.5	0.5	0	0.5	20	0	20.00	0.00	60	394	7.10E-04	1154.95	1054	10.43	Regle, 1994
20	4.5	0.5	0	0.5	20	0	20.00	0.00	60	465	7.10E-04	1067.03	967	13.04	Regle, 1994
20	4.5	0.5	0	0.5	20	0	20.00	0.00	60	557	7.10E-04	856.04	756	19.57	Regle, 1994
20	4.5	0.5	0	0.5	20	0	20.00	0.00	60	587	7.10E-04	680.22	580	20.39	Regle, 1994
20	4.5	0.5	0	0.5	20	0	20.00	0.00	60	668	7.10E-04	396.48	316	21.61	Regle, 1994
20	4.5	0.5	0	0.5	20	0	20.00	0.00	60	749	7.10E-04	297.24	158	20.34	Regle, 1994

APPENDIX FIVE

Weights from the Neural Network Models

The data are arranged in a continuous horizontal sequence in the following order:

$$\theta_1^{(1)}, w_{1,1}^{(1)} \ldots w_{1,22}^{(1)},$$
$$\theta_2^{(1)}, w_{2,1}^{(1)} \ldots w_{2,22}^{(1)},$$
$$\theta_3^{(1)}, w_{3,1}^{(1)} \ldots w_{3,22}^{(1)},$$
$$\theta_4^{(1)}, w_{4,1}^{(1)} \ldots w_{1,22}^{(1)},$$
$$\theta^{(2)}, w_1^{(2)} \ldots w_4^{(2)}$$

Table A5.1a: First member of committee for the yield strength

-0.00963549	0.0965139	0.0925577	0.116975	-0.0618065	0.401545	-0.073527	0.0223006	-0.0422882	-0.00578501	0.00911521	-1.97707
0.526691	-0.0496755	-0.0307015	-0.0244288	0.0102626	0.0328008	-0.14324	0.179606	-0.0141432	0.0350717	0.00245982	-0.129273
4.21674	-0.740116	-0.123192	-0.0433204	-0.0383476	0.00922208	0.0503388	-0.150428	0.70438	-0.00466108	0.0458901	-0.000548582
0.0930819	-2.64046	0.803751	0.00118676	0.00105556	0.00100383	-0.00126966	0.000921421	-0.0011365	-0.00228579	0.0006872240	0.000960586
3.15534e-05	0.000562953	-0.0842606	0.0126547	0.0014289	0.0121175	0.01406	-0.030977	-0.011318	0.107937	0.320192	-0.000796604
-0.00765068	0.0006504	-0.00266111	1.19158	-0.0216612	0.008047	-0.0612125	-0.0739391	-0.000184482	-0.0075718	-0.246463	-0.830796
-0.0287112	-0.021068	0.00341582	0.166202	-2.23336	0.62458	-0.102769	-0.101849	-0.105986	0.124744	0.0254157	-0.171295
0.554864	0.0280342	0.0116805	0.0112502	0.0552873	-0.329057	1.3266	-0.138577	0.0427931	0.0594477	0.029996	0.0351689
-0.0954499	-0.69618	-0.0240259	0.0393423	-0.00391515	0.0172212	1.77225	-1.02043	0.0110008	-0.00360183	-0.00393565	-0.126096
-0.000794104	0.247329	0.493305	-0.0165823	-0.00670078	0.00115444	0.0150564	1.34508	0.505875	-0.0578569	0.0629772	0.0707605
0.0409896	0.00721293	0.0801678	0.566736	-0.010257	0.0180833	0.00381571	0.0897526	-3.91079	0.663554	-0.0846936	0.0894762
0.0983313	-0.0898865	0.000762335	0.0381056	-0.823754	-0.0580365	0.0133889	0.00187751	0.14364	-3.832	0.499408	-0.0166071
-0.00149307	-0.00920792	-0.0182418	-0.0293844	0.058198	-0.617381	-0.00223201	-0.0284824	0.00316078	0.126999	0.181151	-0.251154
0.0067604	0.0743512	0.0625915	0.0755425	-0.0796998	0.00979387	0.1445	-0.0232309	-0.0657325	0.00459906	-0.0402862	1.33049
-1.04415	-0.0204567	-0.100487	-0.112823	-0.109906	0.0151989	-0.163481	0.291148	-0.0223562	-0.00407049	-0.00568125	-0.213171
-1.1985	-0.202536	2.03748	7.76675	-3.90774	6.29014	-0.100933	2.77667	5.48912	7.51574	6.8865	4.89917
-3.7766	-4.79932	5.26614	9.462	5.76393							

Table A5.1b: Second member of committee for the yield strength

0.000479841	-0.080894	-0.0566454	-0.481207	1.19845e-06	-0.026999	0.00291564	0.0958271	-1.25876e-05	0.000363673	0.571339	1.18035
-0.0164984	0.00783428	-0.120645	-0.0969914	1.32047	-0.000268118	-0.0701938	-0.00915339	-0.28708	-0.000239954	0.00258108	-0.112142
0.522203	-0.00837235	-0.020773	0.0669092	0.0307038	-0.159074	-0.000125815	-0.0429729	0.00501487	-0.187528	-7.03826e-05	0.00215657
-0.0388266	4.02114	0.0722661	-0.00389438	0.0900116	0.0372058	-0.369534	-0.000436431	-0.0724181	0.0160896	-0.0114118	-0.000270958
-0.00182226	-0.625313	1.31446	-0.00919318	0.00369866	0.00118469	-0.00486987	-0.081186	-0.000106909	0.0107155	0.0125951	-0.0115773
-6.17585e-05	0.00275412	0.164982	-4.68842	0.0581995	0.0120208	0.0329765	0.0237619	-0.0286545	-6.30028e-06	0.0661794	-0.0136737
0.0443705	1.41052e-05	0.00131798	0.23689	1.85265	-0.0277388	0.0147457	-0.0730213	-0.050437	0.288591	-8.32148e-05	0.02025
0.0202056	0.234573	-8.52194e-05	0.00143649	-0.331085	4.39506	0.0147006	0.00557663	-0.0784979	-0.0585164	-0.814308	-0.000184722
0.0924946	0.0103568	0.0938725	-0.000160631	-0.00203449	0.0407442	-0.724849	0.0117738	-0.00596456	0.0424843	-0.00371166	0.551819
0.000520677	-0.136086	0.0100122	0.0787932	-0.000366828	-0.00192239	0.500614	-1.60109	-0.0249172	0.00413362	-0.0665368	-0.0253032
0.365263	0.000432091	0.0150216	-0.0171807	-0.04984	0.000284983	0.00194207	-0.288606	-0.136877	-0.0244974	0.000665767	2.95024
-4.27317	3.71539	-4.86999	4.73214								

Table A5.1c: Third member of committee for the yield strength

0.0111686	0.000513835	0.000915135	-0.614221	0.0027999	-0.705282	0.0156934	-0.0438029	0.00992358	0.000523633	-0.0107421	2.80273
-0.0013653	0.000344816	0.000446912	0.000840785	-0.45659	-0.00217312	0.705721	0.00142425	0.0228917	-0.00773212	0.00038918	0.0117391
0.00861147	-0.000584812	0.000699813	0.00110132	0.00182711	-0.0718401	0.0041612	1.20762	-0.0135958	-0.080141	0.0144494	-0.00025302
-0.0328696	-0.180552	0.000494674	9.47707e-05	0.000280604	0.000513438	-0.0628378	0.00162964	-0.21303	0.00266005	0.0115696	0.00379684
-0.000298489	-0.00239189	-0.177089	0.000278522	-0.00869256	0.000312494	0.000487341	-0.89976	9.78971e-06	0.054823	0.0218672	-0.0230295
0.000430279	0.000237624	-0.0145111	-4.2505	0.000580097	-0.00598911	-2.19728e-05	7.14292e-05	1.26367	0.00324245	0.0538918	0.0301093
-0.0226274	0.00832274	0.000857329	-0.0225582	4.88311	0.000494719	-0.00136541	-0.00073581	-0.00130109	0.28367	-0.0062407	0.725167
0.00307591	0.00789855	-0.0177861	4.55922e-05	0.0129765	-0.627652	-0.000583237	-0.00137532	0.000780332	0.00113514	-0.0378393	-0.00133812
1.33401	0.0125562	0.0294919	0.000824316	0.000858741	0.0123309	1.17111	0.000867602	0.000513162	0.00056529	-0.0010657	0.234629
-0.00321355	0.407127	-0.00661531	-0.0173622	-0.00983219	0.000396889	0.00662486	-0.255557	-0.000542891	-0.0115531	-0.00105509	-0.00188393
-0.117758	-0.00519656	-0.503067	-0.0220496	0.0228599	-0.0163451	-0.00122879	-0.00600514	3.02262	0.00102054	-0.00116953	0.00119135
0.00196547	0.187605	0.0019297	-0.347273	0.0121794	0.0789616	0.00879436	-0.000722831	0.0016718	-1.03949	0.00128759	0.13138
-6.792	4.22032	-7.96332	-2.44187	10.7267	5.79018	8.23147	-4.24521	5.03287	11.6311	-8.74722	

Table A5.1d: Fourth member of committee for the yield strength

0.159532	0.00290407	0.026766	-0.0421247	0.0300843	-0.00715896	-0.118799	-0.00974685	0.0503236	-0.000934039	0.101898	-2.39015
-0.253355	-0.0085277	-0.000588758	0.00110915	0.0130785	0.00793374	0.000796952	-0.000879590	0.00117743	0.00897762	-0.000168296	0.0419299
0.0487008	-0.0457585	-0.00436873	0.00124661	-0.0079201	0.0189455	0.0114009	0.000957158	-0.00635505	0.00138663	0.0128424	-0.000175083
0.0637722	0.126983	-0.0813309	0.259109	0.0112149	0.0731733	-0.14875	-0.041569	0.00325189	-0.465913	-0.00146259	-0.0267647
-0.00153577	-0.15108	0.632046	-1.47131	-0.00763351	-0.000883071	-0.00269156	0.0148357	0.00909743	0.000984364	-0.00225762	0.00129097
0.0102737	-0.000120321	0.047111	0.0658001	-0.0579833	-0.0490487	-0.000288779	0.00182585	-0.0130966	-0.00261055	-9.3699e-05	-0.151546
-0.0157964	-0.0056739	0.000845638	-0.136263	4.47863	-0.550282	0.0751759	-0.00332587	-0.011507	-0.0302009	0.0461843	-0.0107403
0.555795	0.00726828	0.0499782	-0.00156177	-0.162855	1.83786	-0.773382	-0.0240014	0.00482511	0.0417295	0.00981655	0.0115417
0.00475328	-0.086799	0.00212839	0.0294109	-0.000357487	-0.896385	-0.15953	0.120242	-0.000442462	-0.001402	-0.0147898	0.0223207
0.0126185	0.00118032	-0.00830763	0.00120729	0.0141335	-0.000230848	0.0924055	0.195859	-0.0967801	-0.0914877	0.00138303	0.00715003
0.0438356	-0.0512911	0.00952944	0.0371721	-0.00635303	-0.060733	0.00151042	-0.199299	1.54513	-1.49592	0.0236022	0.000153603
0.00012138	-0.0274921	0.0233275	-0.00543471	0.375913	-0.00390227	0.0344317	-3.62297e-05	-0.49207	-0.636365	-0.371759	-0.13481
0.00963923	0.0692669	-0.0625224	-0.0200018	-0.0100646	-0.599592	-0.00634331	0.00436452	0.000215584	0.188714	-2.31365	-0.138081
-0.0835945	-0.00145542	-0.00638343	0.0184797	0.0205098	-0.00106605	0.322343	-0.0248421	0.0265942	0.00162393	0.105615	-3.46061
0.386295	-0.315707	-0.00631695	-0.0447263	0.0839225	0.0079156	0.0135124	0.389969	0.013607	-0.00587022	-0.000457088	0.142843
-2.66646	0.590344	-0.0585182	0.00786098	0.0564949	-0.0625116	0.00167564	-0.00686104	-0.498317	-0.00735161	0.0200765	-0.000155038
-0.0224441	0.87859	0.0420037	0.00248752	-0.00172136	-0.0197388	0.0239668	0.0127726	0.00151953	-0.00800416	0.000981033	0.0142215
0.000213625	0.115764	0.237914	-0.101812	4.50604	5.63772	-1.47655	-2.12898	-10.477	-1.68101	-3.5525	-10.5474
-6.19706	-2.49771	12.8885	7.89824	-8.85184	-7.14897	7.52268	10.2248	-2.69307			

Table A5.1e: Fifth member of committee for the yield strength

-0.0259302	-0.00365445	-0.00536243	-0.0337601	0.000310952	-0.213329	-0.00941427	-0.0270979	0.0262863	-0.00108941	0.227612	0.589634
0.00677463	-0.0621279	0.00548046	0.00814872	0.102793	-0.000275551	-0.0170769	0.0321402	-0.00259142	0.729878	0.00176537	0.107266
-3.75006	-0.00562428	0.0132497	0.000324811	0.000453659	0.00539878	-5.0641e-05	0.0281538	0.00260119	-0.0265404	-0.0920023	0.00126405
-0.0911509	2.98587	-0.0334892	-0.0690042	0.00171631	0.00262012	-0.379718	-4.23394e-05	0.525282	-0.00551508	-0.0783784	0.423882
-0.000273353	-0.253961	-0.476097	0.00924853	-0.0168103	-0.002659	-0.00400945	-0.0688522	5.55807e-05	-0.0388019	-0.0319606	0.0362799
-0.649416	-0.000516097	0.13173	-3.6579	-0.0103472	-0.0449844	0.00373307	0.00553848	-0.297556	-0.000231097	0.233472	-0.025231
-0.127335	0.315857	0.00190638	0.0727127	0.658191	0.00435382	-0.85127	-16.2858	-7.83256	-18.0333	-11.7221	-7.38475
11.6568											

Table A5.2a: First member of committee for the UTS

1.00194e-05	-0.00449607	-0.0140179	0.083752	0.000132986	-0.00674224	0.000352941	0.0107345	-2.30727e-05	0.00115664	-0.121739	-0.0463532		
-8.15173e-06	7.22279e-06	9.33279e-06	2.93662e-05	-0.000183054	4.05038e-07	1.36027e-05	6.99629e-07	-2.43989e-05	2.86272e-08	-9.0036e-06	0.000256543		
0.000207307	1.32503e-06	1.72093e-05	-0.00549973	-0.0169191	0.0995514	7.9089e-05	-0.00824879	0.000427773	0.0130112	-6.39134e-05	0.00191553		
-0.14521	-0.0130601	-1.14795e-05	0.000171176	-0.0284269	-0.0540541	-0.690413	0.00273164	0.057608	0.000779254	-0.199665	0.00307389		
0.0100769	-0.309797	-1.21296	2.97205e-05	-3.48664e-05	0.00772921	0.023099	-0.127469	-9.6053e-06	0.0107881	0.000531587	-0.0204764		
4.93559e-05	-0.00207339	0.190089	-0.101627	3.78781e-05	0.000390663	-0.0124019	-0.0200093	-0.273655	0.00142268	-0.0153261	0.000354396		
0.0303364	0.00162364	0.0124604	-0.110351	5.05038	7.77396e-05	4.12245e-05	0.0264171	0.11068	0.0782625	0.00137503	0.0491792		
0.00169869	0.0900135	0.00203095	0.00543807	0.646922	0.70837	0.000154631	-9.28845e-05	0.00904841	0.0404087	0.261771	0.00061598		
0.0133764	0.000789421	-0.0108577	0.000893154	0.00228527	-1.34315	-0.463565	9.89333e-05	-1.70044e-05	-0.00201929	-0.00639125	0.0388801		
0.000123867	-0.00292181	-0.000150745	0.00520457	3.84837e-05	0.00065963	-0.0553398	-0.0424107	-1.63177e-05	9.83891e-06	-0.00898159	-0.026614		
0.139487	1.69755e-05	-0.011762	-0.000558349	0.0258918	8.11291e-06	0.00246947	-0.212947	0.162817	-2.66017e-05	0.000886088	-0.0170558		
-0.0366058	0.654992	0.00137122	0.0599953	-0.00202417	0.108544	0.00154575	0.016141	0.532581	-1.12733	9.06099e-05	0.00033529		
-0.0444541	-0.142651	-0.0510537	0.000323983	-0.00293111	0.00175323	0.417036	-0.000133211	-0.00925274	0.112657	-0.849673	-2.47267e-05		
0.00110398	0.00675206	0.0596415	0.136372	0.00234631	-0.013493	0.000355416	-0.0309081	0.00304565	0.0137703	0.0624086	-3.769		
4.08584e-06	0.000422792	0.0334234	0.0697999	-0.420428	-0.0027351	0.00341986	-0.000468818	0.115397	-0.00299455	-0.00516834	-0.207216		
-1.87483	-5.74682e-05	2.03522e-06	-0.011535	-0.0293557	-1.1606	0.000701687	0.0525189	-0.00134293	0.141903	0.000714396	0.0101316		
-0.506287	0.731841	-8.49946e-05	-1.8261e-05	0.00906052	0.0268378	-0.14018	-2.0123e-05	0.0118168	0.00055975	-0.0262453	-4.53733e-06		
-0.00250991	0.214338	-0.16636	1.96635e-05	0.0242118	0.928532	-0.00181482	1.12585	-5.24073	-1.41491	-2.12654	-6.2175		
-3.60747	0.3971	1.50596	6.19473	-4.99662	-3.46794	4.66004	4.73158	-1.51067					

Table A5.2b: Second member of committee for the UTS

0.00266309	-0.000877124	0.000764849	0.171752	0.0088005	-0.00337489	0.00530304	-0.00327245	0.00950929	-0.000350317	-0.149156	0.281726		
-0.0251104	-0.00272268	0.000929556	0.000725187	-0.174725	-0.00894128	0.00349421	-0.00536842	0.00333569	-0.00962627	8.73488e-05	0.151194		
-0.282626	0.025548	-0.00308296	0.039266	0.0444776	0.198868	-6.57098e-05	-0.0507454	-0.0742087	0.117095	0.0128166	-0.0188182		
-0.442262	1.90335	0.030889	0.0378914	-0.0390215	-0.0401346	0.0328211	0.0256818	-0.0466509	-0.218961	-0.143627	0.0168211		
-0.0206349	-0.705752	-0.277975	0.0442456	-0.00230519	0.00060702	-0.000965151	-0.156276	-0.00801179	0.00276749	-0.00487455	0.00290558		
-0.00883028	0.0015532	0.137735	-0.276452	0.02266	0.00894659	-0.00977548	-0.013902	-0.261472	-0.0195949	-0.0395902	-0.0540345		
-0.0655935	-0.0245617	0.0285268	-0.34327	5.51658	0.0546765	-0.102258	0.0836905	0.0883326	-1.20074	-0.0382294	0.110723		
0.075202	0.186583	-0.0155581	0.0269765	0.238716	-0.743301	0.0482235	-0.00269729	0.000906754	0.000742628	-0.173429	-0.00888035		
0.00344216	-0.00534061	0.00330851	-0.00957588	0.000204461	0.150311	-0.282241	0.0253587	0.00262513	-0.000845279	0.000788573	0.169938		
0.00871318	-0.00330235	0.00525941	-0.00323312	0.00943568	-0.000506125	-0.147903	0.281177	-0.0248388	0.0575877	0.000352439	0.00175879		
0.203102	-0.0115632	0.022069	0.0824549	0.00640308	-0.0122525	0.0234343	0.395988	-4.1399	0.00271999	0.0451754	-0.0250978		
-0.0339836	0.871235	-0.031636	-0.0677784	0.014965	0.105369	-0.0419008	0.0178232	-0.506004	1.19559	0.0189046	-0.00258444		
0.000812208	0.000813167	-0.168042	-0.00862083	0.0032268	-0.00521073	0.00319165	-0.00935709	0.000667281	0.146587	-0.280612	0.0245514		
-0.00236864	0.000650438	-0.000933321	-0.158794	-0.00814746	0.00286421	-0.00495194	0.0029708	-0.00894912	0.00138366	0.139714	-0.27743		
0.0230793	0.0273991	-0.0129686	-0.0122439	-0.0613964	0.0150807	-0.0135877	0.120912	-0.0935396	0.0106243	-0.0121976	1.28611		
0.128462	-0.0398728	-0.00271904	0.000926244	0.000727743	-0.174537	-0.00893248	0.00348667	-0.00536451	0.00333176	-0.00961904	0.000104437		
0.151065	-0.282569	0.0255207	-0.574919	1.62247	-1.6474	-5.67043	5.02031	-1.48351	-2.1747	4.89095	-1.63661		
1.60701	-3.85411	4.75653	-1.59067	-1.50726	4.01159	-1.64584							

Table A5.2c: Third member of committee for the UTS

0.00536019	-0.00365323	-0.00374455	0.00287123	0.044019	-0.000956509	0.0315297	0.000270369	0.0114277	-0.00174762	0.0287925	-0.364824
0.00616023	-0.00689612	0.00399365	0.00396585	-0.00281105	-0.0475672	0.00105505	-0.0341416	-0.000361033	-0.0123153	0.00217028	-0.0309939
0.359831	0.00141128	0.00435865	-0.00297204	-0.00305424	0.000503715	0.0293828	-0.000741511	-0.00565099	3.86842e-05	0.009139	-0.00155864
-0.0414419	-0.33127	0.0161293	-0.0157832	-0.00338723	-0.00385564	0.0304572	-0.00762934	-0.00169581	-0.182684	-0.00210317	-0.0354686
0.000231114	1.31061	0.302556	-0.316709	-0.0305457	-0.000474872	0.000383390	0.00237898	0.052719	0.000646706	0.0887717	0.00893044
0.0439046	-0.00832935	0.284666	-4.87683	0.0353703	-0.00728009	0.00430688	0.00450225	-0.00261986	-0.0513464	0.00106399	-0.0364067
0.000381917	-0.0132118	0.00247124	-0.0342298	0.353756	0.000945518	0.00624366	0.00380324	0.00385428	-0.00287542	-0.0454177	0.00100145
-0.0327839	-0.000303866	-0.011807	0.0019759	-0.0295528	0.36298	-0.00101475	-0.0366284	-0.00366461	-0.00428235	0.0606492	-0.0454994
0.000855838	-0.449222	-0.000437004	-0.0711036	0.00532488	-0.608079	-0.776577	0.61579	-0.00406105	-0.000237422	0.000288223	0.0145438
-0.0260157	0.0054139	-0.0693192	0.00138114	-0.0277979	0.00522286	0.645794	-2.42018	0.138786	0.0307242	-0.00110865	-0.00125792
0.0623756	0.0156587	-0.00193345	0.124071	-0.00948324	0.00301435	0.0119207	0.320078	-3.95267	0.137039	0.00535327	-0.00777016
-0.00842157	0.0300379	0.011493	-0.000680287	-0.217257	0.00568004	-0.0479269	0.0040118	-0.159139	1.43472	0.35685	-0.0173283
-0.00091579	-0.000599229	0.0508499	0.0725614	0.000342303	0.566938	-0.00143415	0.0631393	0.0036299	-0.774685	-0.0914317	-0.771357
0.00941636	-0.00612487	-0.00630338	0.0764781	0.0569868	0.00314024	0.219469	-2.25887e-05	-0.00168398	0.00664988	-0.684572	2.08671
0.0563295	0.021485	0.00160655	0.00124126	-0.0521167	-0.0663511	0.00135643	-0.0685732	0.00418759	-0.0509395	-0.0006527	-0.680815
-0.451037	-0.539262	0.00592261	-0.00374095	-0.00381115	0.00289202	0.0447871	-0.000972901	0.0322971	0.000285363	0.0116515	-0.0018977
0.0291341	-0.363726	0.00263818	1.16751	-3.13306	3.41094	-2.53338	6.74894	3.82915	3.68794	3.25021	8.28787
5.11917	-6.04969	-5.93088	8.46761	4.64965	-6.47855	-3.20007					

Table A5.3a: First member of committee for the elongation.

-0.0745008	-0.0105203	-0.0171355	0.0455913	0.0119687	-0.0614878	-0.15747	0.0084879	0.031441	0.00100191	0.254446	-0.113693
0.273654	0.218311	0.0616403	0.0159437	-0.015612	-0.0332434	0.0208012	0.000934114	-0.0407106	-0.405327	-0.0169563	-0.00639367
0.00100904	0.194131	-2.59598	0.232	0.0819451	0.115095	0.0589815	-0.00248828	-0.00502106	0.0316421	0.00188288	-0.0767515
0.932134	-0.0135202	0.00410166	0.00131234	-0.099234	2.29787	-0.0443353	-0.0350258	-0.29659	0.00818787	0.00880872	0.019562
-0.00175117	0.000774314	0.0295598	-0.196915	0.0070217	0.00928947	0.000143244	-0.0030145	0.484183	-0.12256	-0.0248379	-0.0572268
0.00619757	-0.0105519	-0.0244764	-0.00424514	-0.00282516	-0.0280598	-0.313275	-0.00908655	-0.0144753	-0.000342879	0.0557421	-0.0669999
0.0552251	0.0499244	0.125362	0.099921	-0.00320856	-0.00982379	0.0432607	-0.00703065	0.0348196	0.0677272	0.0124424	-0.0245925
0.000485282	0.218079	6.32628	0.210079	-0.134835	-0.0874474	-0.0320355	0.0023913	0.0112909	-0.0164674	0.0114981	-0.0221565
0.135396	-0.00255034	0.0388836	-0.00109095	0.245014	7.64961	0.0544577	-0.013856	0.0748451	-0.000514741	-0.00256434	0.00586549
-0.00136261	-0.000379572	0.00921963	0.0167964	-0.0033729	-0.00446497	-6.5904e-05	0.00682211	-0.238703	0.0321075	0.0139704	0.016394
0.00078661	-0.00338814	-0.00720033	0.000441655	0.000839007	-0.0103522	0.0380523	-0.00407999	-0.00462857	-7.85571e-05	0.0128431	-0.482126
0.0316318	0.0150496	0.0109848	-0.0872472	0.0155377	0.0333181	0.0246819	-0.00096056	-0.0110563	-0.63249	-0.00645007	0.00553504
0.000830717	0.125201	1.26857	0.0696577	0.154407	0.234607	-0.00510571	-0.00425982	-0.0110086	-0.0200238	-0.00281466	0.0118825
0.0148731	-0.0188307	-0.0107491	0.000665439	0.154786	5.3068	-0.177093	-0.103093	-0.477886	-0.0332541	-0.0276029	-0.0561952
0.0350201	0.00726893	-0.0694918	0.531102	-0.0120883	0.00585297	-3.92799e-05	-0.193458	1.34835	0.350898	0.00381134	-0.0627182
0.0503533	0.00400502	0.00861631	0.0394241	-0.000744562	-0.0677136	0.272162	-0.0104532	0.00112558	0.000775704	0.238539	-1.88039
-0.166201	0.0363123	-0.432826	0.00139544	-0.00222183	-0.00441138	0.000761954	0.000789925	0.00578542	0.0115439	-0.00314862	-0.0027303
-4.26697e-05	0.0164396	-0.647315	-0.00621638	0.0111866	0.00784842	-0.0854402	-9.41934	-11.3696	-10.7221	-5.48995	6.35634
15.1834	-7.61171	2.19262	2.80573	10.7522	-8.63799	13.1299	14.1913	2.17388			

Table A5.3b : Second member of committee for the elongation.

0.0301019	0.121517	0.182024	-0.00194643	5.44705e-05	0.0101013	0.12897	-0.0238512	-7.75571e-05	0.000930936	-0.0618289	-6.28198
0.16281	-0.180587	-0.342744	0.0057816	-0.137904	-0.214054	-0.00119854	2.55516e-05	-0.00949255	-0.213071	0.0357813	-1.1789e-05
0.00152644	-0.0257962	4.0593	0.153294	0.0904911	-0.222793	-0.0137223	0.0242711	0.102009	-0.00176617	0.0001988280	0.00343221
0.100601	-0.00300490	0.000604057	0.00167151	-0.00609095	1.06126	0.173169	-0.170512	0.703459	0.00111864	0.00661667	0.0217882
-0.00133588	4.77281e-05	0.00185418	-0.0665885	-0.0120201	0.000129683	0.000619017	-0.00344353	0.32921	0.00266224	-0.0400165	-0.0999159
0.00302706	-0.0587574	-0.121508	0.00314818	-8.77498e-05	0.00711449	0.120833	-0.0420066	-0.000280181	-0.00274657	0.0251753	0.129828
-0.104185	-0.253143	-0.846239	0.0135343	0.00153136	0.0474895	-0.00176051	0.000147364	0.00273694	0.0907888	-0.0345919	0.0004289
0.00125022	0.0251917	-2.03888	-0.0626182	-0.101803	-0.143614	0.0662642	-0.111961	-0.156275	-0.00253351	8.5009e-05	0.0141891
0.188481	0.00998986	0.000175702	0.00509662	-0.00390154	-7.22039	-0.191466	0.123858	0.877387	-0.00220335	-0.00736722	-0.0312849
0.00169266	-5.50113e-05	-0.0020906	0.0944239	0.0154432	-0.000180995	0.000808001	0.00425469	-0.42253	0.0116485	0.0518902	0.129161
0.0246891	-0.0699259	-0.13436	-0.00643982	6.07239e-05	-0.00441801	0.917459	0.0871391	-0.000198693	0.00287858	0.0675696	-0.0964831
0.0255148	0.169637	-0.946907	-0.00166437	0.08478	0.00834102	-0.00225784	-0.000449829	0.00256942	0.241542	0.14702	-0.00123464
-0.00296256	-0.0746134	-5.69595	-0.755812	0.324634	0.6448	-0.039503	-0.229694	-0.304292	0.00281415	0.000228594	-0.00427342
0.141397	-0.0925321	0.000524788	0.00348055	0.0619425	-8.59047	0.0248629	0.116366	0.380848	0.0121133	-0.0605815	-0.0945357
-0.00183616	8.83037e-05	0.0318346	-0.155317	-0.101005	7.10316e-05	-0.00303264	0.0718359	6.68788	0.314799	-0.146146	0.519519
-0.00702782	0.101862	0.108634	0.00662434	-0.000186002	-0.00663234	0.505473	0.0952548	-0.000467822	-0.00303721	0.0560313	0.0718143
-0.133875	0.315246	0.135854	0.010682	-0.0971105	-0.182383	0.00532115	-8.37067e-05	-0.00220235	0.383548	0.00706179	-0.000290045
-0.00274859	-0.040939	0.0193539	0.415258	-0.109892	-0.387889	0.233782	-9.74511	-7.75219	-7.13984	-3.06335	8.79098
-7.13021	16.8943	3.92484	-14.535	-15.9101	-9.30996	-13.0783	14.5079	11.8499			

Table A5.3c : Third member of committee for the elongation

0.0370769	0.0514359	0.0353873	-0.000585384	-0.0156681	0.00338796	-0.566864	0.00050415	-0.00568823	0.00283634	0.00321732	0.354993
-0.366533	0.355984	0.0861148	0.00117097	0.0230824	0.0189446	0.000615662	0.00218215	-0.000449988	-0.443305	-0.00351917	0.00177516
0.00186752	-0.0127677	-1.05622	0.0448273	-0.59614	-0.0752848	0.167228	-0.0611791	-0.0447181	0.00181787	0.00398464	0.00664942
-0.0102759	-0.0774068	0.000461769	-0.00328124	0.0442472	6.88135	-0.161461	-0.359099	0.0108286	0.022324	-0.0466723	-0.039551
-0.000425151	-0.00127799	-0.00313254	-0.985074	-0.00636547	-0.00038825	-0.00263803	0.101341	-0.00376178	-0.0216829	-0.0140537	-0.0262414
0.0259891	0.00286923	-0.0225642	0.00185406	-0.030297	0.00582893	0.113538	-0.0113726	-0.014199	-0.000377488	0.00658813	-5.82291
0.323171	0.195156	0.165512	-0.0154769	0.00357713	0.00461503	0.00154635	0.0034791	-0.0127783	-0.684007	-0.0228538	0.00238445
0.003895	0.0384662	2.28703	0.260629	0.286426	-0.0478254	-0.00995393	0.225249	0.174495	0.00158575	-0.0296509	-0.00396501
0.471634	0.0851422	-0.00798795	0.00220846	-0.0648104	4.45166	-0.269553	-0.26634	0.131066	-0.0967287	-0.128844	-0.0869517
0.00308005	0.0302232	-0.00248292	-0.138239	-0.0115796	0.0117111	0.00151138	0.150832	0.773512	0.342719	0.126994	-0.123916
0.0701628	-0.0604757	-0.0462929	0.00278186	0.0068604	-0.0243401	0.418371	-0.0594458	0.001568	0.00552655	0.0477772	-2.82015
-0.117517	-0.0873828	-0.237285	-0.0326492	-0.111086	-0.0888155	0.00275869	0.00982146	0.00210218	0.292468	-0.00773775	0.00279322
0.000587384	0.0163538	3.92695	0.208295	-0.125505	-0.158683	-0.0441899	-0.0781376	-0.0347271	0.0052771	0.0474481	0.00694641
-1.0843	0.0370285	0.0198197	-0.00187163	0.0386568	-4.52269	-0.0735063	0.212422	0.0424436	-2.06988	-12.6059	-10.2958
8.33286	11.5706	17.1457	12.2333	14.5225	-15.7288	15.8026	14.4659	13.2644			

Table A5.3d : Fourth member of committee for the elongation

-0.020193	0.0448449	0.0339259	-0.009559360	0.00607867	-0.0171082	0.235784	-0.00706618	0.00830511	-0.00158306	-0.0258376	-10.2375
0.0455348	0.015526	0.115596	-0.0111427	0.0336342	0.0286378	-0.010803	0.0276051	0.0149528	-0.0477241	0.00452018	0.0181715
-0.00244213	-0.0641433	-4.82541	-0.232181	0.0272955	0.0732292	0.0751036	0.154373	0.0934853	-0.0250491	-0.0808118	0.0422474
0.0452459	-0.00294873	-0.03657	-0.00462145	-0.103771	0.376437	-0.619407	-0.00139012	0.312204	0.00954491	-0.0242783	-0.00729928
-0.00375946	0.0514059	-0.0456138	-0.285684	-0.00959054	0.0281991	-0.000485044	-0.0798895	10.8936	-0.223225	0.010417	0.0575702
-0.0534281	-0.0958925	-0.068741	-0.00805738	0.0108425	-0.0252296	-0.159321	0.00380677	-0.00218474	-0.00170697	0.0643879	-7.17243
0.0672609	0.0188323	-0.19832	-0.0278828	0.0602626	0.0293837	-0.0290397	-0.0739594	0.0830003	0.202847	0.00561231	-0.0384574
-0.00721035	0.0825382	6.70756	0.0454583	0.0289002	-0.0640086	0.0694243	0.100431	0.0559076	-0.0137281	-0.0759375	0.0656731
-0.644073	0.000999541	-0.0378366	0.00105717	0.0710577	0.324748	-0.223564	-0.0101244	0.121984	0.0009023	-0.00186473	0.000492629
0.00070837	-0.000497952	0.000829272	0.0266968	-0.000165752	7.72062e-05	-0.000160364	0.00748324	0.324458	-0.00959429	0.000864071	-0.00435185
0.0212846	0.00100684	0.000148737	0.000459156	-0.00482937	0.00590924	-0.0638173	-0.00127163	-0.00422942	0.000580833	-0.051817	1.58417
-0.00421807	-0.00376076	-0.0896277	0.00147055	-0.00223882	0.000909066	0.00100498	0.000192739	0.00218195	0.0700261	-0.000373239	0.000576326
0.000537463	0.0194467	0.275985	-0.0178869	0.00269397	-0.0238967	-0.000170069	7.04213e-05	1.14896e-05	1.59254e-06	1.84454e-06	6.70868e-05
0.00191296	-1.19401e-05	2.00777e-06	2.22428e-05	0.000540013	0.0250845	-0.000218694	2.61435e-05	0.000438537	0.0353563	0.0501018	0.0188
0.000304365	-0.0758125	0.0427048	0.0569031	-0.00335015	-0.0425281	-0.000840355	0.0236807	-4.77096	0.0618546	-0.0224205	0.0123008
-0.0289149	-0.0477012	-0.0336078	-0.0101186	0.00531455	0.0109715	-0.735881	-0.00206059	0.000952574	-0.0034055	0.152574	-0.372863
0.386907	0.0110083	-0.164155	-0.184159	-9.95568	-9.18333	12.7581	-8.8568	-10.0412	-12.8849	-14.4681	0.768885
3.59765	2.196	0.051791	8.11692	13.4352							

Table A5.3f : Fifth member of committee for the elongation

-0.090234	0.0205732	0.077368	0.0218687	0.00176121	-0.0414751	0.25648	-0.0062435	0.00128332	0.00105938	-0.00432934	-10.1276
-0.000853758	0.0103565	0.0401002	-0.0967551	0.0650808	0.157336	-0.0792891	0.000243323	0.0761057	-0.218877	-0.00342654	0.000476554
-0.00518596	0.187104	6.50365	-0.0330413	0.0739246	-0.0739554	0.0601146	0.00260953	0.091717	0.0374004	0.00688336	-0.0145799
-0.115905	-0.00187519	0.00458919	0.00171113	0.116514	0.44266	0.104957	-0.0530803	-0.067722	0.00634209	0.0359525	0.0369352
0.00981496	-0.0040129	0.00205756	0.428697	0.000755988	-0.00248303	-0.00254312	-0.237902	-0.0109649	0.39958	-0.0173779	-0.360207
-0.0586657	-0.127212	-0.237429	-0.0134442	0.00467323	0.00563057	0.291094	-0.00252809	0.00245703	-0.00354923	-0.138825	-5.92699
-0.221178	0.0699772	-0.0980035	-0.0141631	0.0362728	0.0285346	0.00412974	-0.0041837	0.00224147	1.04844	3.67414e-05	-0.00266071
-0.00224203	0.163416	0.457109	-0.28733	0.0318935	0.227609	-0.213857	0.0383232	0.103883	-0.0361088	0.00130758	0.0257916
1.60594	0.000473076	0.00108951	0.00245146	-0.349241	0.195557	-0.0286046	0.0467965	-0.120458	0.04546	-0.0501972	-0.0774169
0.0294513	0.00396867	-0.0357505	-0.330947	-0.00463649	0.00235718	0.00159036	-0.136724	11.1711	-0.182287	-0.011839	0.0260563
-0.578728	-7.14487	-8.88831	-5.74086	9.35647	-6.68984	8.58008	-9.60545	-4.86136			

Table A5.3g : Sixth member of committee for the elongation

-0.0832945	0.044772	0.389189	-0.00346995	0.00590356	-0.0242468	-0.933486	-0.0132668	0.0132219	0.0112537	0.0965041	0.105633
-0.418713	0.150403	-0.194985	0.131605	0.00457758	0.0768434	-0.0200813	0.00552868	0.00986155	0.818728	0.0149287	0.00982856
0.0123857	-0.0423408	0.0186902	-0.0943879	-0.00744999	-0.148479	0.0364402	0.0306001	0.157186	0.0110313	-0.00454903	0.0232104
0.0744224	0.000497818	-0.00544221	0.0049015	0.0301545	7.53362	0.240678	-0.13868	-0.0551636	0.0552989	-0.0267163	-0.206242
-0.0259089	-0.00712814	-0.0392377	0.0421706	0.00769304	-0.0102166	0.00556094	-0.0100853	-1.25978	0.0280164	0.0379419	-0.0406369
0.0405625	0.00243521	-0.200488	0.0691052	-0.0240288	-0.0841019	-0.10617	-0.0545487	-0.0364122	0.00986978	-0.0799652	-8.47056
-0.122341	-0.039802	-0.356674	-0.0817946	0.0457894	0.132618	0.02273	-0.0203267	-0.0122117	0.0990098	-0.0716797	-0.027427
0.00240908	-0.00743098	7.49067	3.26751e-05	-0.0884498	-0.509448	0.184845	-0.0602837	-0.339193	-0.0118911	0.00895189	0.00633034
0.0988389	0.0379036	0.00935246	-0.00593667	-0.0233831	-0.511795	0.315044	-0.119116	0.258223	2.03658	-10.9238	-10.3566
14.0747	6.38983	6.5575	-7.07208	-14.7028							

APPENDIX SIX

FORTRAN Program for Thermodynamic Calculations

Introduction

This appendix describes the computer program that was used to calculate the thermodynamic functions in the analysis of the mechanical alloying (Chapter Four). It is presented using documentation defined in the MAP format [Bhadeshia, 1995, http:/www.msm.cam.ac.uk/map/mapmain.html].

MAP FORTRAN LIBRARY

Program MAP_MALLOY

0. Provenance of Source Code

A.Y. Badmos and H.K.D.H. Bhadeshia, Phase Transformation Group, Department of Materials Science and Metallurgy, University of Cambridge, Cambridge, UK.

1. Purpose

To calculate free energy of mixing, configurational enthropy of mixing, enthalpy of mixing, and structural interfacial energy in mechanical alloying as functions of concentration, particle size and temperature.

2. Specification

The program is self-contained

3. Description

Molar entropy of mixing, ΔS_M expressed as a function of atoms per particle is

$$\frac{\Delta S_M}{kN_a} = \frac{(1-x)m_B + xm_A}{m_A m_B} \ln\left\{ N_a \frac{(1-x)m_B + xm_A}{m_A m_B} \right\} - \frac{1-x}{m_A} \ln\left\{ \frac{N_a(1-x)}{m_A} \right\} - \frac{x}{m_B} \ln\left\{ \frac{N_a x}{m_B} \right\}$$

where N_a is Avogadro's number, m_A is atoms per powder particle of A, m_B is atoms per particle of B, and x is the mole fraction of B.

Molar enthalpy of mixing, ΔH_M, is expressed as:

$$\Delta H_M = \Omega \ 2\delta S_V \ x(1-x)$$

where Ω is the regular solution parameter, 2δ is the boundary thickness (two monolayer) and S_V is grain boundary area per unit volume.

Molar interface energy, ΔH_I, is expressed as:

$$\Delta H_I = V_m S_V \sigma$$

where V_m is the molar volume and σ is the interface energy per unit area.

The molar free energy, ΔG_M, is then expressed as:

$$\Delta G_M = \Delta H_M - T\Delta S_M + \Delta H_I$$

4. References

1. A.Y. Badmos, Ph.D. Thesis, University of Cambridge, UK., 1997.

2. A.Y. Badmos and H.K.D.H. Bhadeshia, Metallurgical Transactions, **28A**, 1–5, 1997.

5. Parameters

Input parameters

KTEMP - integer

Temperature in Kelvin at which the thermodynamic functions are to be evaluated.

OMEGA - integer

Regular solution parameter, Ω.

Output parameters

DELTAS - real

Predicted molar configurational entropy of mixing.

DELTAH - real

Predicted molar entropy of mixing.

DELTAE - real

Predicted molar interface energy.

DELTAG - real

Predicted free energy of mixing.

6. Error Indicators

In the case of $\Omega > 0$, the effect is appreciable only when the value of Ω is above about 100.

7. Accuracy

Qualitative

8. Program text

```
      IMPLICIT REAL*8(A-H,K-Z), INTEGER(I,J)
      OPEN(2, FILR='PRN')
      WRITE(*,3)
      WRITE(2,11)
      READ(*,*) KTEMP,OMEGA
      LATP = 2.867D-10
      RGAS = 8.31432D+00
      AVOG = 6.023D+23
      MOLV = 8.634D-7
      ATOD = 2.0*(SQRT(3.0D*00)/2.0D+00)*LATP
      AVOA = LATP**3.0/2.0
      AVOB = AVOA

C  This section defines the particle sizes
       DO 10 J=1,10
       DUMMY = (10.0-1.0*J)
       MA = 10.0D+00**DUMMY
       MB = MA

C  Interface energy per unit area
       MDUMMY = 1.0D+7
       IF(MA .GT. MDUMMY) THEN
       SIGMA = 0.5D+00
       ELSE
       SIGMA = 0.5*(1.0-((MDUMMY-MA)/MDUMMY))
       ENDIF

C
      DO 1 I=1,51
```

```
      X = (I-1)*0.2D-01
      NA = AVOG*(1-X)/MA
      NB = AVOG*X/MB
      SA = 3.0*(NA*(MA*AVOA)**(2.0/3.0) + NB*(MB*AVOB)**(2.0/3.0))
      VT = NA*MA*AVOA + NB*MB*AVOB
      SV = SA/VT
      VB = SV*2.0*ATOD

C  Molar Interface Energy
      DELTAE = SV*SIGMA*MOLV

C
       IF(X .EQ. 0.0D+00 .OR. X .EQ. 1.0D+00) THEN
       DELTAS = 0.0D+00
       TDELTAS = 0.0D+00
       DELTAH = 0.0D+00
       ELSE

C  Molar Entropy
       DELTAS = RGAS*((((1-X)*MB+X*MA)/(MA*MB))*
     &      DLOG(AVOG*(((1-X)*MB+X*MA)/(MA*MB)))
     &      -((1-X)/MA)*DLOG(AVOG*((1-X)/MA))
     &      -(X/MB)*DLOG(AVOG*X/MB))
       TDELTAS = -KTEMP*DELTAS

C  Molar Enthalpy
       DELTAH = X*(1-X)*VB*OMEGA

C  Molar Free Energy
       DELTAG = DELTAH + TDELTAS + DELTAE
       ENDIF
```

```
C
C     WRITE(2,2)MA, MB,X,DELTAS,TDELTAS,DELTAG,KTEMP,SIGMA, DELTAE
2     FORMAT(2D10.2,F6.2,D10.2,2F14.7,F8.0,3F14.7)
3     FORMAT(10x, ' KTEMP, OMEGA')
11    FORMAT(// 7x,'MA, MB, X, DELTAS, TDELTAS, '
     & ' DELTAG, KTEMP, SIGMA, DELTAE'/)
C
1     CONTINUE
      WRITE(2,11)
10    CONTINUE
      STOP

C ***********************************************************************
C     LATP is lattice parameter:  value for iron is used
C     RGAS is Gas constant, R.
C     AVOG is Avogadro constant.
C     MOLV is molar volume calculated for iron.
C     ATOD is diameter of atom.
C     AVOA and AVOB are volume per atom for component A and B respectively.
C     MA and MB are atoms per particle of component A and B respectively.
C     X is mole fraction.
C     NA and NB are number of particles of A and B respectively.
C     SA is total surface area of the particles.
C     VT is total volume of the particles.
C     SV is surface area per unit volume.
C     VB is volume fraction of material within a grain boundary.
C     SIGMA is interface energy per unit area.

C     DELTAE is molar interface energy.
```

APPENDIX SEVEN

FORTRAN Program to Calculate Yield Strength of MA–ODS Steels

Introduction

The progam described in this appendix was used to calculate the components of the yield strength of MA956 in the model discussed in Chapter Six. It is presented using documentation defined in the MAP format [Bhadeshia, 1995, http:/www.msm.cam.ac.uk/map/mapmain.html].

MAP FORTRAN LIBRARY

Program MAP_YSMA956

0. Provenance of Source Code

A.Y. Badmos, Phase Transformation Group, Department of Materials Science and Metallurgy, University of Cambridge, Cambridge, UK.

1. Purpose

To calculate the components of the yield strength of the recrystallized and unrecrystallized mechanically alloyed ODS ferritic steel, MA956.

2. Specification

The program is self-contained

3. Description

The yield strength of the MA956 is calculated as a linear combination of contributions from a number of mechanisms generally expressed as:

$$\sigma_y = \sigma_{Fe} + \sigma_s + \sigma_p + \sigma_g + \sigma_d \tag{7.1}$$

where

σ_{Fe} is the strength of the pure, annealed matrix,

σ_s is solid solution strengthening,

σ_p is the particle strengthening,

σ_g is the grain boundary strengthening,

σ_d is the dislocation strengthening.

The recrystallized alloy has coarse grain structure and there is no contribution from the grain boundary strengthening.

4. References

1. A.Y. Badmos: Ph.D. Thesis, University of Cambridge, UK., 1997.

2. A.Y. Badmos and H.K.D.H. Bhadeshia (1997) - Submitted for publication in *Materials Science and Technology.*

5. Parameters

Input parameters

MO - real

Concentration of molybdenum in wt.%.

CR - real

Concentration of chromium in wt.%.

TI - real

Concentration of titanium in wt.%

PWT - real

Concentration of particles in wt.%.

PRAD - real

Particle radius.

PWT - real

Concentration of particles in wt.%.

PARTD - real

Density of the particle.

MATRD - real

Density of the matrix.

GSIZE - real

Grain size of the unrecrystallised alloy.

DDENS - real

Dislocation density.

AVAC - real

Area associated with a vacancy.

DDIF - real

Constant of difussivity coefficent.

QES - real

Self–difussion activation energy for the alloy.

SRATE - real

Strain rate.

RGAS - real

Gas constant.

BUGV - real

Burgers vector.

SMOD - real

Shear modulus.

A(I,J) - Double precision.

A 13×4 array consisting of temperature in column 1 and corresponding scale factors relative to room temperature for matrix strength in column 2, solid solution strenghtening in column 3 and grain boundary strengthening in column 4.

Output parameters

PIRON - real

Strength of pure iron.

SSOL - real

Solid solution strengthening.

PARTS - real

Particle strengthening.

GRAS - real

Grain size strengthening in the unrecrystallized alloy.

RYST - real

Total yield strength of recrystallized alloy.

URST - real

Total yield strength of of unrecrystallized alloy.

6. Program data

MO = 0.0D0

CR = 20.0D0

TI = 0.5D0

PRAD = 5.695D-09

GSIZE = 0.9D-06

DDENS = 10D+14

RGAS = 8.314510

AVAC = 1.95D-20

DDIF = 5.0D-05

QES = 240000.0

K = RGAS/6.023D23

SMOD = 8.6D+10

BUGV = 2.485D-10

MATRD = 7200.0

PARTD = 5030.0

PWT = 0.5/100

SRATE = 3.3D-4

A(I,J):

20.0d0	1.0d0	1.0d0	1.0d0
100.0d0	0.7334d0	0.9713d0	1.03d0
200.0d0	0.6667d0	0.7856d0	1.03d0
300.0d0	0.6667d0	0.6858d0	1.0d0
400.0d0	0.6667d0	0.5427d0	0.9118d0
500.0d0	0.6667d0	0.4143d0	0.6177d0
600.0d0	0.5999d0	0.3364d0	0.2941d0
700.0d0	0.3333d0	0.2731d0	0.1471d0
800.0d0	0.2425d0	0.2217d0	0.0294d0
900.0d0	0.1765d0	0.1800d0	0.0d0
100.0d1	0.1284d0	0.1461d0	0.0d0
110.0d1	0.0935d0	0.1186d0	0.0d0
120.0d1	0.0680d0	0.0963d0	0.0d0

7. Program text

IMPLICIT DOUBLE PRECISION (A-H,K-Z), INTEGER (I,J)

```
      DOUBLE PRECISION A
      DIMENSION A(20,4)
      OPEN(3, FILE='YIELD')
      IROW1=13
      ICOL=4

C  This do loop reads the data in the array file, A(I,J).
      DO 100 I=1,IROW1
      READ(*,*)A(I,1),A(I,2),A(I,3),A(I,4)
  100 CONTINUE

C  Volume fraction of particle from weight percent
      VFRAC = PWT*MATRD/PARTD

C  Particle spacing
      PSPA = SQRT(2.0*PIE/3.0)*SQRT(PRAD**2.0/VFRAC)

C  Strength of pure iron at room temperature
      PIRON20 = 215.76DO

C  Solid solution strengthening at room temperature.
      SSOL20 = 8.5*CR + 58.0*MO - 107.0*TI

C  Grain boundary strengthening at room temperature
      K = 15.9*(1.0/1000.0)**0.5
      GRAS20 = K*(GSIZE**(-0.5))
      I=1
      DO 1 IJI = 3,15
      KTEMP = 100.0*IJI
      CTEMP = KTEMP-273.15

C  Particle strengthening
```

```
      MODD = (SMOD*BUGV)/PSPA
      EXPT = QES/(RGAS*KTEMP)
      DIFF = DDIF*DEXP(-EXPT)
      LOGN = SRATE*K*KTEMP*PRAD**2.0D0
      LOGD = 4.0D0*PIE*DDENS*BUGV**2.0D0*AVAC*SMOD*PSPA*DIFF
      LOGT = 0.12D0*DLOG10(LOGN/LOGD)
      ENGT = 0.052D0*EXPT
      SPT = 0.51D0 + LOGT + ENGT
      PARTS = MODD*SPT/1E6
      PIRON = PIRON20*A(I,2)
      SSOL = SSOL20*A(I,3)
      GRAS = GRAS20*A(I,4)

C  Recrystallized yield strength
      RYST = PIRON + SSOL + PRAD

C  Unrecrystallized yield strength
      URST = RYST + GRAS

C  Results are in MPa
      WRITE(*,2)CTEMP,KTEMP,PIRON,SSOL,PARTS,GRAS,RYST,URST
      WRITE(3,2)CTEMP,KTEMP,PIRON,SSOL,PARTS,GRAS,RYST,URST

2       FORMAT(2F8.0,6F10.0)
      I = I + 1

1       CONTINUE
      END
```

REFERENCES

Adachi, M., Grant, N.J. (1960)

Trans. TMS-AIME **218** 881.

Aiken, B., Courtney, T., Maurice, D. (1991)

Mat. Sci. Eng. **147A** 229.

Alamo, A., Decours. J., Pigoury, M. and Foucher, C. (1990)

Proc. Conf. on Structural Applications of Mechanical Alloying, ASM Int., Myrtle Beach, South Carolina 89–98.

Alamo, A., Regle, H. and Bechade, J.L. (1992)

Novel Powder Processing, Metal Powder Industries Federation, Princeton, N.J. **7** 169–182.

Andres, F.S., Alexander G.B. and Wartel W.S. (1962)

Metal Progress 88.

Arzt, E. (1984)

*Superalloys 84,*TMS-AIME.

Artz, E. (1988)

Proc. Conf. on New Materials by Mechanical Alloying Techniques, eds. Artz E. and Schultz L., Calw-Hirasu 185.

Arzt, E. and Asby, M. (1982)

Scripta Met. **16** 1285.

Arzt, E. and Wilkinson, D.S. (1986)

Acta Met. **34** 1893.

Asano, K., Kohno, V., Kohyama, A., Suzuki, T. and Kusanagi, H. (1988)

Journal of Nuclear Materials **155** 928–934.

Ashby, M. F. (1966)

Proc. Conf. on Oxide Dispersion Strengthening, Metallurgical Society Conferences 47 , eds.: Ansell, G., Cooper, T., and Lenel, F., Bolton Landing, New York 143.

Ashby, M. F. (1969)

in Physics of Strength and Plasticity, ed. Argon, A., MIT Press 113.

Ashby, M. F. (1973)

Proc. Third Int. Conf. on the Strength of Metals and Alloys, Cambridge, The Institute of Metals **2** 8.

Ashby, M. F and Jones, D. (1980)

Engineering Materials- An Introduction to their Properties and Applications, Pergamon Press.

Balluffi, R. W. and Seigle, L. L. (1955)

Acta Met. **3** 155.

Baloch, M. M. (1989)

Ph.D. Thesis, University of Cambridge.

Baloch, M. M., Bhadeshia, H. K. D. H. (1991)

Materials Science and Technology **6** 1236–1246.

Ben, R. C., Curwick, L. R. and Hack, G. A. J. (1981)

Powder Metallurgy **24** 191.

Benjamin, J. S. (1970)

Metallurgical Transactions **1A** 2943–2951.

Benjamin, J. S. (1988)

Proc. Conf. on New Materials by Mechanical Alloying Techniques, ed. by Arzt, E., Schultz, L., Calw-Hirsau, Germany 3.

Benjamin, J. S. and Bomford, M. J. (1974)

Metallurgical Transactions **5A** 615.

Benjamin, J. S. and Cairns, R. L. (1971)

in Modern Development in Powder Metallurgy, H. H. Hausner, (ed.), volume 5, Plenum Press, New York 47.

Benjamin, J. S. and Volin, T. E. (1974)

Metallurgical Transactions **5A** 1929.

Benjamin, J. S. and Gilman, P. S. (1983)

Metals Handbook, 9th edition, Vol. 7, ASM International, Ohio 722.

Benn, R. C. (1983)

Proc. Conf. on Frontiers of High Temp. Materials II, eds., Benjamin, J. S. and Benn, R. C., London 37.

Benn R. C., Curwick, L. R. and Hack G. A. J. (1981)

Powder Metall. **24** 191–195.

Benn, R. and Mirchandani, P. (1988)

Proc. Conf. on New Materiaals by Mechanical Alloying Techniques, ed. by Arzt, E., Schultz, L. Calw-Hirsau, Germany 19.

Bhadeshia, H. K. D. H. (1995)

MAP – Materials Algorithims Project

Bhadeshia, H. K. D. H., Mackay, D. J. C., and Svensson, L. E. (1995)

Materials Science and Technology **11** 1046–1051.

Bonis, L. J. and Grant, N. J. (1962)

Trans. TMS-AIME **224** 308.

Bricknell R. H, and Woodford, D. A. (1981)

Metallurgical Transactions A **12A** 1673–1680.

Brown, L. and Ham, R. (1971)

Strengthening Methods in Crystals, ed. by Kelly A. and Nicholson R., Elsevier Publishing Company 9.

Cairns, R. L., Curwick, L. R. and Benjamin, J. S. (1975)

Metallurgical Transactions **6A** 179.

Cama, H. (1994)

Ph.D. Thesis, University of Leeds, UK.

Cama, H. and Hughes, T. A. (1993)

Institute of Physics Conference Series No. 138: Section 7, EMAG93, ed. A. Craven, IOP Publishing, Oxford, U. K. 361–364.

Cama, H. and Hughes, T. A. (1994)

Materials for Advanced Power Engineering, Part II Kluwer Academic Publishers, Netherland 1497–1506.

Chaston, J. C. (1945)

Journal of the Institute of Metals **71** 23.

Chou, T.S. and Bhadeshia H.K.D.H. (1993)

Materials Science and Technology **9** 890–897.

Chou, T. S. and Bhadeshia, H. K. D. H. (1994)

Materials Science and Engineering A **A189** 229–233.

Chou, T. S. and Bhadeshia, H. K. D. H. (1995)

Materials Science and Technology **11** 1129–1138.

Cobble, R. L. (1963)

Journal of Applied Physics **34** 1679.

Cool, T. and Bhadeshia, H. K. D. H. (1997)

Mathematical Modelling of Weld Phenomena 3, eds. H. Cerjak and H. K. D. H. Bhadeshia, The Institute of Materials, London 403–442.

Cool, T., Bhadeshia, H. K. D. H., and Mackay, D. J. C. (1997)

Materials Science and Engineering A in press.

Corti, C. W., Cotterill, P. and Fitzpatrick, G. (1974)

Int. Met. Rev. **19** 77-84.

Courtney, T. and Maurice, D. (1989)

Proc. Conf., Solid State Powder Processing, ed. by Clauer, A. by deBarbadillo, J., Indiana, USA 3.

Curwick, L. (1981)

Proc. Conf., Frontiers of High Temps. Materials, ed. by Benjamin, J., New York, USA 3.

Czyrska-Filemonowicz, A., Enniss, P. and Wribel, M. (1993a)

Proc. Conf., MECS 93, Wroclaw, Poland 271.

Czyrska-Filemonowicz, A. and Krantwasser, P. (1992)

Proc. 10th European Congress of Electron Microscopy, EUREM 92, ed. by Rios, A., Arias, J., Megias-Megias, L. and Lopex-Galindo, A., Granada, Spain **2** 245.

Daeubler, M. A., and Froschammer, D. (1990)

Proc. Conf., Structural Application of Mechanical Alloying, ed. by Froes, F.H. and deBarbadillo, J. J., Myrtle Beach 119

Dieter, E. G. (1988)

Mechanical Metallurgy, McGraw-Hill Series, Metric Editions, Materials Science and Engineering 445

Dubiel, P., Osuch, W., Wrobel, M., Czyrska-Filemonowich, A. and Ennis, P. J. (1994)

Materials for Advanced Power Engineering, Part II, D. Coutsouradis *et al.*, (eds.), Kluwer Academic Publisers, Netherlands 1523–1532.

Dyson, B. F. (1976)

Metal Science **10** 349.

Elliott, I., McColvin, G. and Shaw, S. (1991)

Proc. of International Conf. on PM of Aerospace Materials 1991, Laussanne, Switzerland.

Ennis, P. J., Abd El-Azim, M. E. and Schuster, H. (1990)

Proc. Conf., High Temperature Materials for Power Engineering, Liege, Belgium, 143.

Evans, R. W., Preston, J., Wilshire, B. and Little, E. A. (1992)

J. of Nuclear Materials **195** 24–28.

Evans, R. W. and Wilshire, B. (1985)

Creep of Metals and Alloys, Institute of Metals.

Evens, P. J., Martin, J. W. and Little, E. A. (1992)

Materials Science and Technology **8** 531–536.

Fischer, J. J., Astley, I. and Moore, J. P. (1977)

Proc. 3rd Int. Symp. on Superalloys: Metallurgy and Manufacture, Baton Rouge, Louisiana 361.

Fischer, J. and Weber, J. (1990)

Adv. Mat. Proc. **134** 43.

Fleck, R. G., Taplin, D. M. R., and Beavers, C. J. (1975)

Acta Met. **23** 414.

Fleetwood, M. J. (1986)

Mater. Sci. and Technology **2** 1176.

Floreen, S., Kane, R. H., Kelly, J. J. and Robinson, M. L. (1981)

Proc. Conf., Frontiers of High Temp. Materials I, ed. by Benjamin, J.S., New York 94.

Fraser, R. W. and Evans, D. J. I. (1966)

Oxide Dispersion Strengthening, ed. by Ansell, G. S., Cooper, T. D. and Lenel, F.V., Gordon and Breach, New York 375.

Fujii, H., Mackay, D. J. C., and Bhadeshia, H. K. D. H. (1996)

ISIJ International **36** 1373–1382.

Gavard, L., Bhadeshia, H. K. D. H., Mackay, , and Suzuki, S. (1996)

Materials Science and Technology **12** 453–463.

Gessinger, G. H. (1976)

Metallurgical Transactions **7A** 1203.

Gessinger, G. H. (1984)

Powder Metallurgy of Superalloys, Butterworth and Co., London 213–292.

Gilman, P. and Benjamin, J. (1983)

Ann. Rev. Mat. Sci. **13** 279.

Gladman, T., Holmes, B. and McIvor, I. (1971)

Effects of Second Phase Particles on Mechanical Properties of Steels, Iron and Steel Institute, London 68.

Goods, S. H. and Brown, L. M. (1979)

Acta Met. **77** 1.

Gregory, E. and Goetzel, C. G. (1958)

Trans. TMS-AIME **212** 868.

Grundy, E. (1987)

Proc. Conf. on PM Aerospace Materials 87, Switzerland 12.

Grundy, E. and Patton, W. H. (1985)

Proc. Conference on High Temp. Alloys, ed. by Marriott J., Merz,M., Nihoul, J.and Ward, J., Patten, The Netherlands 327.

Hack, G. (1984)

Powder Metallurgy **27(2)** 73–79.

Haeberle, R. (1981)

Proc. Conf., Frontiers of High Temps. Materials, ed. by Benjamin, J., New York 125.

Haghi, M. and Anand, L. (1990)

Metallurgical Transactions **12A** 353.

Hall, E. O. (1951)

*Proc. Conf. Phys. Soc.,*London **64** 747.

Harris, J. E. (1973)

Metallurgical Transactions **7** 1.

Hendrix, P., and Vandermeulen, P. (1982)

BLG 557 - an information sheet of SCK/CEN, Mol, Belgium.

Henrick, R. J. (1981)

Proc. Conf., Frontiers of High Temp. Materials I, ed. by Benjamin, J. S., New York 63.

Herrick, R. S., Weertman, J. R., Petkovic–Luton, R. and Luton, M. J. (1988)

Scripta Metallurgica. **22** 1879.

Herring, C. (1950)

Journal of Applied Physics **21** 437.

Honeycombe, R. W. K. and Bhadeshia, H. K. D. H., (1995)

Steels: Microstructure and Properties, 2nd edition Edward Arnold, London.

Howson, T., Stulga, J. and Tien J. (1980)

Metallurgical Transactions **11A** 1599.

Huet, J. J. and Leroy, V. (1974)

Nuclear Technology **24** 216.

Ichikawa, K., Bhadeshia, H. K. D. H., and Mackay, D. S. C. (1996)

Science and Technology of Welding and Joining **1** 43–50.

IncoMap ()

Information sheet.

Irmann, R. (1949)

SAP : Ein Never Werkstoff der Pulvermetallurgie aus Al, Technische Rundschaw **36** 19–26.

Jaeger, D. M. (1994)

Ph.D. Thesis University of Liverpool, UK.

Jaeger, D. M. and Jones, A. R. (1991)

"Materials for Combined Cycle Power Plant", Proc. conf., Institute of Metals, London 1–11.

Jaeger, D. and Jones, A. (1992b)

AEA-Intec-1082 Report, September.

Jones, J., Mackay, D. J. C., and Bhadeshia, H. K. D. H. (1995)

Proceedings of Advanced Materials, A. Q. Khan Research Laboratories, Pakistan.

Jongenburger, C. and Singer, R. (1988)

Proc. Conf., New Materials by Mechanical Alloying, ed. by Arzt, E. and Schultz, L., Calw-Hirsau, Germany 157.

Jongenburger, P., Verpoort, C. and, Singer, R. (1987)

Int. Conference on Advances in Material Technology for Fossil Power Plants, ASM, Ohio 503.

Kane, R. H., McColvin, G. M., Kelly, T. J. and Davidson, J. M. (1984)

Proc. Conf., Corrossion 84, New Orleans, LA, USA , National Association of Corrossion Engineers, paper 12.

Kawasaki, Y., Ikeda, Y., Kobayashi, T., and Sumiyoshi, T. (1996)

ISIJ International **36** 1208–1214.

Kazimierzak, B., Prignon, M., Lecomte–Mertens, C. and Coutsouradis, C. (1990)

High Temperature Materials for Power Engineering 1990, Kluwer Academic Publishers, 131, quoted by Regle (1994).

Kehagias, T., Coheur, L. and Delavignette, P. (1993)

Journal of Materials Science Lett. **12** 1059.

Kelly, A. and Nicholson, R. B. (1963)

Progress in Materials Science, Macmillan, New York.

Kim, Y. G. and Merrick, H. F. (1979)

NASA CB159–493, Lewis Research Center.

Koch, C. (1989)

Proc. Conf., Solid State Powder Processing, ed. by Clauer, A. and deBarbadillo, J., Indiana, USA 35.

Koch, C. C. (1990)

Structural Applications of Mechanical Alloying, ed. by Froes, F. H. and deBarbadillo, J. J., Materials Park (OH), ASM Int. 193.

Korb, G. (1988)

Proc. Conf., New Materials by Mechanical Alloying Techniques, ed. Arzt, E. and Schultz, L., Calw-Hirsau, Germany 175.

Kramer, K. (1977)

Powder Met. Int. **9** 105.

Krautwasser, P., Czyrska-Filemonowich, A., Widera M. and Carsughi F. (1994)

Materials Science and Engineering A **A177** 199–208.

Lawn, R., Wilson, F. and Desforges, C. (1976)

Powder Metallurgy **19(4)** 196.

Lewis, D. B. and Pickering, F. B. (1983)

Met. Tech. **10** 264.

Little, E. A., Mazey, D. J. and Hanks, W. (1991)

Scripta Metall. Mater. **25** 1115–1118.

Lloyd, D. M. and Cooke, M. J. (1981)

Metall. Mater. Tech. **13** 516.

Lund, R. W. and Nix, W. D. (1976)

Acta Met. **24** 469.

Macdonald, D. M. (1981)

Proc. Conf., Frotiers of High Temp. Materials, New York, Incomap, 101.

Mackay, D. J. C. (1992)

Neural Computation **4** 415–447.

Mackay, D. J. C. (1992)

Neural Computation **4** 448–472.

Mackay, D. J. C. (1997)

Mathematical Modelling of Weld Phenomena 3, eds. H. Cerjak and H. K. D. H. Bhadeshia, The Institute of Materials 359.

Mackay, D. J. C. (1995)

Network: Computation in Neural Systems **6** 469–505.

Mackay, D. J. C. (1994)

Transaction of the American Society of Heating, Refrigeration and Air-Conditioning Engineers **100** 1053–1062.

Martin, J. and Doherty, R. (1980)

Stability of Microstrucure in Metallic Systems, Cambridge Solid State Science Series, ed. Cahn, R., Forty, A. and Ward, I., Cambridge University Press.

McColvin, G. M. and Smith, G. D. (1985)

High Temp. Alloys, ed. by Marriot, J.B., Merze, M., Nihoul, J. and Ward, J., Elsevier Applied Sci. 139.

Mclean, M. (1985)

Acta Met. **33** 545.

Mughrabi, H. (1993)

Materials Science and Technology - A comprehensive treatment, ed. H. Mughrabi, VCH Publishers, NY. and Berlin **6** 1-17.

Murakami, K. (1993)

Ph.D. Thesis, Cambridge University.

Murakami, K., Harada, H. and Bhadeshia, H. K. D. H. (1992)

Heat Treatment '92, ed. I. Tamura, Kyoto, Japan 269–272.

Nabarro, F. R. N. (1948)

Report of a conference on Strength of Solids, Physical Society , London 75.

Nardone, V., Matejczyk, D. and Tien, J. (1984)

Acta Metallurgy **32(a)** 1509.

Nardone, V. C. and Tien, J. K. (1983)

Scripta Metallurgica **17** 467.

Nix, W. D. (1981)

Metals Forum **4** 38.

Nutting, J., Ubhi, S. and Hughes, T. A. (1981)

Proc. Conf., Frontier of High Temp. Materials 33, New York, Incomap.

Okafor, I. C. I. and Carson, O. N. (1978)

Met. Trans. **9A** 1651.

Orowan, E. (1946)

Trans. Inst. Eng., Shipbuilders in Scotland **89** 165.

Perrone, M. P. (1994)

Proceedings 1993 Connectionist Models Summer School, Hillsdale, NJ: Lawrence Erlbaum 364–371.

Perrone, M. P., Cooper, L. N. (1993)

Artificial Neural Networks for Speech and Vission 126–142.

Petch, N. J. (1953)

Journal of Iron and Steel Institute, London **174** 25.

Petkovic-Luton, R., Srolovitz, D. and Luton, M. (1983)

Proc. Conf., Frontiers of High Temperature Materials II, ed. by Benjamin, J., Benn, R., London 73.

Pilling, J. and Ridley, N. (1988)

Res. Mechanica **23** 31.

Preston, J., Wilshire, B. and Little, E. A. (1991)

Scripta Metallurgica et Materialia **25** 183–184.

Raj, R. and Gosh, A. K. (1981)

Met. Trans. **12A** 1291.

Rao, V. K., Taplin, D. M. R. and Rao, P. R. (1975)

Metallurgical transactions A **6** 77–85.

Regle, H. (1994)

Ph.D. Thesis, 'Alliages Ferritiques 14/20 % de chrome Renforces par Dispersion d'Oxydes', Universite de Paris–Sud.

Rösler, J. and Arzt, E. (1990)

Acta Met. Mater. **38(4)** 671.

Rühle, M. and Korb, G. (1991)

Proc. Conf., Heat Resistant Materials, ed. by Natesan, K. and Tillack, D., Fontana, Wisconsin, USA, ASM Int. 45.

Rukwied, A. (1973)

Met. Trans. **3** 3009.

Ruluff, D. and McIntyre, P. E. (1982)

Materials Engineering **95** 34.

Rumelhart, D. E., Hinton, G. E., Williams, R. J. (1986)

Nature **323** 533–536.

Salomom, R. J. (1993)

Journal De Physique IV **3** 697–702.

Schaffer, G. B., Loretto, M. H., Smallman, R. E. and J. W. Brooks (1989)

Acta Metall. **37.** 2551–2558.

Schaffer, G. and McCormick, P. (1992)

Materials Forum **16** 91.

Schneider, K. and Dannhauser, G. (1991)

Proc. of Int. Conf. on PM of Aerospace Materials 1991, Laussanne, Switzerland, Nov., paper 10.

Schroder, J. H. and Arzt, E. (1985)

Scripta Metallurgica **19** 1179.

Seeger, A. (1954)

Philosophical Magazine **45** 771–773.

Sellars, C. M. and Petkovic-Luton, R. A. (1980)

Mat. Sci. Eng. **46.** 75.

Sha, W. and Bhadeshia, H. K. D. H. (1994.)

Metallurgical and Materials Transactions A **25A** 705–714.

Shewfelt, R. S. W. and Brown, L. M. (1974)

Philosophical Magazine **30** 1135–1145.

Shewfelt, R. S. W. and Brown, L. M. (1977)

Philosophical Magazine **35** 945–962.

Singer, R. F. and Gessinger, G. H. (1984)

Powder Metallurgy of Superalloys Gessinger, R. F., (ed.), University Press, Cambridge, UK 213–292.

Smith, D. F., Clatworth, E. F., Tipton, D. G. and Manking W.L. (1980)

"Superalloys 1980", Pcoceedings of the Fouth International Symposium on Superalloys, ASM, Metals Park, O .H. 521–530.

Smith D. F., Smith J. S. and Floreen, S. (1984)

Proceedings of the 5th International Conference on Superalloys, Metal society, AIME, Seven Springs, PA, USA 591-600.

Snykers, M. and Huet, J. J. (1974)

*Proc.Conf. on Creep Strength in Steel and High Temp. Alloys,*Metals Society, London 237.

Spengler, H. (1964)

Metall. **18** 727.

Srolovitz, D., Luton, M., Petkovic-Luton, R., Barnett, D. and Nix, C. (1984a)

Acta Metallurgy **32(7)** 1079.

Srolovitz, D. J., Petkovic-Luton, R. and Luton, M. J. (1982)

Scripta Met. **16** 1401.

Srolovitz, D. J., Petkovic-Luton, R. and Luton, M. J. (1983)

Phil. Mag. **48** 795.

Srolovitz, D. J., Petkovic-Luton, R. and Luton, M. J. (1984)

Scripta Met. **18** 1063.

Sundaresan, R. and Froes, F. H. (1987)

Journal of Metals **39** 22–27.

Takahashi, M. and Bhadeshia, H. K. D. H. (1990)

Materials Science and Technology **6** 592–603.

Tapsell, H. J. (1931)

*Creep of Metals,*Oxford University Press, London.

Tien, J. (1983)

Proc. Conf. on Frontiers of High Temperature Materials II, ed. by Benjamin, J. and Benn, R., London 114.

Tien, J. and Purushothaman, S. (1976)

Proc. Conf. on Properties of High Temperature Alloys with Emphasis on Environmental Effects, ed. by Foroulis, Z. and Pettit, F., AIME, Princeton 3.

Timmins, R. and Arzt, E. (1988)

Scripta Met. **22** 1353.

Tipler, H. R., Taylor, L. H. and Hopkins, B. E. (1990)

Metal Sci. Journal **4** 167.

Tracy, V. A. and Worn, D. K. (1962)

Powder Metallugy **10** 1.

Ubhi, H. S., Huges, T. A., and Nutting, J. (1981)

*Proc. Conf. "Frontiers of High Temperature Materials I" (*ed., Benjamin, J. S.*), New York* 33.

Ubhi, H. (1980)

Ph.D. Thesis, University of Leeds, UK.

Vermeulen, W., Bodin, A., and van der Zwaag, S. (1997)

Steel Research **68** 20–26.

Vermeulen, W., Morris, P. F., de Weijer, A. P., and van der Zwaag, S. (1996)

Ironmaking and Steelmaking **23** 433–437.

Vermeulen, W., van der Zwaag, S., Morris, P., and de Weijer, T. (1997)

Steel Research **68** 72–79.

Weber, J. H. (1980)

Proc. Conf. "Payoff Decade for Advanced Materials", San Diego, Califonia, Society for the Advancement of Materials and Process Engineering 752.

Weisbrodt, A., Penkalla, H., Schubert, F. and Nickel, H. (1990)

Ph.D Thesis, Forschungszentrum KFA, Julich, Germany.

Whittenberger, J. D. (1976)

Metallurgical Transactions A **7A** 611.

Whittenberger, J. D. (1977)

Metallurgical Transactions A **8A** 1155.

Whittenberger, J. D. (1978)

Metallurgical Transactions A **9A** 101.

Whittenberger J. D. (1979)

Metallurgical Transactions A **10A** 1285–1292.

Whittenberger, J. D. (1981)

Metallurgical Transactions A **12A** 845–851.

Whittenberger, J. D. (1984)

Metallurgical Transactions **15A** 1753–1762.

Whittenberger, J. (1989)

Proc. Conf. on Solid State Powder Processing, ed. by Clauer, A. and deBarbadillo, J., Indiana, USA 137.

Wiegert, W. H. and Henricks, J. R. (1980)

Int. Conf. on Superalloys 1980.

Wilcox, B. and Clauer, A. (1972a)

Acta Met. **20** 743.

Wilcox, B. A. and Clauer, A. H. (1972(b))

Superalloys, ed. by Sims C. and Hagel, W., John Wiley and sons 197.

Wilson, F., Knott, B. and Desforges, C. (1978)

Met. Trans. **9A** 275.

Young, C. H. and Bhadeshia, H. K. D. H. (1993)

Programme developed for use internally, University of Cambridge.

Zakine, C., Prioul, C., Alamo, A., and Francois, D. (1993)

Journal De Physique IV **3** 591–596.

Zeizenger, H. and Arzt, E. (1988)

Z. Metallkunde **79(12)** 774.

Zwilsky, K. M. and Grant, N. J. (1961)

Trans. TMS-AIME **221** 371.